2013-03

# LONG-RANGE FORECASTING OF SURFACE AIR TEMPERATURE AND PRECIPITATION FOR THE KOREAN PENINSULA

Reitz, Nicholas J.

Monterey, California. Naval Postgraduate School


# NAVAL POSTGRADUATE SCHOOL

**MONTEREY, CALIFORNIA**

# THESIS

**LONG-RANGE FORECASTING OF SURFACE AIR TEMPERATURE AND PRECIPITATION FOR THE KOREAN PENINSULA**

by

Nicholas J. Reitz

March 2013

Thesis Co-Advisors: Tom Murphree
David Meyer

**Approved for public release; distribution is unlimited**

THIS PAGE INTENTIONALLY LEFT BLANK

# REPORT DOCUMENTATION PAGE

*Form Approved OMB No. 0704–0188*



| **1. AGENCY USE ONLY *(Leave blank)*** | **2. REPORT DATE** March 2013 | **3. REPORT TYPE AND DATES COVERED** Master's Thesis |
|---|---|---|

**4. TITLE AND SUBTITLE**
LONG-RANGE FORECASTING OF SURFACE AIR TEMPERATURE AND PRECIPITATION FOR THE KOREAN PENINSULA

**5. FUNDING NUMBERS**

**6. AUTHOR(S)** Nicholas J. Reitz

**7. PERFORMING ORGANIZATION NAME(S) AND ADDRESS(ES)**
Naval Postgraduate School
Monterey, CA 93943–5000

**8. PERFORMING ORGANIZATION REPORT NUMBER**

**9. SPONSORING /MONITORING AGENCY NAME(S) AND ADDRESS(ES)**
N/A

**10. SPONSORING/MONITORING AGENCY REPORT NUMBER**

**11. SUPPLEMENTARY NOTES** The views expressed in this thesis are those of the author and do not reflect the official policy or position of the Department of Defense or the U.S. Government. IRB Protocol number ____N/A____.

**12a. DISTRIBUTION / AVAILABILITY STATEMENT**
Approved for public release; distribution is unlimited

**12b. DISTRIBUTION CODE**

**13. ABSTRACT (maximum 200 words)**

We have designed, developed, and tested a long-range forecasting system for producing forecasts of surface air temperatures and precipitation rates in the Korean Peninsula region at leads of two months for each calendar month. We tested predictors based on: (1) indices of the Arctic Oscillation, El Niño/La Niña, North Atlantic Oscillation, Pacific/North American Pattern, and the West Pacific Pattern; (2) 850 hectopascal geopotential heights and sea surface temperatures in specific regions; (3) persistence; and (4) year (to represent long-term trends).

Our forecasting system includes 24 multiple linear regression models, one for temperature and one for precipitation for each month. Each model uses a unique set of predictors. We tested each model by conducting 43 years of cross-validated hindcasting for our 1970–2012 study period. The hindcast results showed that, overall, the models had skill in predicting above normal, near normal, and below normal temperatures and precipitation rates for the Korean Peninsula (e.g., Heidke skill scores > 0). We used our January models to successfully forecast temperatures and precipitation for January 2013. We also developed a series of forecaster worksheets to be used to produce forecasts for the Korean Peninsula.

**14. SUBJECT TERMS** Korea, Precipitation, Precipitation Rates, Temperature, Climate, Climate Variations, Climate Anomalies, Climate Prediction, Arctic Oscillation, El Nino, La Nina, West Pacific Pattern, Pacific/North American Pattern, North Atlantic Oscillation, Teleconnection, Long-Range Forecasting, Statistical Forecast, Meteorology

**15. NUMBER OF PAGES** 201

**16. PRICE CODE**

| **17. SECURITY CLASSIFICATION OF REPORT** | **18. SECURITY CLASSIFICATION OF THIS PAGE** | **19. SECURITY CLASSIFICATION OF ABSTRACT** | **20. LIMITATION OF ABSTRACT** |
|---|---|---|---|
| Unclassified | Unclassified | Unclassified | UU |

NSN 7540–01–280–5500

Standard Form 298 (Rev. 2–89)
Prescribed by ANSI Std. 239–18

THIS PAGE INTENTIONALLY LEFT BLANK

**Approved for public release; distribution is unlimited**

# LONG-RANGE FORECASTING OF SURFACE AIR TEMPERATURE AND PRECIPITATION FOR THE KOREAN PENINSULA

Nicholas J. Reitz
Captain, United States Air Force
B.S., Millersville University, 2007

Submitted in partial fulfillment of the
requirements for the degree of

**MASTER OF SCIENCE IN METEOROLOGY**

from the

**NAVAL POSTGRADUATE SCHOOL**
**March 2013**

Author: Nicholas J. Reitz

Approved by: Tom Murphree
Thesis Co-Advisor

David Meyer
Thesis Co-Advisor

Wendell Nuss
Chair, Department of Meteorology

THIS PAGE INTENTIONALLY LEFT BLANK

# ABSTRACT

We have designed, developed, and tested a long-range forecasting system for producing forecasts of surface air temperatures and precipitation rates in the Korean Peninsula region at leads of two months for each calendar month. We tested predictors based on: (1) indices of the Arctic Oscillation, El Niño/La Niña, North Atlantic Oscillation, Pacific/North American Pattern, and the West Pacific Pattern; (2) 850 hectopascal geopotential heights and sea surface temperatures in specific regions; (3) persistence; and (4) year (to represent long-term trends).

Our forecasting system includes 24 multiple linear regression models, one for temperature and one for precipitation for each month. Each model uses a unique set of predictors. We tested each model by conducting 43 years of cross-validated hindcasting for our 1970–2012 study period. The hindcast results showed that, overall, the models had skill in predicting above normal, near normal, and below normal temperatures and precipitation rates for the Korean Peninsula (e.g., Heidke skill scores > 0). We used our January models to successfully forecast temperatures and precipitation for January 2013. We also developed a series of forecaster worksheets to be used to produce forecasts for the Korean Peninsula.

THIS PAGE INTENTIONALLY LEFT BLANK

# TABLE OF CONTENTS

# LIST OF FIGURES

THIS PAGE INTENTIONALLY LEFT BLANK

# LIST OF TABLES

# LIST OF ACRONYMS AND ABBREVIATIONS

| | |
|---|---|
| 14 WS | 14th Weather Squadron |
| AN | above normal |
| AO | Arctic Oscillation |
| Apr | April |
| Aug | August |
| BCC | Beijing Climate Center |
| BN | below normal |
| BSS | Brier skill score |
| C | Celsius |
| CAB | Climate Analysis Branch |
| CFSR | Climate Forecast System Reanalysis |
| CMAP | CPC Merged Analysis of Precipitation |
| CPC | Climate Prediction Center |
| Dec | December |
| DoD | Department of Defense |
| EASM | East Asian summer monsoon |
| EN | El Niño |
| ENLN | El Niño/La Niña |
| ENSO | El Niño-Southern Oscillation |
| ESRL | Earth System Research Laboratory |
| FAR | false alarm rate |
| Feb | February |
| FNMOC | Fleet Numerical Meteorology and Oceanography Center |
| GPH | geopotential height |
| hPa | hectopascal |
| HSS | Heidke skill score |
| IBTrACS | International Best Track Archive for Climate Stewardship |
| IO | Indian Ocean |
| IRI | International Research Institute for Climate and Society |
| Jan | January |
| Jul | July |

| | |
|---|---|
| Jun | June |
| JMA | Japan Meteorological Agency |
| KMA | Korean Meteorological Administration |
| km | kilometer |
| KPI | Korean Precipitation Index |
| KTI | Korean Temperature Index |
| LN | La Niña |
| LR | linear regression |
| LRF | long-range forecast |
| LT | lead time |
| LTM | long-term mean |
| Mar | March |
| MEI | Multivariate ENSO Index |
| MLR | multiple linear regression |
| mm | millimeter |
| NAO | North Atlantic Oscillation |
| NCAR | National Center for Atmospheric Research |
| NCEP | National Centers for Environmental Prediction |
| NN | near normal |
| NOAA | National Oceanic and Atmospheric Administration |
| Nov | November |
| NPS | Naval Postgraduate School |
| OCN | optimal climate normal |
| Oct | October |
| PNA | Pacific/North American Pattern |
| POD | probability of detection |
| PR | precipitation rate |
| R1 | NCEP/NCAR reanalysis |
| Sep | September |
| SO | Southern Oscillation |
| SST | sea [A1]surface temperature |
| USFK | United States Forces Korea |
| WP | West Pacific Pattern |

# ACKNOWLEDGMENTS

I would like to thank my advisors, Dr. Tom Murphree and Mr. David Meyer, for guiding me through my research and thesis writing. Although it took tremendous patience on their part, l learned an extensive amount of material that I will carry with me throughout my career. I would also like to thank Dr. Pat Harr, Mr. Bob Creasey, and Capt. Shane Gillies for helping me along the way. NPS is a great institution and I am honored to be an alumnus.

I want to thank Millersville University (where I received my B.S. degree) for preparing me well for graduate studies in meteorology. I especially want to thank my undergraduate mentor, Dr. Alex DeCaria (a prior NPS student). Without his guidance, I would not be where I am today.

I would also like to thank my parents, Eddie and Terri. They taught me that through hard work and perseverance that I could achieve anything.

THIS PAGE INTENTIONALLY LEFT BLANK

# I. INTRODUCTION

## A. IMPORTANCE

At the end of the Korean War in 1953, the Korean Armistice Agreement was signed, restoring the border between North Korea and South Korea. The objective of the armistice was to “insure a complete cessation of hostilities and all acts of armed force in Korea until a final peaceful settlement is achieved” (FindLaw 2013). A final peaceful settlement has never been reached, and the two nations still technically remain at war. Since the signing of the armistice, there have been many small scale attacks on South Korea by North Korea. As an ally of South Korea, the U.S. has maintained a strong military presence in South Korea to keep North Korea under control. United States Forces Korea (USFK) is comprised of approximately 28,500 U.S. troops (America.gov 2013), all of whom are posted in South Korea.

In 2010, the North launched an artillery strike that killed four South Koreans. In response to the attack, South Korea and the U.S. conducted a joint exercise to demonstrate the strength of the South Korean-U.S. alliance. This four day military exercise involved of the USS George Washington carrier strike group, which carries 75 warplanes and has a crew of over 6,000 (Fox News 2010). North Korea was strongly opposed to this, and their official KCNA news agency stated that due to this exercise, “the Korean Peninsula is inching closer to the brink of war” (USA Today 2010).

With no plans to pull out of Korea, it is vital that the U.S. Department of Defense (DoD) has access to accurate long-range forecasts (LRFs) of environmental conditions in order to prepare for continued military training and for the possibility of war. Since war could erupt at any time, it is imperative that these LRFs cover all 12 months of the year. Although the DoD currently produces LRFs for all 12 calendar months, a detailed study has not been conducted to grade the performance or improve the skill of these LRFs. In our

study, we designed, developed, and tested LRFs of surface air temperature and precipitation rate for the Korean Peninsula region for all 12 months of the year.

## B. KOREAN PENINSULA OVERVIEW

### 1. Geography

Giese (2004) defined four main climatic commonality regions on the Korean Peninsula: the Northeast Highlands, the Northwest Hills and Plains, the Southwest Hills and Plains, and the East Coast Plains (Figure 1). The Northeast Highlands is a very mountainous region that has a peak elevation of 2,744 meters (9,003 feet). There are many rivers in the region that carry rainwater and melted snow eastward to the Sea of Japan and westward to the Yellow Sea. The Northwest Hills and Plains is a series of parallel mountain chains oriented northeast to southwest (Giese 2004). This region contains the densely populated metropolitan areas of Seoul and Pyongyang. The border between North and South Korea is oriented west-east at around 38 degrees N latitude. The Yalu River separates North Korea from China. The Southwest Hills and Plains are made up of mostly coastal plains but also contain the smaller Sobaek mountain range. This mountain range forms an interior divide that separates the northwest area and Seoul from the southeast area and Pusan (the second largest city in South Korea). The volcanic island of Cheju-do is located in the southern portion of this region in the East China Sea and contains the highest elevation in South Korea at 1,950 meters (6,400 feet). There are also many rivers, lakes and marshes in this region, most of which drain into the Yellow Sea. The East Coast Plain is a narrow, ragged plain with short rivers, sandy beaches, inlets, and lowlands parallel to the southern half of the east coast of Korea (Giese 2004). The Taebaek Mountains are less than 1,200 meters (4,000 feet) and make up the western border of this region. The eastern border of this region is the Sea of Japan.

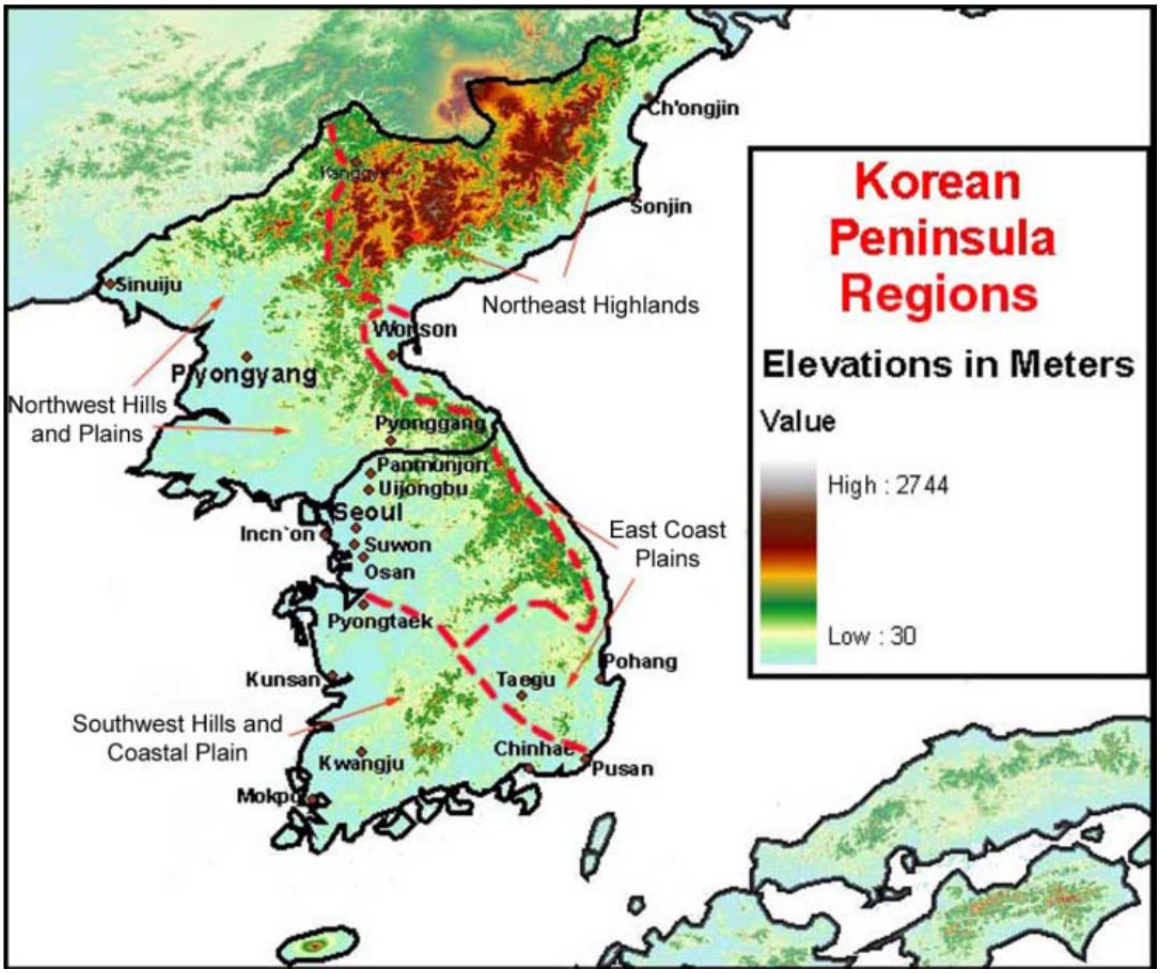


Figure 1. Korean Peninsula climatic commonality regions (Giese 2004).

## 2. Climatology

Korean winters January-March (Jan–Mar) are cold and dry as the predominant lower tropospheric Asian High pressure system blows in Siberian air from the north and northwest. Very little precipitation falls in the winter. Sub-freezing temperatures can persist for days to weeks throughout the peninsula. Snow can be found anywhere in Korea in the winter months, but is heaviest in the Taebaek mountains due to orographic lift and in the Southwest Hills and Plains due to sea effect snow. The spring months April-June (Apr-Jun) are generally mild with greater precipitation than in the winter months. Synoptic low pressure systems and associated cold fronts push through during these transition

seasons, bringing showers and occasional thunderstorms (see Figure 2 for low pressure source regions). The summer months July-September (Jul–Sep) bring monsoonal flow from the south, warm temperatures, and very heavy precipitation. The monsoon cloud and precipitation boundary is called the Changma, and the location of rain and thunderstorms shifts to the north and south as the boundary fluctuates. Korea receives more than half of its annual precipitation in the summer months. In late summer to early autumn (Jul–Oct), Korea is impacted by one to two tropical cyclones on average (Giese 2004). These cyclones can bring heavy rainfall and strong winds to the area. Flooding is common in the summer months from both the Changma and from passing tropical cyclones. The autumn months October-December (Oct–Dec) are generally mild (similar to spring) and feature much less precipitation than the summer months.

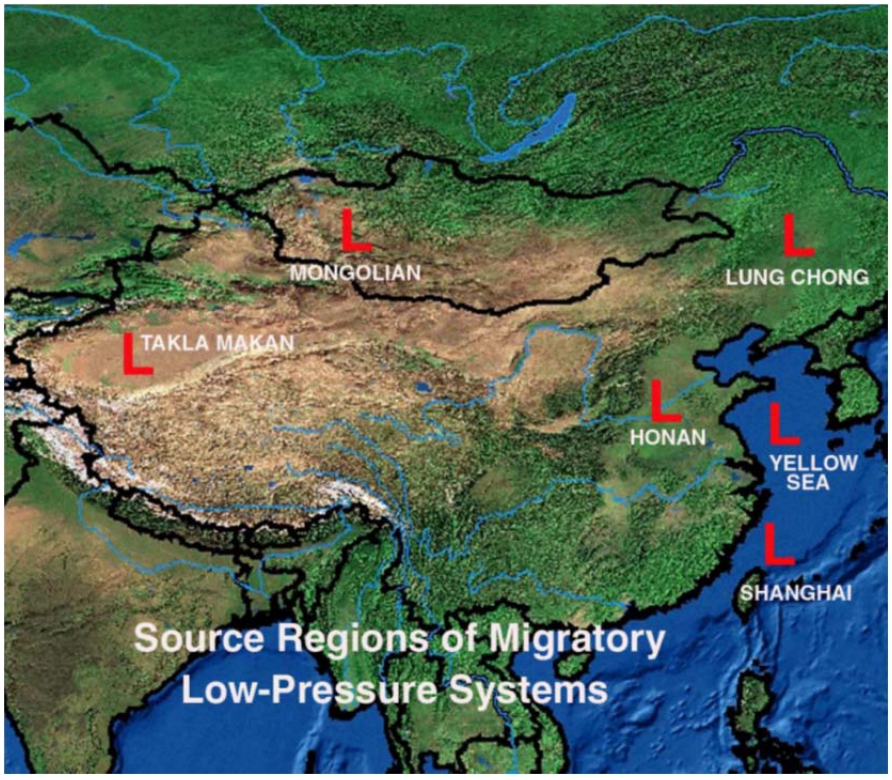


Figure 2. Source regions of migratory synoptic low pressure systems (Giese 2004).

## C. CLIMATE VARIATIONS AND TELECONNECTIONS AFFECTING THE KOREAN REGION

A teleconnection is a link between weather or climate changes occurring in widely separated regions of the globe (cf. AMS 2013). The term teleconnection is most commonly applied to describe linkages and variability on monthly or longer timescales. Sir Gilbert Walker was one of the first scientists to identify teleconnections between weather and climate from widely separated regions. He relied on statistical analyses of long-term weather records to identify many teleconnections that are now well established and used in operational climate analysis and forecasting. Walker stated: “The relationships between weather over the Earth are so complex that it seems useless to try to derive them from theoretical considerations; and the only hope at present is that of ascertaining the facts and of arranging them in such a way that interpretation shall be possible.” (cf. Walker 1932).

Since Walker’s work, many additional teleconnections have been identified and the dynamical explanations for teleconnections have become much clearer (cf. Bridgman and Oliver 2006), helping to improve the scientific understanding of the global climate system. Climate variations, such as El Niño/ La Niña (ENLN), the Arctic Oscillation (AO), and many others have been found to involve teleconnections that affect climate in different parts of the world, even for locations far from the main regions for the variations.

In this study, we investigated the use of teleconnections and indices of well-known climate variations to improve climate prediction for the Korean region. In particular, we identified and applied information about teleconnections between Korean climate and global scale 850 hectopascal (hPa) geopotential heights (GPH) and sea surface temperatures (SSTs). These variables were used as predictors for Korean climate using methods similar to those used by Lemke (2010), DeHart (2011), and Gillies (2012) for predicting climate variations in other regions.

## 1. El Niño and La Niña

El Niño (EN) and La Niña (LN) events are probably the best known and studied climate variations in the global climate system (Bridgman and Oliver 2006). ENLN events are major and complex variations of the tropical Pacific Ocean and atmosphere (Murphree 2012b). One of the atmospheric variations is the Southern Oscillation (SO). ENLN occur about every two to seven years and usually last about one year. They have large impacts on the physical environment of the global tropics and extratropics and tend to produce their maximum extratropical impacts in the winter hemisphere.

For example, ENLN have been shown to impact climate conditions in the general East Asia region. Nitta (1987) and others identified a Rossby wave train response to off-equatorial tropical convection anomalies during the summer that can extend across large portions of the extratropics (Figure 3). This tropical convection is significantly affected by the phase of ENLN. Huang and Wu (1989) found that during summers in which an EN was developing, north and south China were drier than normal and central China was wetter than normal. Wang et al. (2000) and Wang and Zhang (2002) attempted to explain the tendency for increased rainfall throughout the East Asian summer monsoon (EASM) sector following an EN event.

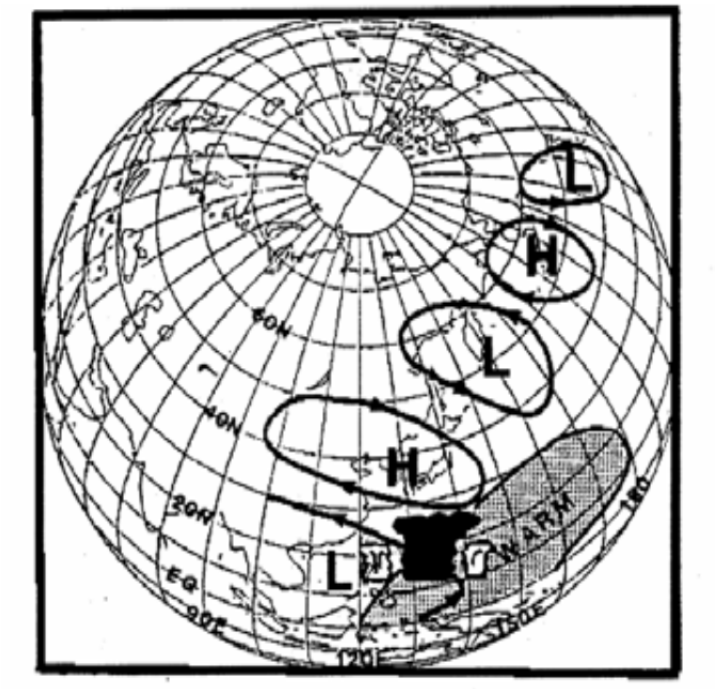


Figure 3. Schematic showing 500 hPa geopotential height (GPH) anomalies associated with increased convection over warmer than normal SST in the tropical western Pacific in the northern summer. H (L) denotes a positive (negative) GPH anomaly. After Nitta (1987)

The Multivariate ENSO Index (MEI) is one of several indices used to monitor and describe the state of ENLN. The MEI is comprised of these six variables in the tropical Pacific: sea-level pressure, zonal and meridional components of the surface wind, SST, surface air temperature, and total cloudiness fraction of the sky (ESRL 2013). The MEI for 1950 through early 2013 can be seen in Figure 4.

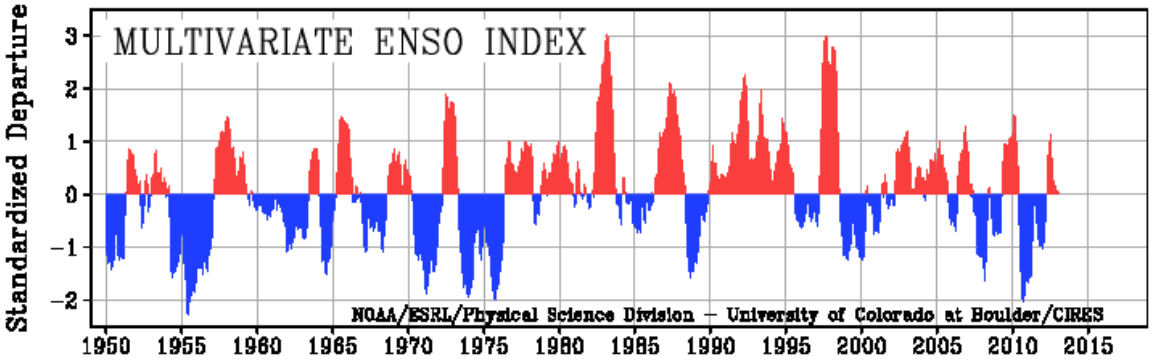


Figure 4. The Multivariate ENSO Index (ME) from 1950–2013 (ESRL 2013)

### 2. Arctic Oscillation

The Arctic Oscillation (AO) is a climate variation in which atmospheric mass oscillates between the northern polar and northern midlatitude regions (Thompson and Wallace 1998). The AO is described by an index that describes the difference between lower tropospheric pressure in the polar region with that in the midlatitudes (e.g., 45°N) (Bridgman and Oliver 2006). The positive (negative) phase occurs when lower (higher) than normal pressures are found in the polar region and higher (lower) than normal pressures are found in the midlatitudes. The AO represents an intraseasonal and interseasonal oscillation in the strength of the northern polar vortex (Murphree 2012c). The positive phase of the AO features a strong, well defined polar vortex and infrequent cold air outbreaks from the polar region, while the negative phase features a weak, poorly defined polar vortex and frequent cold air outbreaks from the polar region (Figure 5).

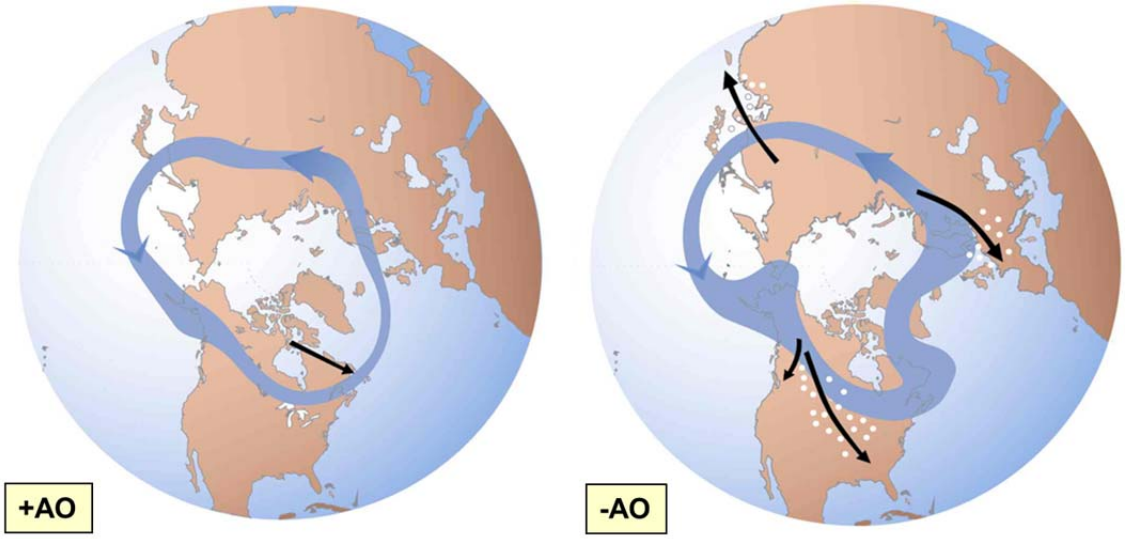


Figure 5. The positive phase of the AO (left) features a strong, well defined polar vortex and infrequent cold air outbreaks from the polar region (Murphree 2012c). The negative phase (right) features a weak, poorly defined polar vortex and frequent cold air outbreaks from the polar region. White dots denote common locations of cold air outbreaks (National Snow & Ice Data Center 2012).

Gong and Ho (2003) examined the relationship between EASM precipitation and the AO. They found strong correlations between the leading AO mode and EASM precipitation, and that direct coupling between the AO and circulation features impacts the EASM. Park et al. (2010) found that in the winter during negative phases of the AO, Korea and Japan experienced stronger cold surges than in the neutral and negative phases. They suggested that it might be possible to predict the occurrence of cold surges based on large-scale climate variation conditions such as AO conditions.

### 3. North Atlantic Oscillation

The North Atlantic Oscillation (NAO) is closely related to the AO and represents an oscillation of mass between the polar-subpolar and midlatitude-subtropical regions of the North Atlantic. The NAO is described by the difference between lower tropospheric pressure at locations representing the centers of actions for the oscillation, typically locations near Iceland and the Azores

(Bridgman and Oliver 2006). This pressure difference is used to derive an index that identifies the phase of the oscillation. The positive (negative) phase is charcterized by a stronger (weaker) than usual midlatitude-subtropical high pressure and a deeper (weaker) than normal Icelandic Low (Bridgman and Oliver 2006). The positive (negative) phase results in anomalously frequent (less frequent) and strong (weak) extratropical cyclones tracking in a more northerly (southerly) path across the North Atlantic Ocean. The NAO is associated with basin-wide anomalies in mass, momentum, energy, moisture, and storm tracks that can extend from North America well into Eurasia (Murphree 2012c). Characteristic anomalies during strong positive phases in winter include: positive low level temperature anomalies in the eastern U.S., extending eastward into northern Europe; negative low level temperature anomalies in Greenland, southern Europe, and Southwest Asia; positive precipitation anomalies in northern Europe; negative precipitation anomalies in southern and central Europe (Murphree 2012c). The opposite anomalies characterize the negative phase. The AO and NAO are closely related, since that they both describe similar variations in the northern hemisphere circulation. Some researchers prefer to view them as separate phenomena, while others view them as the same phenomena viewed from hemispheric-wide (AO) and basin-wide (NAO) perspectives (Murphree 2012c).

Yang et al. (2004) found that for a positive AO and NAO, there is above average extratropical wave activity in the Tibetan Plateau, which leads to colder temperatures at the start of the Asian Summer Monsoon (ASM) and a later and weaker ASM. Watanabe (2004) found that medium-range weather over East Asia is to some extent predictable by carefully monitoring the developing stage of individual NAO events.

### 4. Pacific/North American Pattern

The Pacific/North American Pattern (PNA) is a teleconnection pattern that in which tropospheric pressures fluctuate in characteristic ways over the

subtropical North Pacific, northeast Pacific, Canada, and the southeastern U.S. (Latif and Barnett 1994). For example, when the PNA is in the positive (negative) phase, there is a strong (weak) Aleutian Low and a strong (weak) ridge over western Canada (cf. Bridgman and Oliver 2006). The PNA is associated with a Rossby wave pattern with centers of action over the North Pacific and North America. The PNA tends to be triggered by ENLN events but may be triggered by other climate variations. There have been many studies that have linked the PNA to climate anomalies in North America. For example, Leathers et al. (1991) demonstrated that regional temperatures and precipitation are highly correlated to the PNA Index across the U.S., especially in winter. We are not aware of any studies that have identified clear linkages between the PNA and Korean climate.

### 5. West Pacific Pattern

The West Pacific Pattern (WP) is a primary teleconnection pattern and mode of low frequency variability over the North Pacific in all months (CPC 2013). During winter and spring, the pattern consists of a north-south dipole of anomalies, with one center located over the Kamchatka Peninsula and another broad center of opposite sign covering portions of southeastern Asia and the western subtropical North Pacific. Therefore, strong positive or negative phases of this pattern represent pronounced zonal and meridional variations in the location and intensity of the entrance region of the East Asian–North Pacific jet steam (CPC 2013). The positive phase of the WP pattern is associated with above average temperatures over the lower latitudes of the western North Pacific in both winter and spring, and with below average temperatures over eastern Siberia in all seasons. It is also associated with above average precipitation in all seasons over the high latitudes of the North Pacific, and below average precipitation across the central North Pacific, especially during the winter and spring (CPC 2013). Figure 6 shows the correlation of the WP to precipitation during Jan, Apr, Jul, and Oct. Note the strong positive correlation in Apr extending from East Asia across the North Pacific. This implies that during the

positive phase of the WP, there tends to be increased precipitation over East Asia (including the Korean Peninsula). Ha and Lee (2007) found that the WP pattern in Apr was correlated to the retreat of EASM precipitation in the following summer.

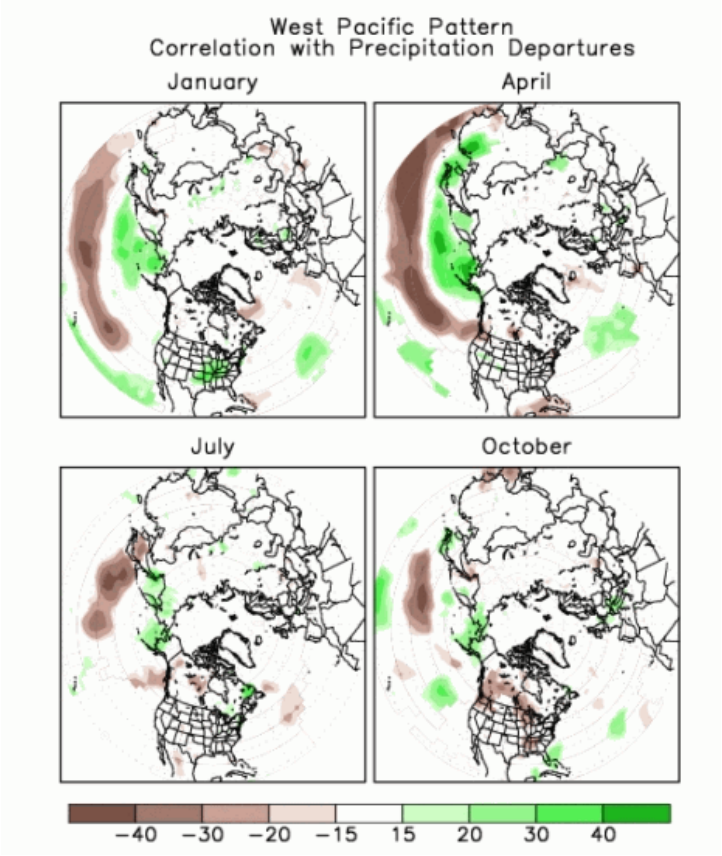


Figure 6. Correlation of the West Pacific (WP) teleconnection pattern with precipitation departures. Note the strong positive correlation in Apr extending from East Asia across the North Pacific (CPC 2013).

## 6. Exploring Additional Teleconnections

The aforementioned climate variations and teleconnections are not the only ones that affect the Korean Peninsula. There is still a tremendous amount to be learned about all the climate variations and teleconnections that affect

Korea. In our study, we explored well known and other climate variations and teleconnection patterns in order to assess the potential for creating better LRF systems for the Korean region.

## D. EXISTING CLIMATE PRODUCTS FOR THE KOREAN PENINSULA

### 1. DoD Products

The 14th Weather Squadron (14 WS) and the Fleet Numerical Meteorology and Oceanography Center (FNMOC) provide climatological support to the Department of Defense (DoD). Most of the climate products from these agencies focus on long-term mean (LTM) conditions. The average high/low temperatures, precipitation amounts, thunderstorm days, and many other fields can be easily accessed from the 14 WS and FNMOC websites. FNMOC has introduced a useful tool for accessing and analyzing climate data called the Advanced Climate Analysis and Forecasting (ACAF). ACAF includes data from the NCEP/NCAR reanalysis dataset, the International Best Track Archive for Climate Stewardship (IBTrACS) dataset, the Climate Forecast System Reanalysis (CFSR) dataset, and other datasets. In recent years, the 14 WS has issued long-range forecast (LRF) discussions. These forecasts are issued monthly for regions of U.S. military interest and have lead times of one to six months. Here is a sample of the Korea Long Range Forecast Discussion issued by the 14 WS on 15 August (Aug) 2012:

*Korea Long Range Forecast Discussion:*

*The following is a long range outlook for the Korea region. Included is: 1) the state of El Niño/ La Niña, 2) forecast summary of conditions, and 3) an annual climatology for the area of interest.*

*El Niño Southern Oscillation Conditions: The latest Climate Prediction Center (CPC) / National Center for Environmental Prediction (NCEP) El Niño Southern Oscillation (ENSO) prediction is for El Niño beginning by Sep 2012.*

*Summary of Forecast Conditions:*

*—Temperatures: During Sep all regions are expected to have below normal temperatures. Oct through Feb all regions are forecast to have near normal to above normal temperatures.*

*—Precipitation: Sep through Nov expect South Korea to have near normal to above normal precipitation while North Korea has near normal to below normal precipitation. Dec through Jan all regions are forecast to have near normal to above normal precipitation.*

*—Ceilings/Cloud Cover: Throughout the period all regions are expected to have near normal to above normal precipitation.*

*—Drought Potential: None expected.*

*—Fog: All season above normal fog is expected for all regions.*

*—Flooding: Some periodic flooding is expected in low lying areas and along river beds in all regions.*

*—Tropical Storms: Early season, expect 2 to 3 tropical storms or remnants to cross S. Korea.*

(14 WS 2012)

The LRF discussions and the ACAF tool represent some of the first uses of advanced climate support by the DoD. Advanced climate support is defined as state-of-the-science basic and applied climatology that directly supports DoD and other national security operations (Murphree 2012a). Additionally, the 14 WS has added LRF figures from the International Research Institute for Climate and Society (IRI), which are discussed later in this chapter.

### 2. Non-DoD Products

#### *a. Climate Prediction Center*

The Climate Prediction Center's (CPC) products include operational predictions of climate variability, real-time monitoring of climate, and assessments of the origins of major climate anomalies. The products focus on analyses and predictions of intraseasonal to interannual climate variations, extending into the future as far as technically feasible, and cover the land, the ocean, and the atmosphere, extending into the stratosphere (CPC 2013). The CPC maintains data on historical conditions, current conditions, and forecasts out to leads of two weeks or longer of ENLN, AO, NAO, and PNA. Climate analyses and forecasts for East Asia and the Korean region are available from CPC, but are not a focus of CPC.

#### *b. Climate Analysis Branch, Earth Systems Research Laboratory*

The Earth Systems Research Laboratory (ESRL) Climate Analysis Branch (CAB) "strives to advance national capabilities to interpret the causes of observed climate variations, and to apply this knowledge to improve climate models and forecasts and develop new climate products that better serve the needs of the public and decision-makers (ESRL 2013)." The CAB is especially focused on climate variations causing floods and droughts in the U.S. and on global-scale impacts of ENLN. The CAB does not produce forecasts specifically for Korea. They do, however, issue daily forecasts for climate variations and teleconnection patterns such as WP, NAO, and PNA at lead times of 1–14 days.

#### *c. International Research Institute for Climate and Society*

The mission of the International Research Institute for Climate and Society (IRI) is "to enhance society's capability to understand, anticipate and manage the impacts of climate in order to improve human welfare and the environment, especially in developing countries (IRI 2013)." IRI issues monthly

multi-model probability forecasts of temperature and precipitation. The valid periods for these LRFs are three months long, and the lead times are one to six months. Figure 7 is an example of a LRF from IRI for temperature over land for Mar-Apr-May 2013 issued in Jan 2013. Note that the 2.5° resolution is quite coarse and that the Korean Peninsula only has a few grid cells over it. Figure 8 is a sample verification chart from IRI showing Heidke skill scores (HSS) for 1.5 month lead forecasts of January-March (Jan-Mar) surface air temperature. In this example, the HSS for the Korean region is between 0.0–0.24. The IRI also issues a probabilistic El Niño/Southern Oscillation (ENSO) forecast, SST forecasts, and some additional experimental forecasts. A big disadvantage of the IRI LRFs for the Korean Peninsula is that their spatial and temporal resolutions are coarse.

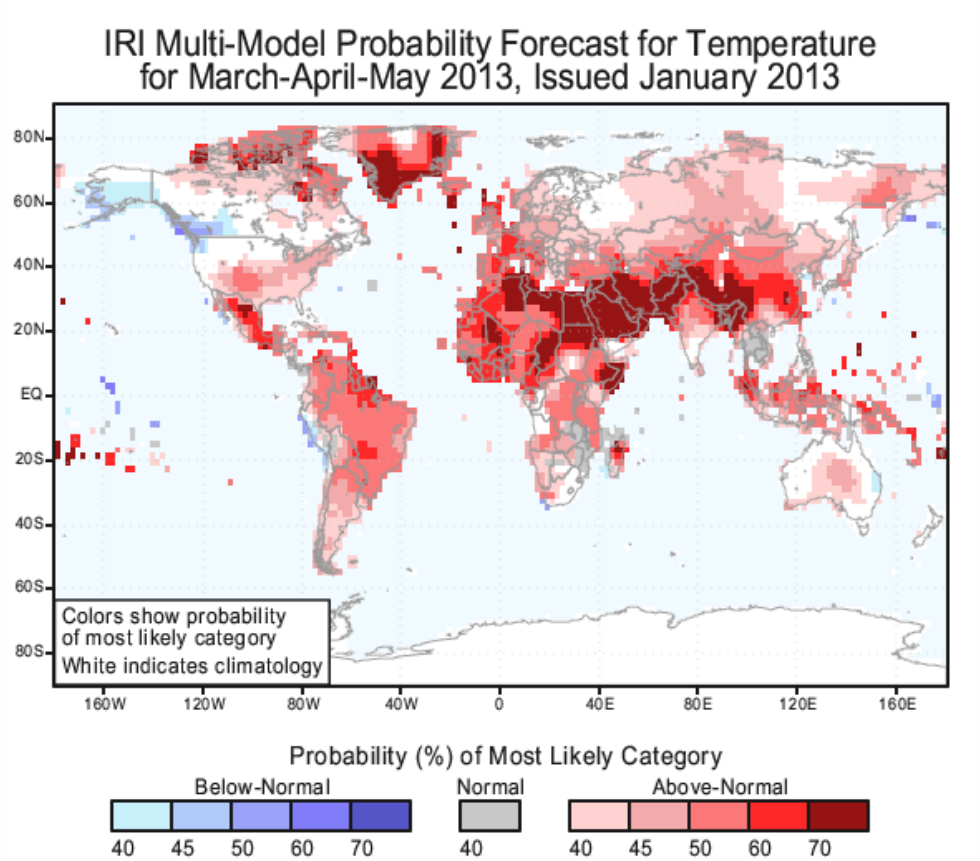


Figure 7. Example of a long-range forecast (LRF) from the International Research Institute for Climate and Society (IRI). This example is a forecast for temperature (degrees C) [A2]over land for a Mar-Apr-May 2013 valid period issued in Jan 2013. In this example, the forecast for the Korean region is a 45–50% probability of above normal temperatures.

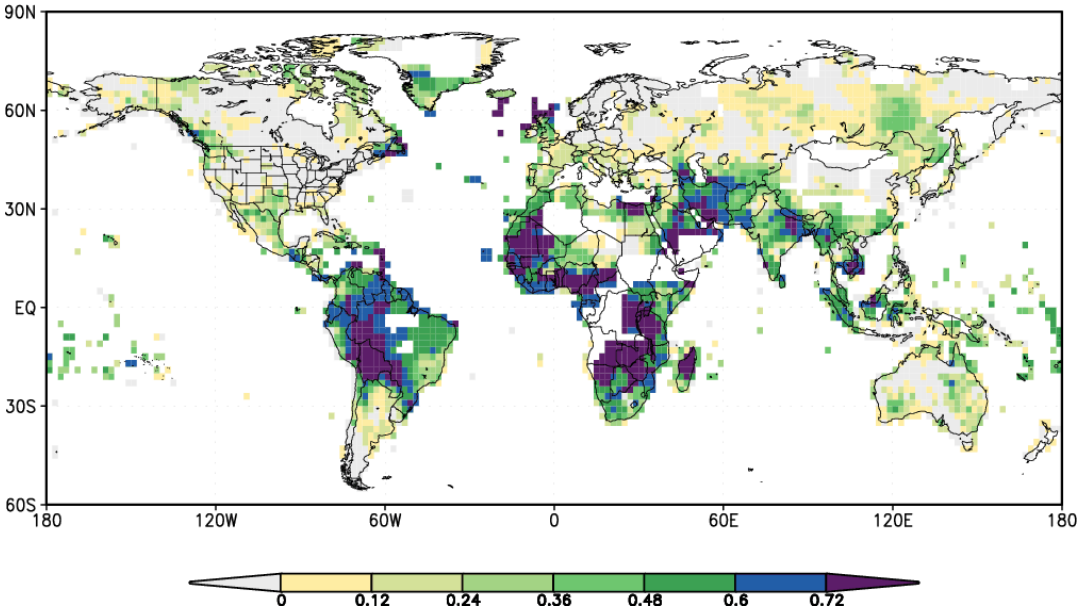


Figure 8. Example of a long-range forecast (LRF) verification chart from the International Research Institute for Climate and Society (IRI). This chart shows the Heidke Skill Scores (HSS) at a 1.5 month lead for Jan–Mar temperature forecasts. In this example, the HSS for the Korean region is between 0.0 - 0.24.

### *d. The Korean Meteorological Administration and Other Asian Weather Agencies*

The Korean Meteorological Administration (KMA) is the government weather and climate forecast authority for South Korea. The KMA produces LRFs at one, three, and six month lead times. The one month lead LRFs are issued three times a month for 10-day and 30-day 850 hPa temperatures, precipitation, sea level pressure, and 500/200 hPa heights. The three month lead LRFs are issued monthly for one month mean 850 hPa temperatures and precipitation. The six month lead LRFs are issued twice a year for one month mean 850 hPa temperatures and precipitation. The KMA's one and three month lead LRFs include northern hemisphere images displayed at a 2.5° x 2.5° spatial resolution (KMA 2013). Since the KMA is a Korean organization, the Korean Peninsula is often their focus area. The Figure 9 is an example of KMA's one month lead 850 hPa temperature forecast.

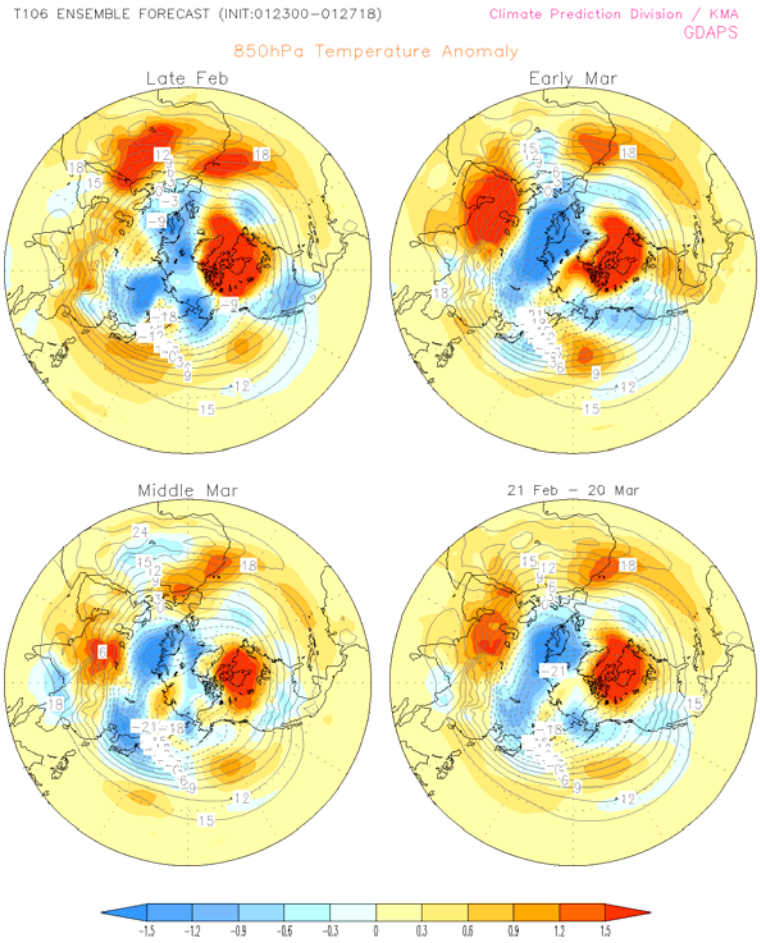


Figure 9. Examples of one month lead 850 hPa temperature anomaly (degrees C) forecasts for February-March (Feb-Mar) 2013 from the Korean Meteorological Administration (KMA). From KMA (2013).

The Japan Meteorological Agency (JMA) issues LRFs only for Japan temperature, precipitation, and sunshine (JMA 2013). The Beijing Climate Center (BCC) from China issues monthly and seasonal global climate forecasts for temperatures, precipitation, 500 hPa GPHs, and several other variables (BCC 2013). BCC uses a coupled (ocean/atmosphere) global climate model to produce forecasts with lead times ranging from 10–90 days. BCC also have a written discussion that is available in Chinese and English, though it only focuses on

China. The BCC website could be used to produce LRFs for the Korean Peninsula, but the skill of the BCC forecasts for the Korean region would need to be determined first.

### 3. The Need to Update Existing DoD Products

Vorhees (2006) described the stark disparities between DoD climate products and those of the civilian community. He emphasized that the DoD's lack of climate forecasting put them well behind many of the civilian institutions. Since 2006, the 14 WS has shortened the gap between the DoD and the civilian institutions by incorporating advanced climate support. They have introduced LRF discussions to characterize the ever-changing global climate. They have also added IRI LRF charts to their website, which convey useful climate forecasts to DoD customers. In the 14 WS LRF discussions, they include a forecast of ENLN obtained from the CPC. Although ENLN events can have huge global impacts on climate, the 14 WS LRF discussions generally do not clearly relate this global scale climate variation to regional and local climate variations. Additionally, other important climate variations and teleconnections that may have significant effects on local weather conditions are not considered.

Only since the mid-1990s has the NCEP/NCAR reanalysis (R1) dataset (Kalnay et al. 1996; Kistler et al. 2001) been created and made available to the public (see Chapter II for a further description of this dataset). The R1 dataset, and other reanalysis datasets that have been developed since, have greatly extended the potential to analyze climate variations, teleconnections, and predictor-predictand relationships, and to develop the statistical and dynamical basis for LRF systems. There is a critical need for the DoD to take advantage of reanalysis data to develop statistical LRF models that incorporate many climate oscillations for specific regions of military interest. These models must incorporate the appropriate climate variations that uniquely affect each region. Ford (2000) and Vorhees (2006) used reanalysis data to identify mechanisms and impacts of climate oscillations. Tournay (2008), Lemke (2010), DeHart

(2011), and Gillies (2012) developed LRF models using reanalysis data for Korea, Horn of Africa, and Pakistan precipitation. These were important steps on the road to integrating advanced climate support into the DoD weather community.

## E. MOTIVATION AND OUTLINE OF STUDY

### 1. Motivation

Prior to studying at the Naval Postgraduate School, I was the weather flight commander for the 51st Fighter Wing at Osan Air Base in South Korea. I was asked many times by decision makers to provide a LRF for the upcoming weeks and months. I told them that my weather team could not forecast out that far and that the best thing that I could provide them with is the LTM climatology. My greatest motivation for this study was the knowledge that we can do better than providing our decision makers with just LTM climatology products. Lemke (2010), DeHart (2011), and Gillies (2012) developed LRF models for seasonal precipitation for the Horn of Africa and Pakistan. These were very useful studies, but they did not focus on the Korean Peninsula. Tournay (2008) developed a LRF model for summertime precipitation for the Korean Peninsula. This too was an important study, but Tournay's model was only designed for precipitation forecasts and only for a few months of the year. Skillful LRFs with year-round coverage of temperatures and precipitation would provide military leaders with a valuable planning tool.

### 2. Scope of this Study

The 14 WS identified in 2012 several research projects that would be useful in determining how to extend the LRF capabilities of the 14 WS (S. Gillies 2012, personal communication). One of these projects was an investigation of how known climate variations (e.g., ENLN, AO) affect specific regions (e.g., Korea) and of the potential to use existing LRFs of these variations to predict conditions in those regions (e.g., to use 14-day lead LRFs of the AO from CPC to

predict Korean conditions). Our research project is an attempt to address this and related 14 WS needs, with a focus on LRFs of Korean surface air temperature and precipitation for all months. An important objective for our study was to develop a system for generating these LRFs that could be readily adapted for operational use by the 14 WS.

Due to our limited research time, we focused solely on LRFs of Korean surface air temperature and precipitation climate variations at two-month lead times. To develop our LRF systems, we applied the methods described by Gillies (2012), who developed and tested a process for creating statistical forecast systems for specific forecast targets (e.g., specific predictand regions and variables).

## 3. Research Questions for this Study

The main questions for this research project were:

(1) What are the statistical and dynamical relationships at intraseasonal to seasonal scales between Korean climate variations and other climate variations and teleconnections (e.g., ENLN, AO, NAO, WP, PNA)?

(2) What is the potential to use forecasts of climate variations and teleconnections to produce intraseasonal to seasonal forecasts of Korean climate variations?

(3) What climate system variables are the most viable predictors of intraseasonal to seasonal climate variations in Korea?

# II. DATA AND METHODS

## A. DATASETS

We assessed two reanalysis datasets for use in our study, each with pros and cons. We considered the following factors when we selected our surface air temperature and precipitation rate datasets:

1. Availability of dataset on a monthly basis for long-range forecasting
2. Accessibility to data by long-range forecasters
3. Length of the data record
4. Spatial and temporal resolution
5. Evidence of the accuracy of the data
6. Effectiveness of data in conducting long-range forecasts for Korea

The reanalysis datasets that were considered in this study were the NCEP/NCAR Atmospheric Reanalysis Data (R1) and the National Centers for Environmental Prediction (NCEP) Climate Forecast System Reanalysis (CFSR) (Saha et al. 2010). We used the six factors listed above to compare these two datasets and determine which to use in our study. The Climate Prediction Center (CPC) Merged Analysis of Precipitation (CMAP) was not considered, since it is included in the CFSR dataset (Saha et al. 2010). The University of Delaware (UDEL) precipitation dataset was also not considered since it only uses rain gauge data over land (Willmott et al. 1994).

The climate variations and teleconnection patterns that we investigated in our study are represented by the following indices: AO index, NAO index, PNA index, MEI (for ENLN), and the WP index. We obtained the data for these indices from the CPC website (for the AO, NAO, PNA, and WP indices) and from the ESRL website (for the MEI) (CPC 2013, ESRL 2013).

We conducted a number of analyses of climate anomalies. For all of these, we used a long-term mean base period of 1981–2010.

### 1. NCEP/NCAR Reanalysis

The primary data source for this study was the NCEP/NCAR reanalysis dataset (Kalnay et al. 1996), acquired from the Earth Systems Research Laboratory (ESRL) via their website, http://www.cdc.noaa.gov (accessed 3 Feb 2013). This dataset will be referred to simply as “R1” throughout this paper. The R1 reanalysis process uses a fixed, state-of-the-art global data assimilation system to collect and analyze land surface, ship, rawinsonde, pibal, aircraft, satellite, and other observational data to produce a temporally consistent analysis of global fields for a variety of atmospheric and oceanic variables (Kalnay et al. 1996). Data was available for most variables from 1948 through the present, and at a spatial resolution of 2.5° and a temporal resolution of 6 hours. Only data from 1970–2012 were considered in our study. In order to maximize the positive impacts of satellite data in the reanalysis data, years prior to 1970 were excluded. Although it is often better to use the longest period possible to identify climate patterns, it is imperative that the data is of the highest quality. Kistler et al. (2001) identifies three major phases of the global observing system: 1940s–1957 as the “early” period, 1958–1978 as the “modern rawinsonde network” period, and 1979-present as the “modern satellite” period. The “early” period, which lacks significant amounts of upper-air observations, is missing essential data from the atmosphere that is crucial to a climate study such as ours. We included some years from the end of the “modern rawinsonde network” period so that our study period would include a relatively large number of both strong EN and strong LN events (e.g., the 1973–1975 LN event). The 1970–2012 period is sufficiently long to identify intraseasonal to interannual variations, and some aspects of decadal climate variations. The primary variables used from the R1 data set that we used were surface air temperatures, precipitation rate (PR), geopotential heights (GPH), wind direction/speed, and sea surface temperatures.

In the following sections, we have in some places shortened the term *surface air temperature* to just *temperature*, for brevity. If another temperature is meant, then when we have added modifiers to indicate that something other than surface air temperature is referred to.

A major advantage of the R1 dataset is that daily and monthly composites are available almost immediately (typically three days) after the end of each month. This makes R1 data especially suitable for operational applications. R1 data is also very easy to access, analyze, and download from the ESRL website, which is important for both research and operational applications.

### 2. Climate Forecast System Reanalysis

In Jan 2010, NCEP released CFSR, a new global, high resolution, coupled atmosphere-ocean-land surface-sea ice system to provide the best reanalyses of the state of these coupled domains (Saha et al. 2010; UCAR 2013). CFSR atmospheric, oceanic, and land surface output products are available at an hourly temporal resolution and 0.5° spatial resolution for 1979–2010. CFSR is considerably more accurate than the previous global reanalysis (R1) made at NCEP in the 1990s (Saha et al. 2010). The CFSR precipitation reanalysis contains the following datasets: CMAP pentad dataset at a 2.5° x 2.5° resolution and a global interpolation of quality-controlled rain gauge reports from approximately 30,000 stations, and many other national and international collections at a 0.5° x 0.5° resolution (Saha et al. 2010). A drawback for using CFSR data is that it only spans from 1979–2010. It takes several months or longer for updates of the CFSR reanalysis data to be released, so the CFSR dataset cannot be used in near-real time operational applications. Additionally, the data is not easy to access from the web and is only available in GRIB2 format.

## 3. Comparison of Datasets

The R1 dataset is the most accessible and is available for the longest period; however the resolution is a coarse 2.5° (~200 km, depending on latitude). The CFSR dataset is less accessible and is available for only a 31 year period, but the resolution is much finer, at 0.5° (~38 km, depending on latitude). The biggest issue here is determining the acceptable resolution for this study (e.g., if 2.5° resolution is sufficient, then the R1 dataset might be the better choice). Figure 10 shows the area that we referred to in our study as the Korean Peninsula.


Figure 10. Korean Peninsula (ESRL 2013).

Figure 11 shows R1 and CFSR area averaged surface air temperature data for the Korean Peninsula for 1979–2009 for four representative months. CFSR is generally slightly cooler than R1, but the two vary together and have a correlation of 0.97 or better for each month. These results suggest that R1 may be as suitable as CFSR for our study.

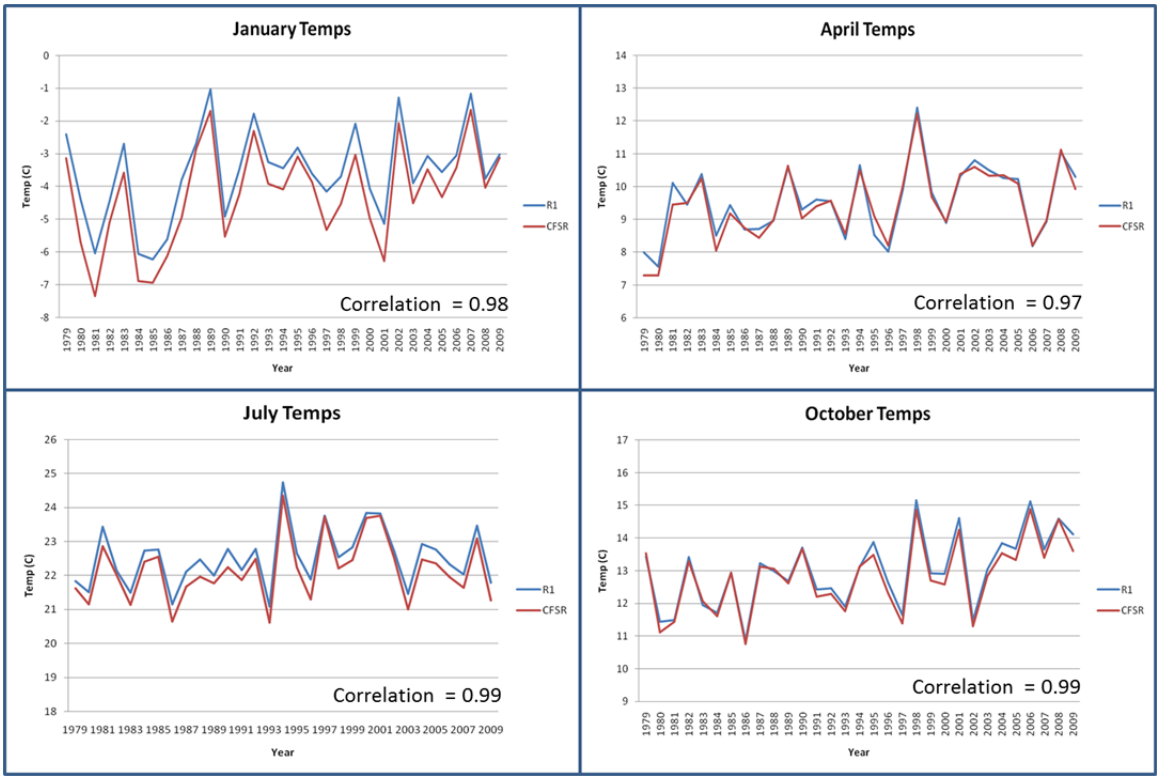


Figure 11. Comparison of area averaged surface air temperature (degrees C) from the NCEP/NCAR reanalysis (R1, blue) and C limate Forecast System Reanalysis (CFSR, red) for the Korean Peninsula (Figure 11) for Jan, Apr, Jul, and Oct of 1979–2009. Note that for all months, the two datasets are very similar, with correlations of 0.97 or greater.

Figure 12 shows R1 and CFSR area averaged precipitation rate (PR) data for the Korean Peninsula for 1979–2009 for four representative months. CFSR is generally wetter than R1, but the two vary together and have correlations ranging between 0.75 (Jul) and 0.93 (Jan and Apr). The difference between the two datasets is most likely because the higher resolution CFSR is better at capturing the mesoscale convection that is common in the summertime in Korea. Korea receives approximately half of its annual precipitation in the summer months and accuracy during these months is crucial. Compared to R1, CFSR uses observed global precipitation analyses as direct forcing to the land surface analysis, rather

than the typical analysis approach of using precipitation from the assimilating background atmospheric model (Saha et al. 2010).

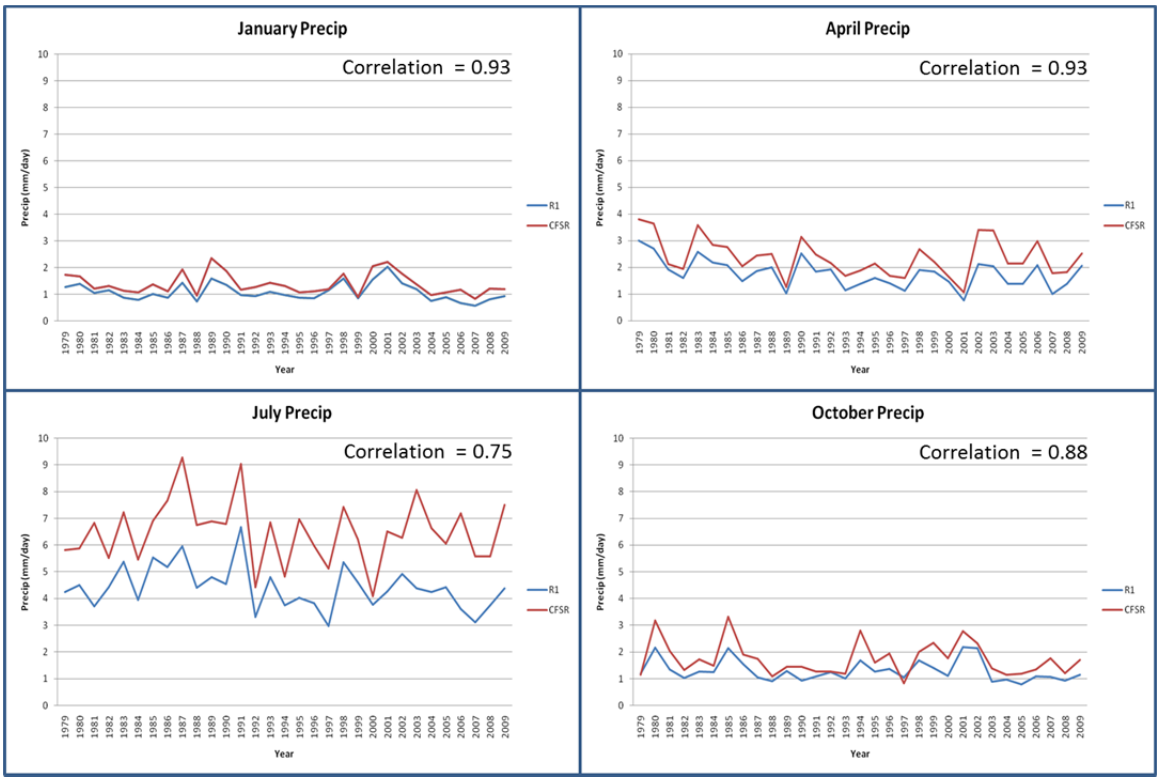


Figure 12. NCEP/NCAR reanalysis (R1) precipitation rate (mm/day) (blue) and Climate Forecast System Reanalysis (CFSR) precipitation rate (mm/day) (red) for Jan, Apr, Jul, and Oct of 1979–2009. Note that the CFSR values are consistently greater than the R1 values. The two datasets are fairly well correlated, except for the summer months where in Jul, for example, the correlation is only 0.75.

There was an important factor to consider when considering the use of CFSR variables as predictors for our study: CFSR data currently cannot be used operationally for describing intraseasonal to seasonal LRF predictors, because that data takes several months to years to become available. This issue, however, becomes less important if the most skillful predictor(s) turn out to be existing climate variations for which data is readily available at intraseasonal to seasonal lead times (e.g., ENLN). For example, if the Arctic Oscillation (AO) and

the West Pacific (WP) are the main predictors for Korean precipitation, then forecasters will not need to use R1 or CFSR data in the production of LRFs. But if, for example, 850 hPa GPH in the Bering Strait is the best predictor for Korean precipitation, R1 data would work to describe that predictor but CFSR data would not work. We determined early in our research that 850 hPa GPHs and SSTs were commonly the best predictors for Korean temperatures and precipitation. This, we decided that R1 would be used exclusively in our study, since R1 data for these predictors is updated in near real time (within a few days of real time).

## B. DETERMINING SPECIFIC TELECONNECTIONS FOR KOREA

Many known climate variations have impacts on Korean climate. In our study, we identified additional teleconnections that have not previously been identified using correlation analyses. The results our study include many correlations maps, most of which are based on correlations of 43 years of data. For 43 years of data, correlations greater than 0.256 are statistically significant with 95% confidence.

### 1. Korean Temperature Indices

We developed a set of indices based on geopotential height (GPH) differences to characterize the circulation anomalies associated with Korean temperature variations, and especially the circulation anomalies that occur at two month or longer lead times. We referred to these as the Korean temperature indices (KTIs). We developed, tested, and applied the KTIs to: (a) characterize climate variations and teleconnections that are related to Korean climate variations; and (b) potentially use as predictors of temperature in our LRF system. KTIs were calculated from past 850 hPa GPH patterns and are intended to represent precursor circulation patterns that strongly contribute to temperature anomalies in Korea at lead times of two months or more. KTIs indicate teleconnection patterns and were developed to both explain the dynamics of Korean temperatures variations and to predict those variations. A single unique

KTI was developed for each predictand month, based on optimized 850 hPa GPH patterns from two months or longer before the predictand month. This lead time for the KTIs was chosen to allow us to focus on two month lead LRFs.

In developing KTIs for each month, we searched for dipoles of significant positive/negative correlation located over or near East Asia in the maps of correlations between Korean temperature and 850 hPa GPHs. These correlation dipoles allowed us to identify potential predictors and to also infer anomalous circulation and temperature advection patterns that might explain the precursor conditions that led to Korean temperature variations two months later. For example, a correlation dipole that indicates that anomalously low temperature anomalies in Korean tend to be associated with an anomalously weak Aleutian Low and an anomalously strong Arctic Low might indicate that a KTI based on the 850 hPa GPH difference between the Aleutian Low and the Arctic Low might: (a) be a good predictor of Korean temperature; and (b) explain the physical mechanisms (e.g., temperature advection processes) that enable them to be good predictors.

Our first step in determining the KTI for a given month was to use the linear correlation page at the ESRL site to correlate Korean surface air temperatures with 850 hPa GPH from two months prior. In a few cases, higher correlations were found when using the 850 hPa GPH from three months prior. We then searched for a highly correlated positive/negative dipole that was close to the Korean Peninsula. Boxes were then drawn around the positively and negatively correlated areas to mark the regions of the two dipole centers within which the GPHs would be area averaged for use in calculating the GPH difference between the two dipole centers. The rectangular box dimensions remained constant throughout this study at 30 degrees longitude long and 15 degrees latitude wide. It was easier to keep the box dimensions constant, and this size was suitable for each month. A suitable size meant that the box was large enough to represent most of the region with the same correlation sign and

small enough to avoid representing areas with differing correlation signs. Due the spherical nature to the Earth, the physical sizes of the boxes varied according to their latitude (e.g., boxes closer to the equator will be physically larger). We calculated the KTI by averaging the monthly mean 850 hPa GPH values within the two dipole boxes and then subtracting the average value in the positively correlated box from that in the negatively correlated box. This positive minus negative method was consistently used in our study and meant that the resulting difference and KTI was positive (negative) for warm (cold) events in Korea. In a few cases, the correlation results did not allow us to develop a KTI based on a correlation dipole. In those cases, we based the KTI on a single high magnitude correlation region. In all cases in which we used a correlation dipole, we determined that the KTI was better correlated with the corresponding Korean surface air temperature than the 850 hPa GPH in either of the two individual dipole centers by themselves. We used the following notation the valid period and lead time associated with each of the KTIs: KTI_MMML, where MMM indicates the valid month and L indicates the lead time. For example, the KTI for Jun with a two month lead time (which used 850 hPa GPH from Apr) was notated as KTI_JUN2.

Figures 13-14 show an example of this process for a one month lead KTI based on correlating R1 850 hPa GPHs from Dec with R1 Jan surface air temperatures for the Korean Peninsula (Figure 10). Remember that correlations greater than 0.256 are considered statistically significant. In Figure 13, the orange to red areas have a high positive correlation and the dark blue to purple areas have a high negative correlation. Note the high positive correlation to the south of Korea/Japan and the high negative correlation in the Chukchi Sea region of the Arctic. These two areas were selected as the dipole centers for KTI_JAN1.

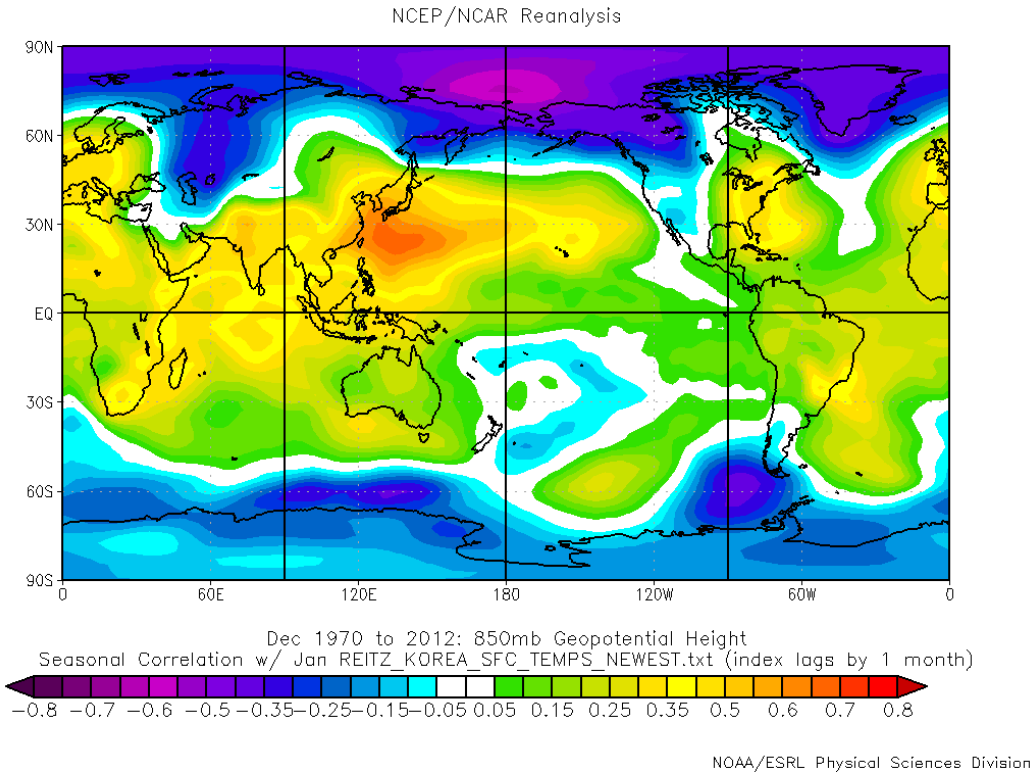


Figure 13. Correlation of 850 hPa geopotential heights (GPHs, m) for Dec with Jan surface air temperatures in Korea region during 1970–2012. Correlations greater than 0.256 are statistically significant with 95% confidence. Note the high positive correlation to the south of Korea and the high negative correlation in the Arctic near the dateline.

Figure 14 is the same as Figure 13 but zoomed in on the Asia–North Pacific region. The averaged 850 hPa GPH in the positively correlated box (south of Korea/Japan) minus that in the negatively correlated box (in the Arctic near the dateline) equals the KTI_JAN1. The KTI for this case indicates that a positive (negative) KTI_JAN1 value for Dec is likely to be followed by above (below) normal temperatures for Jan in Korea.

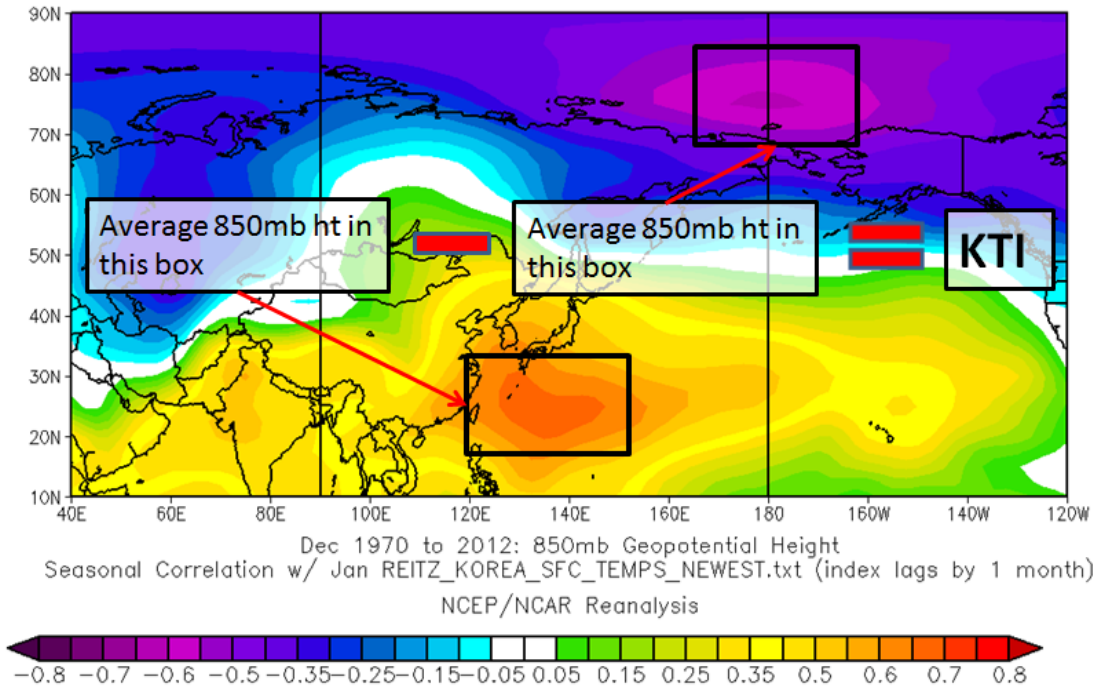


Figure 14. Correlation of 850 hPa geopotential heights (GPHs, m) for Dec with Jan surface air temperatures in Korea region during 1970–2012. Correlations greater than 0.256 are statistically significant with 95% confidence. The black boxes mark the areas with the highest positive and negative correlations, which are the areas used to construct the corresponding KTI.

### 2. Korean Precipitation Indices

We developed a set of 12 Korean precipitation indices (KPIs) that were exactly analogous to the KTIs (Chapter II, section B.1), except that they are based on correlations between 850 hPa GPHs and Korean precipitation rates (rather than Korean surface air temperatures). The notation for referring to the KPIs is the same as for the KTIs.

## 3. Sea Surface Temperatures

We also evaluated the use of SSTs as predictors of Korean surface air temperatures and precipitation, using methods similar to those used by Gillies (2012). The SST predictors we selected had a minimum lead time of two months and were different for each month.

We used the ESRL site to correlate Korean temperature and precipitation rate with global SSTs, with SSTs leading by two or more months. The region of maximum correlation magnitude was identified and a rectangular box was then drawn around the area. Unlike the KTI and KPI, these box dimensions varied for each SST area. We changed the dimensions of the boxes based on the SST patterns for each month. The SST high correlation areas varied in shape and size, so we determined that we should adjust the predictor regions accordingly. Each month has a maximum of one SST area as a predictor, to keep the forecast process relatively simple. The SST areas were different for each predictand (temperatures and precipitation) as well. We area averaged the SSTs within each potential SST predictor area to develop the SST predictor for that area. We used the following notation to designate the predictand, valid period, and lead time associated with each of the SST predictors: SST_PMMML, where P indicates the predictand, MMM indicates the valid month, and L indicates the lead time. For example, the SST predictor for temperature (precipitation rate) for Jun with a two month lead time (which used area averaged SSTs from Apr) was notated as SST_TJUN2 (SST_PJUN2).

Figure 15 shows an example of this process for SST_TJAN2 based on correlating the R1 SSTs from November (Nov) with R1 Jan surface air temperatures for the Korean Peninsula (Figure 10). Note the highest correlation magnitude is to the northeast of Madagascar in the Indian Ocean.

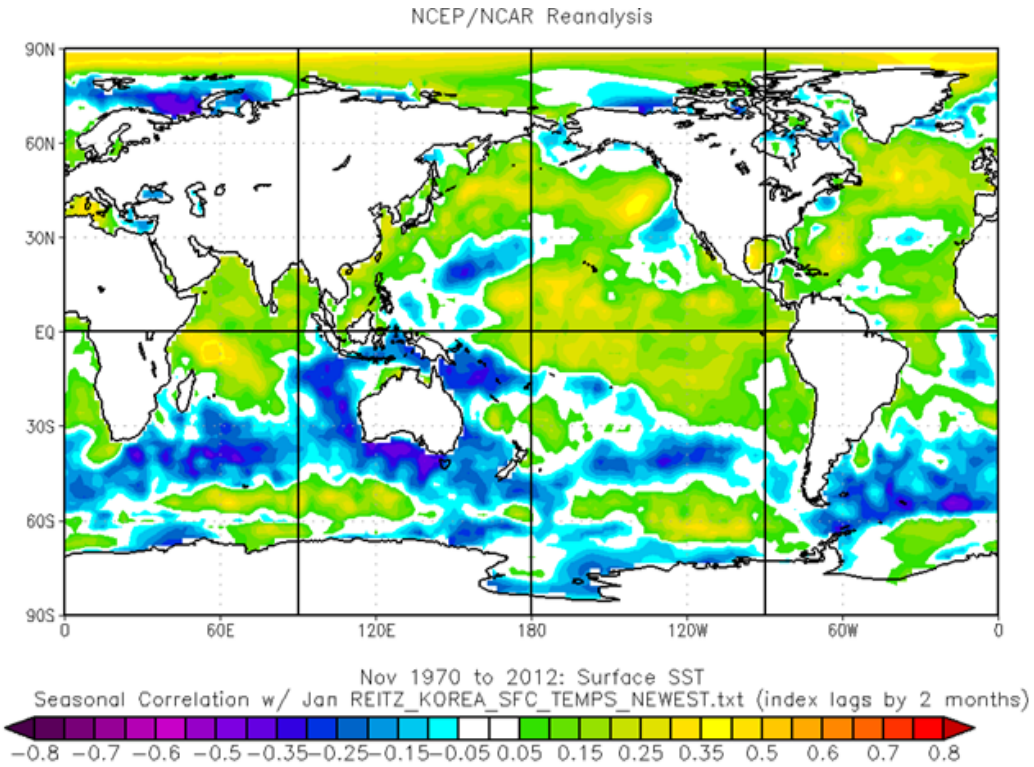


Figure 15. Correlation of sea surface temperatures (SSTs) for Dec with Jan surface air temperatures in Korea region during 1970–2012. Correlations greater than 0.256 are statistically significant with 95% confidence. Note the highest correlation area in the Indian Ocean.

Figure 16 is a zoomed in view of SSTs from Nov correlated with Jan Korean surface temperatures. For each Nov during 1970–2012, the area averaged SST in the Indian Ocean region marked by the black box is the SST_TJAN2 for that Nov. For some months the highest correlated area was in the tropical central or east Pacific Ocean. However, we avoided selecting SST areas in the tropical central or east Pacific, since the MEI already accounts for SSTs from this region.

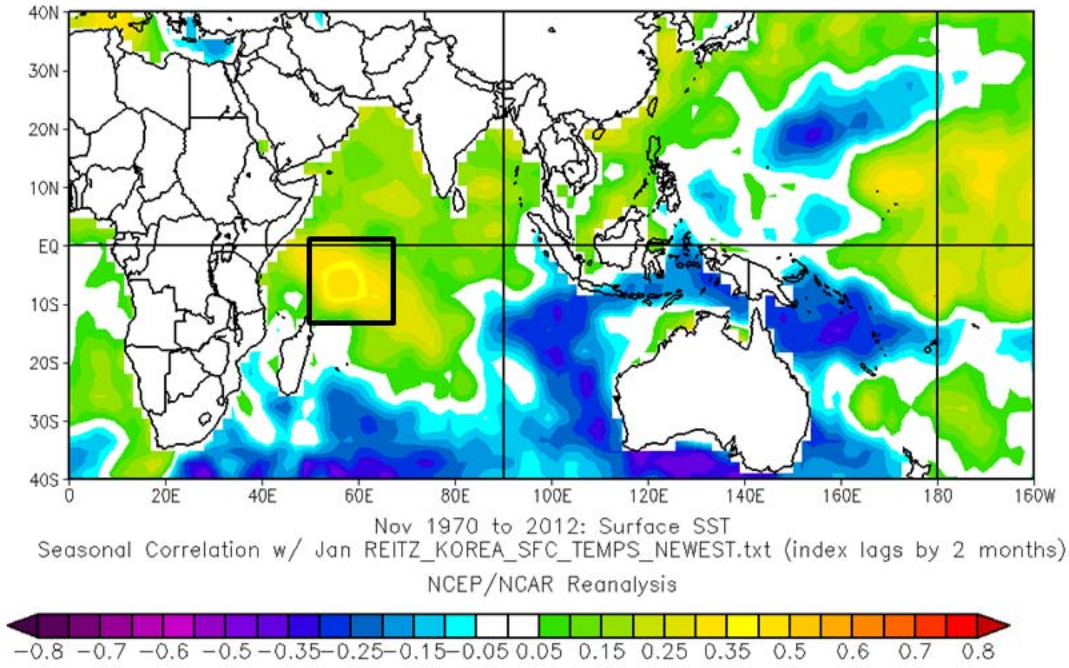


Figure 16. Correlation of sea surface temperatures (SSTs) for Dec with Jan surface air temperatures in Korea region during 1970–2012. Correlations greater than 0.256 are statistically significant with 95% confidence. The black box marks the area of highest correlation, which was used to construct the SST predictor area. For each Dec during 1970–2012, the SST predictor area that we used to characterize the precursor circulation patterns for the following Jan was calculated as the area average SST in the box. The SST area was different for each month, lead time, and predictand (temperature and PR). In this example, the SST predictor was labeled as SST_TJAN2, where Jan2 indicates the target month and lead time and the T indicates the predictand variable as temperature.

## 4. Persistence

It is a forecaster's goal is to be able to beat climatology and persistence. In some cases, however, persistence is the best forecast. Persistence in weather forecasting is approximately defined as "forecasting for tomorrow what you observed today." In our long-range forecasting study, we defined persistence as using a prior monthly average temperature (PR) to forecast a future monthly average temperature (PR). Persistence from the immediately preceding one month was not considered in our study, since our focus was on lead times of two

months or longer. Persistence was only considered from at least two months prior. For example, we tested Apr Korean temperatures as a predictor of Jun Korean temperatures, and we referred to this predictor as “persistence from Apr.” In some cases persistence was used from three months prior, because that gave better skill.

## C. LONG-RANGE FORECAST DEVELOPMENT

Gillies (2012) designed, developed, and tested a process for creating an LRF system. We followed GIllies’ LRF development process, but did not use his multimodel and ensemble methods. Instead, we used a single multiple linear regression (MLR) LRF model for each month and predictand.

Gillies (2012) used a lagged average ensemble approach (Hoffman and Kalnay 1983). He created cumulative forecasts that included all forecast members available at the time of the forecast issuance. His lagged average ensembles represented the forecasts from multiple models at all available leads times. Although our LRF models did not incorporate lagged averaging (or even ensembling), they did use forecast members with different lead times that ranged from two and six months.

Gillies’ LRF development process consists of three sequential phases: (1) select the forecast target, (2) develop the forecast system, and (3) apply the forecast system. The entire conceptual process is presented in Figure 17. This LRF development process was followed in our study as closely as possible. We conducted Phases (1) and (2) for our study of LRFs of Korean temperatures and PR. We also tested Phase (3) by producing LRFs for Jan-Apr 2013. In the future, Phase (3) will be conducted by climate forecasters who use our LRF models (e.g., forecasters at the 14 WS). Our major deviations from the Gillies’ process were not using multiple models for a given forecast month and predictand, and not optimizing ensemble members (step 2. f.), since we did not use ensembling.

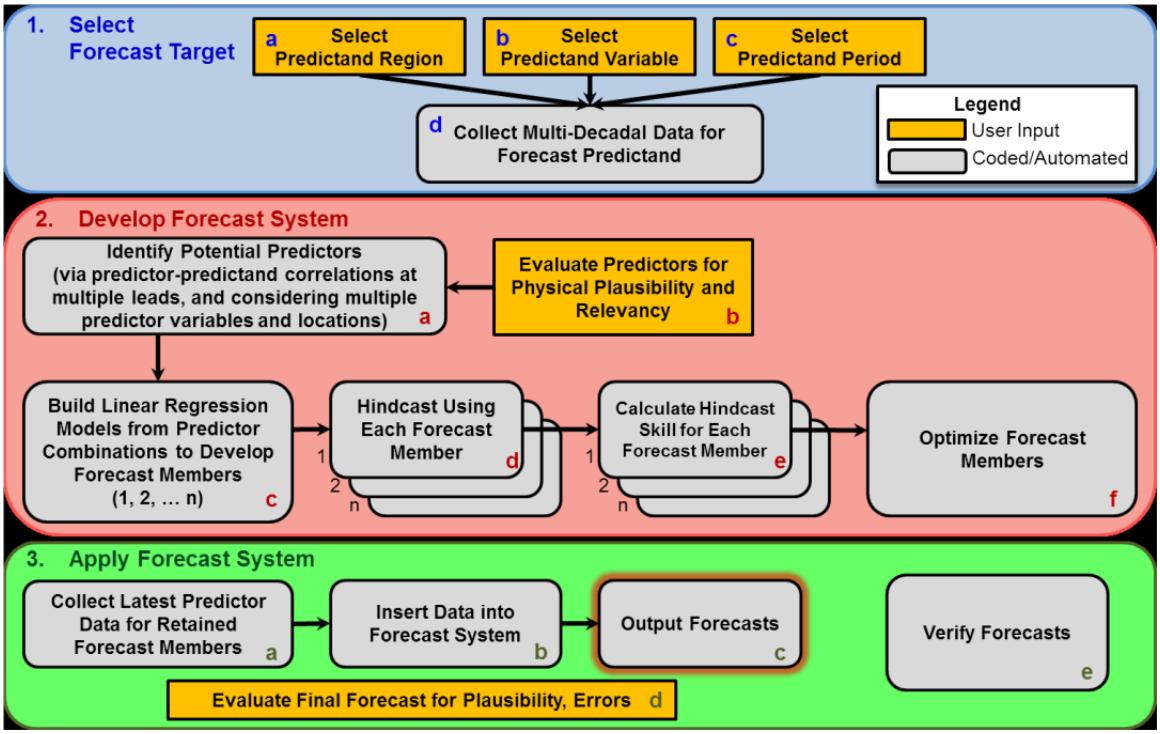


Figure 17. Conceptual schematic of the LRF development process. The concept consists of three sequential phases: (1) select forecast target (blue); (2) develop forecast system (red); and (3) apply forecast system (green). Gray-filled steps indicate high potential for automation. Orange-filled steps indicate steps that require forecaster inputs (Gillies 2012).

## 1. Select Forecast Target

### *a. Select Predictand Region*

The selection of the predictand region was highly dependent on the operational needs of the DoD. South Korea needed to be included since it is used extensively for military training and would be vital for wartime operations. North Korea needed to be included in case war was to break out between the nations. It was also useful to include the surrounding waters for applications to naval operations. Thus, for operational needs of the DoD, it seemed important to include in our predictand region both North Korea and South Korea and surrounding areas.

In addition to meeting operational needs, the predictand region must also satisfy some climatological requirements. Since our goal was to be able to predict temperature and precipitation anomalies, we needed to select a predictand region that has anomaly patterns that are relatively uniform both temporally and spatially. A predictand region should have fairly uniform climate and should be uniformly affected by major climate processes. If the region does not meet these requirements, it may be necessary to break the region down into sub-regions. For example, the entire continental U.S. may not be an ideal predictand region, since it lacks climatological uniformity. The U.S. is immense in size and contains deserts, marshes, glaciers and forested terrain that are affected differently by large scale climate processes. We had to determine in our study if North Korea and South Korea are climatologically uniform enough to combine or if smaller sub-regions were needed.

The Korean Peninsula is small in geographical size at around 85,000 square miles (approximately the size of Minnesota). Although small in size, as discussed in Chapter I, the Korean Peninsula does have different climate zones. Due to the coarseness of the R1 reanalysis data, we could not separate the Korean Peninsula into its four climate commonality regions. We could, however, break up the peninsula into North and South Korea, although combining them would, if justified, allow for simpler LRF modeling. In the remainder of this sub-section, we will discuss the plausibility of combining North Korea and South Korea into a single predictand region.

Figure 18 shows Jan temperatures for 1970–2012 for the northern and southern portions of the Korean Peninsula based on a north-south division at 37.5°N (Figure 19). This division was based on the R1 dataset's resolution of 2.5° x 2.5°. Note that although the northern area is clearly colder, the two areas vary together and are highly correlated (0.89). In particular, the temperature variations in the two areas tend to be very similar in phasing, duration, and

amplitude. We obtained similar results for other months (not shown). These results indicated that it might be reasonable to use a single Korean Peninsula predictand region for temperature.

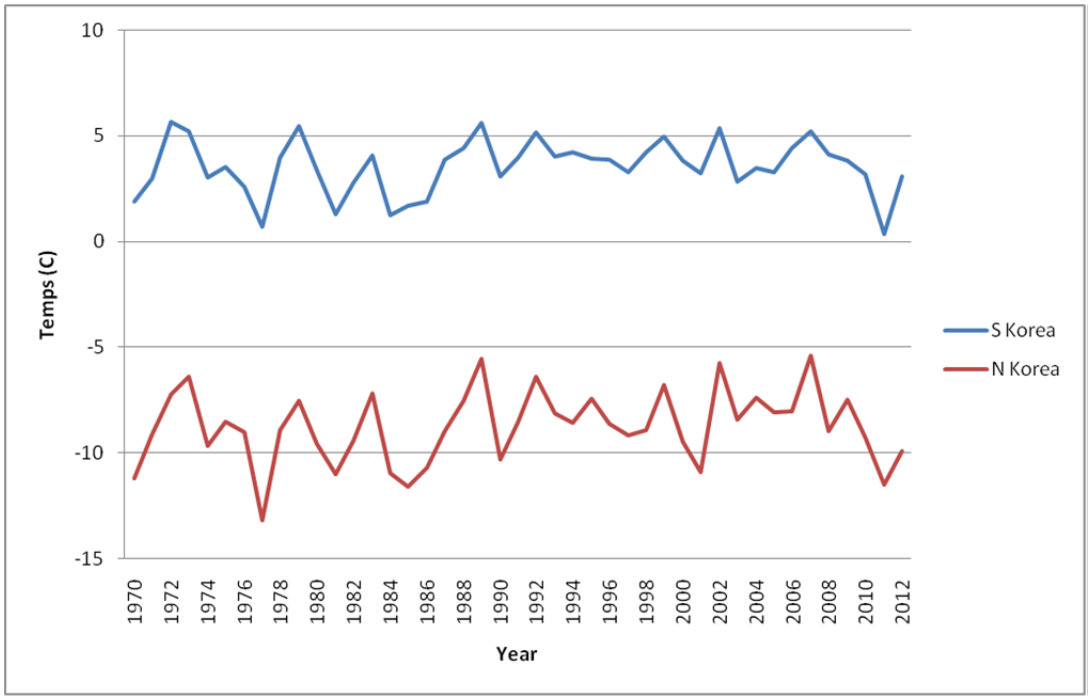


Figure 18. Jan temperatures (degrees C) for southern and northern areas of the Korean Peninsula for 1970–2012. Note that although the northern area is clearly colder, the two areas vary together and are highly correlated (0.89). This suggests that combining the two areas into one predictand region may be reasonable.

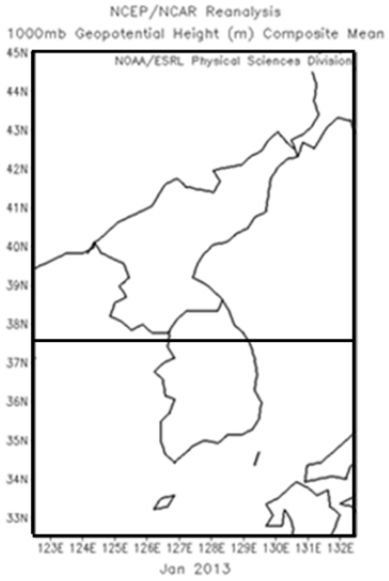


Figure 19. North Korea (top) and South Korea (bottom). The division of the Koreas is denoted by the solid black line (37.5° N). These two geographical areas were compared to see if they met our climatological uniformity standards.

Figure 20 shows Jan precipitation rates (PR) for 1970–2012 for the northern and southern portions of the Korean Peninsula based on a north-south division at 37.5°N (Figure 19). Note that although the southern area is generally wetter, the two areas tend to vary together and are fairly well correlated (0.62). In particular, the PR variations in the two areas tend to be very similar in phasing, duration, and amplitude. We obtained similar results for other months (not shown). The similarities between the two areas for PR are not as strong as for temperature. One possible explanation for the disparity for Jan is that the southern area tends to get more sea-effect snow than the northern area. These results indicate that it might be reasonable to combine the two areas into a single predictand region for PR.

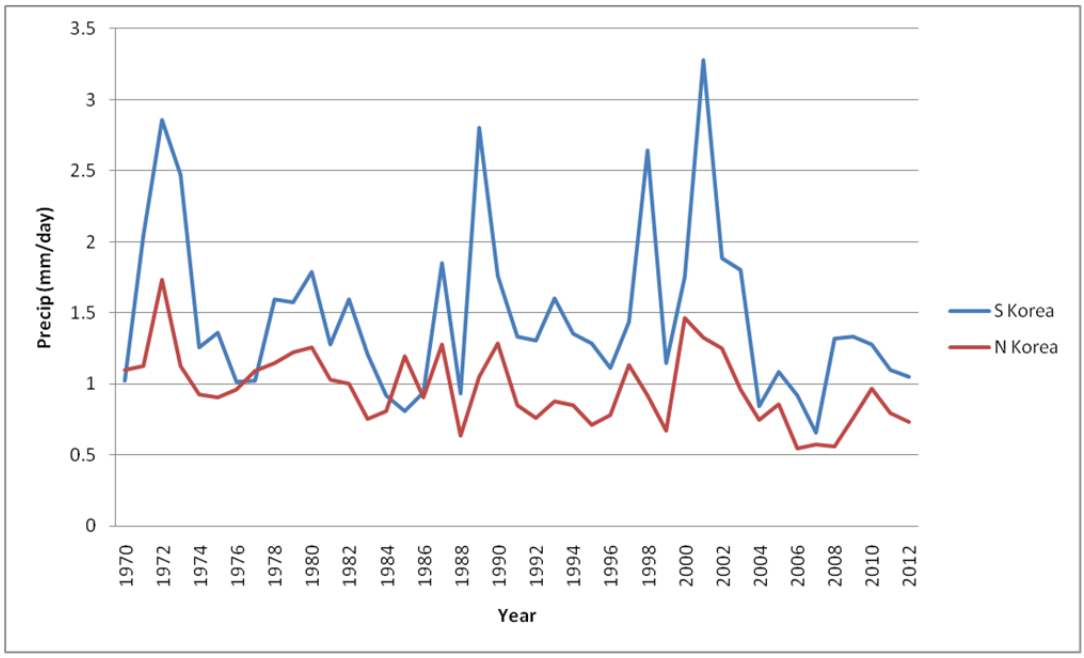


Figure 20. Jan precipitation rates (PR, mm/day) for the southern and northern areas of the Korean Peninsula for 1970–2012. Note that although the southern area is generally wetter, the two areas vary together and are highly correlated (0.62). This suggests that combining the two areas into one predictand region may be reasonable.

Figure 21 shows the 1970–2012 LTM Jan temperature and LTM Jul PR for the Korean Peninsula. The temperature panels show that the northern area is colder than the southern area in Jan, but as shown in Figure 18, the temperatures in these two areas tend to vary together. Similarly, the PR panels show that the northern area is wetter than the southern area in Jul, but, as shown in Figure 20, the PRs in these two areas tend to vary together.

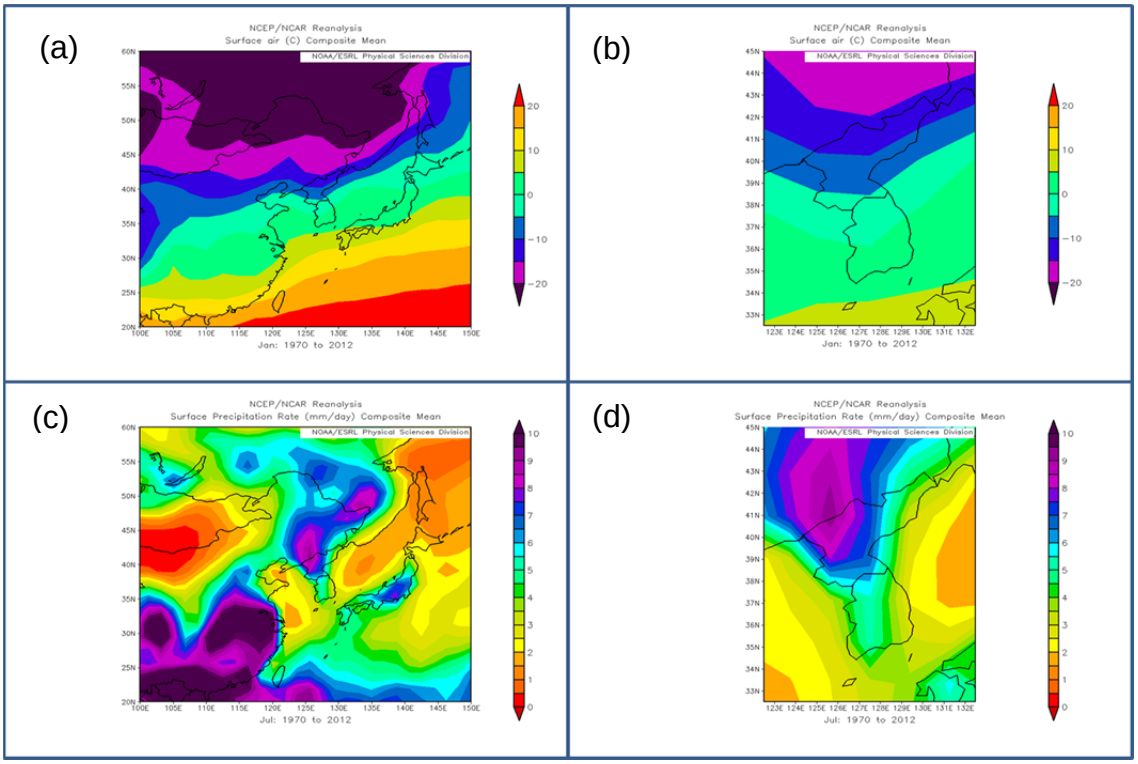


Figure 21. Jan long-term mean (LTM) temperatures (degrees C, (a) and (b)) and Jul LTM precipitation rates (mm/day, (c) and (d)) for the Korean Peninsula for 1970–2012.

Figure 22 shows the surface temperature anomalies for the eight coldest and eight warmest Jans for the Korean Peninsula during 1970–2012. Figure 22 (a)-(b) shows that when North Korea has much colder than normal Jan temperatures, South Korea tends to also be much colder than normal. Figure 22 (c)–(d) shows that when North Korea has much warmer than normal Jan temperatures, South Korea to also be much warmer than normal. These results support the use a single Korean Peninsula predictand region for Jan temperature.

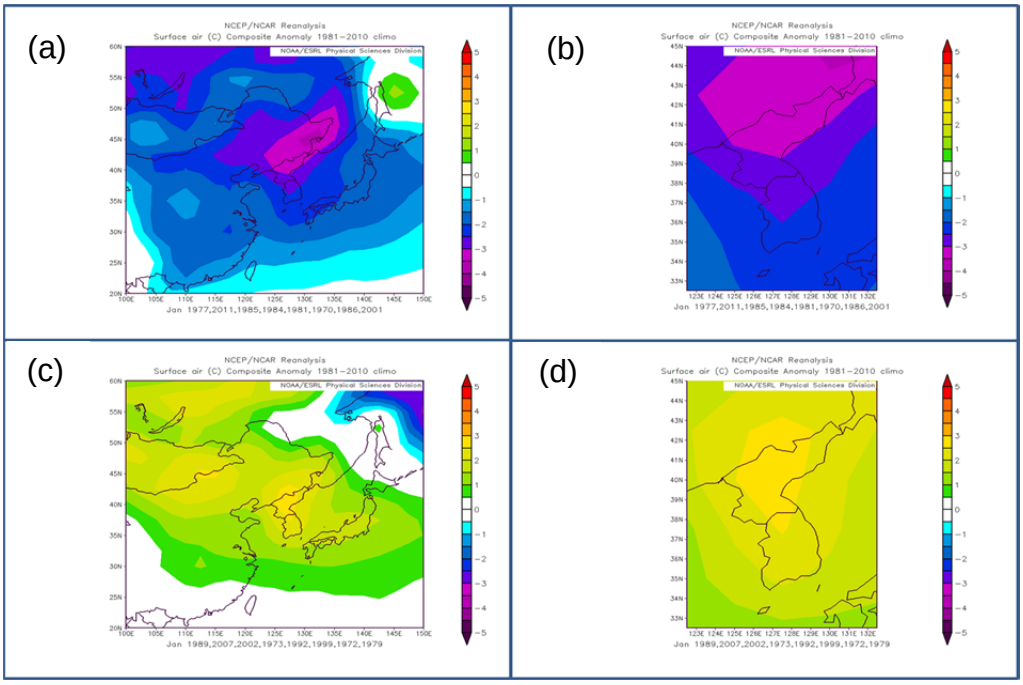


Figure 22. Surface temperature anomalies (degrees C) for the eight coldest (panels (a) and (b)) and eight warmest (panels (c) and (d)) Jans for the Korean Peninsula during 1970–2012. Panels (a) and (b) show that when North Korea has much colder than normal Jan temperatures, South Korea tends to also be much colder than normal. Panels (c) and (d) shows that when North Korea has much warmer than normal Jan temperatures, South Korea to also be much warmer than normal.

Figure 23 shows PR anomalies for the eight driest and eight wettest Juls for the Korean Peninsula 1970–2012. Panels (a) and (b) illustrate that when North Korea has much lower than normal Jan PRs, South Korea tends to also, but to a lesser extent. Panels (c) and (d) illustrate that when North Korea has much higher than normal Jan PRs, South Korea tends to also, but to a lesser extent. It is important to note that although the values are not the same for the PR anomalies, the sign is the same (positive). Figure 23 shows that the most extreme PR positive and negative anomalies tend to occur in the northern portion of the Korean Peninsula region, centered over northeast China. However, the sign of these anomalies is uniform over almost the entire region. These results

support the use a single Korean Peninsula predictand region for Jan PR. Thus, we decided to treat the Korean Peninsula region as a single predictand region for Jan temperature and PR.

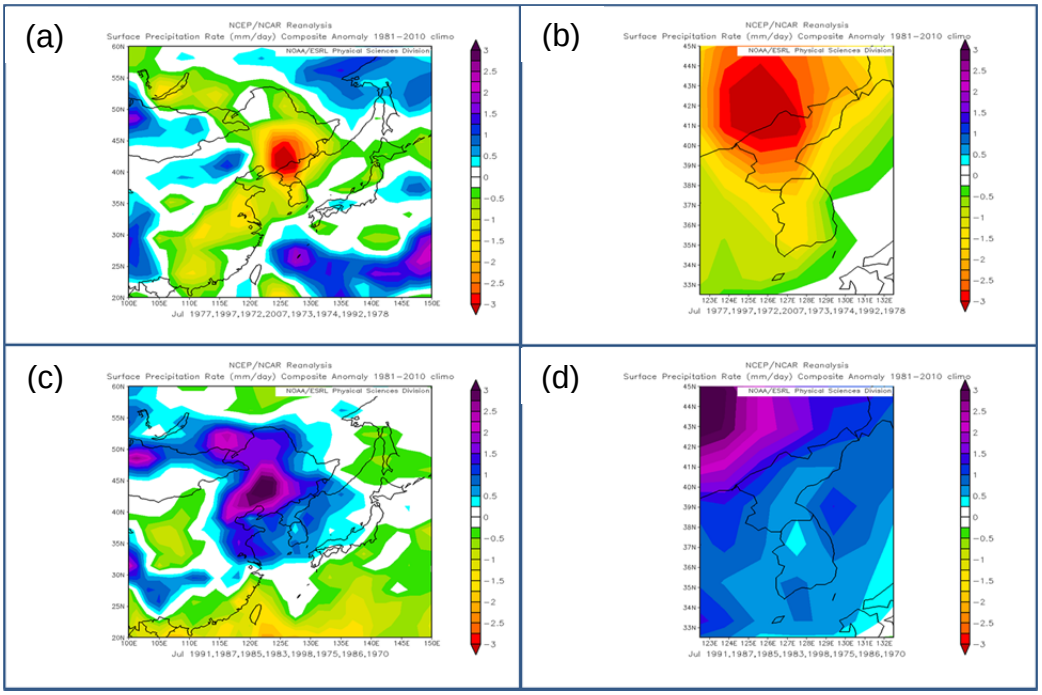


Figure 23. Precipitation rate (PR, mm/day) anomalies for the eight driest ((a) and (b)) and eight wettest (panels (c) and (d)) Juls for the Korean Peninsula 1970–2012. Panels (a) and (b) illustrate that when North Korea has below normal Jan PRs, so does South Korea, but to a much lesser extent. Panels (c) and (d) illustrate that when North Korea has above normal Jan PRs, so does South Korea, but to a lesser extent.

We conducted similar assessments of the climatological uniformity of temperature and PR in the Korean Peninsula region (Figure 19) for all months. We determined that there was sufficient overall uniformity to use the entire region as a single predictand region.

Figures 25 and 26 show our final selection for our predictand region, which includes North Korea and South Korea and surrounding areas. The coordinates for our predictand region are 32.5N to 45N latitude and 122.5E to

132.5E longitude. We used the surface air temperature data for the area enclosed by these coordinates. For the PR data, we used the area enclosed by 33.3N to 44.8N latitude and 121.9E to 133.1E longitude, which is the closest match to the temperature area that is available for the Gaussian grid on which the R1 PR data is provided by ESRL.


Figure 24. The Korean Peninsula predictand region for our study is outlined by the black box (Wikimedia Commons 2013).

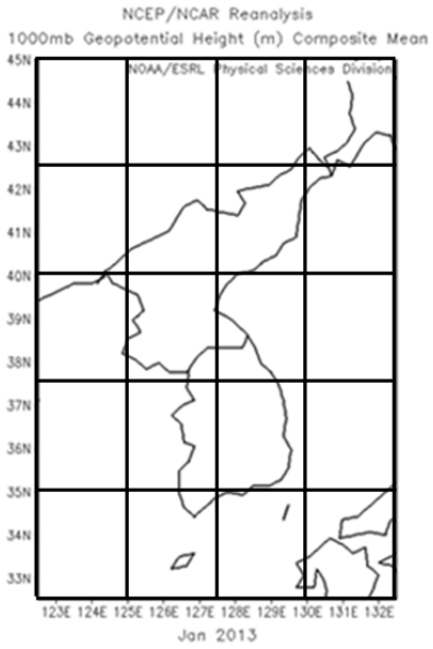


Figure 25. The Korean Peninsula predictand region, extending from 32.5N to 45N latitude and 122.5E to 132.5E longitude. The grid boxes represent the 2.5° x 2.5° resolution of the R1 dataset (ESRL 2013).

### *b. Select Predictand Variables*

The predictand variables for our study were monthly mean surface air temperature (degrees Celsius) and PR (mm/day). The monthly averaging kept our LRF models simple and was sufficient to describe longer term intraseasonal climate variations, but not shorter term (e.g., intra-monthly) variations. Our focus was on predicting these two variables at a two month lead times. A two-month lead time is defined in our study as using monthly predictors based on a data for a given month to forecast for a forecast valid period that is two calendar months in the future. For example, using the averaged AO from 1–31 Jan to forecast the averaged Korean temperatures for 1–31 Mar is considered to be a two-month lead time.

### *c. Select Predictand Period*

This step entails the selection of the time period that the LRF will be designed to predict (i.e., the selection of the forecast valid period). Our study is different from Tournay (2008), Lemke (2010), DeHart (2011) and Gillies (2012) in that our predictand periods were each calendar month, Jan–Dec. These prior studies focused on wet seasons of just two to three months. The advantage of including all months in the predictand period is that predictions can be made year-round by climate forecasters.

### *d. Collect Multi-Decadal Data for Forecast Predictand*

This study period should ideally be long enough to resolve interannual, decadal, and interdecadal variations. We were limited on the length of the study period by the R1 dataset (1948–present). We limited ourselves further by the years that included satellite data in the reanalysis dataset: 1970–2012 (see Chapter II, Section A.2).

An optimal climate normal (OCN) approach was used by Lemke (2010), DeHart (2011), and Gillies (2012). This approach looks at more recent years and gives them extra weight (or even all the weight) in the LRF models. Barnston et al. (2003) and van den Dool (2007) found that a focus on a shorter base period can provide important information on recent decadal and shorter period variations and yield more skillful predictions. Gillies (2012) used two periods in his study: 1970–2010 (41 years) and 1995–2010 (16 years) to apply an OCN approach in the development of his LRF models. In order to keep our study as simple as possible, we only used the period 1970–2012. Since our study uniquely looks at LRF production for all 12 calendar months and for two predictand variables, it was important to limit ourselves to one study period. Additionally, using the OCN approach can sometimes yield inferior results due to the use of a smaller sample size.

## 2. Develop Forecast System

### *a. Identify Potential Predictors*

The predictors that we considered were indices of the following known climate variations and teleconnections: AO, ENLN, NAO, PNA, and WP. We also analyzed global 850 hPa GPH fields (KTI and KPI), persistence, year, and SSTs to identify additional predictors (see Chapter II, Section B). It may seem odd to use year as a predictor, but year can be a good proxy for describing long-term trends.

One of our early steps in evaluating potential predictors was to analyze Korean temperatures correlated with global temperatures and Korean PR correlated with global PR. Figure 26 shows an example for Jan temperature in which the pattern of: (a) positive (negative) correlations with the tropical central-eastern (western) Pacific indicate possible teleconnections between Korean temperature and ENLN; and (b) negative correlations with the high latitudes indicate possible teleconnections between Korean temperature and the AO. We used this type of analysis to evaluate the spatial coherence of our temperature and PR predictands, to assess potential predictors, to identify potential physical mechanisms that might explain the variations of the predictands, and to assess the physical plausibility of predictor-predictand relationships (done more extensively in the next step).

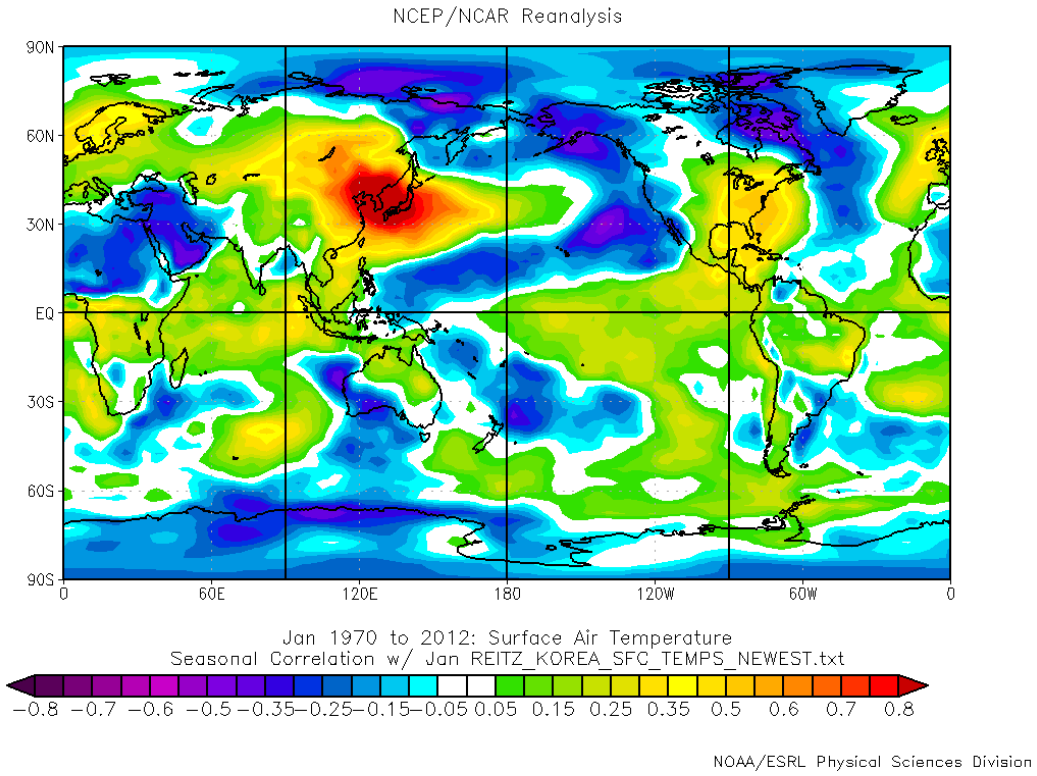


Figure 26. Jan Korea surface temperatures (degrees C) correlated with Jan global surface temperatures, 1970–2012. For 43 years of data, correlations of 0.257 or higher are considered statistically significant with 95% confidence. The correlations with the tropical Pacific indicate possible teleconnections between Korean surface temperatures and El Nino/La Nina (ENLN). The negative correlations with the high latitudes indicate possible teleconnections between Korean temperature and the Arctic Oscillation (AO).

### *b. Evaluate Predictors for Physical Plausibility*

We used statistical methods to identify and test predictors. We also conducted assessments of the physical plausibility of the predictors. Figure 26 can be used to describe an example of these assessments. This figure shows that Jan Korean surface air temperature is positively (negatively) correlated with surface air temperature in most of the northern midlatitudes (northern polar and subpolar regions). These correlations patterns suggest that: (a) the AO plays a

large role in creating Jan Korean surface air temperature anomalies; (b) the AO may be a useful predictor Jan Korean temperature anomalies; and (c) the correlations have a dynamical basis and are physically plausible.

### *c. Develop Forecast Members*

Indices of the climate variations and teleconnections at lead times (LTs) of two to six months were correlated with Korean temperatures and PR for each month. The LT that had the highest correlation for each oscillation was considered the optimal LT and was selected as a predictor. For example, if the AO index values from Oct had the highest correlation (compared to AO from Nov, Sep, Aug, and Jul) with the following Jan Korean temperatures, then Oct AO was chosen as a potential predictor for those Jan temperatures. Most often, the shortest (two month) LT produced the highest correlation.

We created multiple linear regression (MLR) models for each month and predictand variable (24 total) using the backward elimination process (Wilks 2006). The initial MLR model for each month and variable was constructed by including all nine predictors (i.e., five known climate oscillations at their optimal LTs, one KTI/KPI predictor, one SST predictor, persistence, and year). The predictors were ordered based on their contribution to the linear least-squares relationship with the predictand. Contribution was defined by the amount of reduction in error sum of squares, which increases the magnitude of the F-statistic and reduces the probability of committing a type-I error with respect to the hypothesis that the sum of squares due to the regression is significantly larger than the sum of squares due to the errors (P. Harr 2013, personal communication). For each MLR model, the predictor with the smallest F-ratio was removed and the regression was repeated. This process was repeated until all predictors had sufficiently large F ratios, such that the probability of a type-I error (i.e., p-value) was .05 or less. An example of the MLR model trials process that we used to develop the 24 MLR models is provided in Table 1 (Jan Korean surface temperatures). The table contains nine separate MLR trial models,

separated by black lines. MLR Trial #1 (contained all nine variables) was examined and the variable with the highest p-value was eliminated (highlighted in red). MLR was conducted repeatedly until only one predictor remained (MLR Trial #9). MLR Trial #7 was selected as the final as the final MLR model to predict Korean temperatures for Jan. It was selected since it was the one with the most predictors that each had a p-value of 0.05 or less (highlighted in yellow). The MLR model for Jan Korean surface temperatures contained the following predictors: NAO, KTI, and persistence.

Table 1. Multiple linear regression models (MLRs) for Jan Korean surface temperatures. This table contains nine separate MLR trial models, separated by black lines. MLR Trial #1 (contains all nine variables) was examined and the variable with the highest p-value was eliminated (red). MLR was conducted repeatedly until one variable remained (MLR Trial #9). MLR Trial #7 was selected as the final MLR model to predict Korean temperatures for Jan. It was selected since it was the one with the most variables that had p-values or 0.05 or less (highlighted in yellow). The MLR model for Jan Korean surface temperatures contained the following variables: NAO, KTI, and persistence.

| MLR Trial #1 | | MLR Trial #2 | | MLR Trial #3 | | MLR Trial #4 | | MLR Trial #5 | | MLR Trial #6 | | MLR Trial #7 | | MLR Trial #8 | | MLR Trial #9 | |
|---|---|---|---|---|---|---|---|---|---|---|---|---|---|---|---|---|---|
| *Variable* | *P-value* | *Variable* | *P-value* | *Variable* | *P-value* | *Variable* | *P-value* | *Variable* | *P-value* | *Variable* | *P-value* | *Variable* | *P-value* | *Variable* | *P-value* | *Variable* | *P-value* |
| KTI | 0.00389 | KTI | 0.00306 | KTI | 0.00259 | KTI | 0.00030 | KTI | 0.00030 | KTI | 0.00017 | KTI | 0.00009 | KTI | 0.00003 | KTI | 0.00001 |
| Persist | 0.02404 | Persist | 0.02355 | NAO | 0.00488 | NAO | 0.00613 | Persist | 0.00531 | NAO | 0.00890 | Persist | 0.00822 | Persist | 0.02026 | | |
| WP | 0.12978 | NAO | 0.08777 | Persist | 0.01213 | Persist | 0.01305 | NAO | 0.00542 | Persist | 0.01135 | NAO | 0.01722 | | | | |
| NAO | 0.13336 | SST | 0.10358 | SST | 0.11664 | Year | 0.10476 | WP | 0.04457 | WP | 0.10537 | | | | | | |
| Year | 0.16960 | WP | 0.13191 | Year | 0.13137 | WP | 0.12833 | Year | 0.20262 | | | | | | | | |
| SST | 0.22827 | Year | 0.14576 | WP | 0.13197 | SST | 0.15980 | | | | | | | | | | |
| PNA | 0.32296 | PNA | 0.22551 | PNA | 0.22336 | | | | | | | | | | | | |
| AO | 0.56533 | AO | 0.56177 | | | | | | | | | | | | | | |
| MEI | 0.72988 | | | | | | | | | | | | | | | | |

Here is an example formula for a three variable MLR:

$$y = b + m_1 x_1 + m_2 x_2 + m_3 x_3$$

This is a simple linear equation where y is the predicted value, the m values are the slopes, the x values are the inputted predictor values, and b is the y-intercept.

The appropriate MLR model variables for each month and predictand variable were determined using the process stated above. Several statistical quantities for each model were noted in this process, such as the p-values, R^2, and correlation. See Table 2 in Chapter III for a list of all MLR model variables for each month and predictand variable.

### *d. Hindcasting*

Each MLR model was tested by using it to hindcast Korean conditions during 1970–2012. The hindcasting was done using cross-validated MLR models based on the leave-one-out method of cross-validation (Wilks 2006). This method involves creating a separate MLR model for each variable for each of the 43 years in our dataset, with no information about the year being hindcasted used in the development of the MLR model for that year. The 1980 MLR model, for example, was based on data from 1970–1979 and 1981–2012, but not from 1980. This method ensured that only independent data was used in the calculations and minimized the risk of over-estimating model skill. The results from the hindcasting were 43 discrete values (hindcasts) for each month (Jan-Dec) and for each the two predictands (Korean surface air temperature and PR).

### *e. Calculate Hindcast Performance Metrics*

Statistics such as R^2 show the *goodness of fit* of our MLR models. We also assessed the MLR models by verifying their hindcasts. We used tercile matching in order to calculate hindcast verification metrics, such as probability of detection (POD, also known as hit rate), false alarm rate (FAR), and Heidke skill score (HSS) (Wilks 2006).

Tercile matching was done by taking the observed conditions for the 43 year hindcast period for each month and variable, and breaking them into

terciles (three equal parts). Since 43 is not divisible by three, we created the above normal (AN) tercile using data from the 14 years with the highest observed values, the below normal (BN) tercile using data from the 14 years with the lowest observed values, and the near normal (NN) tercile suing data from the remaining 15 years. The hindcasted terciles were determined by comparing the hindcasted values to the range of values for the observation based terciles. For example, a hindcast would be considered AN if the hindcast value was above the observation based AN threshold. The hindcast tercile for a given year was then compared to the observed tercile for that year. Table 2 shows an example of this process for hindcasts of Jan surface temperatures. The observed temperature and predicted temperature columns show the discrete observed and hindcasted values, respectively. The observed temperature tercile and predicted temperature tercile columns show the tercile categories corresponding to the observed and hindcasted values, respectively. The performance of the 43 years of hindcasts was assessed using tercile matching. For example, 2009 was considered a successful hindcast since both the hindcast and actual temperature were above normal (AN). 2012 was considered an unsuccessful hindcast since the hindcast was for AN temperatures and the actual temperature was below normal (BN).

Table 2. Jan Korean surface air temperature cross-validated hindcasting results for 43 years of two-month lead hindcasting.

| Year | Observed Temp | Observed Temp Tercile | Predicted Temp | Predicted Temp Tercile |
|---|---|---|---|---|
| 1970 | -5.997 | Below | -6.145 | Below |
| 1971 | -4.317 | Normal | -4.250 | Normal |
| 1972 | -2.116 | Above | -3.454 | Normal |
| 1973 | -1.770 | Above | -3.014 | Above |
| 1974 | -4.581 | Below | -4.377 | Below |
| 1975 | -3.661 | Normal | -4.550 | Below |
| 1976 | -4.359 | Below | -3.179 | Above |
| 1977 | -7.622 | Below | -4.485 | Below |
| 1978 | -3.766 | Normal | -4.271 | Normal |
| 1979 | -2.407 | Above | -3.324 | Normal |
| 1980 | -4.390 | Below | -4.295 | Normal |
| 1981 | -6.033 | Below | -5.052 | Below |
| 1982 | -4.459 | Below | -6.089 | Below |
| 1983 | -2.683 | Above | -3.441 | Normal |
| 1984 | -6.052 | Below | -5.016 | Below |
| 1985 | -6.216 | Below | -5.960 | Below |
| 1986 | -5.600 | Below | -4.050 | Normal |
| 1987 | -3.792 | Normal | -4.751 | Below |
| 1988 | -2.697 | Above | -2.485 | Above |
| 1989 | -1.028 | Above | -3.235 | Normal |
| 1990 | -4.904 | Below | -3.364 | Normal |
| 1991 | -3.473 | Normal | -3.147 | Above |
| 1992 | -1.771 | Above | -2.131 | Above |
| 1993 | -3.244 | Normal | -2.985 | Above |
| 1994 | -3.443 | Normal | -1.947 | Above |
| 1995 | -2.808 | Above | -2.911 | Above |
| 1996 | -3.599 | Normal | -3.467 | Normal |
| 1997 | -4.147 | Normal | -4.471 | Below |
| 1998 | -3.683 | Normal | -5.445 | Below |
| 1999 | -2.076 | Above | -3.422 | Normal |
| 2000 | -4.067 | Normal | -3.458 | Normal |
| 2001 | -5.139 | Below | -4.506 | Below |
| 2002 | -1.287 | Above | -2.926 | Above |
| 2003 | -3.897 | Normal | -5.183 | Below |
| 2004 | -3.059 | Above | -4.051 | Normal |
| 2005 | -3.556 | Normal | -3.076 | Above |
| 2006 | -3.041 | Above | -3.304 | Normal |
| 2007 | -1.158 | Above | -1.815 | Above |
| 2008 | -3.758 | Normal | -2.951 | Above |
| 2009 | -3.015 | Above | -2.757 | Above |
| 2010 | -4.246 | Normal | -4.557 | Below |
| 2011 | -6.755 | Below | -5.426 | Below |
| 2012 | -4.739 | Below | -2.548 | Above |

The hindcasting results were verified using 2x2 contingency tables for each tercile. The following contingency table performance metrics were then calculated: POD, FAR, and HSS. Probability of detection (POD) or hit rate, is the number of “yes” forecasts that were actually “yes” and should be as close to one as possible. False alarm rates (FAR) are ratios of “yes” forecasts divided by the total number of forecasts and should be as close to zero as possible. HSS is a skill score based on the proportion correct as the basic accuracy measure (Wilks 2006). Perfect forecasts receive HSS=1, forecasts with no skill receive HSS<0, and forecast with some skill receive 0<HSS<1. See DeHart (2011) and Wilks (2006) for a more in-depth explanation of 2x2 contingency tables and associated performance metrics. Table 3 shows an example of contingency table results, in this case for 43 years of Jan Korean surface air temperature hindcasts at a two month lead time. The Heidke Skill Score (HSS) was 0.26 for the AN tercile, 0.43 for the below normal tercile, and -0.09 for the near normal (NN) tercile . In this example, our LRF model had significant skill for the AN and BN terciles, but had no skill for the NN tercile.

Table 3. Jan Korean surface air temperature 2x2 contingency table results for 43 years of hindcasts.

| | | Observed | |
|---|---|---|---|
| | | **Above** | **Not Above** |
| | **Above** | **7** | **7** |
| Forecast | **Not Above** | **7** | **22** |
| | | 14 | 29 |
| | Above Score | | |
| HSS: | 0.25862069 | | |
| FAR: | 0.5 | | |
| POD: | 0.5 | | |
| | Observed | | |
| | | **Below** | **Not Below** |
| | **Below** | **9** | **6** |
| Forecast | **Not Below** | **5** | **23** |
| | | 14 | 29 |
| | Below Score | | |
| HSS: | 0.428053204 | | |
| FAR: | 0.4 | | |
| POD: | 0.642857143 | | |
| | Observed | | |
| | | **Normal** | **Not Normal** |
| | **Normal** | **4** | **10** |
| Forecast | **Not Normal** | **11** | **18** |
| | | 15 | 28 |
| | Normal Score | | |
| HSS: | -0.091898428 | | |
| FAR: | 0.714285714 | | |
| POD: | 0.266666667 | | |

## 3. Apply Forecast System

This forecasting phase is intended to be conducted by climate forecasters at agencies such as the 14 WS. However, we conducted several trial runs of this phase, including forecasting for Jan 2013 (see Chapter III, Section C). In this phase, we used our MLR models from phase two to produce forecasts for Korean surface temperatures and precipitation. It is important to note that for MLR models that have HSS≤0, it is generally best to not even disseminate a forecast.

### *a. Collect Latest Predictor Data*

The climate forecaster can obtain up-to-date values for the known climate variation predictors at the CPC (http://www.cpc.ncep.noaa.gov) and

ESRL (http://www.esrl.noaa.gov) websites. For KTI, KPI, SST, and persistence, the climate forecaster will have to obtain R1 reanalysis data from the ESRL website. R1 data is available on their website by the third or fourth day of the month. For example, Feb data will be available by Mar 3 or 4. The climate forecaster will enter the latest predictor data into the forecast worksheets that we created (Tables 12–15). The tables will tell forecasters, for each predictand and forecast valid month, which climate variations to use, which geographical boxes to enter on the ESRL website for KTI, KPI, SST and persistence, and which lead times to use. These forecast worksheets are included in Chapter III, Section C.

### *b. Insert Data into Forecast System*

The latest predictor data will be entered into the MLR model equation. The formulas for each of the 24 predictands are located in Tables 12 and 14. LRF outputs in the form of a discrete forecast values will be obtained by solving the MLR models into which the predictor data has been entered.

### *c. Output Forecasts*

The discrete value LRF outputs obtained in the prior step can be used as the forecasts issued to customers. For customers that prefer tercile (AN, NN, or BN) forecasts, the climate forecaster will assign terciles to the discrete value forecasts (Tables 12 and 14). The terciles thresholds are based on the R1 values for 1970-2012 and are located in the Chapter III, Section C for each month and predictand variable. An example of a final output is shown in Chapter III, Section C.

### *d. Evaluate Final Forecast for Plausibility and Errors*

This step requires the user to confirm that the LRFs are reasonable and contain no obvious errors. If the LRF is completely unreasonable, then perhaps the forecaster collected incorrect predictor data or incorrectly entered that data, should repeat the collection and/or entry steps. This is also the step in

which the forecaster should decide if the performance of the model being used (determined from its skill in the 1970–2012 hindcasts and in prior forecasts) is acceptable enough to justify issuing the LRF to customers. For example, if the model has HSS values that are close to or less than zero, then it is probably best, in general, to withhold the forecast and instead provide alternative guidance (e.g., LTM information) to customers.

### *e. Verify Forecasts*

This final step is completed after the forecast valid month has past and the R1 data for that month has been posted on the ESRL website. It is important to see how the LRF models perform over time and we recommend that the climate forecasters keep metrics on the forecast system. We also recommend that climate forecasters compare their metrics to those from alternate forecasting systems (e.g., those from IRI).

THIS PAGE INTENTIONALLY LEFT BLANK

# III. RESULTS

## A. OVERVIEW

The LRF models that we developed were intended to skillfully predict Intraseasonal variations from long-term mean (LTM) conditions. Thus, we began our study by examining the LTM seasonal cycles of surface air temperature and precipitation rate in the Korean Peninsula region, and the standard deviations in those quantities, as shown in Figure 27. The Korean Peninsula experiences sub-zero temperatures in the winter. The standard deviation in temperatures is highest in the winter, indicating higher variability. As shown in Figure 27, the Korean Peninsula is wettest in the summer. The standard deviation in PR is also highest in the summer, indicating higher variability.

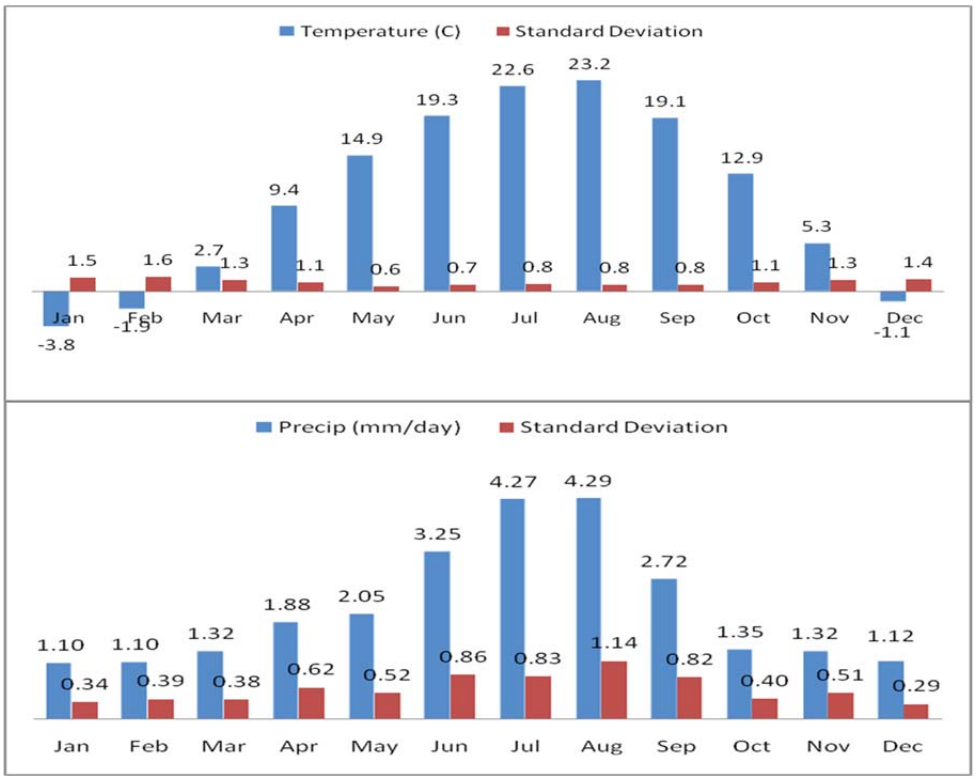


Figure 27. Long-term mean (LTM) surface air temperatures by month for the Korean Peninsula region (top), 1970–2012. LTM precipitation rate (PR) by month for the Korean Peninsula region (bottom), 1970–2012.

To forecast the variations from the seasonal cycles shown in Figure 27, we developed 24 LRF models that we evaluated through cross-validated hindcasting for the 1970–2012 study period. This chapter describes in detail our model development and hindcasting results for four key months: Jan, Apr, Jul and Oct —as well as our forecasts and verification results for Jan 2013. Results for all months of the year are summarized in Appendices A and B.

Table 4 summarizes the MLR models we developed for forecasting surface air temperature for Jan-Dec at two-month lead times. The predictors column shows which variables were chosen as the MLR predictors for each month. The next column shows the p-values. The adjusted R^2 and correlations between the predicted temperature and the actual temperature are listed in the two rightmost columns. As discussed in Chapter II, predictors that had p-values greater than 0.05 were removed. For 43 years of data, correlations of 0.257 or higher are considered statistically significant with 95% confidence. For more details on the selection of predictors, the use of p-values, and other details of the MLR process, see Chapter II.

Table 4. Summary descriptions of the multiple linear regression (MLR) models we developed for generating for 2-month lead surface air temperature forecasts for Jan-Dec for the Korean Peninsula region. The predictors column shows which variables were chosen as the MLR predictors for each month. The next column shows the p-values. The adjusted R^2 and correlations between the predicted temperature and the actual temperature are listed in the two rightmost columns.

| Month | Predictors | P-Values | Adjusted R^2 | Correlation |
|---|---|---|---|---|
| Jan | NAO<br>KTI<br>Persistence | 0.017<br><0.001<br>0.008 | 0.49 | 0.73 |
| Feb | Year<br>KTI<br>PNA | <0.001<br><0.001<br><0.001 | 0.54 | 0.76 |
| Mar | SST<br>KTI | 0.013<br>0.001 | 0.31 | 0.58 |
| Apr | SST<br>KTI | 0.003<br><0.001 | 0.41 | 0.66 |
| May | SST<br>Year | 0.003<br>0.011 | 0.33 | 0.61 |
| Jun | AO<br>SST<br>KTI | 0.022<br><0.001<br>0.004 | 0.54 | 0.75 |
| Jul | SST<br>PNA | 0.035<br>0.037 | 0.17 | 0.45 |
| Aug | SST<br>KTI | 0.002<br>0.006 | 0.35 | 0.62 |
| Sep | MEI<br>Year<br>KTI | 0.021<br><0.001<br>0.0460 | 0.50 | 0.73 |
| Oct | SST<br>KTI<br>PNA | 0.002<br>0.002<br>0.006 | 0.51 | 0.74 |
| Nov | SST<br>KTI | 0.010<br>0.002 | 0.34 | 0.61 |
| Dec | SST<br>KTI | 0.001<br>0.001 | 0.39 | 0.65 |

Table 5 is like Table 4 but summarizes the MLR models we developed for forecasting precipitation rate (PR) for Jan-Dec at two-month lead times. The predictors column shows which variables were chosen as the MLR predictors for each month. The next column shows the p-values. The adjusted R^2 and correlations between the predicted PR and the actual PR are listed in the two rightmost columns. Predictors that had p-values greater than 0.05 were removed from the MLRs, except for Feb KPI, Jul SST, and Sep KPI, for which we decided that these predictors were important and that their p-values were acceptably small (0.078 or less).

Table 5. Multiple linear regression (MLR) results for 2-month lead for precipitation rate (PR) forecasts, Jan-Dec. The predictors column shows which variables were chosen as the MLR predictors for each month. The next column shows the p-values. The adjusted R^2 and correlations between the predicted temperature and the actual temperature are listed in the two rightmost columns.

| Month | Predictors | P-Values | Adjusted R^2 | Correlation |
|---|---|---|---|---|
| Jan | SST<br>KPI | 0.006<br>0.037 | 0.25 | 0.54 |
| Feb | NAO<br>KPI<br>SST | 0.002<br>0.070<br>0.001 | 0.51 | 0.74 |
| Mar | KPI | 0.003 | 0.18 | 0.45 |
| Apr | SST<br>KPI | 0.014<br>0.002 | 0.30 | 0.57 |
| May | MEI<br>SST<br>KPI | 0.010<br>0.018<br>0.003 | 0.33 | 0.62 |
| Jun | SST<br>KPI | 0.014<br>0.020 | 0.26 | 0.55 |
| Jul | SST<br>KPI | 0.075<br><0.001 | 0.32 | 0.59 |
| Aug | SST<br>KPI | 0.010<br>0.003 | 0.33 | 0.60 |
| Sep | SST<br>KPI | 0.025<br>0.078 | 0.23 | 0.51 |
| Oct | SST1<br>SST2<br>KPI | 0.016<br>0.007<br>0.041 | 0.36 | 0.63 |
| Nov | MEI<br>SST<br>KPI | 0.017<br>0.011<br>0.007 | 0.45 | 0.70 |
| Dec | SST<br>KPI | <0.001<br><0.001 | 0.46 | 0.70 |

Tables 6–8 show the HS, FAR, and POD verification results for the Korean surface air temperature hindcasts for 1970–2012. To be a perfect model, the HSS should be 1, the FAR should be 0 (no false alarms), and the POD should be 1 (no misses). Note that the HSS and POD are generally higher and the FAR is generally lower for the AN and BN terciles. This indicates that the overall results for the NN tercile were not as good. The best performing month for surface temperature hindcasts was for the AN tercile for Feb with a HSS of 0.67, a FAR of 0.17, and a POD of 0.71. The worst performing month for surface temperature hindcasts was for the NN tercile for Jan with an HSS of -0.09, a FAR of 0.71, and a POD of 0.27.

Table 6. Verification results for Korean surface air temperature hindcasts for Jan–Apr 1970–2012.

| Month | Tercile | Heidke Skill Score | False Alarm Rate | Prob. of Detection |
|---|---|---|---|---|
| Jan | AN | 0.26 | 0.50 | 0.50 |
| | BN | 0.43 | 0.40 | 0.64 |
| | NN | -0.09 | 0.71 | 0.27 |
| Feb | AN | 0.67 | 0.17 | 0.71 |
| | BN | 0.45 | 0.33 | 0.57 |
| | NN | 0.33 | 0.47 | 0.67 |
| Mar | AN | 0.39 | 0.44 | 0.64 |
| | BN | 0.26 | 0.50 | 0.50 |
| | NN | 0.05 | 0.62 | 0.33 |
| Apr | AN | 0.45 | 0.33 | 0.57 |
| | BN | 0.51 | 0.31 | 0.64 |
| | NN | 0.17 | 0.56 | 0.53 |

Table 7. Verification results for Korean surface air temperature hindcasts for May–Aug 1970–2012.

| Month | Tercile | Heidke Skill Score | False Alarm Rate | Prob. of Detection |
|---|---|---|---|---|
| May | AN | 0.38 | 0.36 | 0.50 |
| | BN | 0.33 | 0.29 | 0.36 |
| | NN | 0.11 | 0.60 | 0.67 |
| Jun | AN | 0.31 | 0.50 | 0.64 |
| | BN | 0.61 | 0.18 | 0.64 |
| | NN | 0.01 | 0.64 | 0.33 |
| Jul | AN | 0.26 | 0.50 | 0.50 |
| | BN | 0.38 | 0.17 | 0.36 |
| | NN | 0.27 | 0.52 | 0.73 |
| Aug | AN | 0.17 | 0.50 | 0.29 |
| | BN | 0.59 | 0.11 | 0.57 |
| | NN | 0.17 | 0.58 | 0.73 |

Table 8. Verification results for Korean surface air temperature hindcasts for Sep–Dec 1970–2012.

| Month | Tercile | Heidke Skill Score | False Alarm Rate | Prob. of Detection |
|---|---|---|---|---|
| Sep | AN | 0.55 | 0.35 | 0.79 |
| | BN | 0.24 | 0.43 | 0.31 |
| | NN | 0.19 | 0.53 | 0.56 |
| Oct | AN | 0.45 | 0.33 | 0.57 |
| | BN | 0.62 | 0.23 | 0.71 |
| | NN | 0.17 | 0.56 | 0.53 |
| Nov | AN | 0.09 | 0.57 | 0.21 |
| | BN | 0.43 | 0.30 | 0.50 |
| | NN | 0.00 | 0.65 | 0.60 |
| Dec | AN | 0.36 | 0.33 | 0.43 |
| | BN | 0.43 | 0.30 | 0.50 |
| | NN | 0.06 | 0.63 | 0.60 |

Figure 28 shows the Heidke skill scores (HSS) by tercile for all months for the surface air temperature hindcasts for 1970–2012. The HSS values for the BN and AN terciles are positive, and thus skillful, for all months. The NN tercile, however, is the poorest performing tercile and is near or below zero for Jan, Jun, and Nov. The less skillful performance of the NN tercile may be due this tercile being bounded at both the high and low ends. The AN tercile is only bounded at the lower end, and the BN tercile is only bounded at the upper end, but the NN tercile is bounded on both ends. Thus, it is easier for observed conditions to "escape" the bounds of NN than the bounds of AN or BN (cf. van den Dool and Toth 1991).

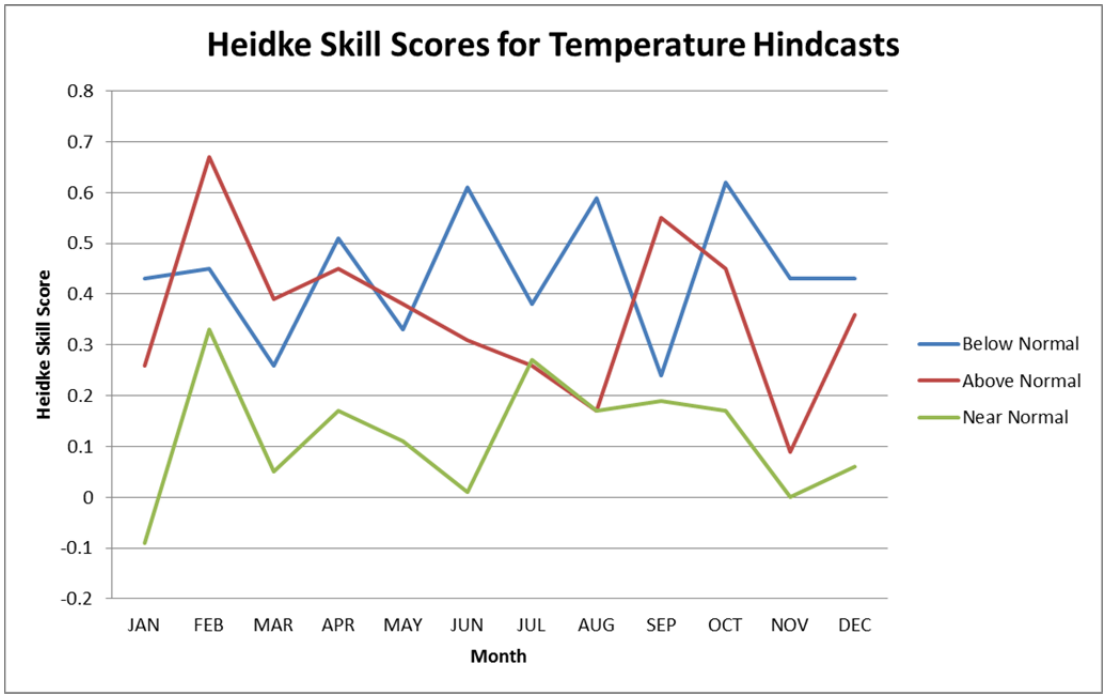


Figure 28. Heidke skill scores (HSS) by tercile for Jan through Dec for temperature hindcasts for 1970–2012.

Tables 9–11 show the HS, FAR, and POD verification results for the Korean PR hindcasts for 1970–2012. Note that the HSS and POD are generally higher and the FAR is generally lower for the AN and BN terciles. This indicates that the overall results for the NN tercile were not as good. The PR hindcasting results were less skillful overall than the surface temperature results. There were a few months with near zero or negative HSSs, representing no forecast skill. The best performing month for PR hindcasts was for the AN tercile for Feb with a HSS of 0.72, a FAR of 0.09 and a POD of 0.71. The worst performing month for PR hindcasts was for the NN tercile for Jun with a HSS of -0.39, a FAR of 0.83 and a POD of 0.27.

Table 9. Verification results for Korean precipitation rate (PR) hindcasts for Jan–Apr 1970–2012.

| Month | Tercile | Heidke Skill Score | False Alarm Rate | Prob. of Detection |
|---|---|---|---|---|
| Jan | AN | 0.08 | 0.63 | 0.50 |
| | BN | 0.25 | 0.33 | 0.29 |
| | NN | -0.22 | 0.77 | 0.27 |
| Feb | AN | 0.72 | 0.09 | 0.71 |
| | BN | 0.41 | 0.38 | 0.57 |
| | NN | 0.33 | 0.47 | 0.67 |
| Mar | AN | 0.30 | 0.20 | 0.29 |
| | BN | 0.21 | 0.43 | 0.29 |
| | NN | 0.18 | 0.58 | 0.87 |
| Apr | AN | 0.30 | 0.46 | 0.50 |
| | BN | -0.04 | 0.75 | 0.07 |
| | NN | -0.01 | 0.65 | 0.60 |

Table 10. Verification results for Korean precipitation rate (PR) hindcasts for May–Aug 1970–2012.

| Month | Tercile | Heidke Skill Score | False Alarm Rate | Prob. of Detection |
|---|---|---|---|---|
| May | AN | 0.32 | 0.47 | 0.57 |
| | BN | 0.51 | 0.31 | 0.64 |
| | NN | 0.18 | 0.53 | 0.47 |
| Jun | AN | -0.14 | 0.80 | 0.14 |
| | BN | 0.12 | 0.56 | 0.29 |
| | NN | -0.39 | 0.83 | 0.27 |
| Jul | AN | 0.47 | 0.36 | 0.64 |
| | BN | 0.29 | 0.38 | 0.36 |
| | NN | 0.16 | 0.57 | 0.60 |
| Aug | AN | 0.40 | 0.25 | 0.43 |
| | BN | 0.36 | 0.33 | 0.43 |
| | NN | 0.17 | 0.58 | 0.73 |

Table 11. Verification results for Korean precipitation rate (PR) hindcasts for Sep–Dec 1970–2012.

| Month | Tercile | Heidke Skill Score | False Alarm Rate | Prob. of Detection |
|---|---|---|---|---|
| Sep | AN | 0.17 | 0.40 | 0.21 |
| | BN | 0.31 | 0.40 | 0.43 |
| | NN | 0.11 | 0.61 | 0.73 |
| Oct | AN | 0.39 | 0.48 | 0.79 |
| | BN | 0.33 | 0.29 | 0.36 |
| | NN | 0.18 | 0.53 | 0.47 |
| Nov | AN | 0.34 | 0.42 | 0.50 |
| | BN | 0.01 | 0.67 | 0.21 |
| | NN | 0.03 | 0.64 | 0.53 |
| Dec | AN | 0.47 | 0.22 | 0.50 |
| | BN | 0.38 | 0.36 | 0.50 |
| | NN | 0.36 | 0.48 | 0.80 |

Figure 28 shows the Heidke skill scores (HSS) by tercile for the PR hindcasts for 1970–2012. For all three terciles, the HSS values are positive in most of the 12 months—including Jul, Aug, and Sep, three of the four months with the highest PR (see Figure 27). The skill is also relatively good for the AN and BN terciles during Dec, Jan, Feb, and Mar, four of the driest months of the year. The HSS results are poorest in Apr, Jun, and Nov, for which two of the three terciles had little or no skill. This is likely due to challenges inherent in forecasting seasonal transitions (see Figure 27), especially: (1) the transition in Apr to greater spring precipitation; (2) the transition in Jun to the summer wet period of Jun-Sep (the four months of the year with the highest precipitation); and (3) the transition in about Nov to reduced winter precipitation. The NN tercile has the poorest performance overall, most likely for the reasons discussed earlier in this section.

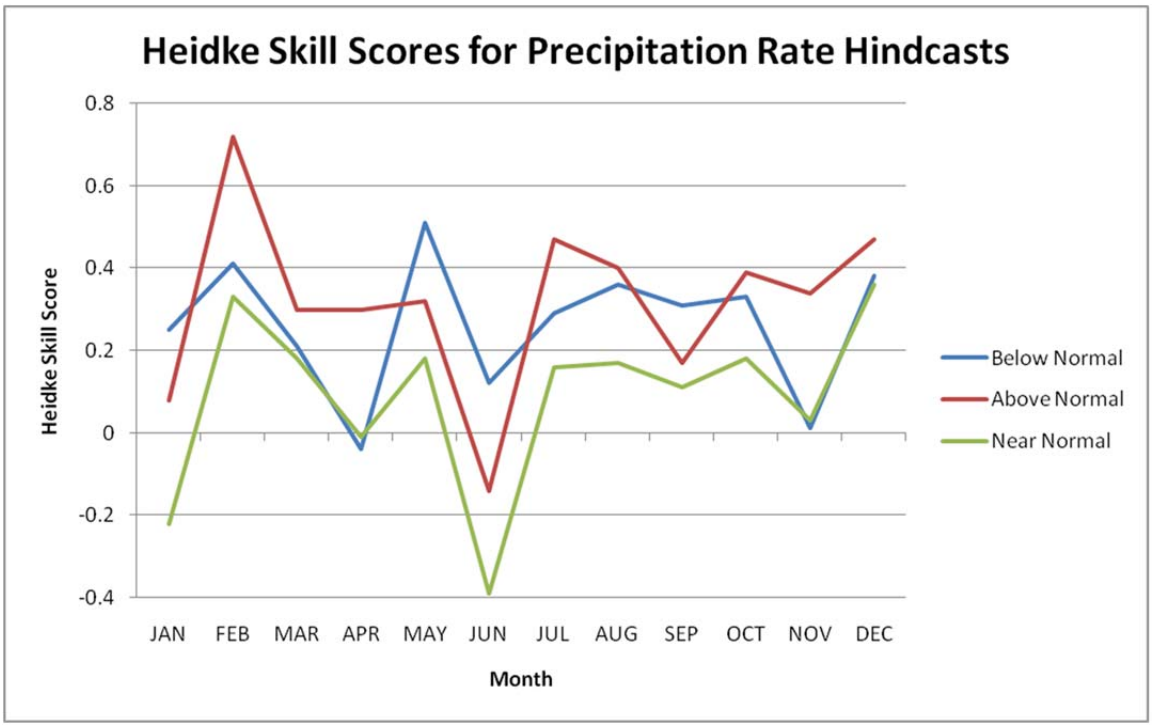


Figure 29. Heidke skill scores (HSS) by tercile for Jan through Dec for precipitation rate hindcasts for 1970–2012.

## B. PREDICTOR SELECTION AND HINDCASTING RESULTS FOR KEY MONTHS

This section focuses on results for four representative months: Jan, Apr, Jul, and Oct. Jan results are described in full detail, with discussions of the physical processes that underlie Jan temperature variations in the Korean region, the predictor variables used for predicting those variations, and the MLR model hindcasting verification results. For Apr, Jul, and Oct, summary discussions of the predictor variables and the hindcasting verification results are presented. Appendix A summarizes the predictors that were included in our final MLR models for all 12 months for both surface temperatures and PR. Appendix B summarizes the hindcasting results for all 12 months for both surface temperatures and PR.

### 1. January

Analyses of the eight coldest and eight warmest Januarys during 1970–2012 indicate that variations in these two features, and other lower tropospheric circulation features, help explain anomalously cold and warm conditions during Jan.

Analyses of the Jan LTM 850 hPa GPH (Figure 30 (a)) reveal two significant semi-permanent features that tend to strongly influence Korean temperature: the Aleutian Low and the Asian High. Figure 30 (b)-(c) shows that the most notable differences in the cold Jans compared to the LTM were: (1) anomalously high heights in the Arctic, especially north of Siberia; (2) anomalously low heights in the northern subpolar and midlatitude regions, especially in the Aleutian Low region (cf. Figure 26). Note that these height anomaly patterns indicate that the cold Jans tended to occur during the negative phase of the AO. Figure 31 shows a zoomed in view of the LTM compared to the composite for the eight coldest Jans. During the cold Jans, the stronger Aleutian Low and presence of the high centered north of Siberia tended to bring stronger northerly winds and colder temperatures to the Korean Peninsula. It is also important to note that the flow over Siberia and into Korea had a more pronounced northerly component in the cold Jans. These results indicate that the cold Jans tended to be associated with the negative phase of the AO, and with anomalously northerly flow and cold air advection over the Korean Peninsula.

[A3]

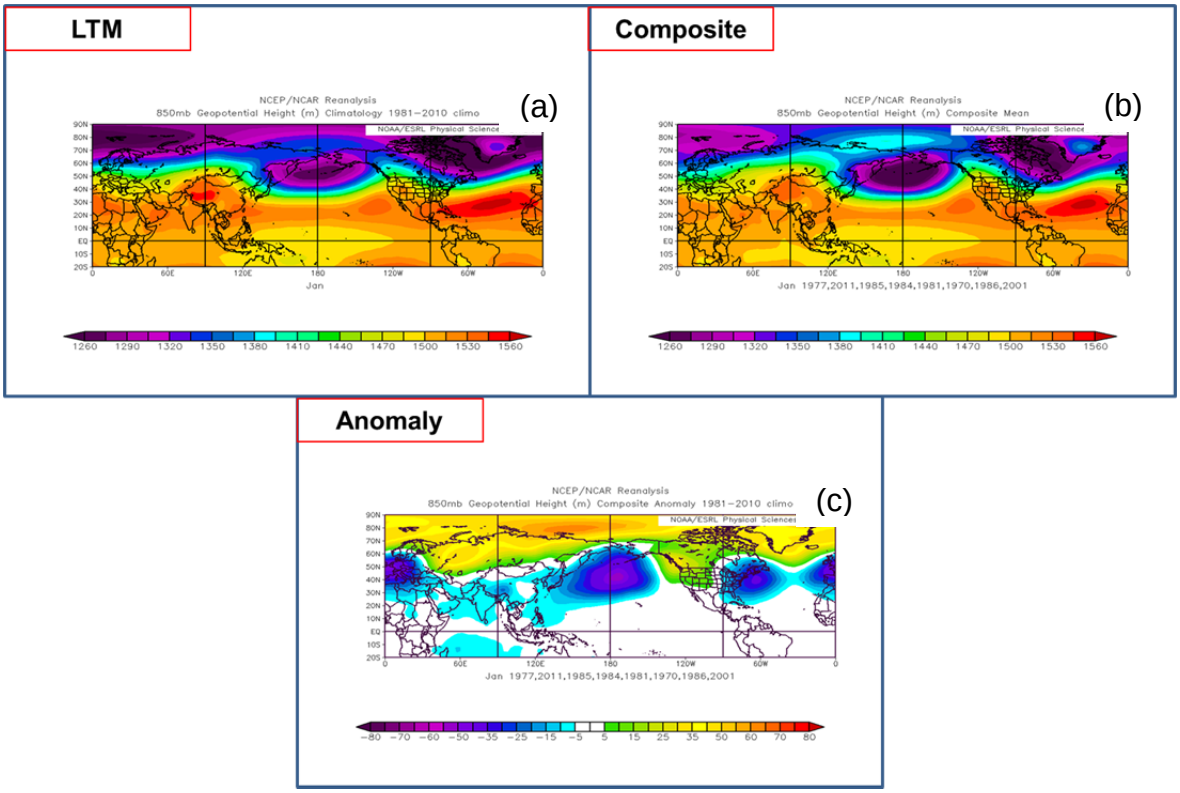


Figure 30. Jan 850 hPa geopotential heights (GPH, m): (a) long-term mean (LTM); (b) composite of the eight coldest years in the Korean study region during the 1970–2012 study period; and (c) anomaly for those eight coldest years. Note in the composite and anomaly figures the anomalously high heights over the Arctic and the anomalously low heights over much of the northern subpolar and midlatitude regions, especially to the north and east of Korea.

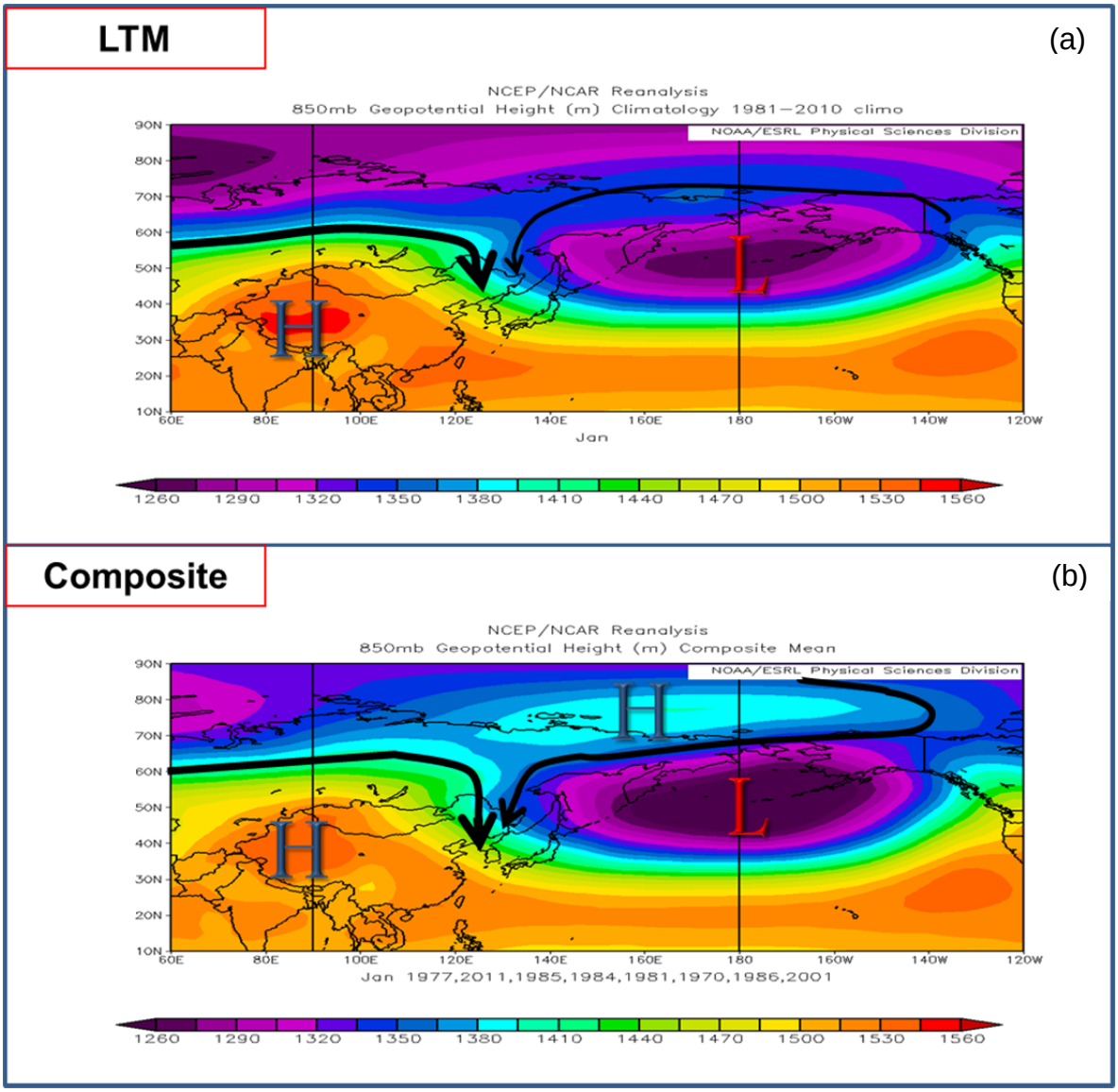


Figure 31. Jan 850 hPa geopotential heights (GPH, m): (a) long-term mean (LTM) and (b) composite of the eight coldest years in the Korean region during 1970-2012. In the LTM chart (a), the implied lower tropospheric winds over Korea tend to be: (1) relatively strongly from the west through Siberia and southward through eastern Russia and China; and (2) less strongly from the east and north, from along the north flank of the Aleutian Low. In the composite chart (b): (1) the winds from the west and north originate from further north and have a more northerly component than in the LTM; and (2) the winds from the east originate much further north, near the North Pole, and are stronger.

Figure 32 shows that the most notable differences in the warm Jans compared to the LTM are: (1) the anomalously low heights in the polar latitudes, especially over much of Russia and north of Siberia; and (2) the anomalously high heights over much of the subpolar and midlatitude regions, especially in and near the Aleutian Low region. Note that these height anomaly patterns indicate that the warm Jans tended to occur during the positive phase of the AO. Figure 33 shows a zoomed in view of the LTM compared to the composite for the eight warmest Jans. During the warm Jans: (1) the winds from Siberia tended to have a weaker northerly component than in the LTM; and (2) the northeasterly winds from the northern flank of the Aleutian Low tended to be much weaker and to originate at lower latitudes. These results indicate that the warm Jans tended to be associated with the positive phase of the AO, and with anomalously southerly flow and warm air advection over the Korean Peninsula.

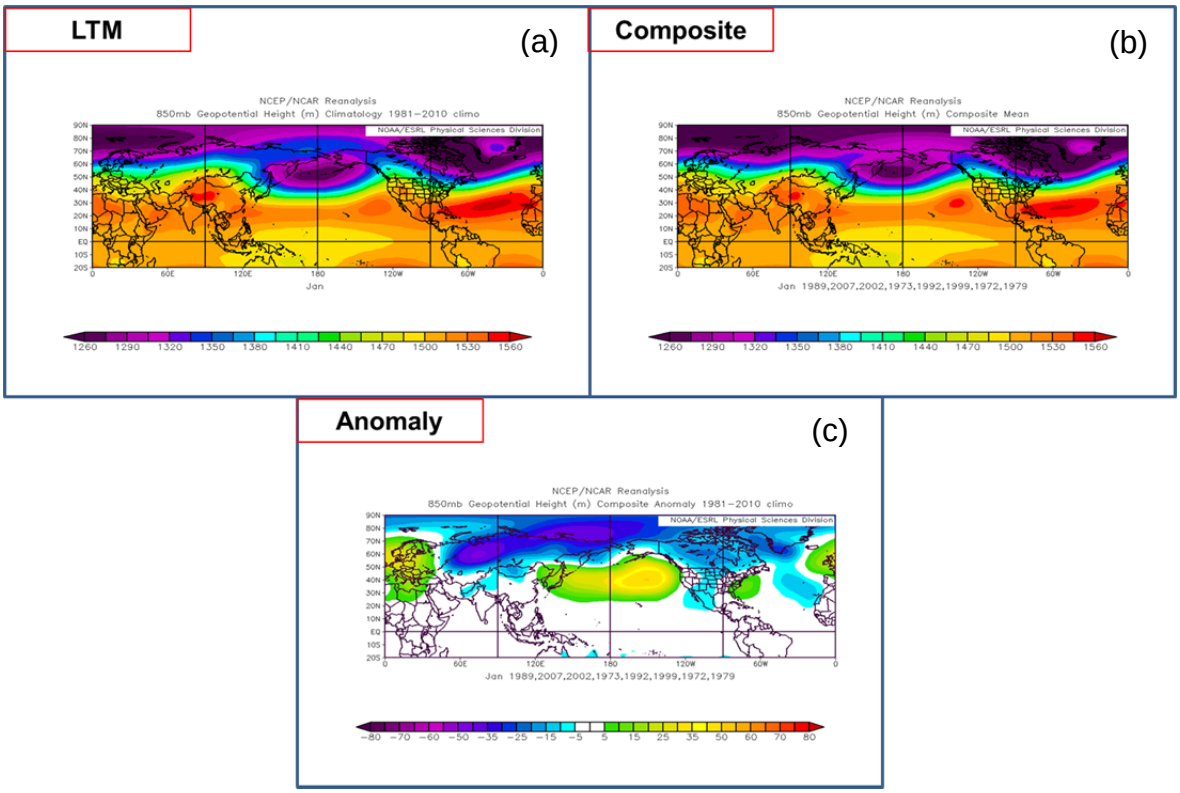


Figure 32. Jan 850 hPa geopotential heights (GPH, m): (a) long-term mean (LTM); (b) composite of the eight warmest years in the Korean study region during the 1970–2012 study period; and (c) anomaly for those eight coldest years. Note in the composite and anomaly figures the anomalously low heights in the polar latitudes and the anomalously high heights over much of the subpolar and midlatitude regions.

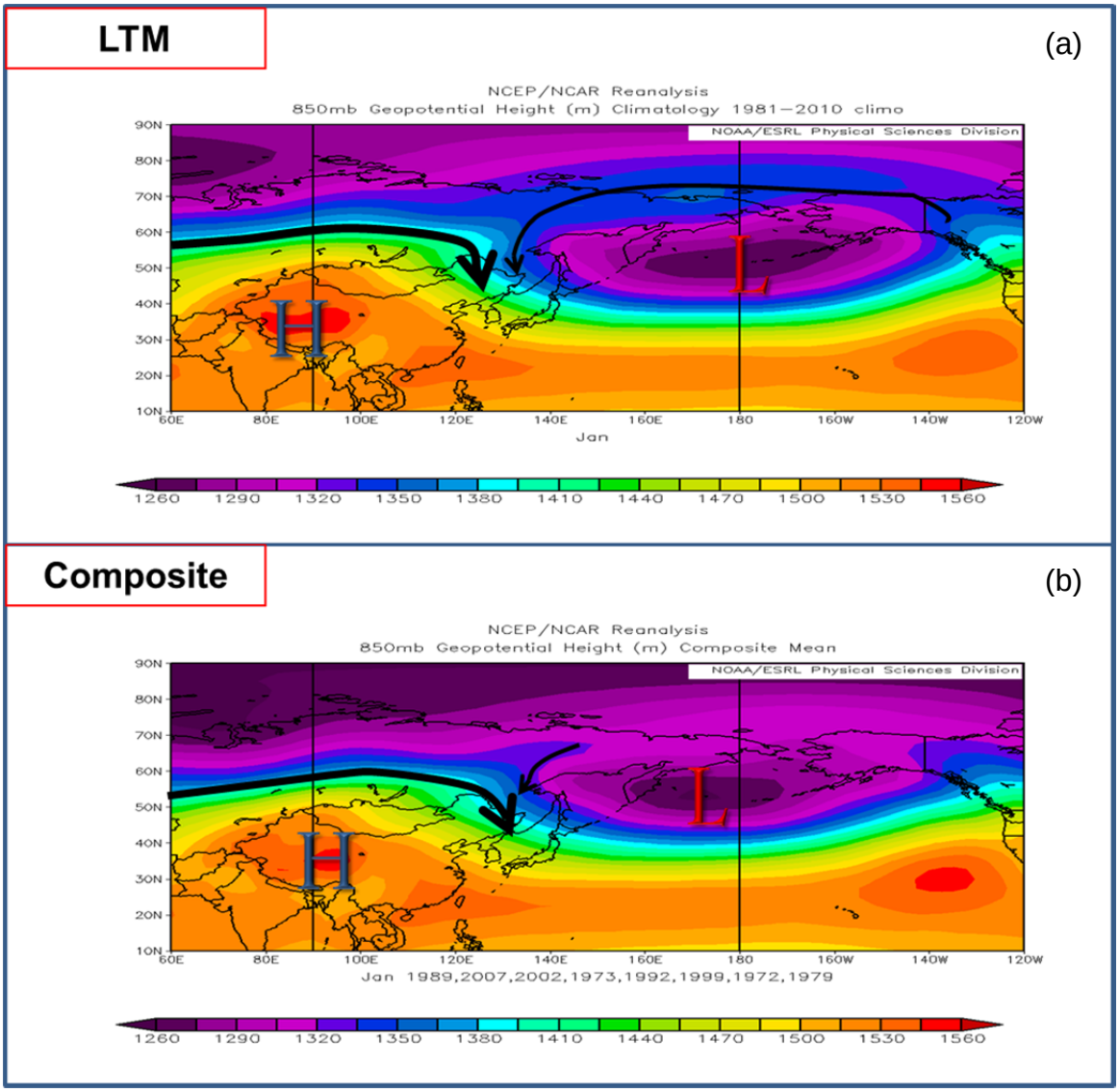


Figure 33. Jan 850 hPa geopotential heights (GPH, m): (a) long-term mean (LTM) and (b) composite of the eight warmest years in the Korean region during 1970-2012. During the warm Jans (b), the winds from Siberia tended to have a weaker northerly component than the LTM. Also, the northeasterly winds from the northern flank of the Aleutian Low tended to be much weaker and to originate at lower latitudes.

Once we had characterized the types of anomalous circulation patterns that tended to occur during anomalously cold and warm Jans, we looked back in time to identify the precursor conditions that led to those patterns. We focused on the changes from Oct to Jan, since Oct-Nov represented the lead times of

interest for our LRFs of Jan conditions. Figure 34 shows the LTM 850 hPa GPH for the Asian–North Pacific region for the Oct–Jan period. Note that from Oct to Jan: (1) the Asian High does not move very much; (2) the Aleutian Low strengthens and extends to the west; (3) heights in the Arctic become much lower; (4) the North Pacific High weakens considerably and contracts to the south and east; and (5) winds over Korea become much stronger and more northerly. These seasonal evolutions in the major features of the lower tropospheric circulation were useful in identifying the anomalies that tended to precede anomalously cold and warm Jans in Korea.

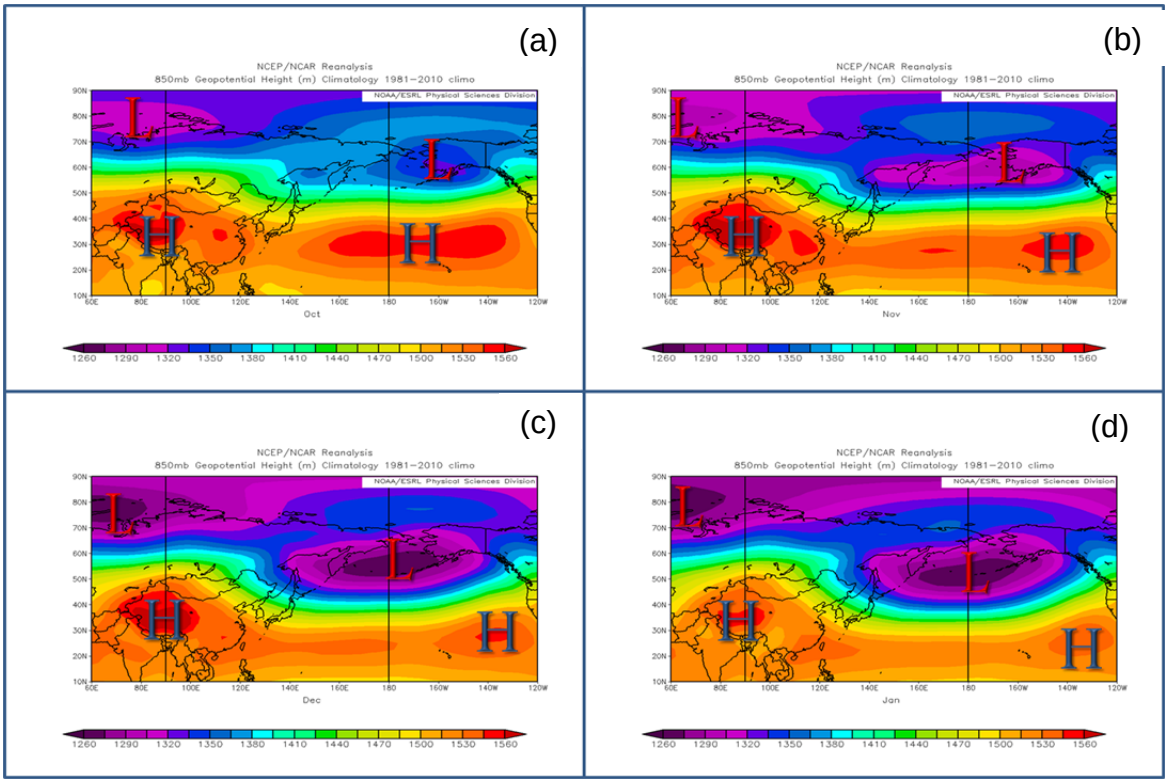


Figure 34. Long-term mean (LTM) 850 hPa geopotential heights (GPH, m) for: (a) Oct, (b) Nov, (c) Dec, and (d) Jan.

Figure 35 shows that for the Octs preceding the cold Jans, the lower tropospheric heights tend to be anomalously high over northern Russia and low in the Aleutian Low region. Figure 36 shows approximately the opposite patterns

for the Octs preceding the warm Jans. Note that these anomaly patterns are similar to those for the following Jans (Figures 30 and 32). That is, the low level circulation anomalies that tended to produce cold (warm) Jans tended to be in place three months earlier in the Asia–North Pacific region. This indicates that, for at least the most extreme cold and warm Jans, the anomalous lower tropospheric conditions that produced the Jan temperature extremes tended to be initiated several months earlier. If so, then these preceding Oct conditions may be useful as predictors of the Jan temperature extremes. Note too that these Oct GPH anomalies for the cold (warm) composite resembled the negative (positive) AO conditions in the corresponding Jan composite anomalies, but were more limited in areal extent and magnitude than in Jan. This suggests that the value of the AO index in Oct may not be a good indicator or predictor of Jan temperatures, even though northern Russia and North Pacific GPH variations in Oct that appear to be associated with the AO may be good predictors.

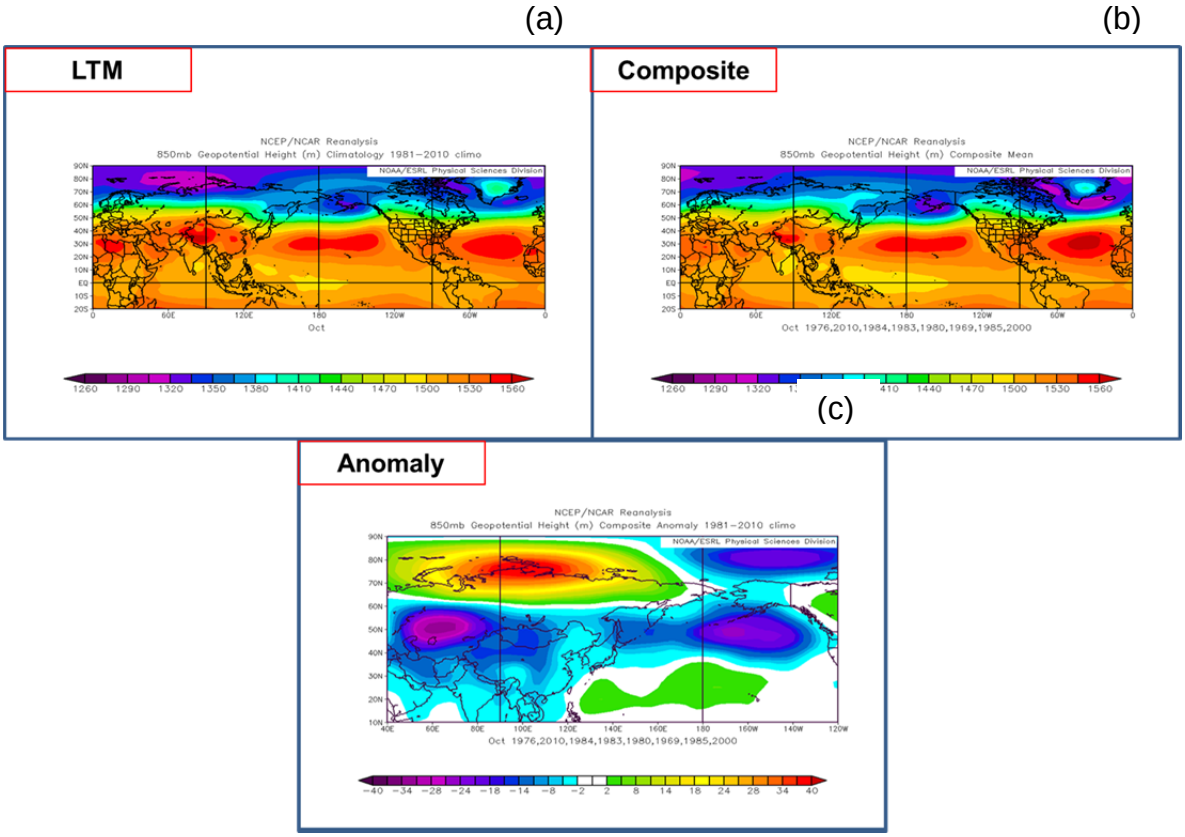


Figure 35. Oct 850 hPa geopotential heights (GPHs, m): (a) long-term mean (LTM); (b) composite of the eight coldest years for the Korean study region during the 1970–2012 study period; and (c) anomaly for the eight coldest years. Note the positive (negative) height anomalies over northern Russia (North Pacific, especially in the Aleutian Low region).

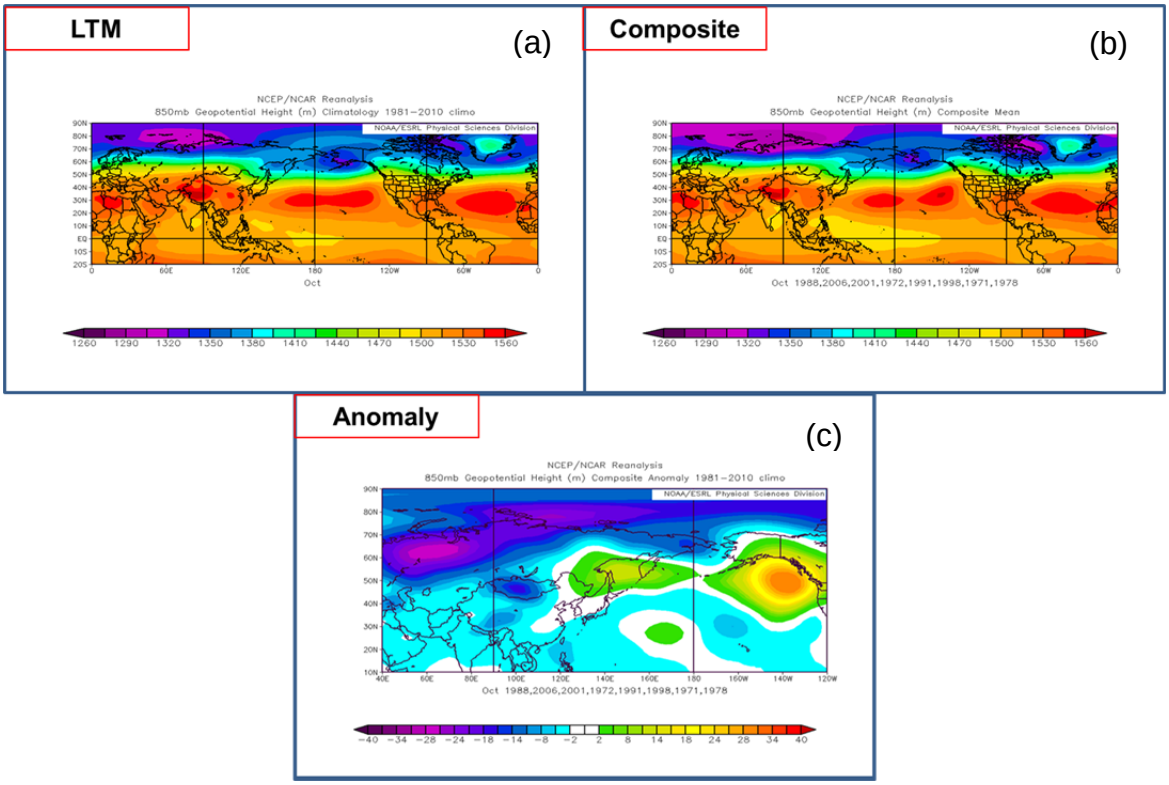


Figure 36. Oct 850 hPa geopotential heights (GPHs, m): (a) long-term mean (LTM); (b) composite of the eight warmest years for the Korean study region during the 1970–2012 study period; and (c) anomaly for the eight warmest years. Note the negative (positive) height anomalies over northern Russia (North Pacific, especially in the Aleutian Low region).

The results in Figures 35–36 led us to investigate the correlations of Oct 850 hPa GPH with Jan Korean surface air temperatures. Figure 37 shows those correlations. The highest correlations are over northern Russia and in the Aleutian Low region, consistent with the results in Figures 35-36. We used these correlation results to develop a potential three month lead KTI predictor based on the Oct 850 hPa GPH in these two regions (see black boxes in Figure 36), which we designated as KTI_JAN3. We defined KTI_JAN3 as the Oct area average 850 hPa GPH for the box south of Alaska minus that for the box over northern Russia (Figure 37). Note that the locations of these predictor boxes are similar to the locations of the northern Russia and North Pacific height anomalies for Octs preceding cold and warm Jans (Figures 35-36). We also investigated the

corresponding two month lead based on correlation results like those in Figure 3 but for Nov GPHs. However, we chose to use the Oct KTI (i.e., KTI_JAN3) rather than the Nov KTI (i.e., KTI_JAN2) because the correlations were higher than those at a two-month lead time.

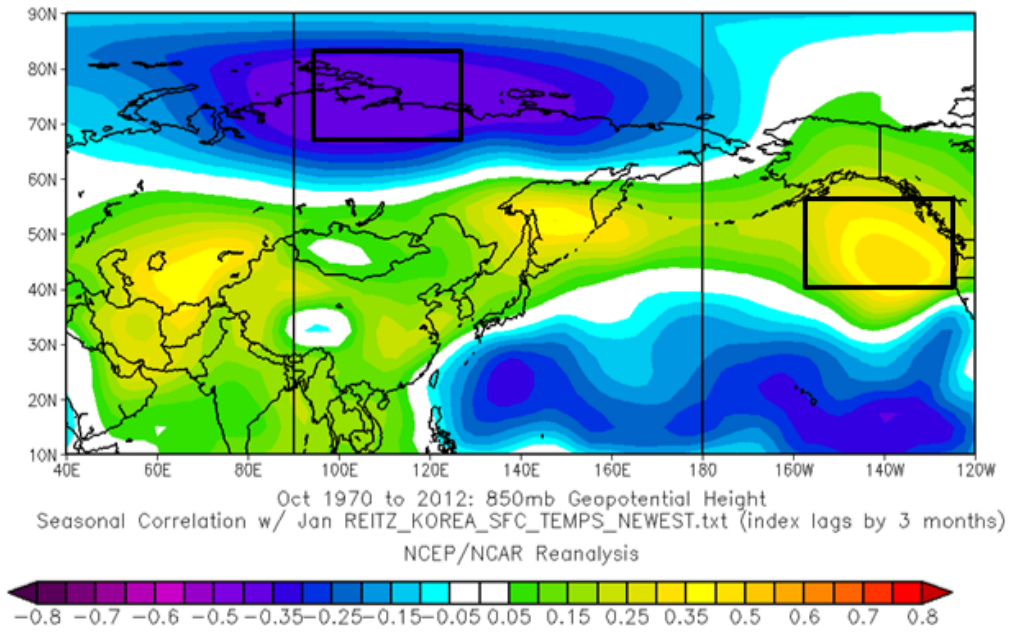


Figure 37. Correlation of 850 hPa geopotential heights (GPHs) for Oct with Jan surface air temperatures in the Korea region during 1970–2012 (heights leading by three months). Correlations greater than 0.256 are statistically significant with 95% confidence. The black boxes mark the areas with the highest positive and negative correlations, which are the areas used to construct the Jan KTI. KTI_JAN3 is defined as the average 850 hPa GPH from the box south of AK minus the corresponding GPH in the box in northern Russia. KTI_JAN3 was developed with a three month lead time, since the correlations were higher than for the corresponding KTI at a two month lead time. KTI_JAN3 was used in the final multiple linear regression (MLR) model for Jan temperatures.

Figure 38 shows Jan global surface temperatures correlated with KTI_JAN3. Remember that for 43 years of data, correlations of 0.257 or higher are considered statistically significant with 95% confidence. The high correlation over Korea (over 0.6) indicates that the KTI_JAN3 may be a good predictor for

Jan Korean surface temperatures. Note that the area of positive correlation centered over Korea extends eastward-southeastward over Japan, indicating that the KTI_JAN3 may also be a good predictor of Jan surface temperatures in Japan.

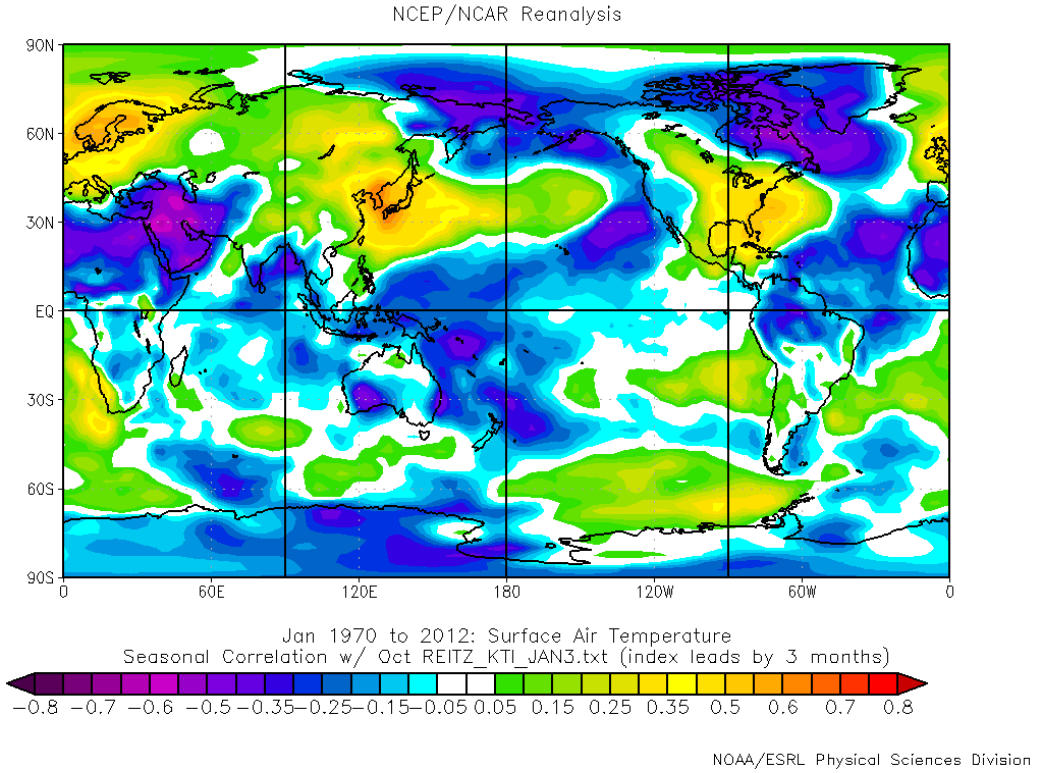


Figure 38. Correlation of the Oct Korean temperature index (KTI_JAN3) with Jan surface temperatures during 1970–2012 (KTI_JAN3 leading by three months). Correlations greater than 0.256 are statistically significant with 95% confidence. The high correlation over Korea (over 0.6) indicates that the KTI_JAN3 may be a good predictor for Jan Korean surface temperatures. Note that the area of positive correlation centered over Korea extends eastward-southeastward over Japan, indicating that the KTI_JAN3 may also be a good predictor of Jan surface temperatures in Japan.

Based on these KTI results, we chose KTI_JAN3 as one of the potential predictors for Jan Korean temperature. After conducting multiple MLR model trials process (Chapter II, Section C.2.c), we selected KTI_JAN3 as one of the

three predictors for the final MLR model for Jan temperature, along with the NAO and persistence (as summarized in Table 4 and discussed later in this section). Note that the correlation patterns that led to the development of KTI_JAN3 (Figure 37) resemble those associated with the AO and WP (see Chapter I, sections C.2, C.5). Thus, KTI_JAN3 may be a proxy for the AO and WP that focuses on the features of the AO and WP that are most related to Jan Korean temperature variations. If so, then this may explain why the AO and WP indices, which we all tested as potential predictors for Jan Korean temperature, did not survive our MLR model trials (i.e., due to multi-colinearity). Also note that the KTIs for Feb and Mar were similar to the KTI for Jan (KTI_JAN3), and also resembled the AO and WP patterns (see Appendix A).

The Nov NAO was chosen as a predictor for Jan Korean surface temperatures through our MLR model trial process (Chapter II, Section C.2.c). Figure 39 shows the correlation of the Nov NAO index with Jan global surface temperatures. The correlations over Korea were relatively high (around 0.35). and extended westward over much of eastern China and southward and eastward over southern Japan and nearby ocean regions. This indicates that the Nov NAO may also be a good predictor of Jan surface temperatures in a much larger region surrounding Korea. Also note that the correlation pattern in: (1) the tropical Pacific resembles patterns associated with ENLN, suggesting that there may be substantial overlap between the NAO and MEI potential predictors. If so, this may explain why the NAO survived as a predictor for Jan Korean temperatures but the MEI did not (cf. Li and Lau 2011). Note also that the correlation pattern in the North Atlantic resembles the quadripole pattern associated with the NAO (Murphree 2012c).

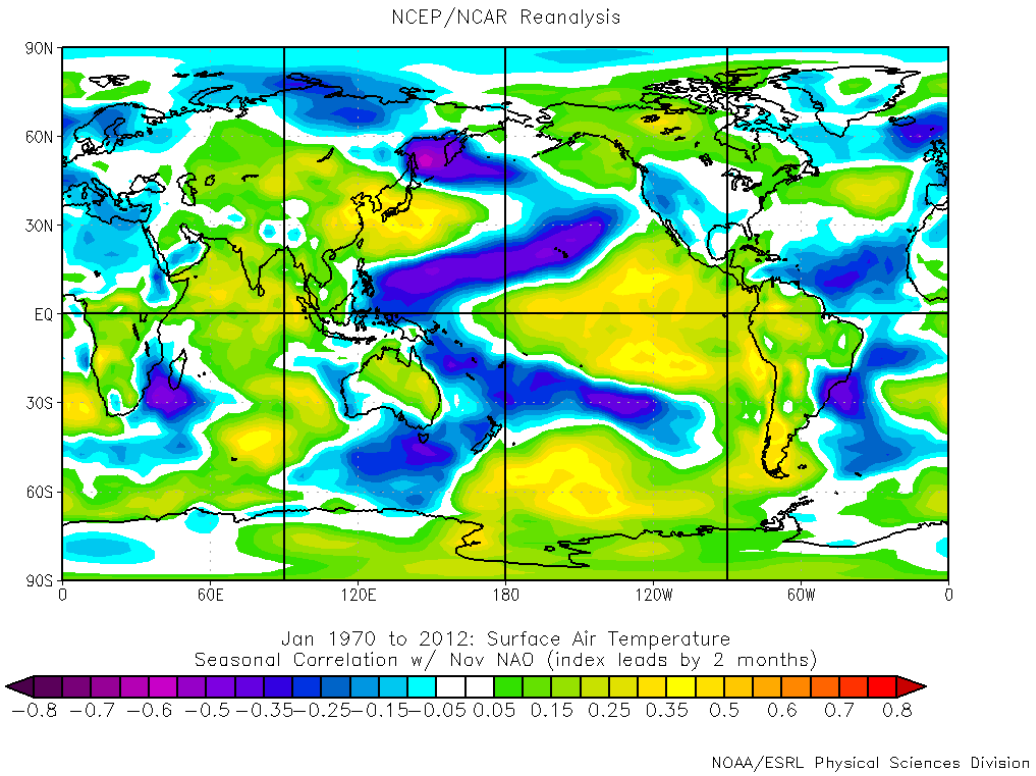


Figure 39. Correlation of the Nov North Atlantic Oscillation (NAO) index with Jan global surface temperatures (NAO leading by two months) during 1970–2012. For 43 years of data, correlations of 0.257 or higher are considered statistically significant with 95% confidence.

Persistence from Oct was evaluated as a predictor for Jan Korean surface temperatures through our MLR model trials process. For the definition of persistence that we used for this study, see Chapter II, Section B. Figure 40 shows Oct global surface temperatures correlated with Jan Korean surface temperatures. Note the relatively high correlations over Korea (around 0.35) and the general resemblance to the corresponding correlations with the NAO index (Figure 39). Persistence showed high potential as a predictor of Korean surface air temperature for nearly every month, especially the winter months. Persistence with a one month LT generally had the best results for each month, but was not considered due to minimum LT requirement of two-month for our study.

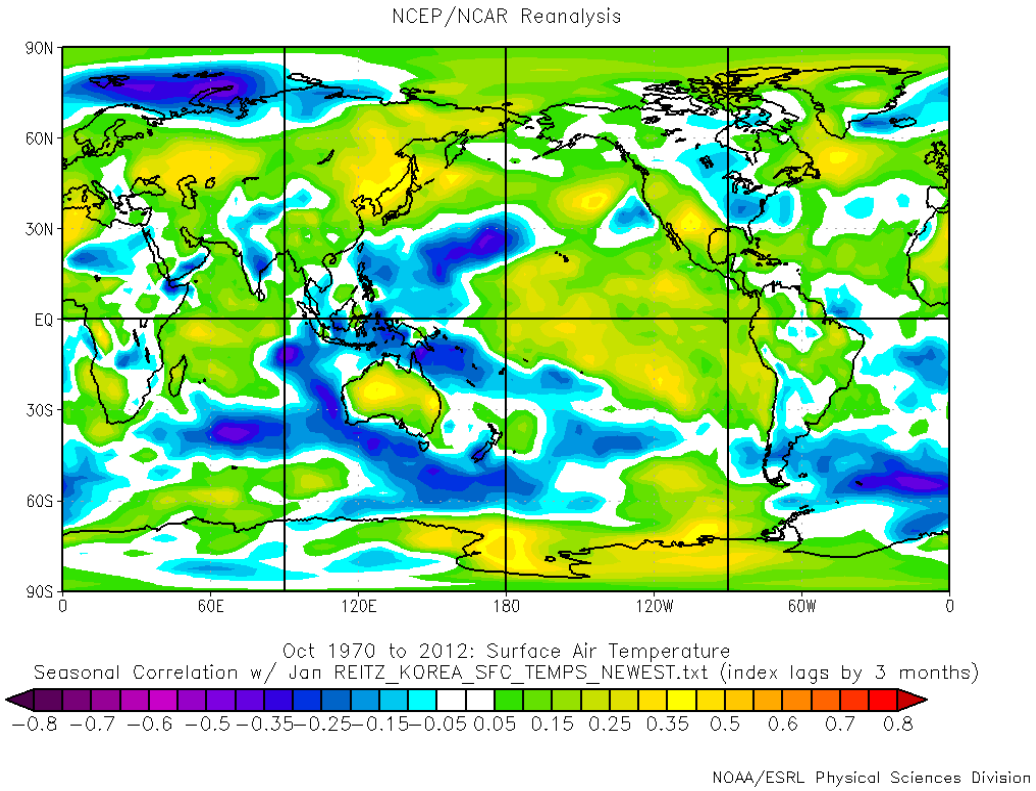


Figure 40. Correlation of Oct global surface temperatures with Jan Korean surface air temperatures for 1970-2012 (global temperatures leading by three months). For 43 years of data, correlations of 0.257 or higher are considered statistically significant with 95% confidence. These results indicate the potential for using persistence from Oct as a predictor of Jan Korean surface air temperatures.

We investigated the correlations of Nov 850 hPa GPH with Jan Korean PR. Figure 41 shows those correlations. The highest correlations are over the Gulf of Alaska and in the central North Pacific. We used these correlation results to develop a potential two month lead KPI predictor based on the Nov 850 hPa GPH in these two regions (see black boxes in Figure 41), which we designated as KPI_JAN2. We defined KPI_JAN2 as the Nov area average 850 hPa GPH for the southern box minus that in the northern box (Figure 41).

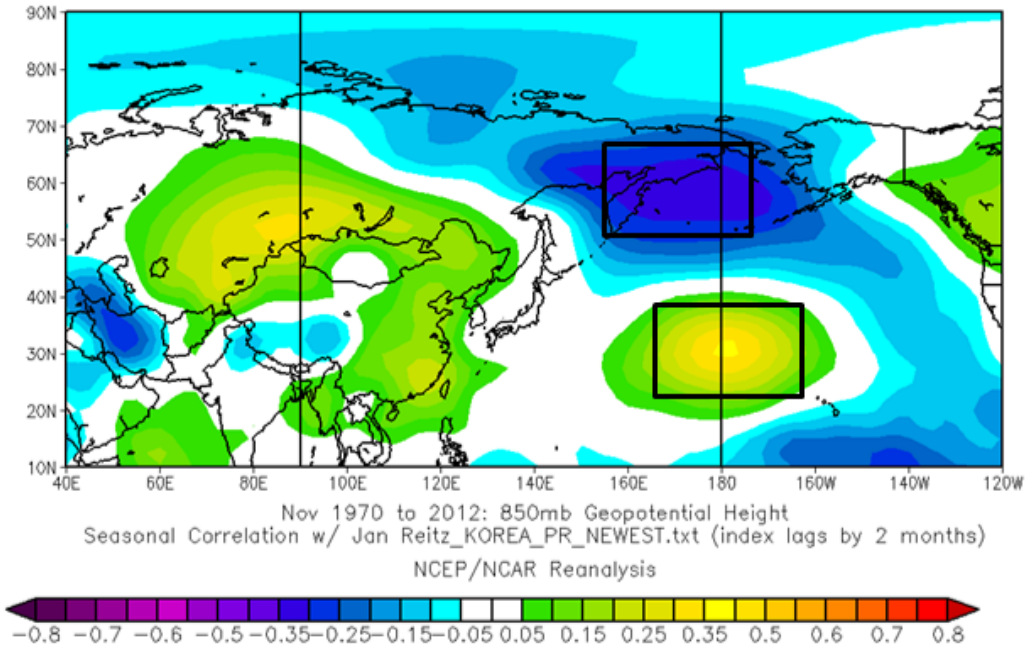


Figure 41. Correlation of 850 hPa geopotential heights (GPHs) for Nov with Jan precipitation rate (PR) in the Korea region during 1970–2012. Correlations greater than 0.256 are statistically significant with 95% confidence. The black boxes mark the areas with the highest positive and negative correlations, which are the areas used to construct the Jan KPI. KPI_JAN2 is defined as the average 850 hPa GPH from the box southern box minus that in the northern box. This KPI was designed for a 2 month lead time. KPI was used in the final multiple linear regression (MLR) for Jan PR.

Figure 42 shows Jan global PRs correlated with KPI_JAN2. The high correlation over Korea (over 0.3) indicates that the KPI_JAN2 may be a good predictor for Jan Korean PR. KPI_JAN2 resembles the PNA pattern and to a lesser extent MEI, which may explain why PNA and MEI did not survive our MLR analysis due to multi-colinearity.

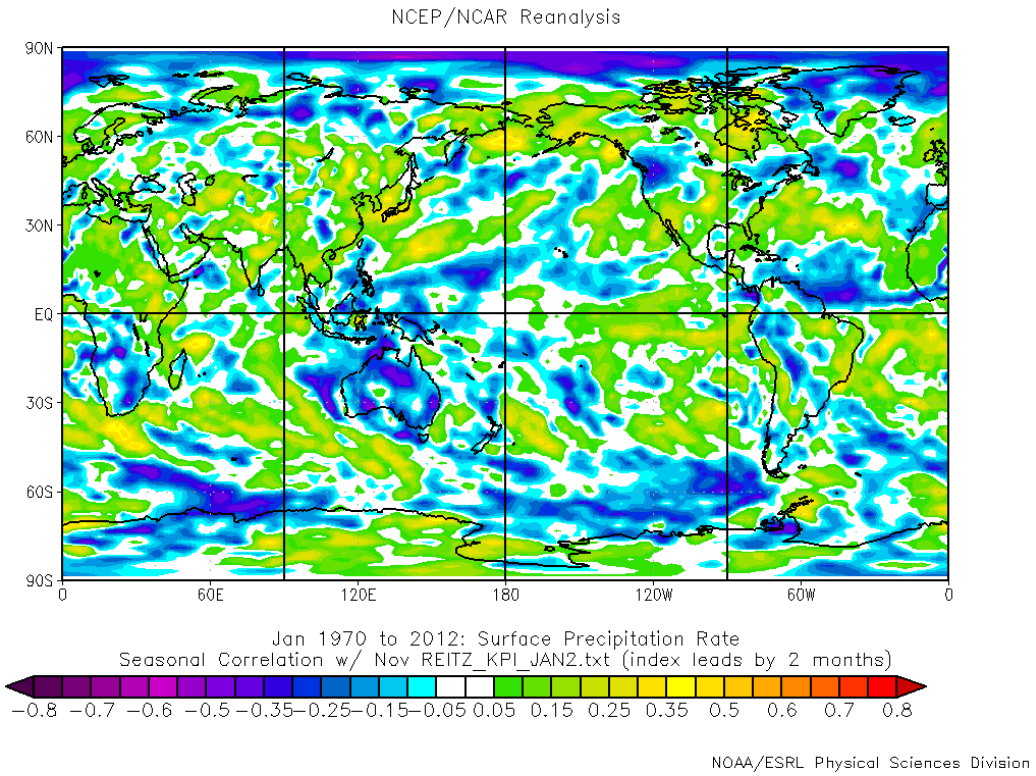


Figure 42. Correlation of Jan precipitation rate (PR) with the Nov Korean precipitation index (KPI_JAN2) during 1970–2012. For 43 years of data, correlations of 0.257 or higher are considered statistically significant with 95% confidence. There are significant correlation values (around 0.3) over Korea.

Based on these KPI results, we chose KPI_JAN2 as one of the potential predictors for Jan Korean PR. After conducting multiple MLR model trials process (Chapter II, Section C.2.c), we selected KPI_JAN2 as one of the two predictors for the final MLR model for Jan PR, along with SST_PJAN3 (as summarized in Table 5 and discussed later in this section). Note that the correlation patterns that led to the development of KPI_JAN2 (Figure 42) resemble those associated with the PNA and MEI (see Chapter I, Sections C.2, C.5). Thus, KTI_JAN3 may be a proxy for the PNA and MEI that focuses on the features of the PNA and MEI that are most related to Jan Korean PR variations. If so, then this may explain why the PNA and MEI indices, which we all tested as potential predictors for Jan Korean PR, did not survive our MLR model trials (i.e., due to multi-colinearity).

SST_PJAN3 was chosen as a predictor for Jan Korean PR through our MLR model trial process (Chapter II, Section C.2.c). Figure 43 shows the correlation of Oct SSTs with Jan Korean PR. Although it is very far from Korea, the Caribbean Sea region was chosen since there were no highly correlated regions closer. For some predictor regions (such as this one), we were unable to explain the physical plausibility. SST_PJAN3 was developed with a three month lead time, since the correlations were higher than those at a two-month lead time.

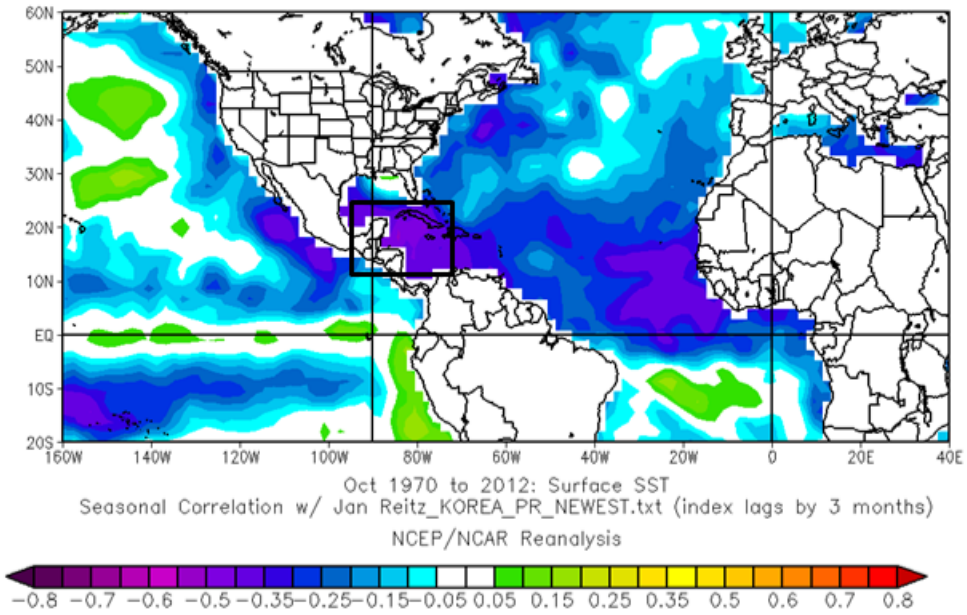


Figure 43. Correlation of Oct sea surface temperatures (SST) with Jan Korean precipitation rate (PR) during 1970–2012. Correlations greater than 0.256 are statistically significant with 95% confidence. This area in the Gulf of Mexico was selected because it has a higher correlation than anywhere else in the world. This variable is defined as SST_PJAN3, since it can be obtained with a three month lead time. SST was used in the final multiple linear regression (MLR) for Jan precipitation rate (PR).

Figure 44 compares the hindcasting results for Jan Korean temperature anomalies with the corresponding observed anomalies for 1970–2012. The hindcasts and the observations have a correlation of 0.73 with each other. Note

that most of the coldest and warmest extremes are represented in the hindcasts, although the hindcasted amplitudes were generally lower than those in the observations. With only a few exceptions, the model predicted temperatures equally well throughout the 43 year study period. This suggests that the OCN approach probably would not have added much skill to the hindcasts and that the model used in the hindcasting is likely to be skillful in future forecasting, barring significant climate regime shifts (e.g., those associated with global climate change). The corresponding results for the winter months (Dec-Feb) were similar to those shown in Figure 44; in particular, all showed a high correlation between the hindcasts and observations (see Appendix B).

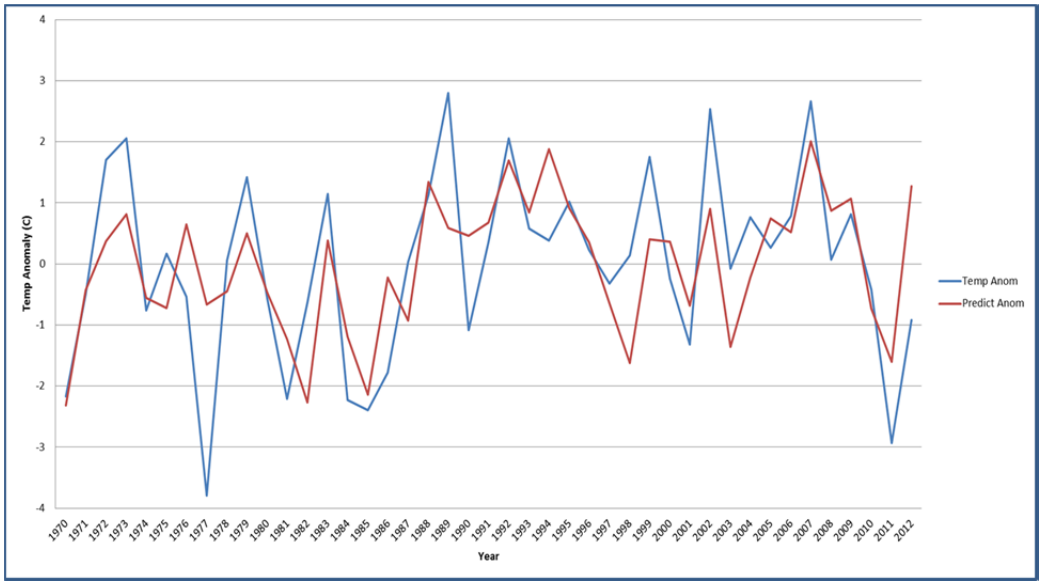


Figure 44. Comparison of Jan Korean surface air temperature anomaly hindcasts (red) and the corresponding observed anomalies (blue) for 1970–2012. The two time series have a relatively high correlation with each other of 0.73. Note that most of the coldest and warmest extremes were represented in the hindcasts, although generally with less amplitude than observed.

Figure 45 compares the hindcasting results for Jan Korean PR anomalies with the corresponding observed anomalies for 1970–2012. The hindcasts and the observations have a correlation of 0.54 with each other. Note that most of the

driest and wettest extremes are represented in the hindcasts, although the hindcasted amplitudes were generally lower than those in the observations. The correlation of 0.54 is statistically significant with 95% confidence, but note that the model has missed extremes in 1972 and 2001. Results for the fall and winter months (Oct-Feb) were the best for the year. In fact Jan was the poorest performing month in that period. Jan is, on average, the driest month of the year (and the winter is the driest season). This means that a rare big Jan storm that may be missed by our LRF model (such as in 1972 and 2001) could lead to significant misses in the forecast.

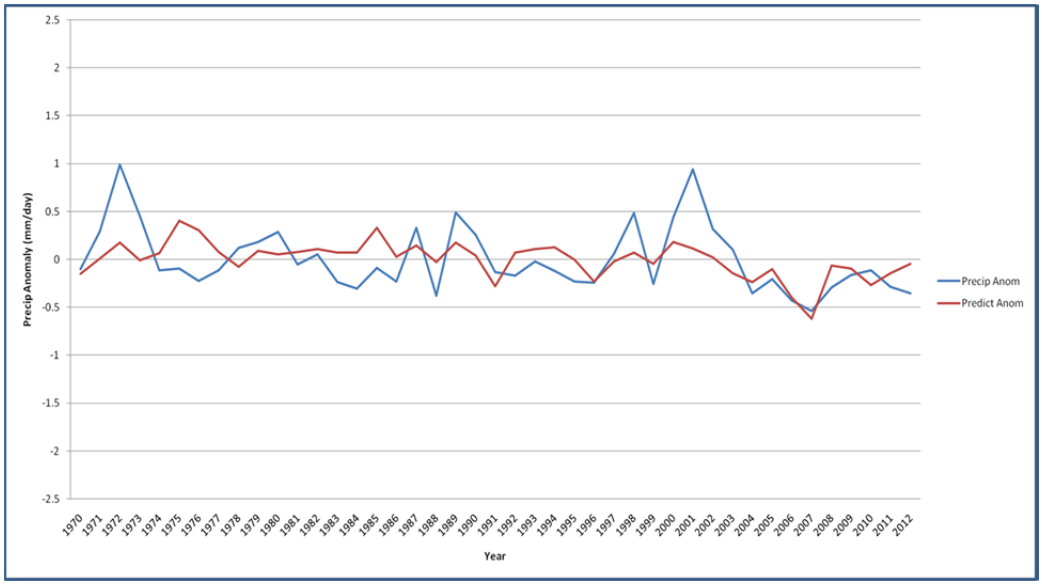


Figure 45. Comparison of Jan Korean precipitation rate (PR) anomaly hindcasts (red) and the corresponding observed anomalies (blue) for 1970–2012. The two time series have a relatively high correlation with each other of 0.54. Note that most of the driest and wettest extremes were represented in the hindcasts, although generally with less amplitude than observed.

## 2. April

Our MLR analysis was done the same way for Feb-Dec as it was for Jan. Our MLR model trials process led us to select these two predictor inputs for Apr Korean surface temperature: KTI_APR2 and SST_TAPR2. KTI_APR2 is defined

as the area average 850 hPa GPH from the box in eastern North America (Figure 46). We selected this single region for the Apr KTI, since it was the only area where the 850 hPa GPH from Feb was highly correlated with Apr temperatures in Korea. The eastern North American/Atlantic selection for KTI is unique for the months of Apr and Nov. This pattern for Apr and Nov resembles the AO and NAO climate oscillations and is possibly the reason that AO and NAO did not survive the MLR analysis (due to multi-colinearity) for either month. SST_TAPR2 is defined as the average SST from the box in eastern Pacific Ocean (Figure 47). This SST pattern shows a slight resemblance to ENLN.

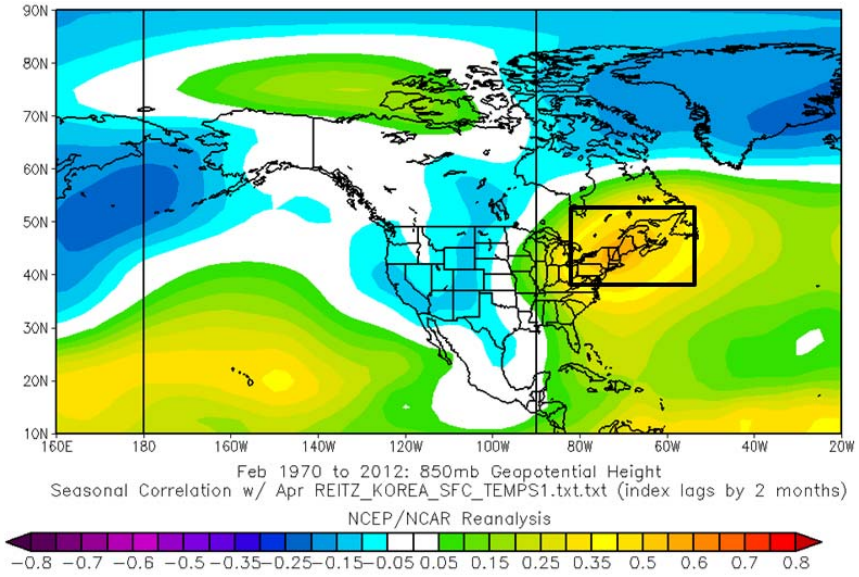


Figure 46. Correlation of 850 hPa geopotential heights (GPHs) for Feb with Apr surface air temperatures in Korea region during 1970–2012. Correlations greater than 0.256 are statistically significant with 95% confidence. KTI_APR2 is defined as the average 850 hPa GPH from the box in eastern North America. KTI_APR2 was used in the final multiple linear regression (MLR) for Apr temperatures.

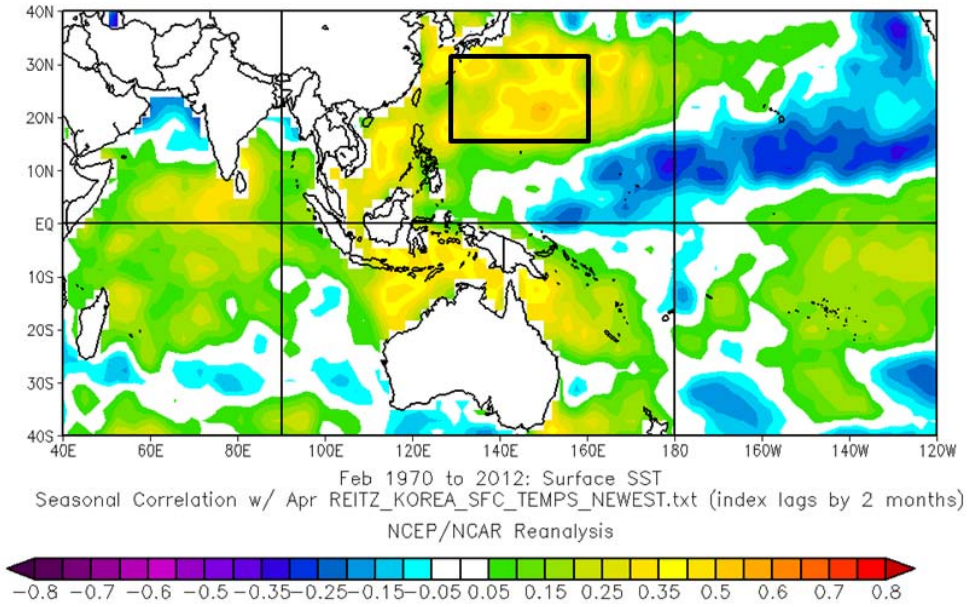


Figure 47. Correlation of Feb sea surface temperatures (SST) with Apr Korean temperatures during 1970–2012. Correlations greater than 0.256 are statistically significant with 95% confidence. This variable is defined as SST_TAPR2. SST_TAPR2 was used in the final multiple linear regression (MLR) for Jan precipitation rate (PR).

Our MLR model trials process led us to select these two predictor inputs for Apr Korean PR: KPI_APR2 and SST_PAPR2. KPI_APR2 is defined as the area average 850 hPa GPH from the southern box minus that in the northern box (Figure 48). The Apr KPI is calculated from a similar region as for Jan and resembles the PNA teleconnection pattern. This may explain why PNA did not survive our MLR analysis for PR (due to multi-colinearity). SST_PAPR4 is defined as the average SST from the box in western Pacific Ocean (Figure 49). SST_PAPR4 resembles ENLN as this may explain why MEI did not survive our MLR analysis for PR (due to multi-colinearity). The following months have SST predictor areas that resemble ENLN: Feb, Apr, May, Jun, Jul, Aug, Sep, and Dec.

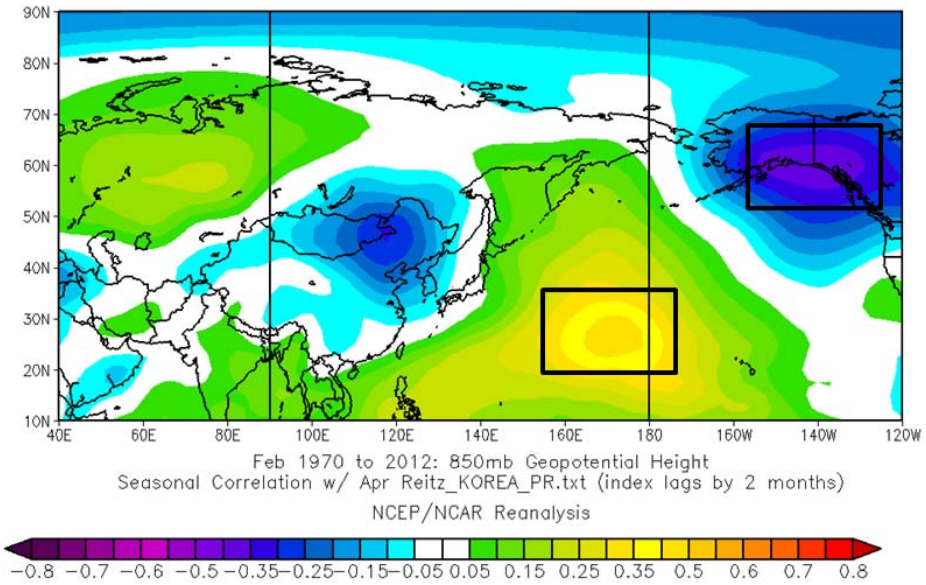


Figure 48. Correlation of 850 hPa geopotential heights (GPHs) for Feb with Apr precipitation rate (PR) in Korea region during 1970–2012. Correlations greater than 0.256 are statistically significant with 95% confidence. The black boxes mark the areas with the highest positive and negative correlations, which are the areas used to construct the Apr KPI. KPI_APR2 is defined as the average 850 hPa GPH from the box southern box minus that in the northern box. KPI_APR2 was used in the final multiple linear regression (MLR) for Apr PR.

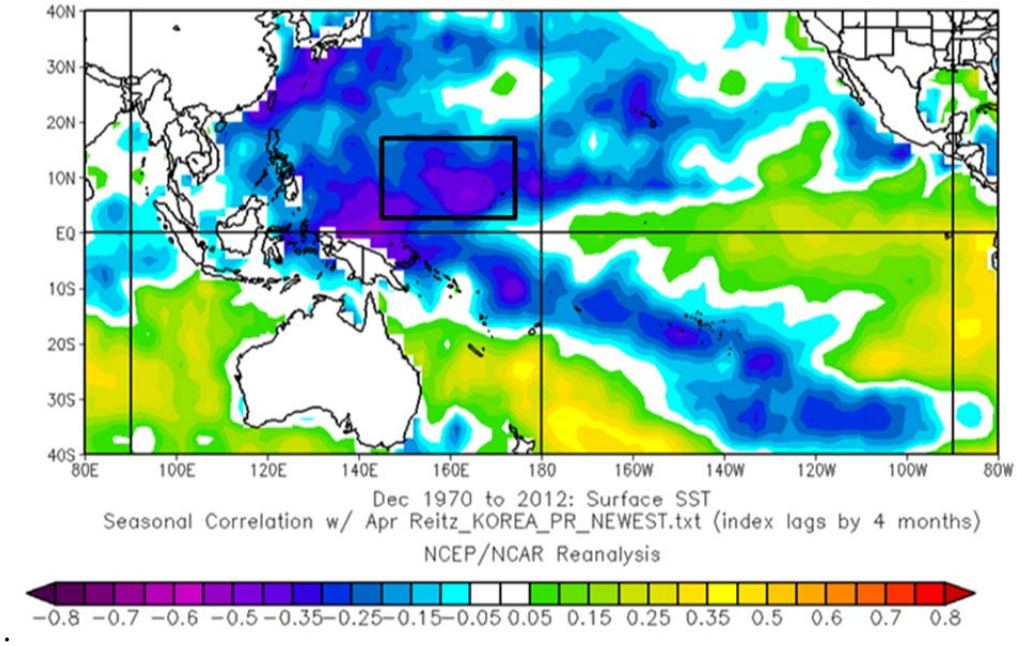


Figure 49. Correlation of Dec sea surface temperatures (SST) with Apr Korean precipitation rate (PR) during 1970–2012. Correlations greater than 0.256 are statistically significant with 95% confidence. This variable is defined as SST_PAPR4. SST_PAPR4 was used in the final multiple linear regression (MLR) for Jan precipitation rate (PR).

Figure 50 compares the hindcasting results for Apr Korean temperature anomalies with the corresponding observed anomalies for 1970–2012. Note the high correlation of 0.66 and that most of the coldest and warmest extremes are represented in the hindcasts. With only a few exceptions, the model predicted temperatures equally well throughout the 43 year study period. This means that the OCN approach would not have added much value here and that this model should continue being successful for future forecasts barring significant impacts due to climate change.

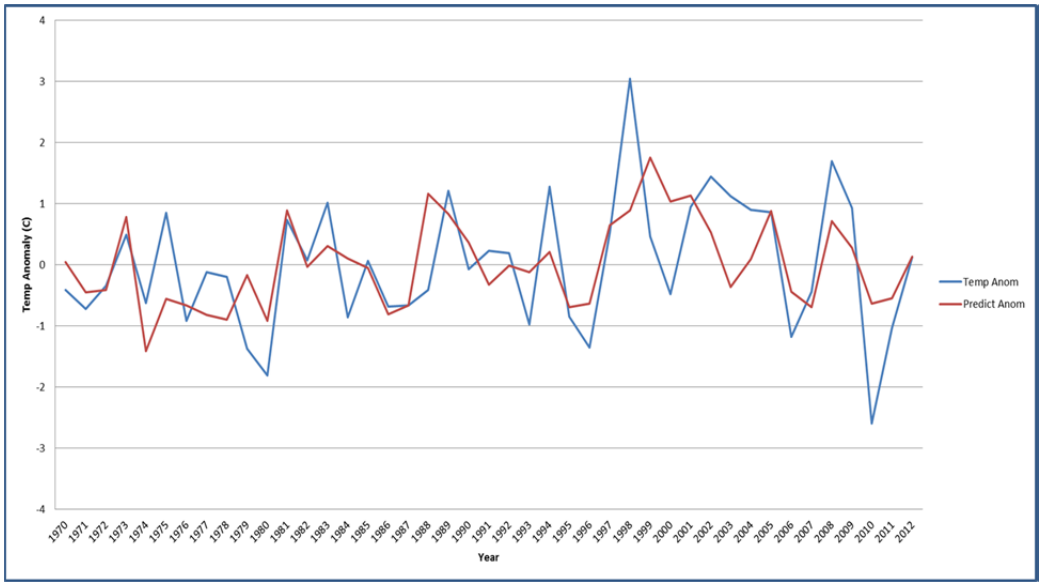


Figure 50. Comparison of Apr Korean surface air temperature anomaly hindcasts (red) and the corresponding observed anomalies (blue) for 1970–2012. The two time series have a relatively high correlation with each other of 0.66. Note that most of the coldest and warmest extremes were represented in the hindcasts, although generally with less amplitude than observed.

Figure 51 compares the hindcasting results for Apr Korean PR anomalies with the corresponding observed anomalies for 1970–2012. The hindcasts and the observations have a correlation of 0.57 with each other, which is statistically significant with 95% confidence. The spring months (Mar-Jun) did not perform as well as the winter months. In fact, the Mar MLR model for PR was the poorest performing of all 12 months. The spring models most likely do not perform as well as the winter models due to the difficulty in predicting the transition season.

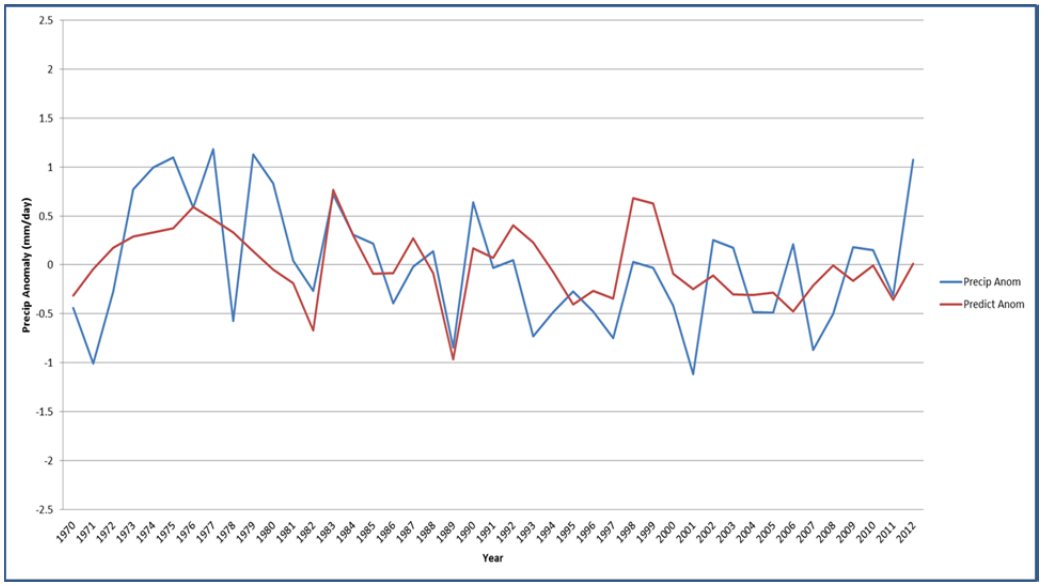


Figure 51. Comparison of Apr Korean precipitation rate (PR) anomaly hindcasts (red) and the corresponding observed anomalies (blue) for 1970–2012. The two time series have a relatively high correlation with each other of 0.57. Note that the model performed exceptionally well in the 1980s, and that the model's performance declinced since then.

### 3. July

Our MLR model trials process led us to select these two predictor inputs for Jul Korean surface temperature: PNA from Apr and SST_TJUL2. SST_TJUL2 is defined as the average SST from the box in western Pacific Ocean (Figure 52). This SST pattern shows a slight resemblance to ENLN. Figure 53 shows the correlation between Apr PNA and Jul global surface temperatures. Note the "bull's eye" of high negative correlation (around -0.40) over the Korean Peninsula. PNA was also used in the MLR model for Korean temperatures in Feb and Oct.

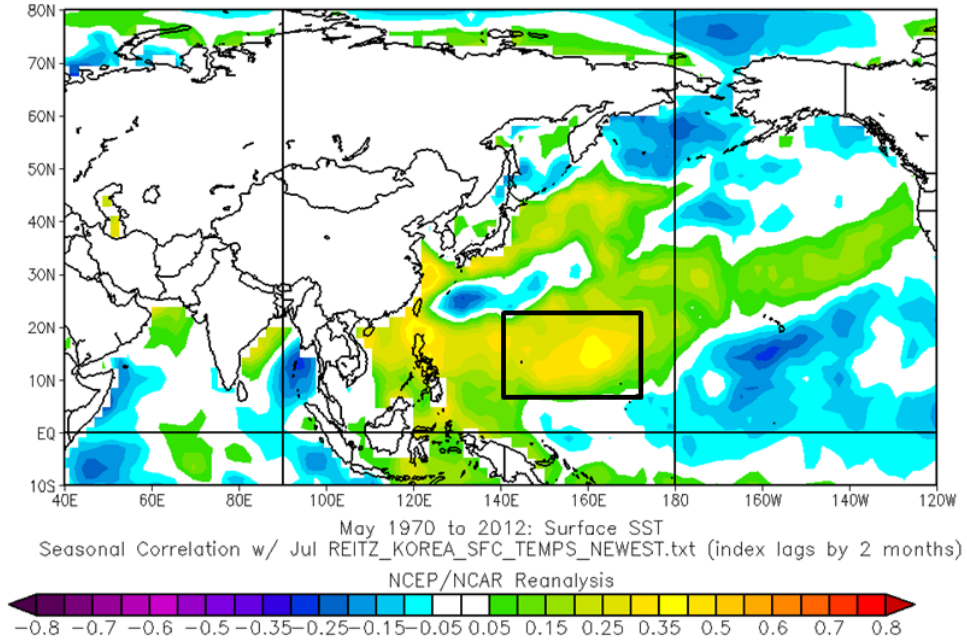


Figure 52. Correlation of May sea surface temperatures (SST) with Jul Korean temperatures during 1970–2012. Correlations greater than 0.256 are statistically significant with 95% confidence. This variable is defined as SST_TJUL2. SST_TJUL2 was used in the final multiple linear regression (MLR) model for Jul surface temperatures.

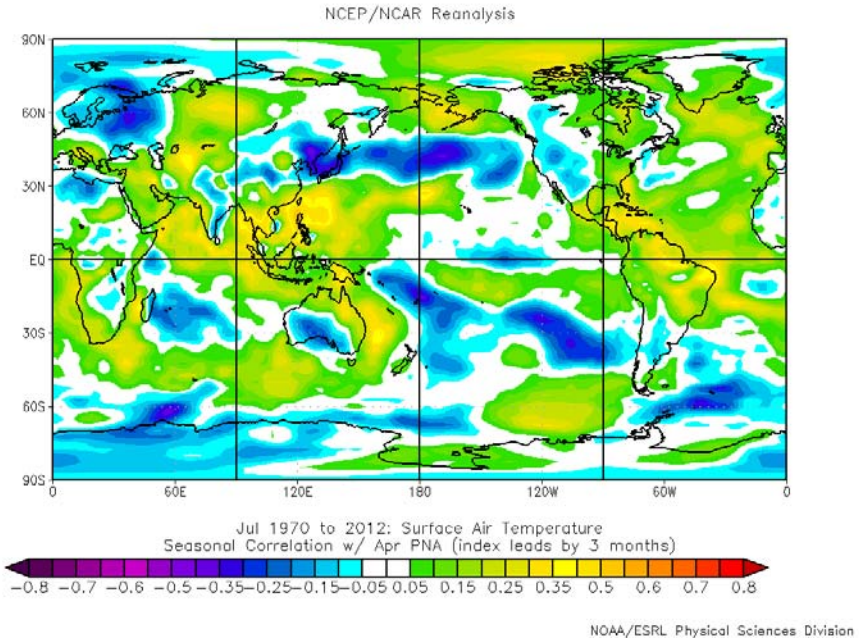


Figure 53. Correlation of Apr Pacific/North American Pattern (PNA) with Jul global surface temperatures (PNA leading temperature by three months). For 43 years of data, correlations of 0.257 or higher are considered statistically significant with 95% confidence. PNA was used in the final multiple linear regression (MLR) for Jul temperatures. Note the fairly high correlations over Korea (around -0.40).

Our MLR model trials process led us to select these two predictor inputs for Jul Korean PR: KPI_JUL2 and SST_TJUL2. KPI_JUL2 is defined as the area average 850 hPa GPH from the box in the South Atlantic Ocean (Figure 54). This KPI predictor region is unique to the month of Jul. SST_PJUL2 is defined as the average SST from the box in central Pacific Ocean (Figure 55). This SST pattern shows a slight resemblance to ENLN.

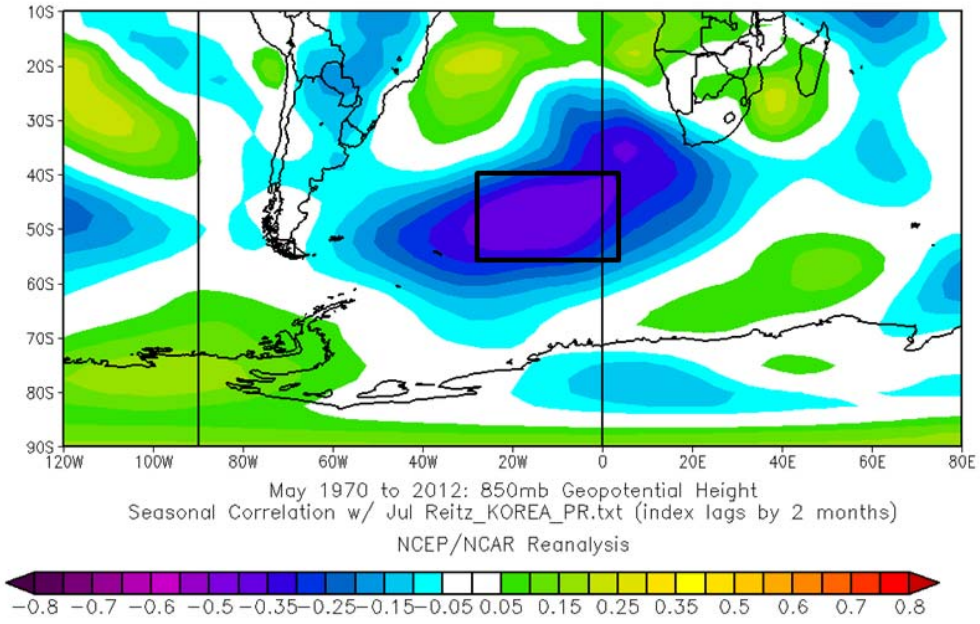


Figure 54. Correlation of 850 hPa geopotential heights (GPHs) for May with Jul precipitation rate (PR) in the Korea region during 1970–2012. Correlations greater than 0.256 are statistically significant with 95% confidence. KPI_JUL2 is defined as the average 850 hPa GPH from the box in the South Atlantic Ocean. KTI_JUL2 was used in the final multiple linear regression (MLR) for Apr PR.

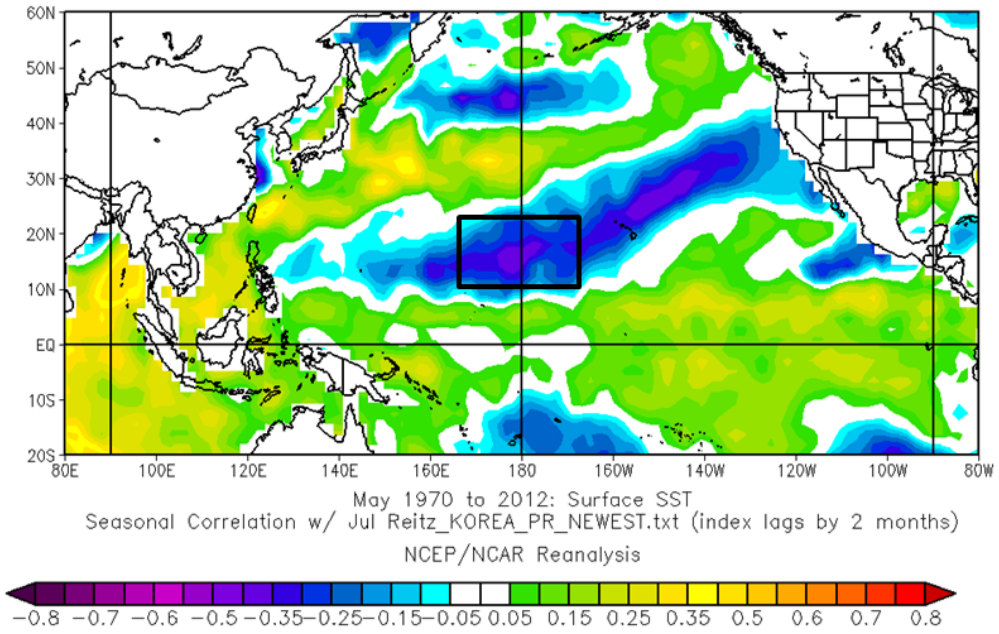


Figure 55. Correlation of May sea surface temperatures (SST) with Jul Korean precipitation rate (PR) during 1970–2012. Correlations greater than 0.256 are statistically significant with 95% confidence. This variable is defined as SST_PJUL2. SST_PJUL2 was used in the final multiple linear regression (MLR) model for Jul PR.

Figure 56 compares the hindcasting results for Jul Korean temperature anomalies with the corresponding observed anomalies for 1970–2012. Although still statistically significant, the MLR model for Jul is the worst performing month for temperature forecasts with a correlation of 0.45 between the hindcasts and observations. The model performed better in the second half of the study period. An OCN approach may have yielded a better model for Jul temperatures.

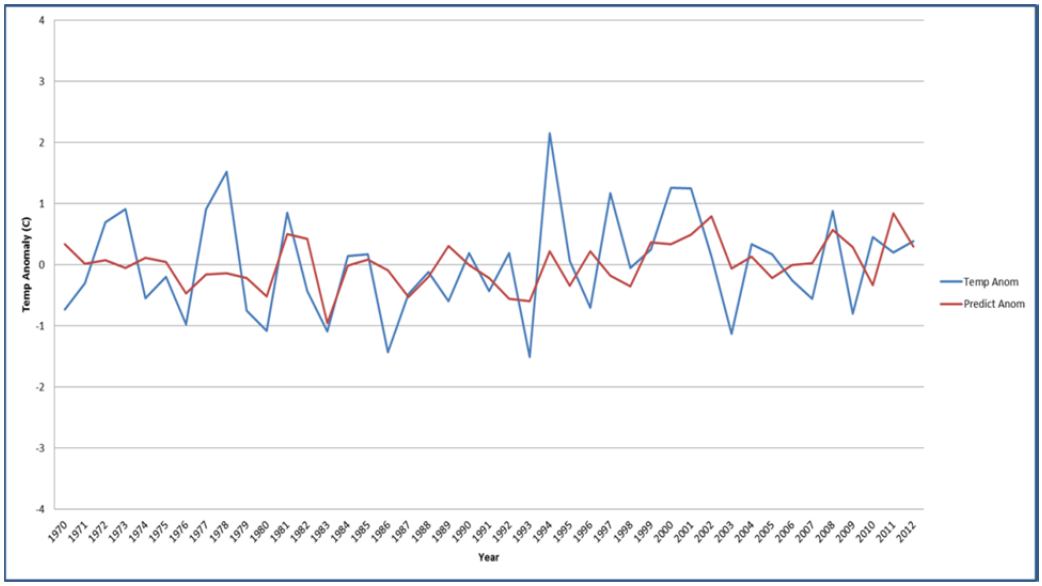


Figure 56. Comparison of Jul Korean temperature anomaly hindcasts (red) and the corresponding observed anomalies (blue) for 1970–2012. The two time series have a correlation to each other of 0.45. Although still statistically significant, the MLR model for Jul is the worst performing month for temperature forecasts. Note that most of the coldest and warmest extremes were represented in the hindcasts, although generally with less amplitude than observed.

Figure 57 compares the hindcasting results for Jul Korean PR anomalies with the corresponding observed anomalies for 1970–2012. The hindcasts and the observations have a correlation of 0.59 with each other, which is statistically significant with 95% confidence. The summer months (Jul-Sep) MLR PR models all performed well with correlations to the observed temperatures of between 0.51 and 0.60. It is encouraging to see positive results for this time period, since most of Korea's annual precipitation falls during the summer months.

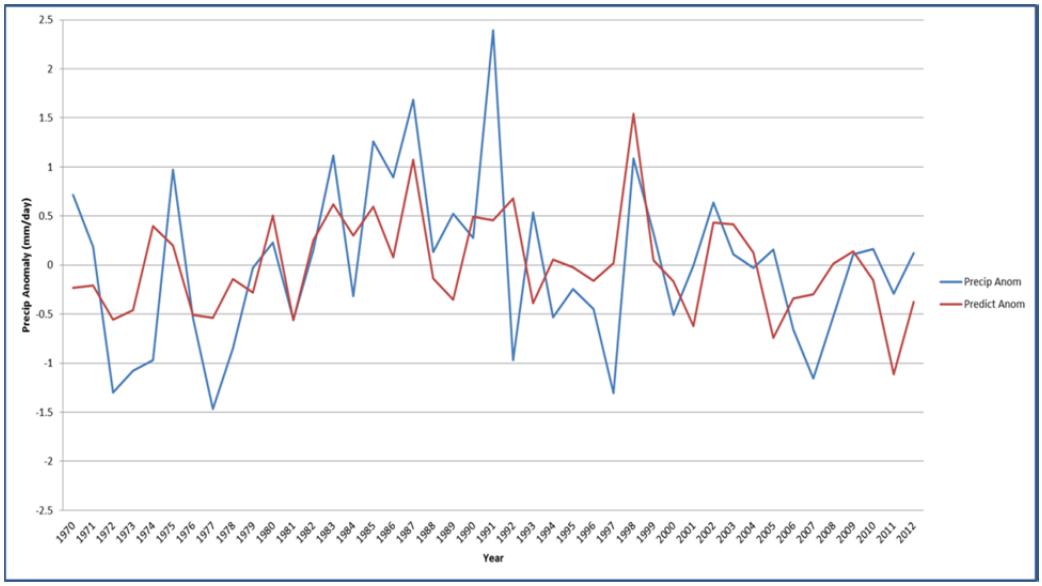


Figure 57. Comparison of Jul Korean precipitation rate (PR) anomaly hindcasts (red) and the corresponding observed anomalies (blue) for 1970–2012. The two time series have a relatively high correlation with each other of 0.59.

### 4. October

Our MLR model trials process led us to select these three predictor inputs for Oct Korean surface temperature: KTI_OCT_2, SST_TOCT2, and PNA from Aug. KTI_OCT2 is defined as the area average 850 hPa GPH from the box in the North Pacific minus the corresponding GPH in the box in the Gulf of AK (Figure 58). SST_OCT2 is defined as the average SST in the box near northern Japan (Figure 59). Figure 60 shows the correlation between Aug PNA and Oct global surface temperatures. Note the fairly high correlations over Korea (around 0.35). Also note that the area of positive correlation centered over Korea extends eastward over Southern Japan, indicating that the Aug PNA may also be a good predictor of Oct surface temperatures in Japan.

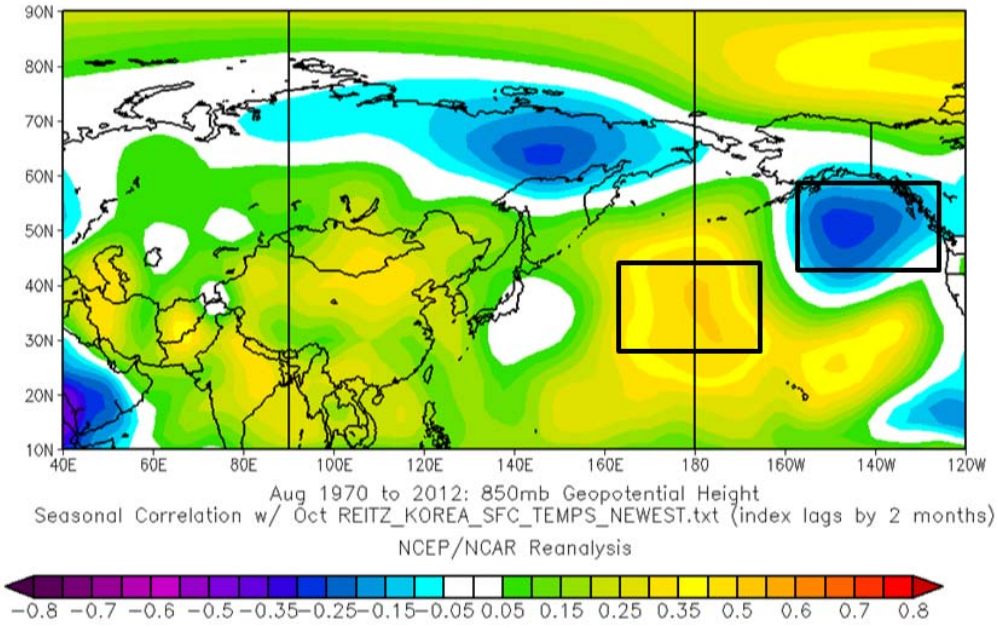


Figure 58. Correlation of 850 hPa geopotential heights (GPHs) for Aug with Oct surface air temperatures in Korea region during 1970–2012. Correlations greater than 0.256 are statistically significant with 95% confidence. The black boxes mark the areas with the highest positive and negative correlations, which are the areas used to construct the Oct KTI. KTI_OCT2 is defined as the average 850 hPa GPH from the box in the North Pacific minus the corresponding GPH in the box in the Gulf of AK. KTI_OCT2 was used in the final multiple linear regression (MLR) for Oct temperatures.

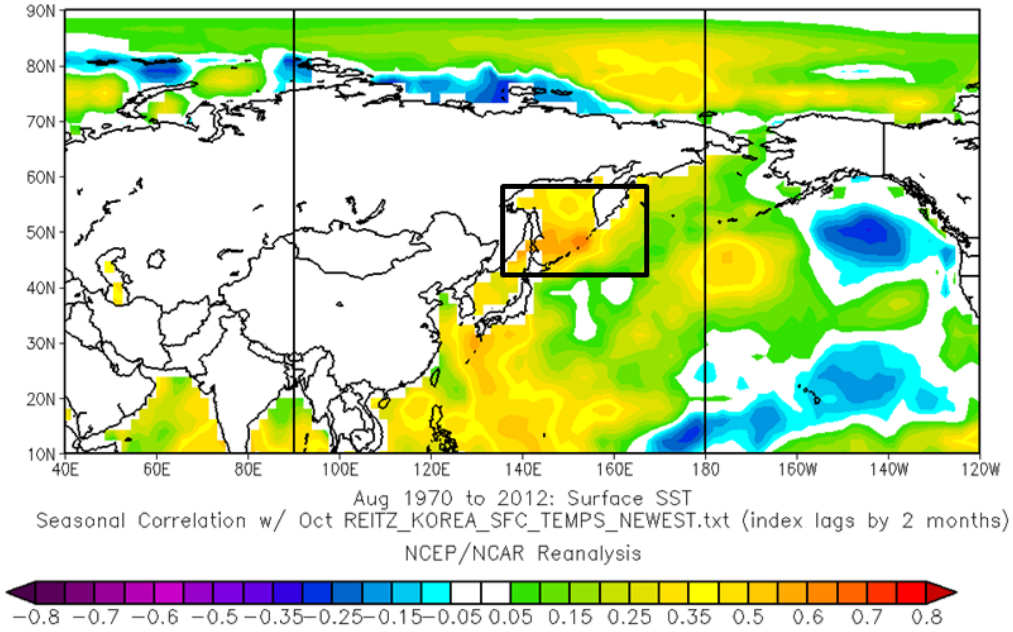


Figure 59. Correlation of Aug sea surface temperatures (SST) with Oct Korean temperatures during 1970–2012. Correlations greater than 0.256 are statistically significant with 95% confidence. The average SST in the black box is defined as SST_TOCT2. SST_TOCT2 was used in the final multiple linear regression (MLR) model for Jul surface temperatures.

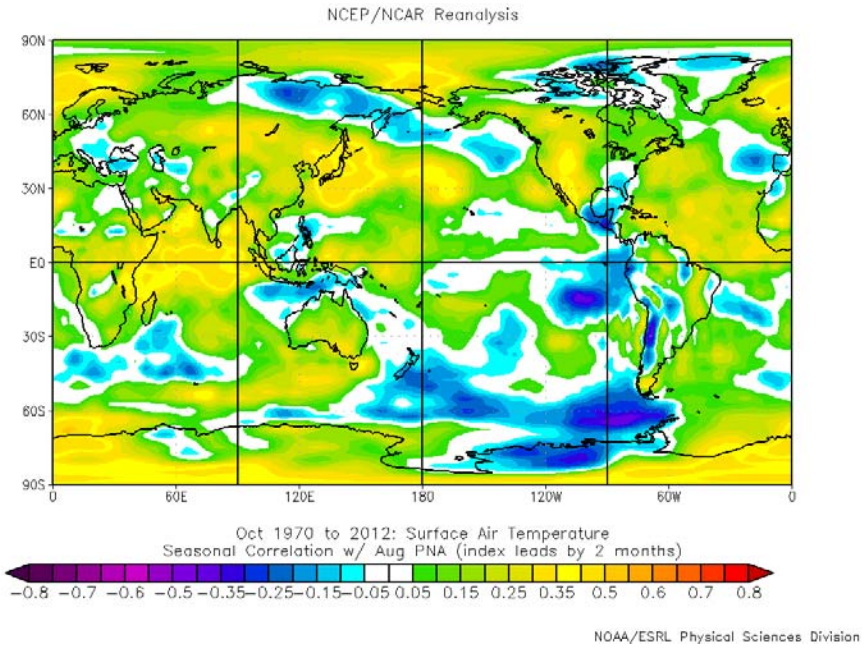


Figure 60. Correlation of Aug Pacific/North American Pattern (PNA) with Oct global surface temperatures (PNA leading temperature by three months). For 43 years of data, correlations of 0.257 or higher are considered statistically significant with 95% confidence. PNA was used in the final multiple linear regression (MLR) for Oct temperatures. Note the fairly high correlations over Korea (around 0.35).

Our MLR model trials process led us to select these three predictor inputs for Oct Korean PR: KPI_OCT2, SST_POCT2, and SST_POCT3. KPI_OCT2 is defined as the area average 850 hPa GPH from the box in eastern North America minus that in the box in the Arctic Ocean (Figure 61). SST_POCT2 is defined as the average SST from the box in the northern Pacific Ocean (Figure 62). SST_POCT3 is defined as the average SST from the box in the eastern Pacific Ocean (Figure 63). An exception was made for the Oct PR MLR model to include two SST predictor regions. The exception was made in order to improve the model's poor performance when only one of the SST predictor regions was used.

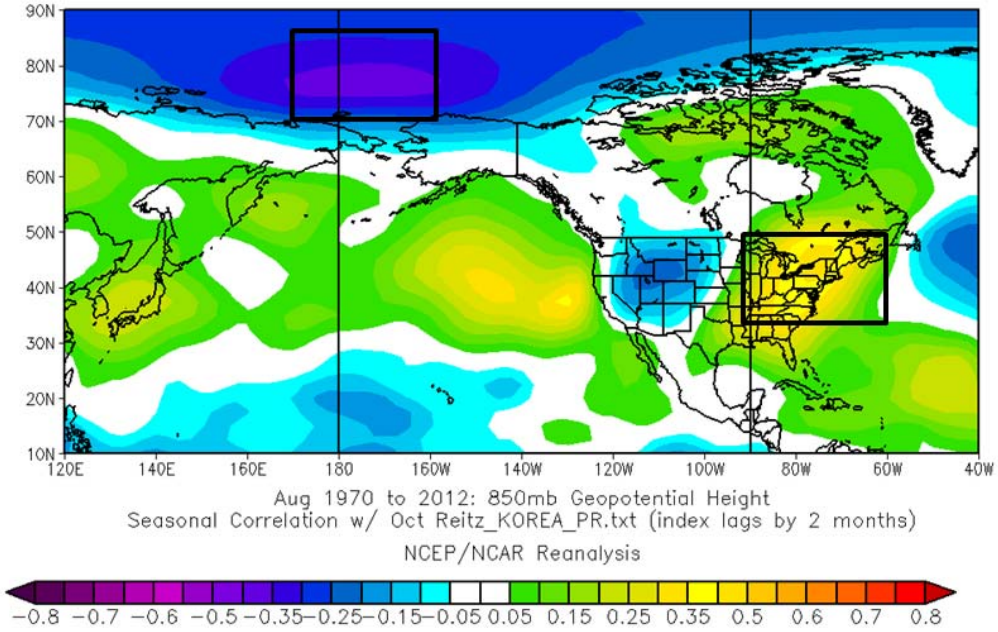


Figure 61. Correlation of 850 hPa geopotential heights (GPHs) for Aug with Oct precipitation rate (PR) in Korea region during 1970–2012. Correlations greater than 0.256 are statistically significant with 95% confidence. The black boxes mark the areas with the highest positive and negative correlations, which are the areas used to construct the Oct KPI. KPI_OCT2 is defined as the average 850 hPa GPH from the box in eastern North America minus that in the box in the Arctic Ocean. KPI_OCT2 was used in the final multiple linear regression (MLR) for Oct PR.

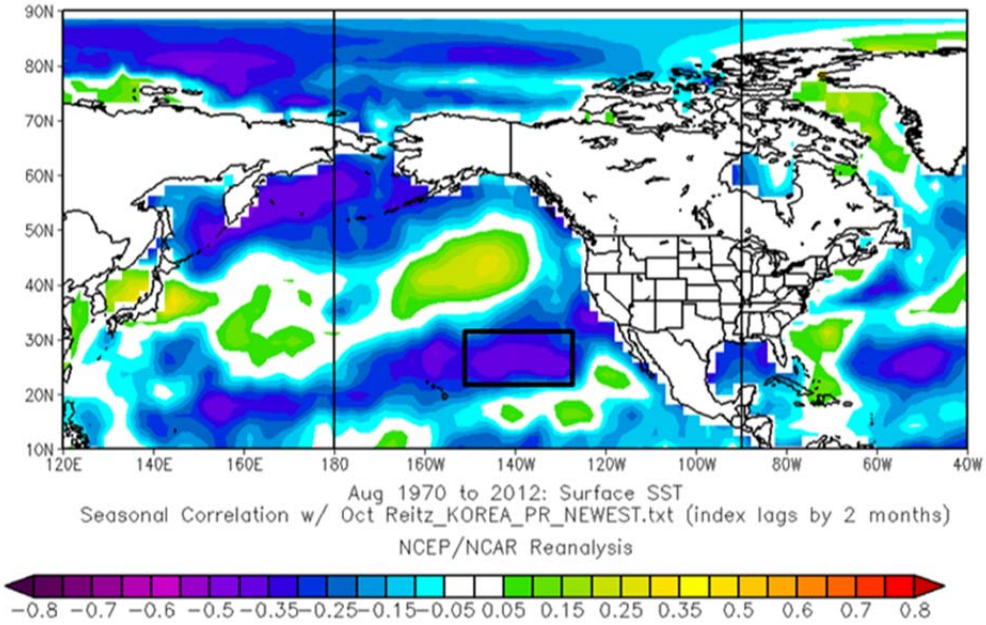


Figure 62. Correlation of Aug sea surface temperatures (SST) with Oct Korean precipitation rate (PR) during 1970–2012. Correlations greater than 0.256 are statistically significant with 95% confidence. Two SST areas were used as predictors for the month of Oct. This variable is defined as SST_POCT2. Both SST predictor regions (SST_POCT2 and SST_POCT3) were used in the final multiple linear regression (MLR) model for Oct PR.

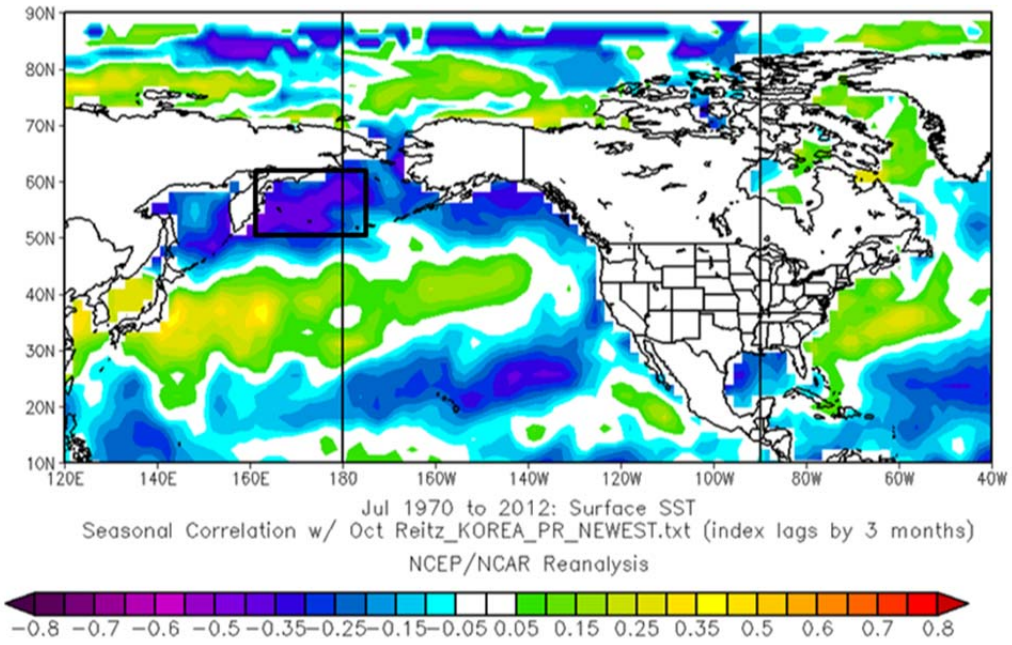


Figure 63. Correlation of Jul sea surface temperatures (SST) with Oct Korean precipitation rate (PR) during 1970–2012. Correlations greater than 0.256 are statistically significant with 95% confidence. Two SST areas were used as predictors for the month of Oct. This variable is defined as SST_POCT3. Both SST predictor regions (SST_POCT2 and SST_POCT3) were used in the final multiple linear regression (MLR) model for Oct PR.

Figure 64 shows the hindcasting results for Oct Korean temperature anomalies 1970–2012. The blue line is R1 reanalysis data for the Korean peninsula and represents the actual temperature. The red line is the hindcast for temperatures based on the MLR for Oct. Note the high correlation of 0.74 and that most of the coldest and warmest extremes are captured by the model. With only a few exceptions, the model predicted temperatures equally well throughout the 43-year study period. This means that the OCN approach would not have added much value here and that this model should continue being successful for future forecasts barring significant impacts due to climate change. Also note the overall positive trend in Oct temperatures from 1970–2012, indicating a long-term warming trend for the Korean Peninsula.

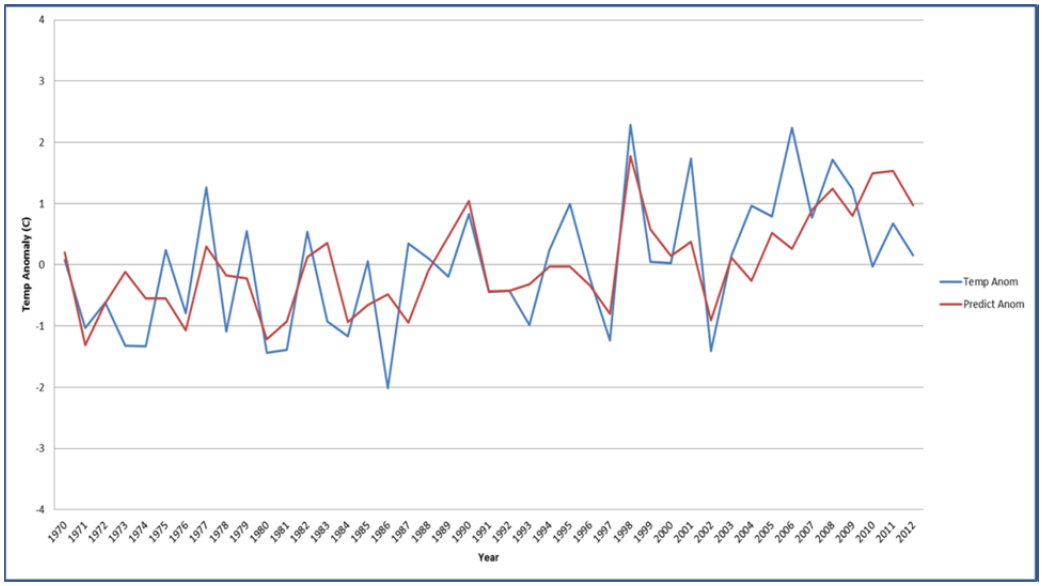


Figure 64. Comparison of Oct Korean temperature anomaly hindcasts (red) and the corresponding observed anomalies (blue) for 1970–2012. The two time series have a high correlation to each other of 0.74. Note that most of the coldest and warmest extremes were represented in the hindcasts. Also note the warming trend throughout the 43 year period.

Figure 65 shows the hindcasting results for Oct Korean PR anomalies 1970–2012. The blue line is R1 reanalysis data for the Korean peninsula and represents the actual PR. The red line is the hindcast for PR based on the MLR for Oct. The correlation of 0.63 is statistically significant with 95% confidence. The autumn months (Oct-Nov) MLR PR models all performed very well with correlations to actual PRs of between 0.63 and 0.70.

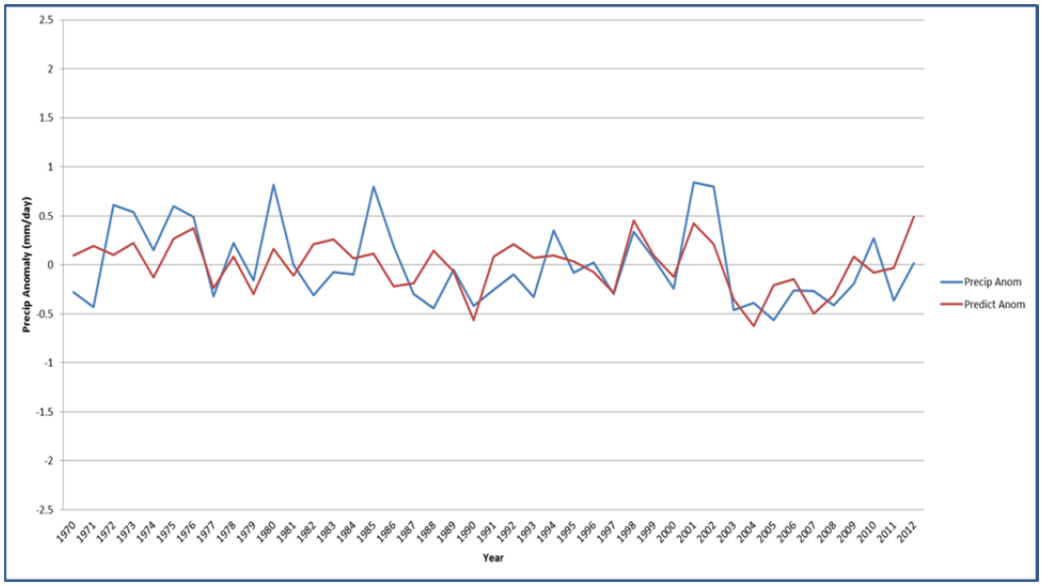


Figure 65. Comparison of Oct Korean precipitation rate (PR) anomaly hindcasts (red) and the corresponding observed anomalies (blue) for 1970–2012. The two time series have a correlation to each other of 0.63.

## 5. Overall Trends

Figure 66 shows the annual average surface air temperature for the Korean Peninsula during 1970–2012. This positive trend in temperatures is most likely due to climate change. Although the focus of our study was not to investigate global warming, this consistent warming trend was large enough to be an important factor in our LRF models. This trend alone does not indicate climate change; it only indicates that the Korean Peninsula has warmed from 1970–2012.

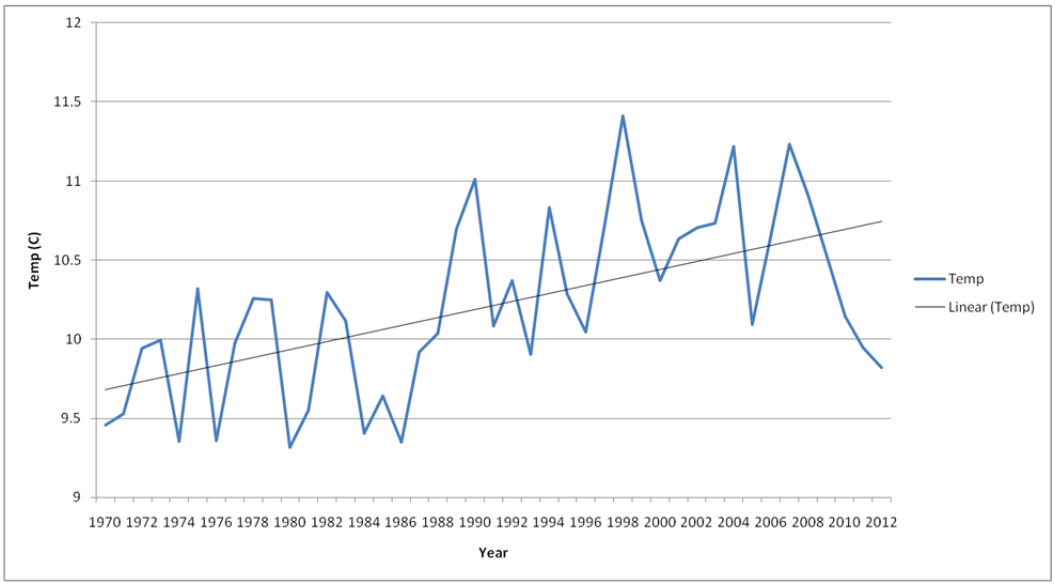


Figure 66. Annual average temperatures by year for the Korean Peninsula for Jan-Dec 1970–2012. During this study period, the annual average surface air temperature of the Korean Peninsula region increased by 1° C (from 9.7° C to 10.7°).

The warming trend shown in Figure 66 was also seen in each of the 12 months during 1970–2012 (see Appendix B). This led us to using year was selected as a predictor in the surface air temperature LRF models for three of the 12 months (Feb, May, and Sep; Table 4). In eight of the remaining nine LRF models, SST was used as a predictor and may have also accounted for the warming trend.

In addition to the warming trend, our hindcasting results revealed an overall drying trend in PRs from 1970–2012. For 9/12 months, the Korean Peninsula saw a drying trend in PRs from 1970–2012. Note the negative trend (drying) of the average annual PRs for the Korean Peninsula (Figure 67). SST was used as a predictor for 11 of the 12 months (all except for Mar; Table 5) and accounted for the drying trend seen in the observations.

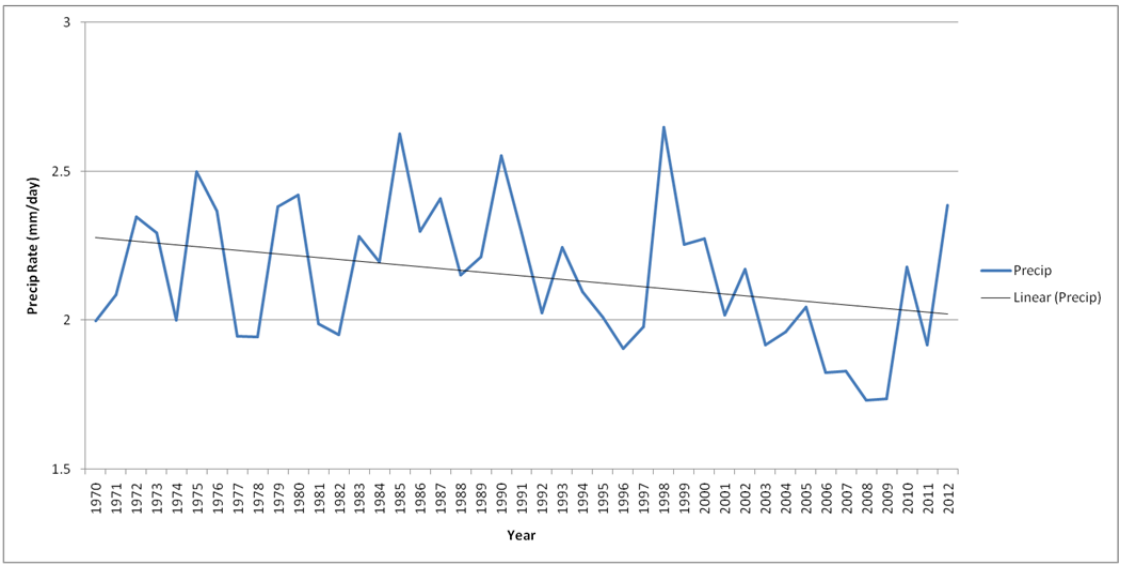


Figure 67. Annual precipitation rates (PRs) by year for the Korean Peninsula for Jan–Dec 1970–2012. During this study period, the annual average PR of the Korean Peninsula region decreased by 0.3 mm/day (from 2.3 mm/day to 2.0 mm/day).

## C. FORECAST SYSTEM APPLICATION

### 1. January 2013 Forecast

The forecast system developed in our study can be used directly to produce LRFs for the Korean Peninsula. See the next section for the tables that are to be used to produce the LRFs (Tables 12–15). In order to test the application of our forecast system, we produced two month lead temperature and PR forecasts for Jan 2013. Our forecasts were issued on 05 Dec 2012 and were valid for 01–31 Jan 2013. We forecasted below normal temperatures and below normal precipitation for the Korean Peninsula predictand region, both of which verified as correct (Figure 68).

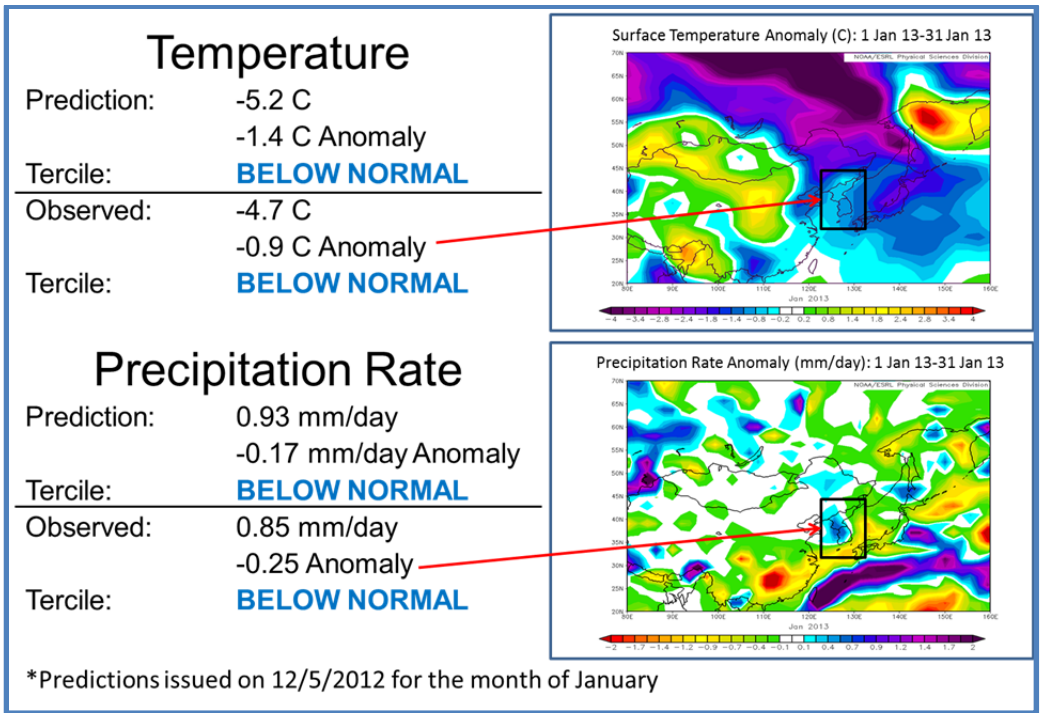


Figure 68. Example of two actual forecasts and verification results for two-month lead forecasts of Korean temperature and precipitation rate for Jan 2013. The inset maps in this figure show the observed anomalies, with the predictand region marked by black boxes. The forecasts were correct for both temperature and precipitation rate.

As mentioned in Chapter II, we recommended that users of our MLR models verify their forecasts and calculate verification as an ongoing effort to test the models' performance. It is also important to mention that the LRF models that we developed will not work forever. With our ever-changing climate system, there is an "expiration date" for our models at which point they will no longer have skill. This is an important reason why the climate forecaster should monitor the performance metrics of our models is to determine this expiration date.

### 2. Forecast Tables

Table 12 is a forecaster worksheet and Table 13 is a look-up table that shows forecasters how to use the final MLR model equations to forecast temperatures for the Korean Peninsula for each of the twelve months. The y-

intercept and slopes of the lines (m1, m2, m3) are given in Table 12. Climate forecasters will obtain the latest predictor values for the given month (highlighted in yellow) and enter them into the formula under Table 12.

The output from each model will be a discrete forecast. If forecasters want a tercile output, then they must use the values in the tercile bounds columns to convert the discrete forecasts to tercile forecasts. For example, if the discrete forecast is less than or equal to the BN-NN tercile boundary value, then the tercile forecast would be BN. If the discrete forecast is greater than or equal to the AN-NN tercile boundary value, then the tercile forecast would be AN. And if the discrete forecast is between the AN-NN and BN-NN tercile boundaries, then the tercile forecast would be NN.

Table 12. Forecaster worksheet for developing two month lead surface air temperature forecasts for the Korean Peninsula region for all months of the year. The b, m, and x columns in the Jan-Dec rows indicate the input terms used in the MLR forecast model for each month. The MLR formula is located below this table. The yellow highlighting indicates MLR model predictors for which forecasters must obtain and enter data. The rightmost two columns show the tercile boundaries that must be used to produce tercile forecasts from the discrete forecasts that are the direct output of the MLR models.

| Month | b | | m1 | | x1 | | m2 | | x2 | | m3 | | x3 | BN-NN | NN-AN |
|---|---|---|---|---|---|---|---|---|---|---|---|---|---|---|---|
| January | -11.7352 | + | 0.4290 | x | NOV NAO | + | 0.0167 | x | KTI_JAN3 | + | 0.4469 | x | OCT PERS | -4.323 | -3.218 |
| February | -152.7723 | + | 0.0755 | x | YEAR | + | 0.0117 | x | KTI_FEB2 | + | -0.7835 | x | AUG PNA | -2.681 | -1.147 |
| March | -14.6680 | + | 0.8983 | x | SST_TMAR2 | + | 0.0117 | x | KTI_MAR2 | | | | | 2.269 | 3.191 |
| April | -40.1138 | + | 0.9642 | x | SST_TAPR2 | + | 0.0203 | x | KTI_APR2 | | | | | 8.872 | 9.869 |
| May | -36.97993 | + | 0.6679 | x | SST_TMAY2 | + | 0.0172 | x | YEAR | | | | | 14.623 | 15.159 |
| June | -133.3468 | + | -0.1233 | x | FEB AO | + | 1.1036 | x | SST_TJUN3 | + | 0.0805 | x | KTI_JUN2 | 18.897 | 19.437 |
| July | 2.8467 | + | 0.7060 | x | SST_TJUL2 | + | -0.2446 | x | APR PNA | | | | | 22.148 | 22.794 |
| August | -6.6809 | + | 1.0594 | x | SST_TAUG2 | + | 0.0114 | x | KTI_AUG3 | | | | | 22.839 | 23.553 |
| September | -100.8044 | + | -0.2357 | x | JUL MEI | + | 0.0310 | x | YEAR | + | 0.0376 | x | KTI_SEP2 | 18.596 | 19.385 |
| October | -36.3788 | + | 0.5582 | x | SST_TOCT2 | + | 0.0270 | x | KTI_OCT2 | + | 0.3243 | x | AUG PNA | 12.413 | 13.255 |
| November | -10.4571 | + | 0.7507 | x | SST_TNOV3 | + | 0.0166 | x | KTI_NOV2 | | | | | 4.779 | 6.010 |
| December | -38.0663 | + | 1.3131 | x | SST_TDEC3 | + | 0.0181 | x | KTI_DEC2 | | | | | -1.712 | -0.282 |

$$y = b + m_1 x_1 + m_2 x_2 + m_3 x_3$$

Table 13 shows the geographic regions for forecasters to use in obtaining the GPH and SST data needed to calculate the KTI and SST predictors in the MLR models are listed for each month. The data for predictors that are climate variation or teleconnection indices will be obtained from the CPC or ESRL sites for the indicated preceding month or months. These website addresses are: http://www.cpc.ncep.noaa.gov and http://www.esrl.noaa.gov/psd. The current year will be entered for the variable YEAR. Persistence will be entered for the indicated preceding month for the variable PERS. The same notation from Chapter II is used in Tables 12–15 for the SST and KTI/KPI predictors. KTI_JAN3, for example, means that the forecaster will calculate the Jan KTI from three months prior (Oct). The latitude and longitude values are in decimal degrees. Positive (negative) values for latitude correspond to the Northern (Southern) Hemisphere. Longitude values are not broken down into hemispheres and start from the prime meridian (0–359°). For KTI_APR2, there is only an Area #1 (Table 13), so the average 850 hPa GPH will be averaged for that area only. For KTI_JAN3, the 850 hPa GPH will be averaged for Area #1 and Area #2 and the value for Area #2 will be subtracted from that in Area #1.

Table 13. Forecaster look-up table for use by forecasters in obtaining data for the KTI and SST predictors used in producing two month lead Korean surface air temperature forecasts (cf. Table 12). The latitude and longitude values are in decimal degrees. Positive (negative) values for latitude are in the Northern (Southern) Hemisphere. Longitude values are not broken down into hemispheres and start from the prime meridian (0–359°).

| | | Area #1 | | | Area #2 | |
|---|---|---|---|---|---|---|
| Month | Variable | Latitude | Longitude | | Latitude | Longitude |
| January | KTI_JAN3 | 40 to 55 | 205 to 235 | - | 67.5 to 82.5 | 95 to 125 |
| February | KTI_FEB2 | 35 to 50 | 137.5 to 167.5 | - | 72.5 to 87.5 | 145 to 175 |
| March | SST_TMAR2 | 27.6 to 41.0 | 144.4 to 174.4 | | | |
| | KTI_MAR2 | 17.5 to 32.5 | 120 to 150 | - | 57.5 to 72.5 | 177.5 to 207.5 |
| April | SST_TAPR2 | 18.1 to 33.3 | 129.4 to 159.4 | | | |
| | KTI_APR2 | 37.5 to 52.5 | 277.5 to 307.5 | | | |
| May | SST_TMAY2 | 4.8 to 20.0 | 99.4 to 129.4 | | | |
| June | SST_TJUN3 | 14.3 to -1.0 | 135.0 to 165.0 | | | |
| | KTI_JUN2 | 2.5 to -12.5 | 255 to 285 | | | |
| July | SST_TJUL2 | 8.6 to 21.9 | 140.6 to 170.6 | | | |
| August | SST_TAUG2 | 10.5 to -4.8 | 129.4 to 159.4 | | | |
| | KTI_AUG3 | 55 to 70 | 145 to 175 | - | 42.5 to 57.5 | 250 to 280 |
| September | KTI_SEP2 | 15 to 30 | 185 to 215 | | | |
| October | SST_TOCT2 | 42.9 to 58.1 | 136.9 to 166.9 | | | |
| | KTI_OCT2 | 27.5 to 42.5 | 162.5 to 192.5 | | | |
| November | SST_NOV3 | 35.2 to 50.5 | 174.4 to 204.4 | | | |
| | KTI_NOV2 | 32.5 to 47.5 | 320 to 350 | - | 60 to 75 | 310 to 340 |
| December | SST_DEC3 | 14.3 to 29.5 | 210.0 to 240.0 | | | |
| | KTI_DEC2 | -15 to -30 | 90 to 120 | - | -47.5 to -62.5 | 135 to 165 |

Tables 14 and 15 are the corresponding forecaster worksheet and look-up table for producing two month lead Korean region PR forecasts for Jan-Dec.

Table 14. Forecaster worksheet for developing two month lead precipitation rate (PR) forecasts for the Korean Peninsula region for all months of the year. The b, m, and x columns in the Jan-Dec rows indicate the input terms used in the MLR forecast model for each month. The MLR formula is located below this table. The yellow highlighting indicates MLR model predictors for which forecasters must obtain and enter data. The rightmost two columns show the tercile boundaries that must be used to produce tercile forecasts from the discrete forecasts that are the direct output of the MLR models.

| Month | b | m1 | x1 | m2 | x2 | m3 | x3 | BN-NN | NN-AN |
|---|---|---|---|---|---|---|---|---|---|
| January | 13.2447 | + -0.4565 x | SST_PJAN3 | + 0.0020 x | KPI_JAN2 | | | 0.893 | 1.163 |
| February | 18.2627 | + 0.1415 x | SEP NAO | + 0.0018 x | KPI_FEB2 | + -0.5742 x | SST_FEB2 | 0.880 | 1.278 |
| March | 1.6170 | + 0.0122 x | KPI_MAR2 | | | | | 1.146 | 1.533 |
| April | 19.2735 | + -0.6385 x | SST_PAPR4 | + 0.0051 x | KPI_APR2 | | | 1.481 | 2.062 |
| May | 9.469952 | + 0.1657 x | NOV MEI | + -0.3717 x | SST_PMAY2 | 0.0127 | KPI_MAY4 | 1.878 | 2.193 |
| June | 125.8499 | + -0.6004 x | SST_PJUN2 | + -0.0721 x | KPI_JUN2 | | | 2.818 | 3.596 |
| July | 19.5616 | + -0.6404 x | SST_PJUL2 | + -0.0156 x | KPI_JUL2 | | | 3.816 | 4.467 |
| August | -37.4990 | + 1.4383 x | SST_PAUG3 | + 0.0088 x | KPI_AUG3 | | | 3.777 | 4.856 |
| September | -8.5541 | + 0.5199 x | SST_PSEP3 | + 0.0181 x | KPI_SEP3 | | | 2.462 | 3.297 |
| October | 10.5448 | + -0.3234 x | SST_POCT2 | + 0.0034 x | KPI_OCT2 | + -0.2701 x | SST_POCT3 | 1.078 | 1.423 |
| November | 18.5533 | + 0.1710 x | JUL MEI | + -0.6017 x | SST_PNOV3 | + 0.0056 x | KPI_NOV3 | 1.053 | 1.481 |
| December | -4.5115 | + 0.2693 x | SST_PDEC4 | + 0.0059 x | KPI_DEC2 | | | 0.996 | 1.265 |

$$y = b + m_1 x_1 + m_2 x_2 + m_3 x_3$$

Table 15. Forecaster look-up table for use by forecasters in obtaining data for the KPI and SST predictors used in producing two month lead Korean precipitation rate (PR) forecasts (cf. Table 12). The latitude and longitude values are in decimal degrees. Positive (negative) values for latitude are in the Northern (Southern) Hemisphere. Longitude values are not broken down into hemispheres and start from the prime meridian (0–359°).

| | | Area #1 | | | Area #2 | |
|---|---|---|---|---|---|---|
| Month | Variable | Latitude | Longitude | | Latitude | Longitude |
| January | SST_PJAN3 | 10.5 to 23.8 | 264.4 to 288.8 | | | |
| | KPI_JAN2 | 22.5 to 37.5 | 165 to 195 | - | 50 to 65 | 155 to 185 |
| February | KPI_FEB2 | 42.5 to 57.5 | 200 to 230 | - | 37.5 to 52.5 | 75 to 105 |
| | SST_FEB2 | -2.9 to -14.3 | 159.4 to 181.9 | | | |
| March | KPI_MAR2 | 22.5 to 37.5 | 115 to 145 | - | 15 to 30 | 222.5 to 252.5 |
| April | SST_PAPR4 | 2.9 to 18.1 | 144.4 to 176.3 | | | |
| | KPI_APR2 | 20 to 35 | 155 to 185 | - | 52.5 to 67.5 | 202.5 to 232.5 |
| May | SST_PMAY2 | -14.3 to -39.0 | 270.0 to 288.8 | | | |
| | KPI_MAY4 | -25 to -40 | 190 to 220 | - | 5 to -10 | 225 to 255 |
| June | SST_PJUN2 | -18.1 to -41.0 | 200.6 to 219.4 | | | |
| | KPI_JUN2 | 2.5 to -12.5 | 300 to 330 | | | |
| July | SST_PJUL2 | 10.5 to 21.9 | 166.9 to 191.3 | | | |
| | KPI_JUL2 | -40 to -55 | 332.5 to 2.5 | | | |
| August | SST_PAUG3 | 21.9 to -1.0 | 110.6 to 129.4 | | | |
| | KPI_AUG3 | -27.5 to -42.5 | 160 to 190 | - | -42.5 to -57.5 | 210 to 240 |
| September | SST_PSEP3 | 25.7 to 37.1 | 165.0 to 195.0 | | | |
| | KPI_SEP3 | 35 to 50 | 120 to 150 | - | 25 to 40 | 75 to 105 |
| October | SST_POCT2 | 21.9 to 31.4 | 208.1 to 232.5 | | | |
| | KPI_OCT2 | 35 to 50 | 270 to 300 | - | 70 to 85 | 170 to 200 |
| | SST_POCT3 | 50.5 to 61.9 | 161.3 to 183.8 | | | |
| November | SST_PNOV3 | 18.1 to -8.6 | 142.5 to 161.3 | | | |
| | KPI_NOV3 | 55 to 70 | 35 to 65 | - | 45 to 60 | 105 to 135 |
| December | SST_PDEC4 | 29.5 to 39.0 | 187.5 to 211.9 | | | |
| | KPI_DEC2 | 55 to 70 | 105 to 135 | - | 30 to 45 | 355 to 25 |

# IV. SUMMARY, CONCLUSION, AND RECOMMENDATIONS

## A. SUMMARY AND CONCLUSION

In our study, we designed, developed, and tested a system of MLR models for producing Intraseasonal LRFs of surface air temperature and precipitation rate for the Korean Peninsula. We carefully determined the predictand region, predictor and predictand variables, input datasets, and lead times of our LRF models. Our LRF system produced forecasts for surface air temperature and precipitation rate at lead times of two months for each calendar month (24 models total) for the Korean Peninsula. The predictors that we considered were the following known climate variations and teleconnection patterns: AO, ENLN, NAO, PNA, and WP. We also analyzed global 850 hPa GPH fields (KTI and KPI), global SSTs, persistence, and year as potential predictors.

Our study was similar to Lemke (2010), DeHart (2011), and Gillies (2012), in that we created predictor regions to forecast for a specific predictand region far away. Our study was also similar to Tournay (2008), in that we considered known climate variations as predictors for Korean climate. These prior studies only investigated LRFs of precipitation for a few months of the year. Our study expanded on that by creating LRF models for predicting both temperature and precipitation for all 12 months. Our forecast system was uniquely designed for ease of use and immediate implementation into climate forecasting operations.

Tables 16 and 17 are summary tables for the temperature and PR LRF models. The red X's indicate the predictors used for each particular model. As seen in both tables, KTI/KPI and SST were used as predictors for temperature for most months. The KTI/KPI and SST predictors were tailored for the Korean Peninsula, so it is not surprising that they were selected so many times. If the KTI/KPI and SST predictors were removed from our MLR analysis, the remaining climate variations and teleconnections would have been used more often. The

removal of these predictors, however, would decrease the skill our models. It is interesting to see that the AO or WP were not used for the temperature LRFs for Jan–Mar, even though those climate variations are known to have impacts on the midlatitudes in the winter months. This is very likely because the climate variability represented by the KTIs for Jan–Mar very much resembles the variability associated with the AO and WP, which led to the AO and WP being eliminated from the MLR analysis for reasons of multi-colinearity. The year and SST predictors in Table 16 have the potential to account for the positive temperature trend that we have observed over the past 43 years (note that at least one of these two predictors was selected for 11 of the twelve months). Although ENLN was only used in the MLR model for Sep temperatures, and for May and Nov PR, several other predictors appear to represent much of the variability associated with ENLN.

Table 16. Summary of predictors for Korean surface air temperatures, by month. The red X's indicate the predictors used. May, for example, used year and SST as predictors.

| Month | Jan | Feb | Mar | Apr | May | Jun | Jul | Aug | Sep | Oct | Nov | Dec |
|---|---|---|---|---|---|---|---|---|---|---|---|---|
| KTI | X | X | X | X | | X | | X | X | X | X | X |
| AO | | | | | | X | | | | | | |
| NAO | X | | | | | | | | | | | |
| WP | | | | | | | | | | | | |
| PNA | | X | | | | | X | | | X | | |
| ENLN | | | | | | | | | X | | | |
| Year | | X | | | X | | | | X | | | |
| SST | | | X | X | X | X | X | X | | X | X | X |
| Persistence | X | | | | | | | | | | | |

Table 17. Summary of predictors for Korean precipitation rate (PR), by month. The red X's indicate the predictors used. May, for example, used KPI, ENLN, and SST as predictors.

| Month | Jan | Feb | Mar | Apr | May | Jun | Jul | Aug | Sep | Oct | Nov | Dec |
|---|---|---|---|---|---|---|---|---|---|---|---|---|
| KPI | X | X | X | X | X | X | X | X | X | X | X | X |
| AO | | | | | | | | | | | | |
| NAO | | X | | | | | | | | | | |
| WP | | | | | | | | | | | | |
| PNA | | | | | | | | | | | | |
| ENLN | | | | | X | | | | | | X | |
| Year | | | | | | | | | | | | |
| SST | X | X | | X | X | X | X | X | X | X | X | X |
| Persistence | | | | | | | | | | | | |

Throughout the development of our LRF system, we kept the physical plausibility of predictors in mind. As an example, a detailed description of the physical plausibility for the Jan temperature LRF model can be found in Chapter III, Section B.

We conducted cross-validated two month lead hindcasts using the 24 LRF models and found significant forecast skill for each of them. We took the discrete value hindcasts and broke them down into terciles. By comparing the hindcasted terciles with the observed terciles, we created 2x2 contingency tables and calculated the HSS, FAR, and POD for each of the 24 models. The LRF models for Korean surface air temperatures performed overall better than the LRF models for Korean PR. The AN and BN terciles had notably better performance than the NN tercile for both temperature and PR. We applied our models to produce two month lead forecasts for Jan 2013, which were correct for both temperature and PR. We also identified multi-decadal warming and drying trends for the Korean Peninsula for 1970–2012 which were at least partially accounted for by the year predictors, and probably also by the SST predictors.

In conclusion, we were able to use global scale climate variations and teleconnections to skillfully predict surface air temperatures and PRs for the Korean Peninsula at two month lead times for most of the terciles and months. We have provided forecaster worksheets and look-up tables (Tables 12–15), so that climate forecasting agencies, such as the 14 WS, can create future predictions. These forecasts can be easily prepared using our forecast tables for all 12 calendar months.

## B. RECOMMENDATIONS

We recommend that our forecast system be operationally tested and applied by agencies such as the 14 WS for use in providing long lead support for military operations. On-going verification should be conducted as part of that testing process, and as part of any operational implementation.

We recommend the following future research and applications:

1. Compare the skill of forecasts with comparable forecasts from other organizations (e.g., CPC, IRI, KMA, BCC).

2. Work on improving our forecast system to obtain positive HSS scores for all months and predictands.

3. Repeat this study considering other types of statistical analysis, such as non-linear regression.

4. Repeat this study using quintiles (or another type of division) instead of terciles to divide the predictands.

5. Repeat this study using multi-model, lagged average ensemble, and/or OCN approaches (cf. Gillies 2012).

6. Conduct a similar study for Korea for longer lead times, for smaller predictand regions (e.g., North Korea and South Korea separately), and using the higher resolution CFSR dataset.

7. Apply our forecast development process to other regions of military interest.

THIS PAGE INTENTIONALLY LEFT BLANK

# APPENDIX A. PREDICTORS BY MONTH

This appendix contains all of the predictors used in our MLR models for each month for both temperatures and PR. The captions will be abbreviated in this appendix and the following descriptions will be used.

For the KTI (KPI) predictors, the figures will show correlation of 850 hPa GPHs for the optimal preceding month with the surface air temperatures (PR) in the Korea region during 1970–2012 for the indicated month (see Figure 37 for a full caption example). The black boxes mark the areas with the highest positive and negative correlations, which are the areas used to construct the KTIs (KPIs). The area average 850 hPa GPH from the positively correlated box minus that of the negatively correlated box equals the KTI (KPI) for a given month. If there is only one box for a given month, the area average 850 hPa GPH for that box alone will be used.

For the SST predictors, figures will show correlation of SSTs for the optimal preceding month with the surface air temperatures (PR) in the Korea region during 1970–2012 for the indicated month (see Figure 43 for a full caption example). The area average SST contained in the black box will be used as the SST predictor for the indicated month.

For the climate variation/teleconnection and the persistence predictors, figures will show correlation of the predictor for the optimal preceding month with the surface air temperatures (PR) in the Korea region during 1970–2012 for the indicated month (see Figures 39 and 40 for full caption examples).

For the year predictor, figures will show correlation of year with the surface air temperatures (PR) in the Korea region during 1970–2012 for the indicated month.

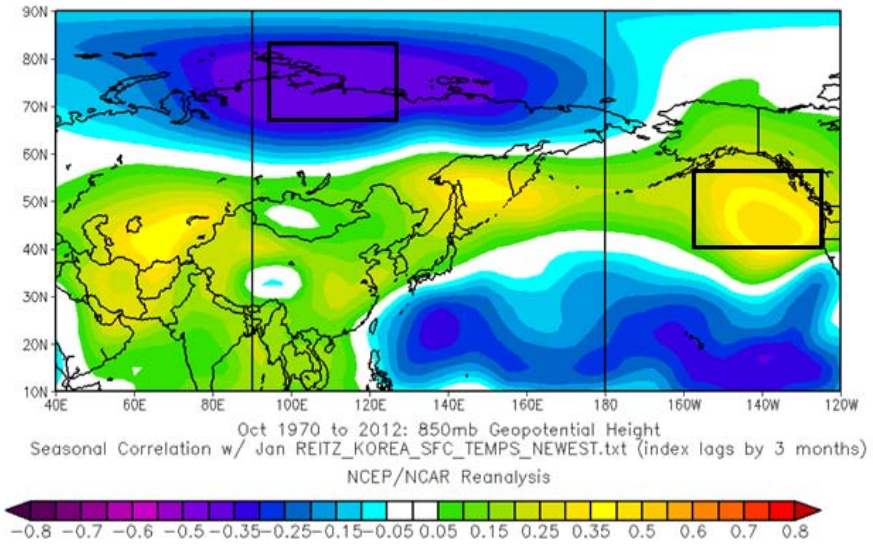


Figure 69. Inputs for KTI_JAN3, used as a predictor for Jan surface air temperatures.

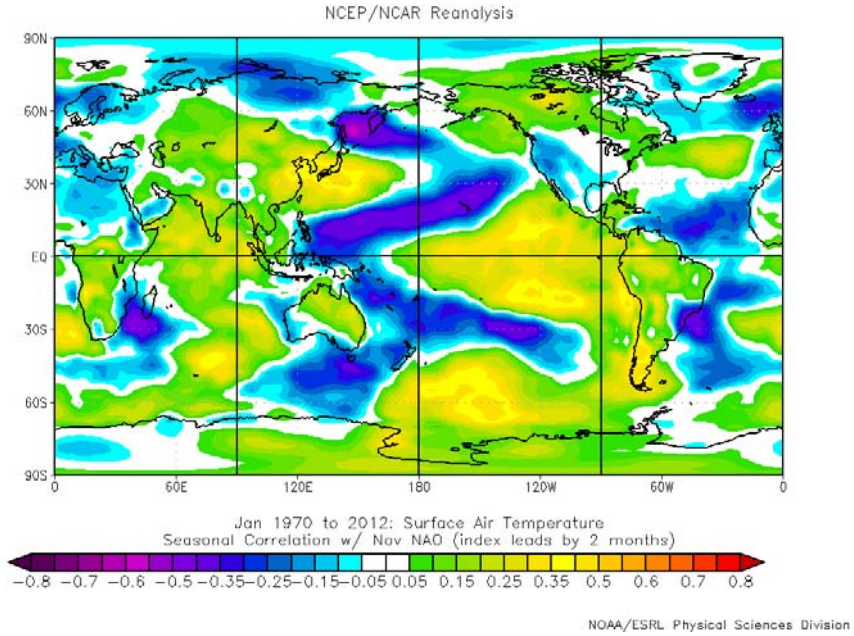


Figure 70. Nov NAO, used as a predictor for Jan surface air temperatures.

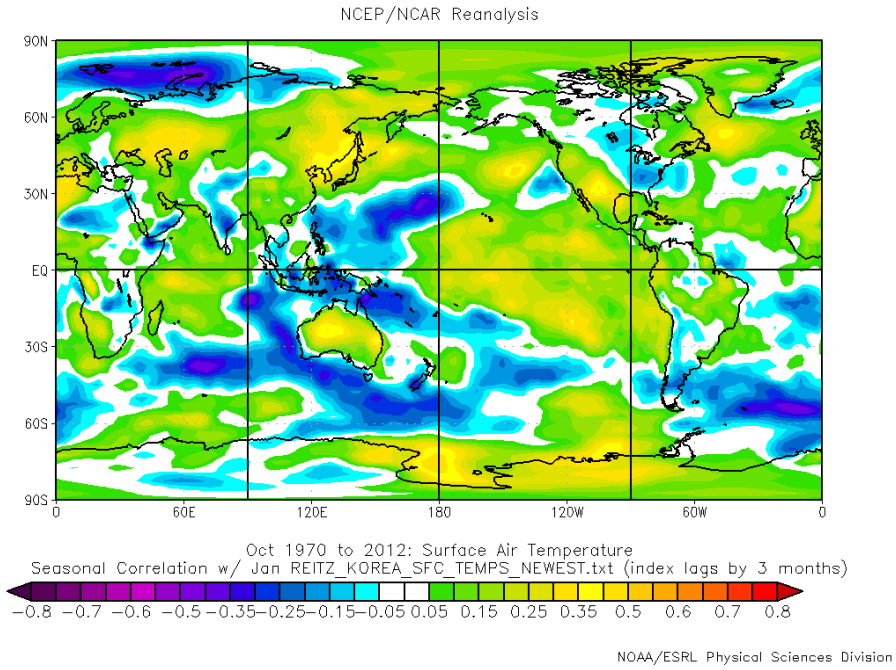


Figure 71. Persistence from Oct, used as a predictor for Jan surface air temperatures.

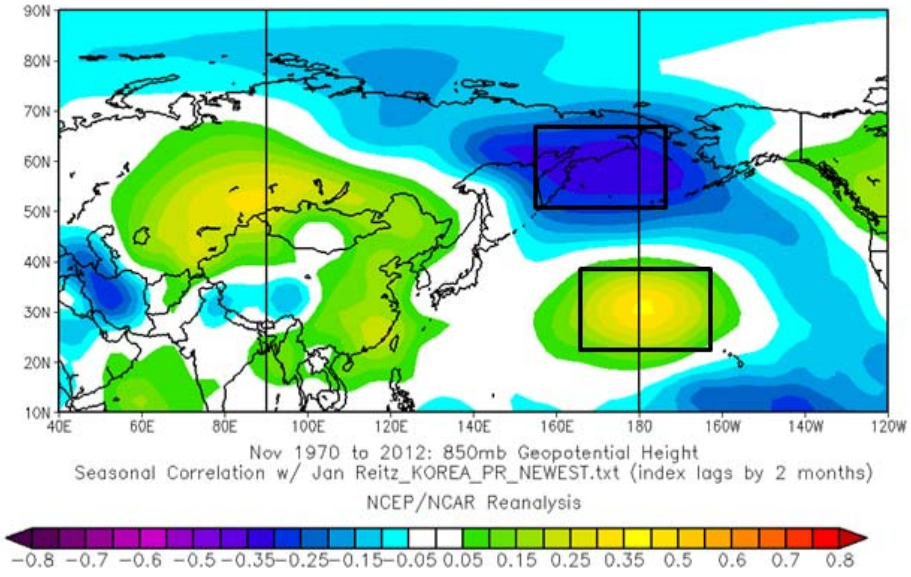


Figure 72. Inputs for KPI_JAN2, used as a predictor for Jan PR.

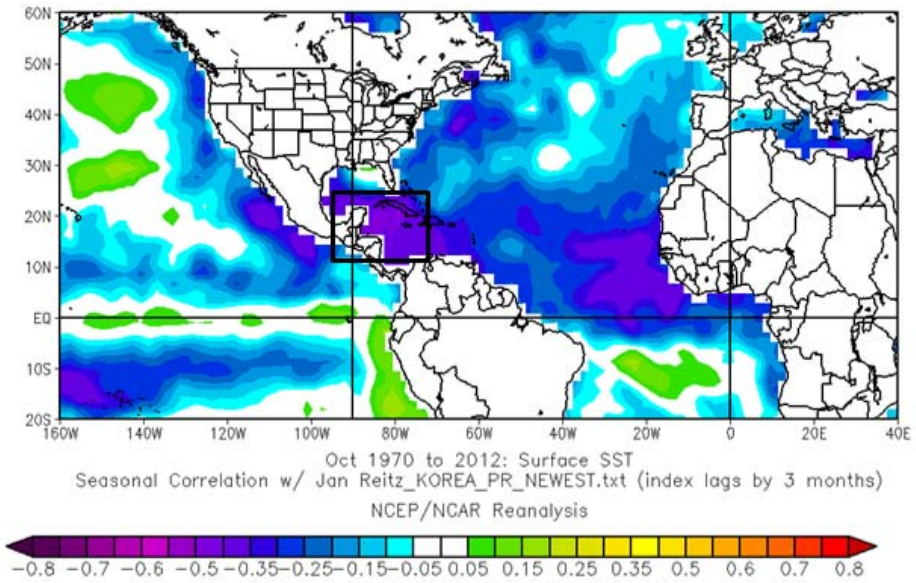


Figure 73. SST_PJAN3, used as a predictor for Jan PR.

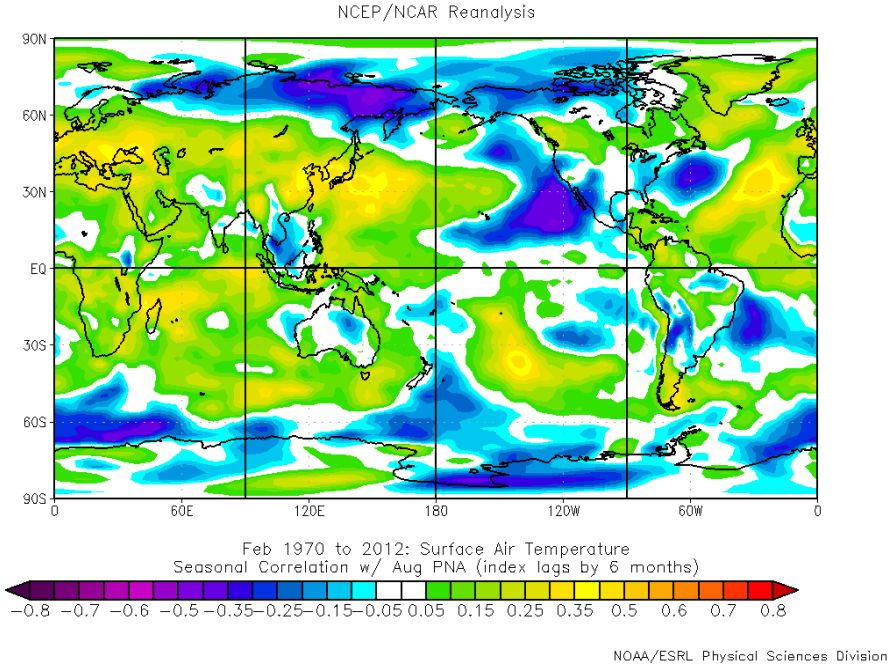


Figure 74. Aug PNA, used as a predictor for Feb surface air temperatures.

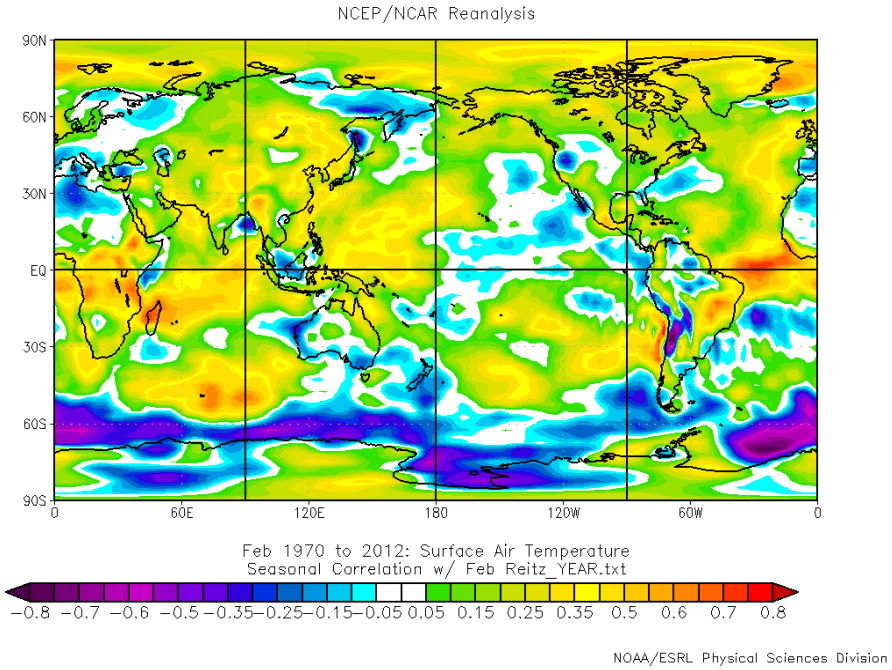


Figure 75. Year, used as a predictor for Feb surface air temperatures.

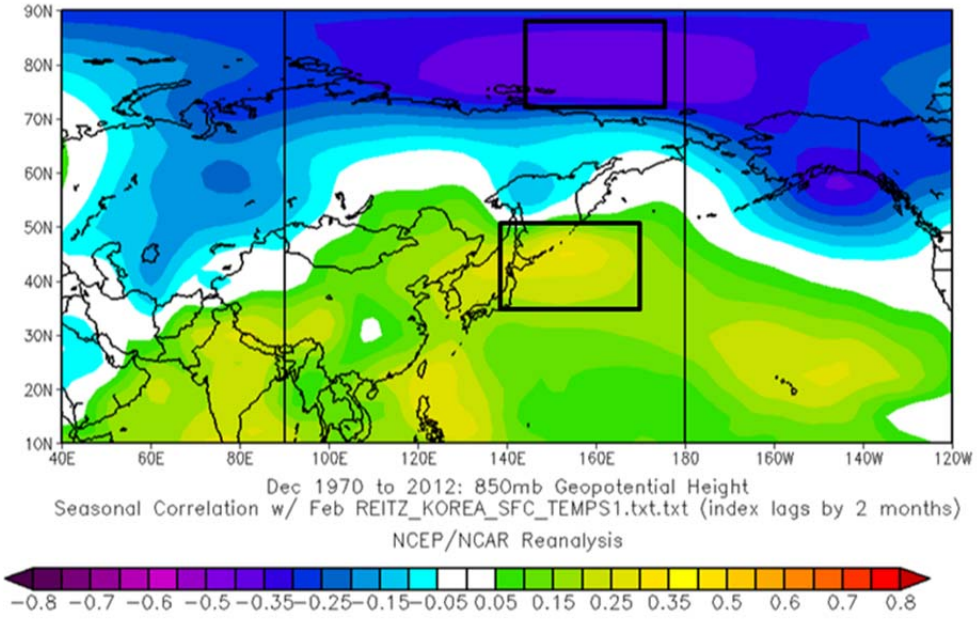


Figure 76. Inputs for KTI_FEB2, used as a predictor for Feb surface air temperatures.

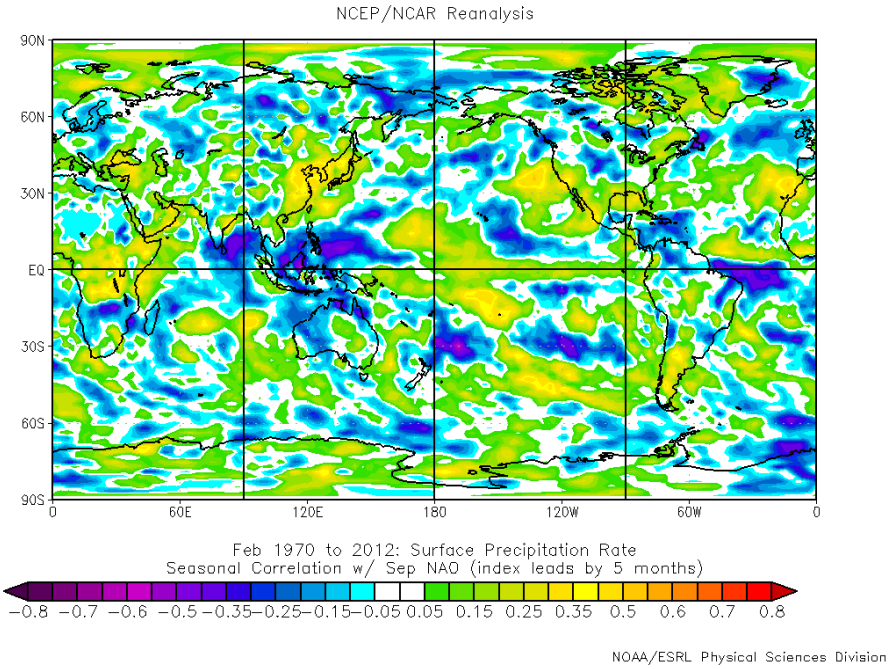


Figure 77. Sep NAO, used as a predictor for Feb PR.

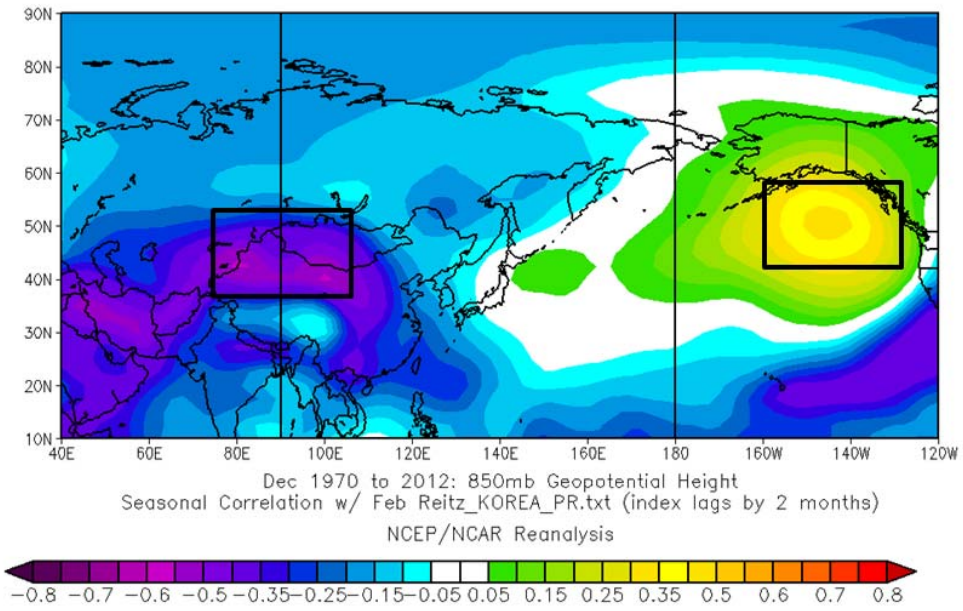


Figure 78. Inputs for KPI_FEB2, used as a predictor for Feb PR.

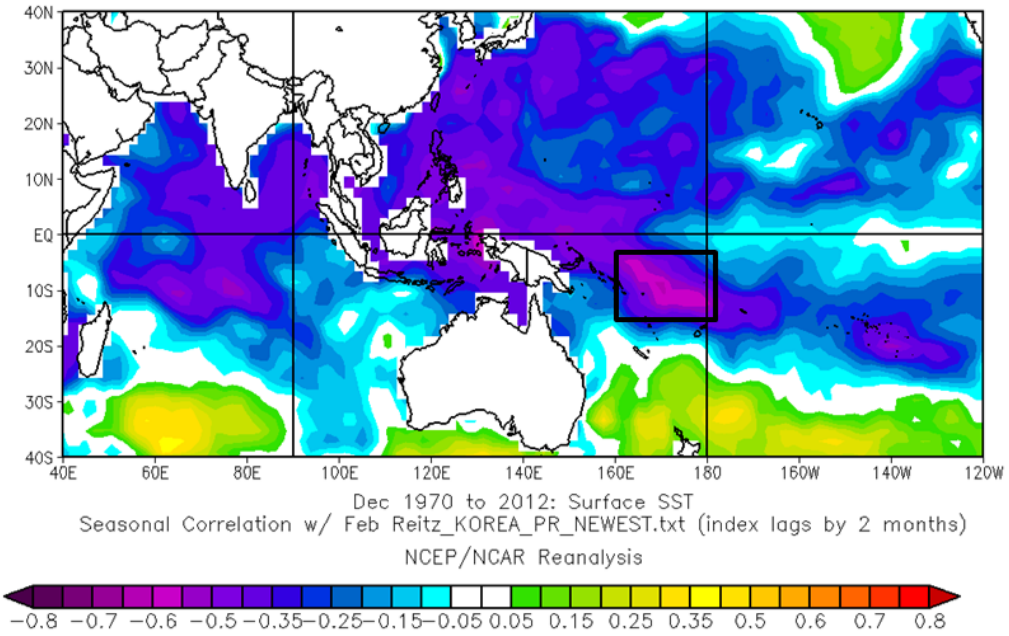


Figure 79. SST_PFEB2, used as a predictor for Feb PR.

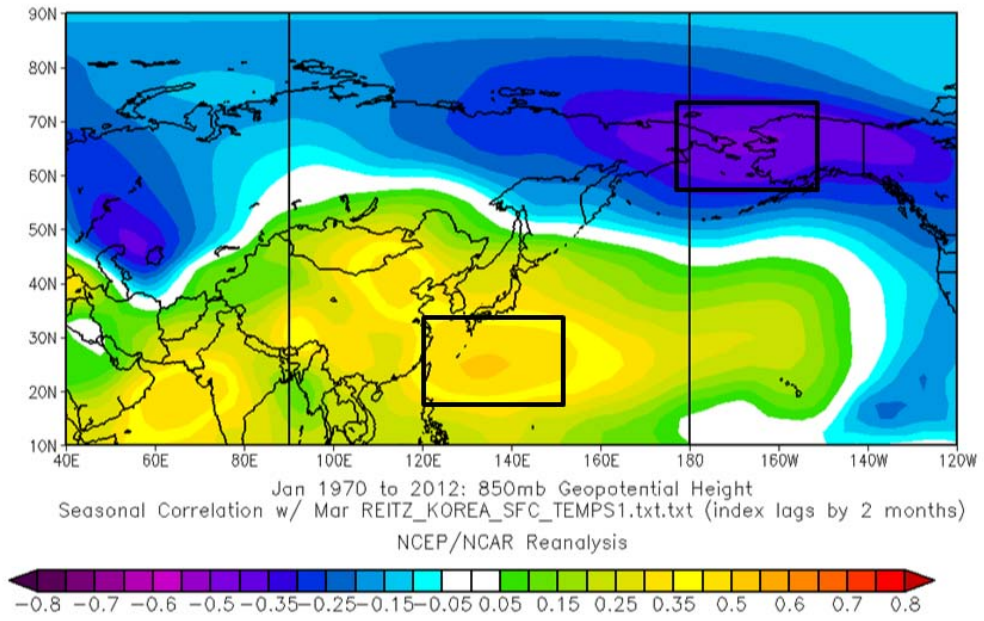


Figure 80. Inputs for KTI_MAR2, used as a predictor for Mar surface air temperatures.

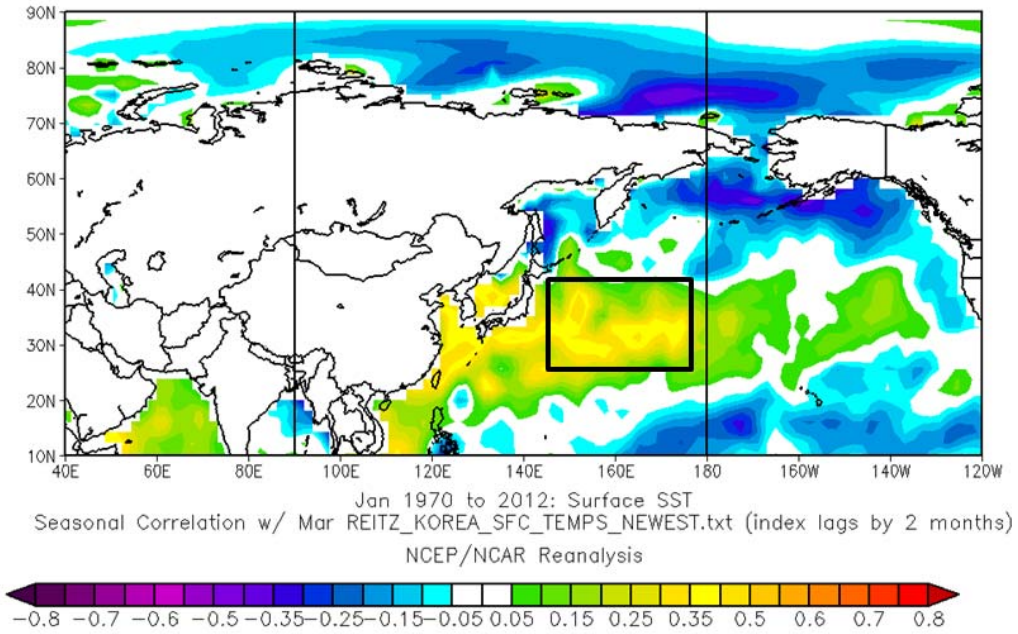


Figure 81. SST_TMAR2, used as a predictor for Mar surface air temperatures.

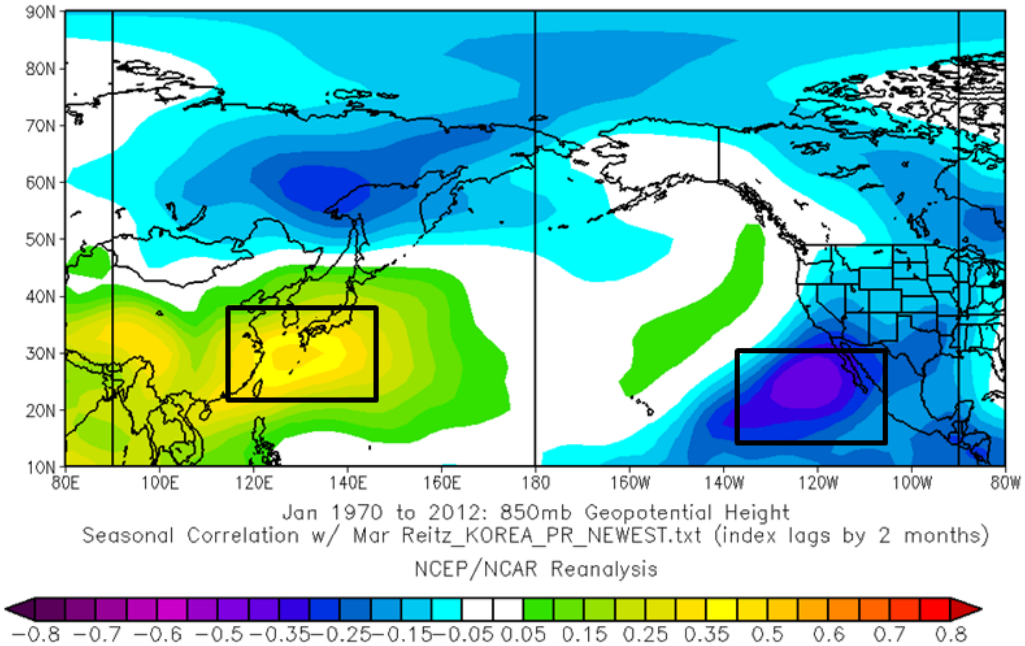


Figure 82. Inputs for KPI_MAR2, used as a predictor for Mar PR.

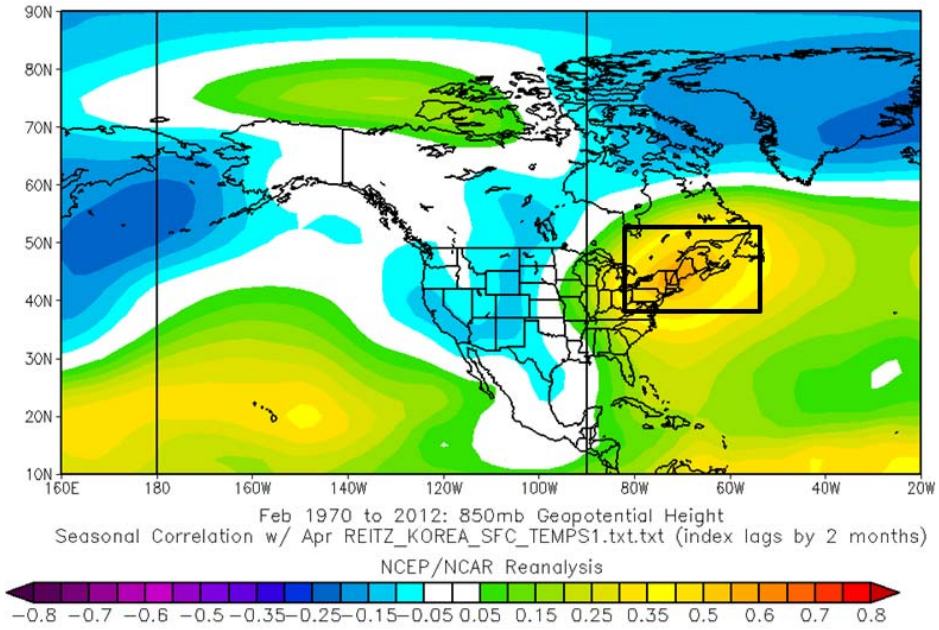


Figure 83. Inputs for KTI_APR2, used as a predictor for Apr surface air temperatures.

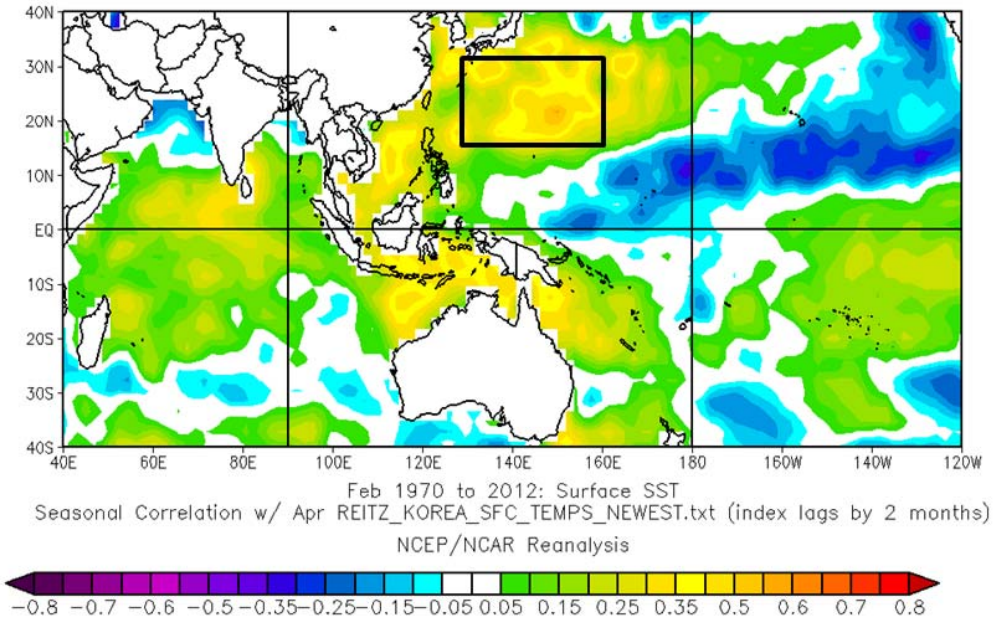


Figure 84. SST_TAPR2, used as a predictor for Apr surface air temperatures.

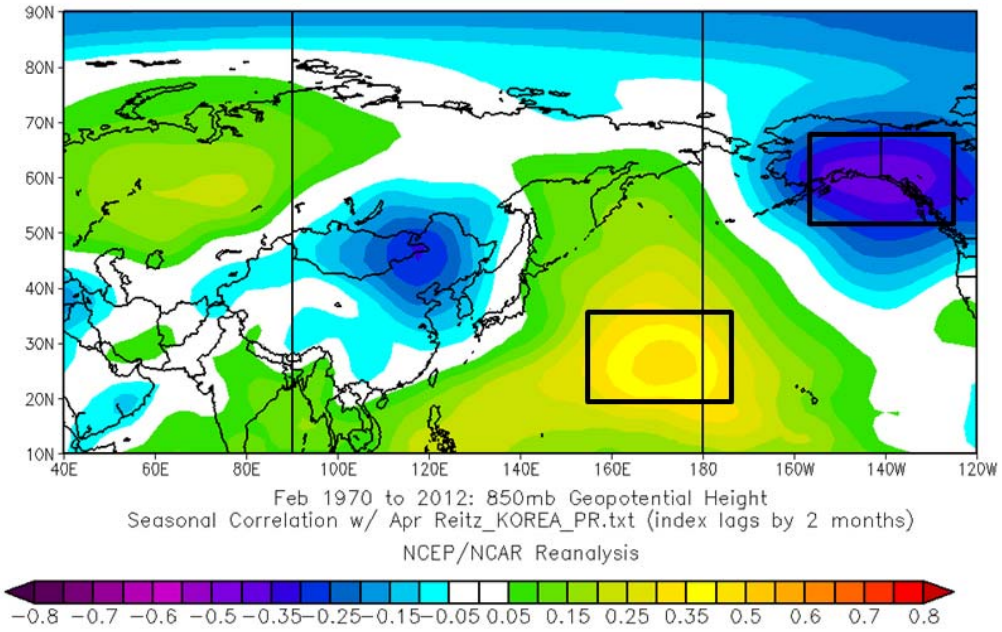


Figure 85. Inputs for KPI_APR2, used as a predictor for Apr PR.

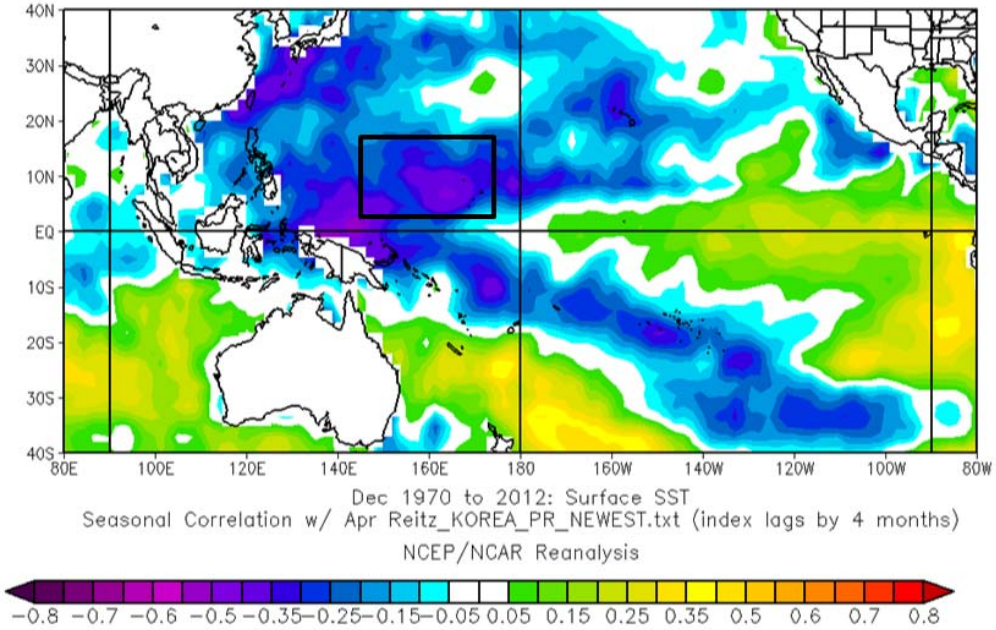


Figure 86. SST_PAPR4, used as a predictor for Apr PR.

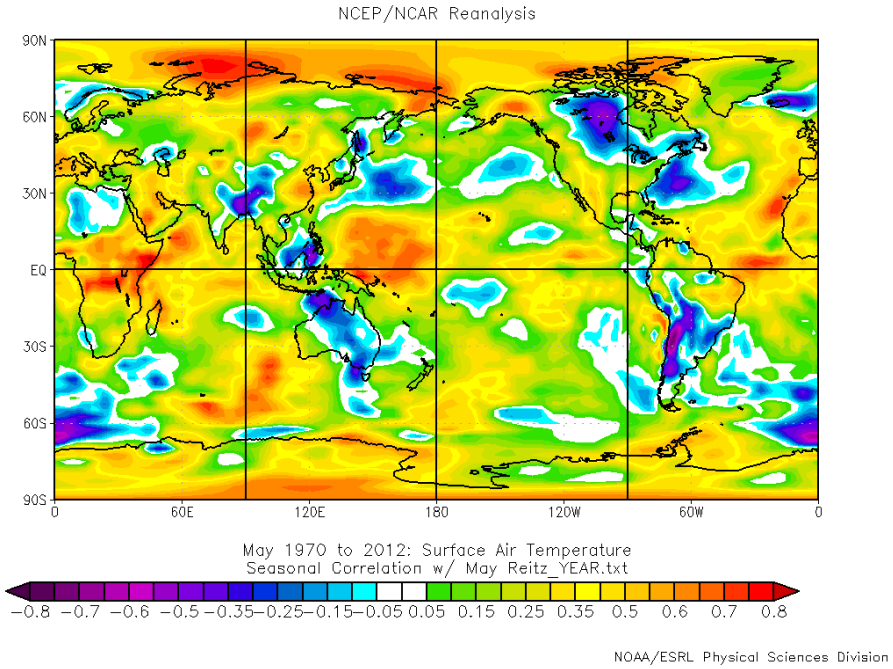


Figure 87. Year, used as a predictor for May surface air temperatures.

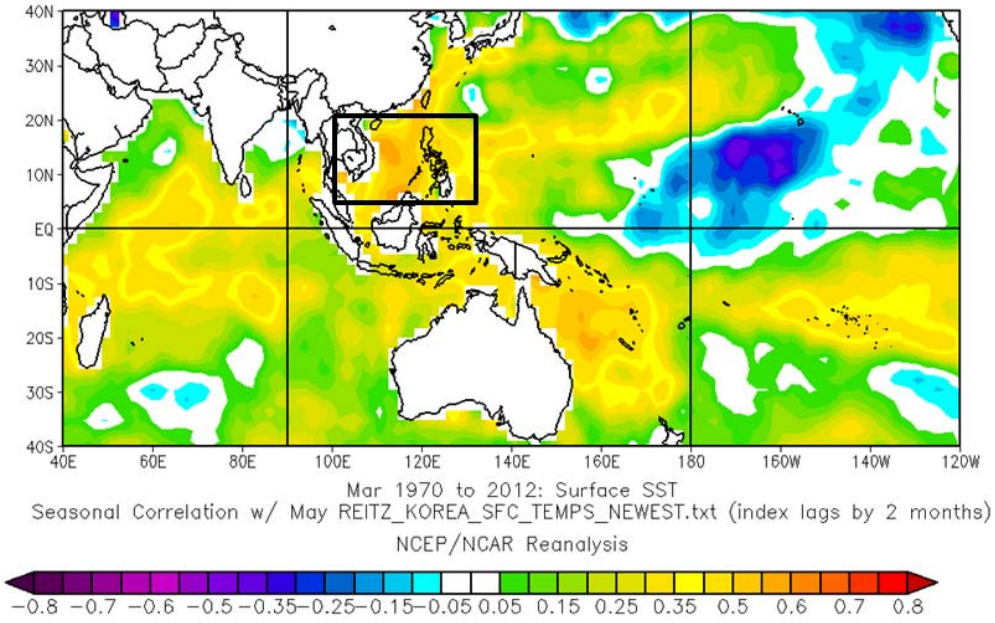


Figure 88. SST_TMAY2, used as a predictor for May surface air temperatures.

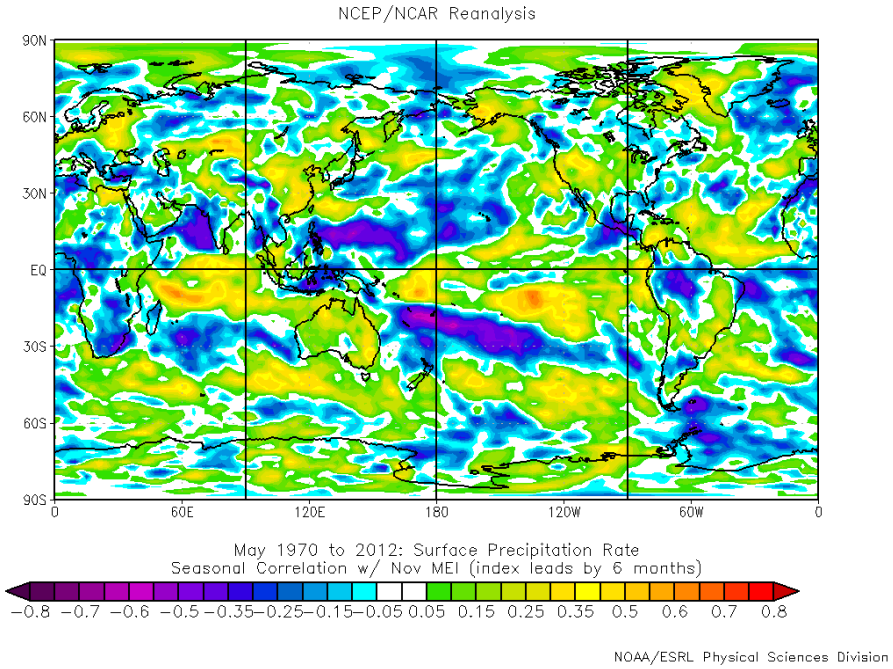


Figure 89. Nov MEI, used as a predictor for May PR.

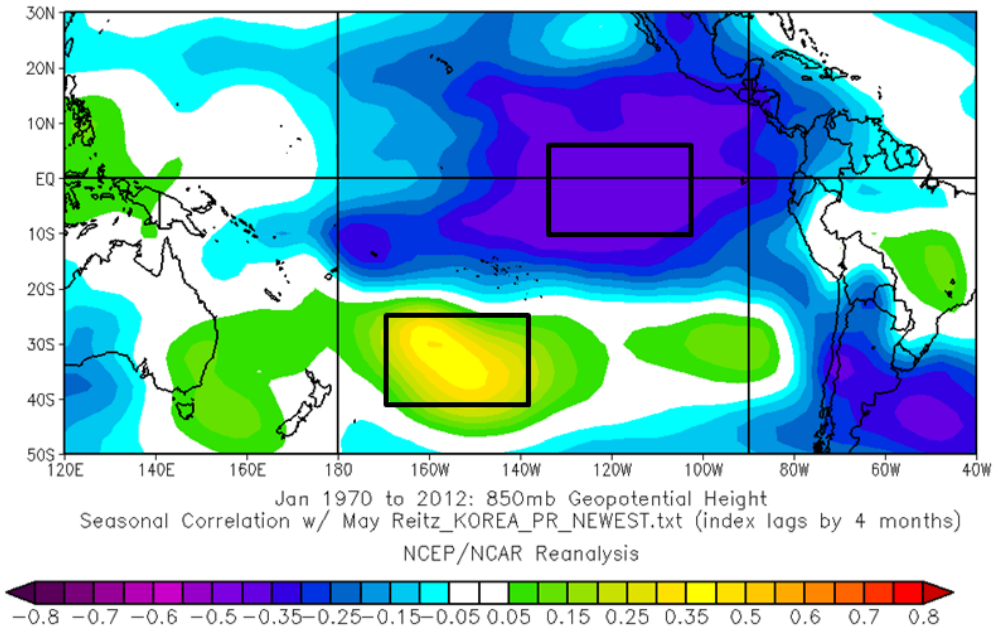


Figure 90. Inputs for KPI_MAY4, used as a predictor for May PR.

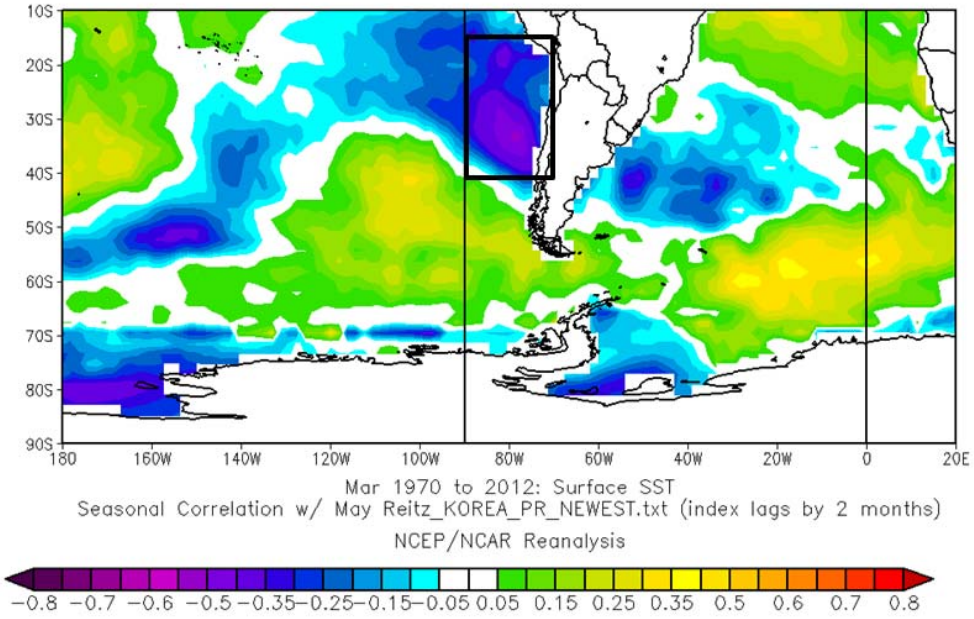


Figure 91. SST_PMAY2, used as a predictor for May PR.

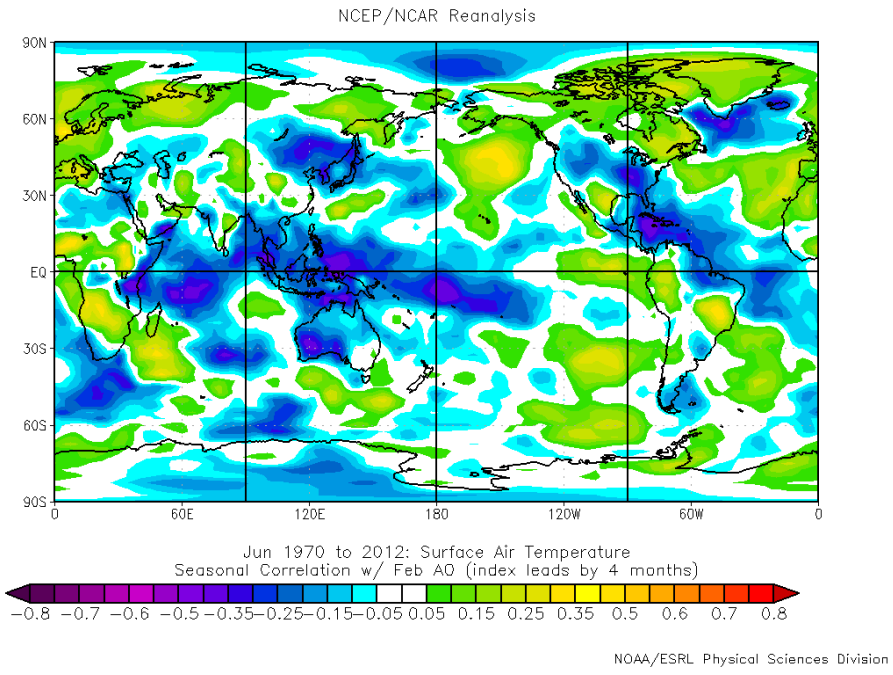


Figure 92. Feb AO, used as a predictor for Jun surface air temperatures.

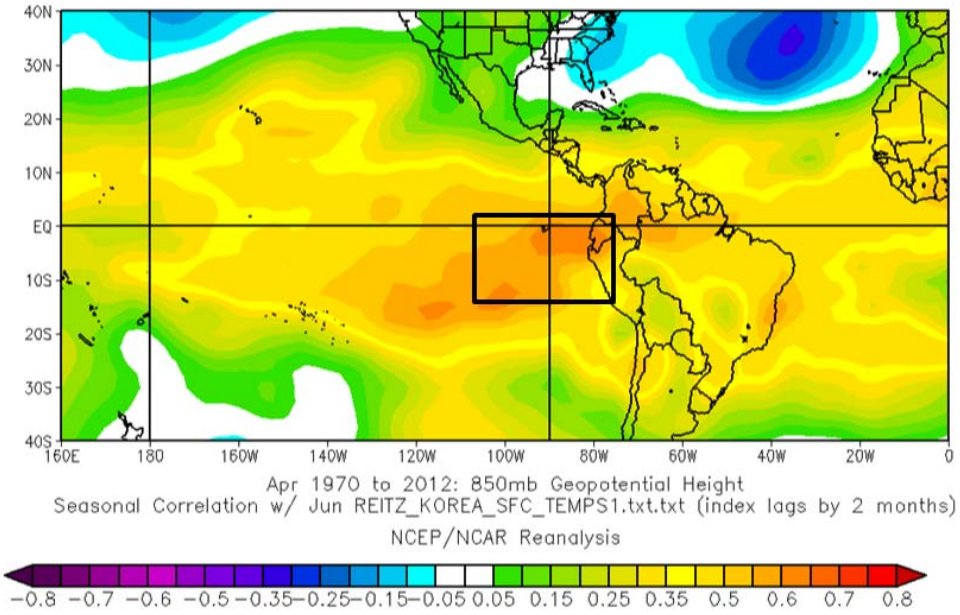


Figure 93. Inputs for KTI_JUN2, used as a predictor for Jun surface air temperatures.

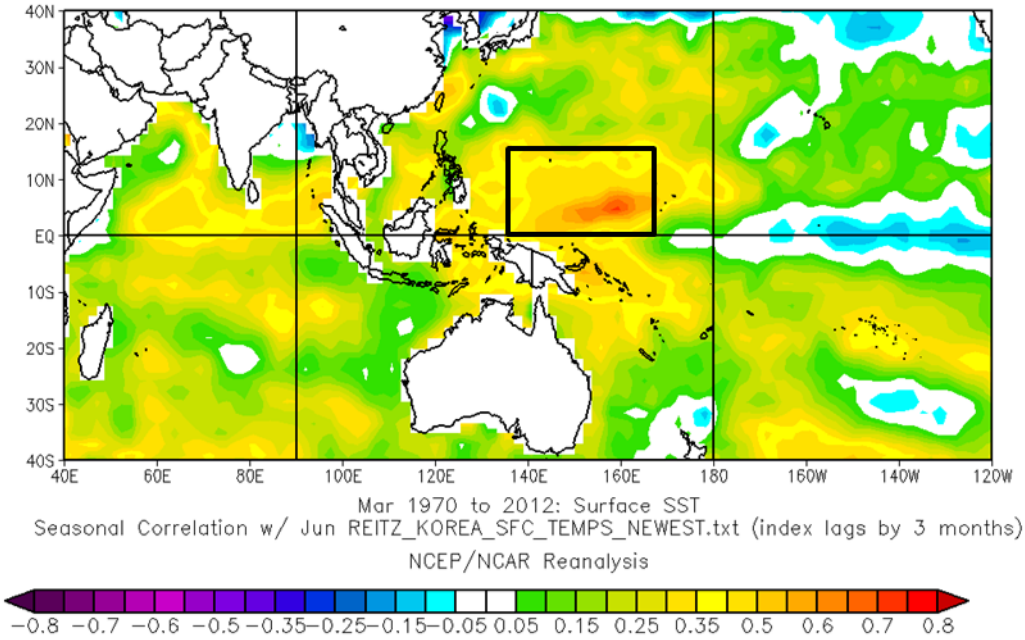


Figure 94. SST_TJUN3, used as a predictor for Jun surface air temperatures.

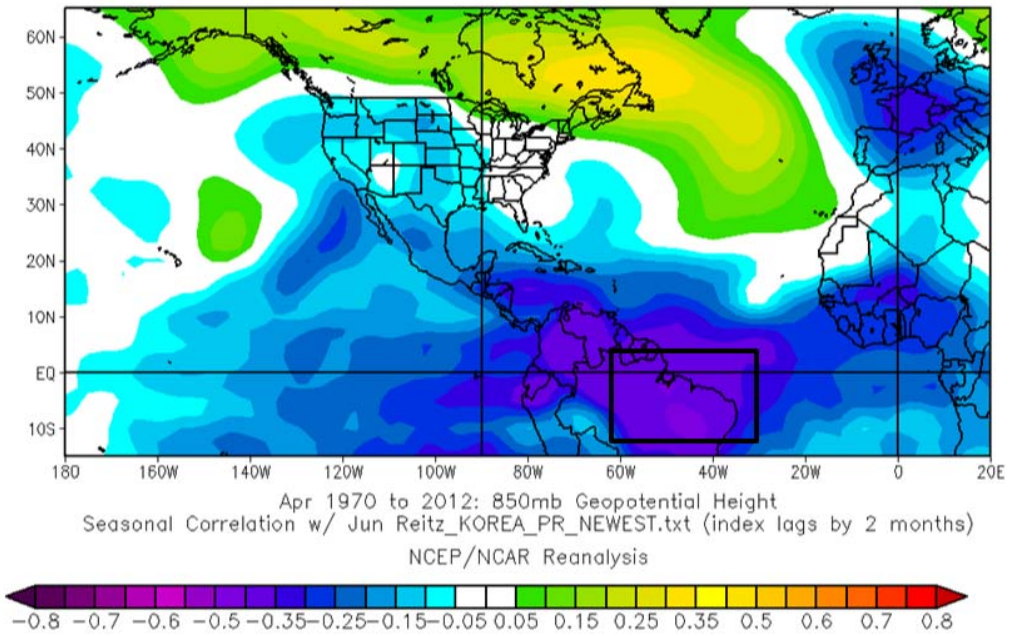


Figure 95. Inputs for KPI_JUN2, used as a predictor for Jun PR.

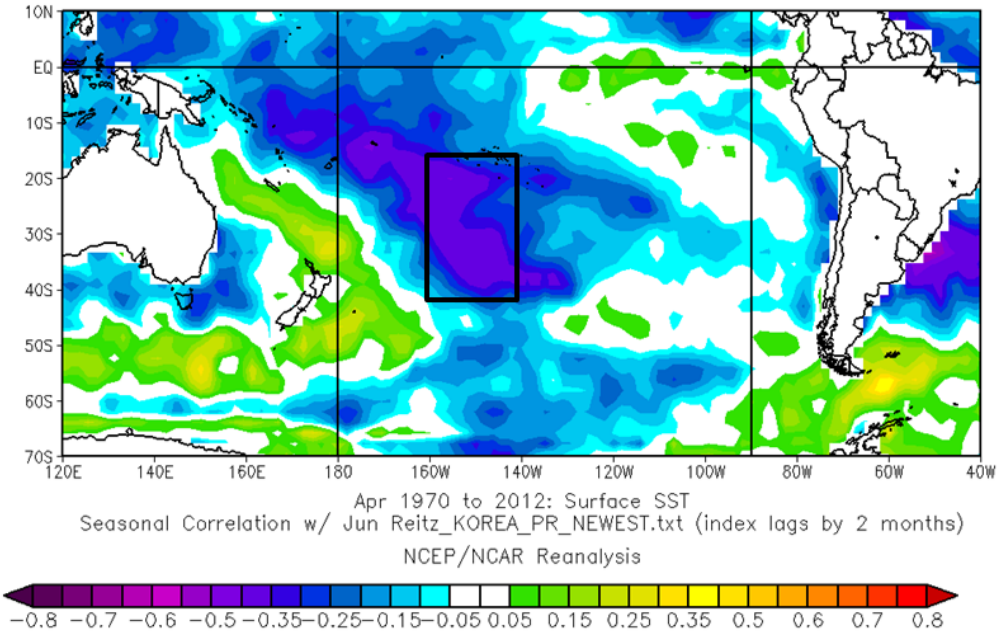


Figure 96. SST_PJUN2, used as a predictor for Jun PR.

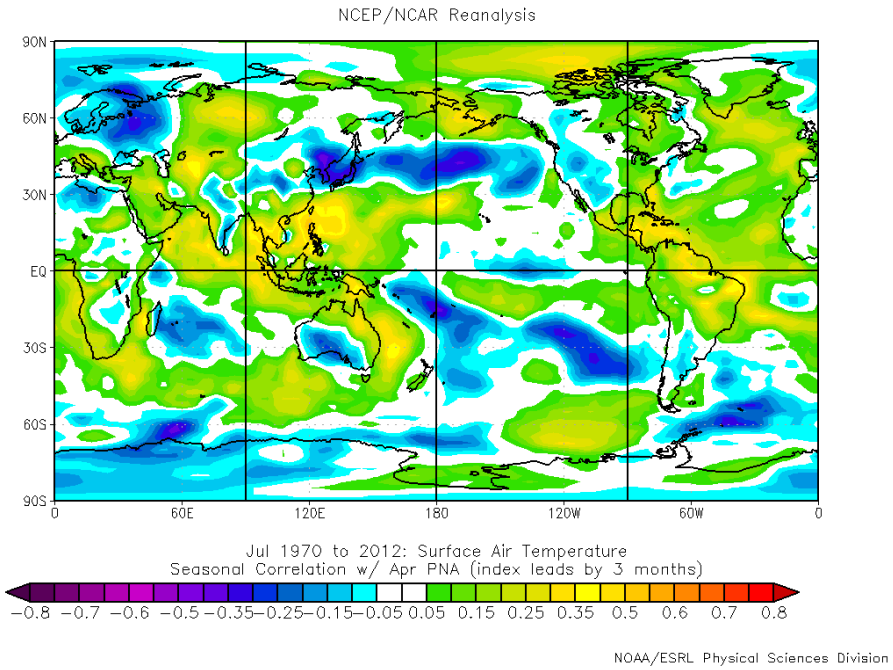


Figure 97. Apr PNA, used as a predictor for Jul surface air temperatures.

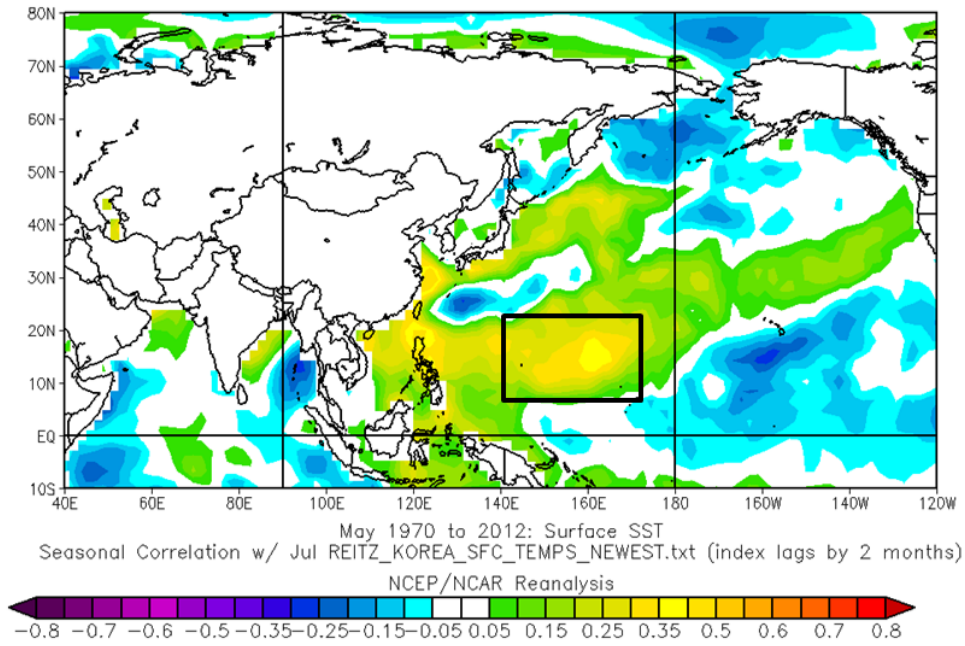


Figure 98. SST_TJUL2, used as a predictor for Jul surface air temperatures.

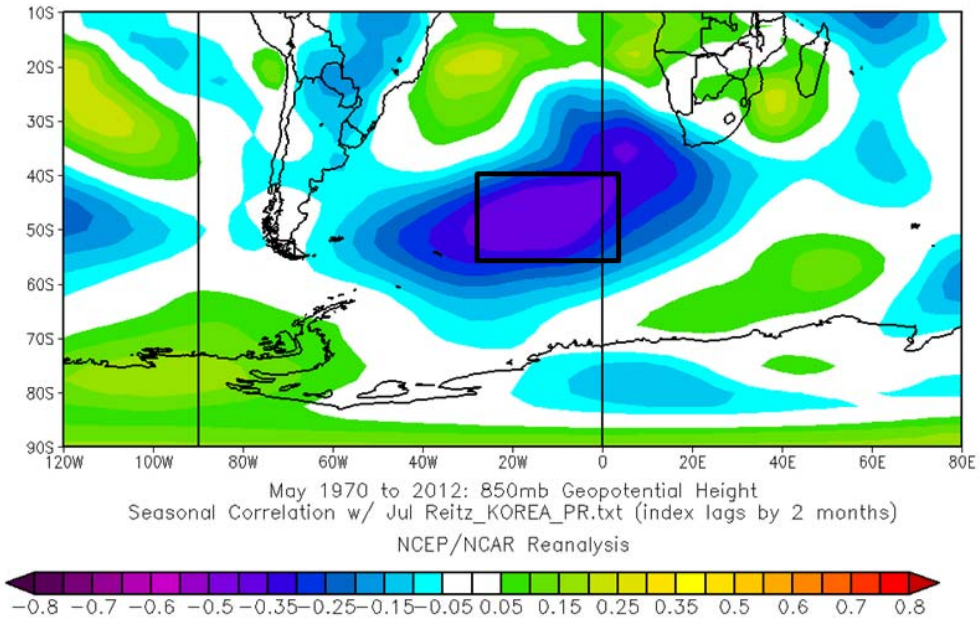


Figure 99. Inputs for KPI_JUL2, used as a predictor for Jul PR.

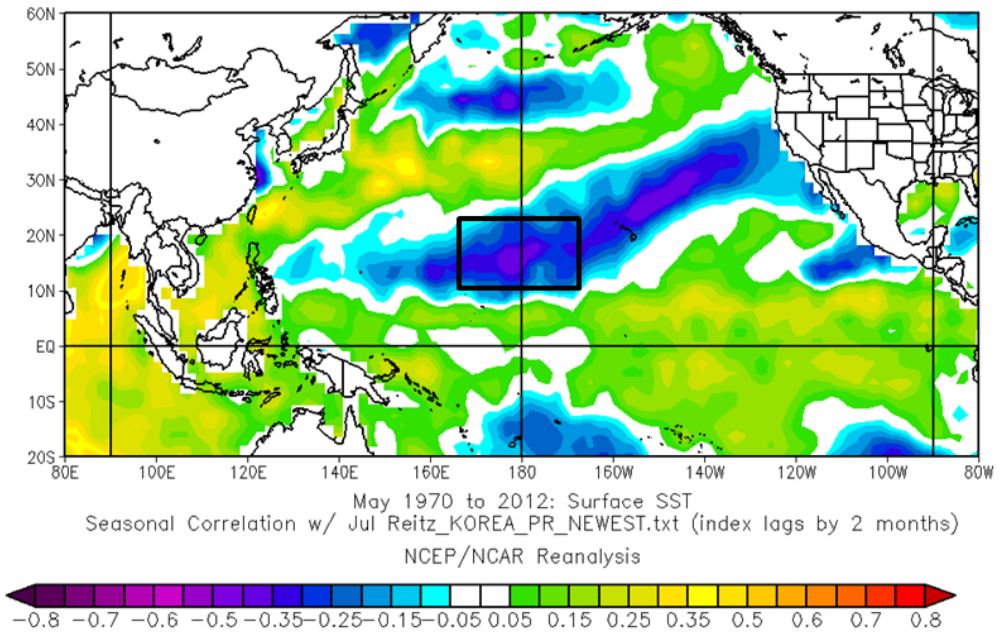


Figure 100. SST_PJUL2, used as a predictor for Jul PR.

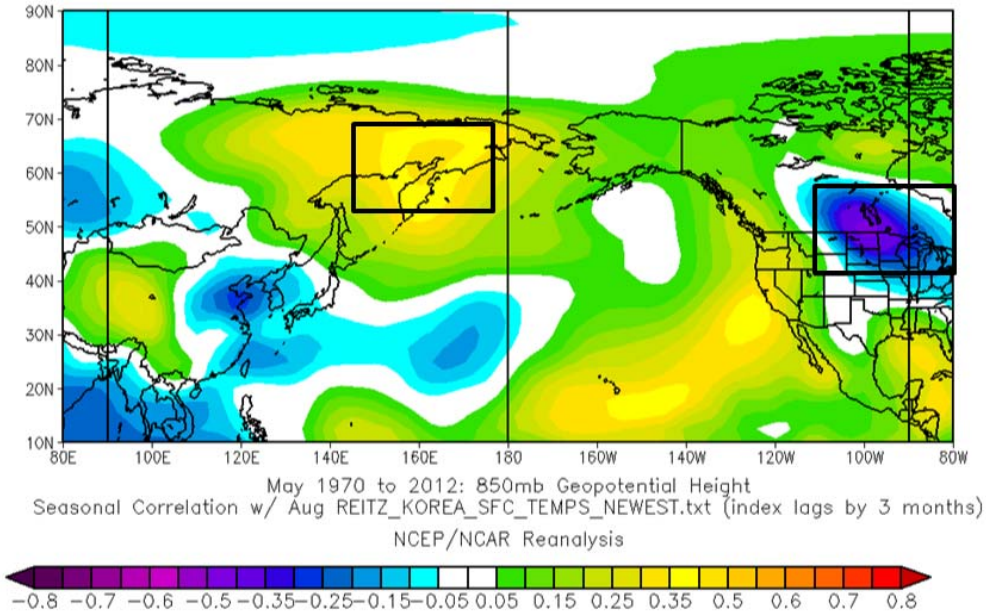


Figure 101. Inputs for KTI_AUG3, used as a predictor for Aug surface air temperatures.

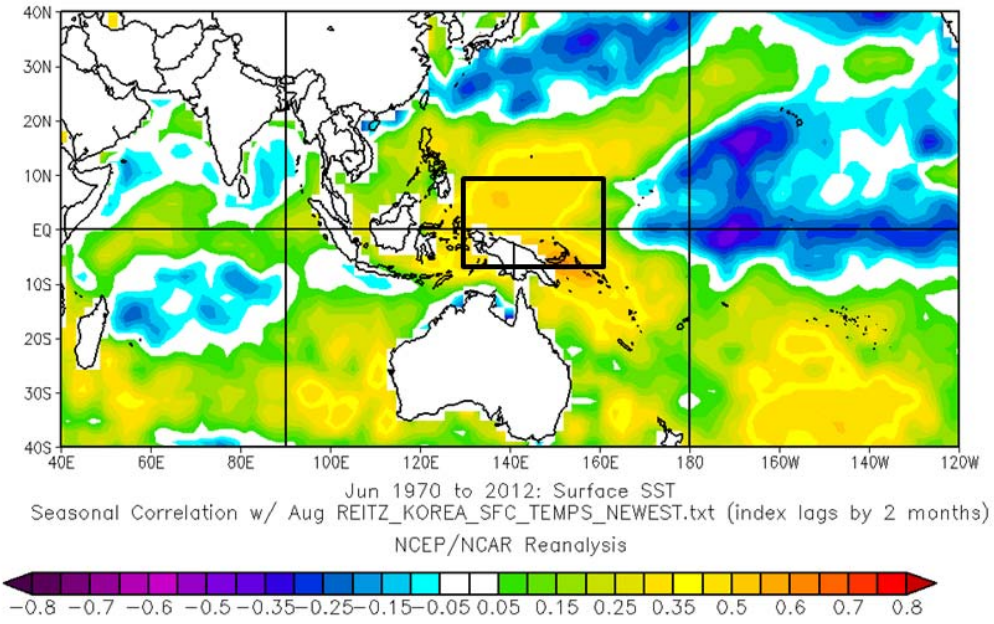


Figure 102. SST_TAUG2, used as a predictor for Aug surface air temperatures.

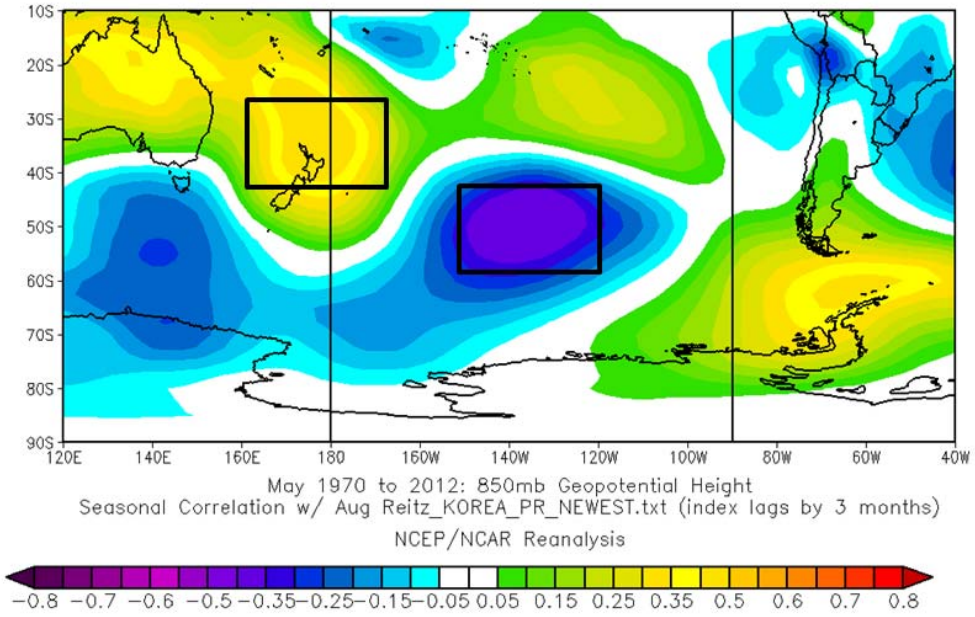


Figure 103. Inputs for KPI_AUG3, used as a predictor for Aug PR.

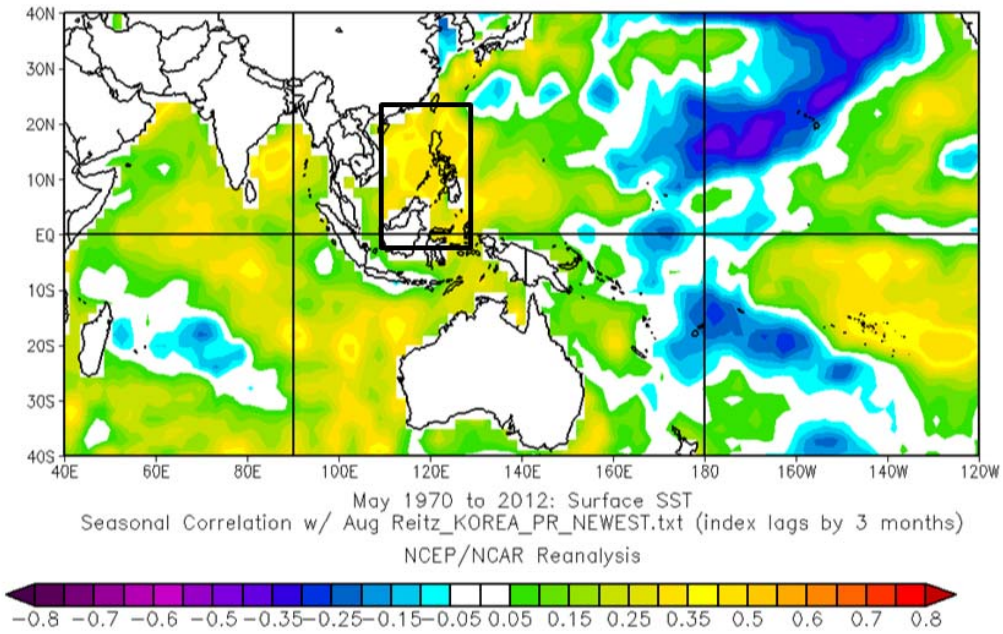


Figure 104. SST_PAUG3, used as a predictor for Aug PR.

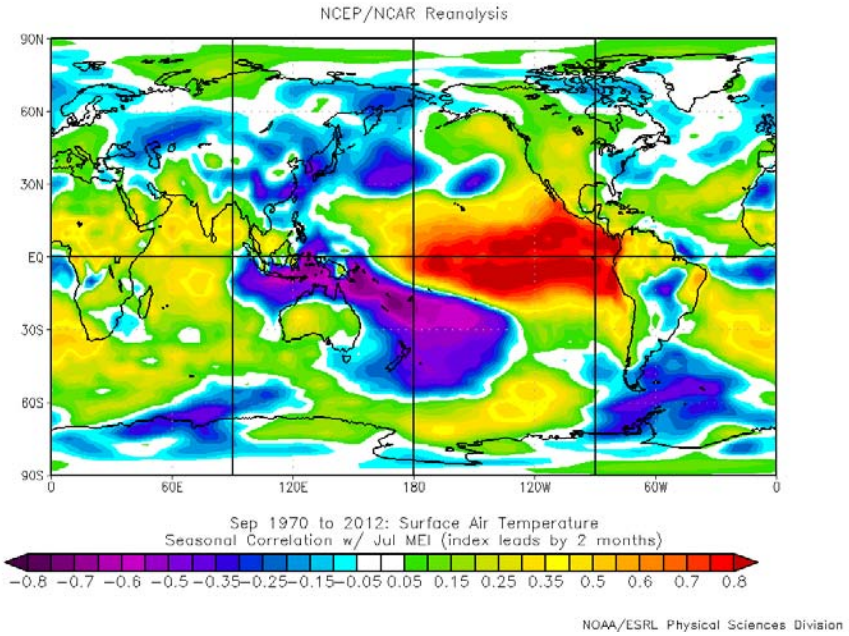


Figure 105. Jul MEI, used as a predictor for Sep surface air temperatures.

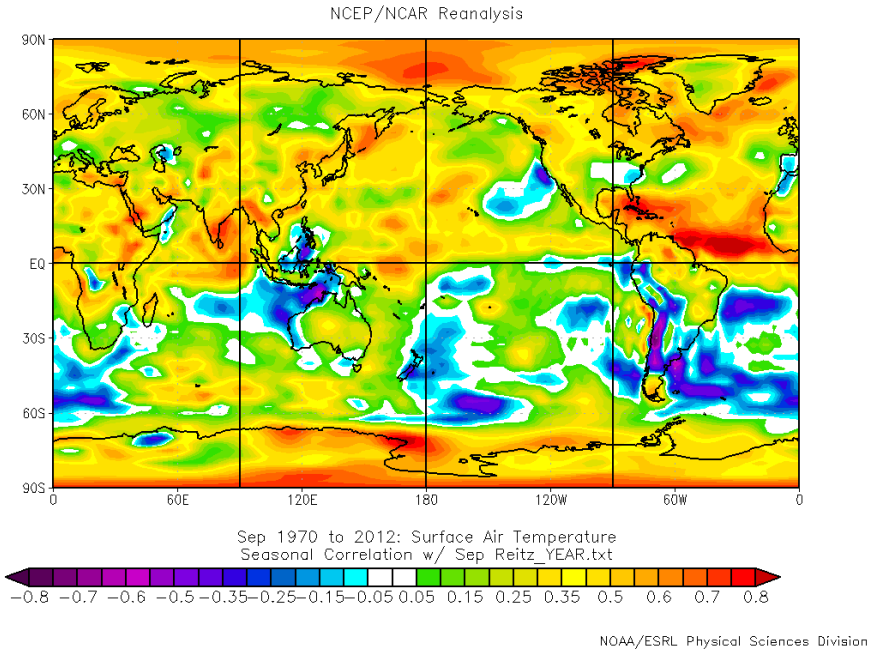


Figure 106. Year, used as a predictor for Sep surface air temperatures.

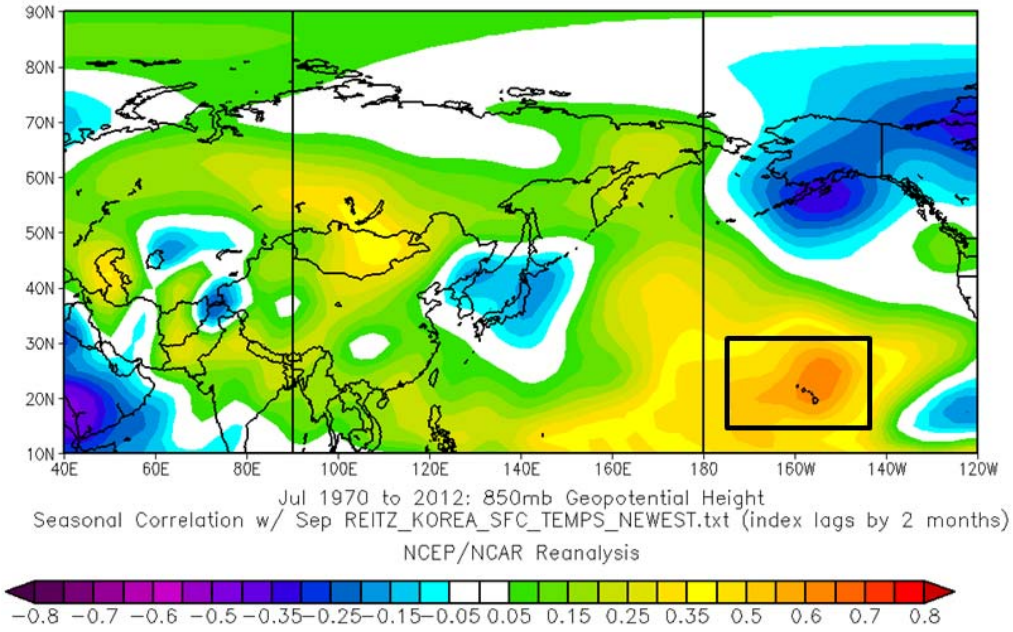


Figure 107. Inputs for KTI_SEP2, used as a predictor for Sep surface air temperatures.

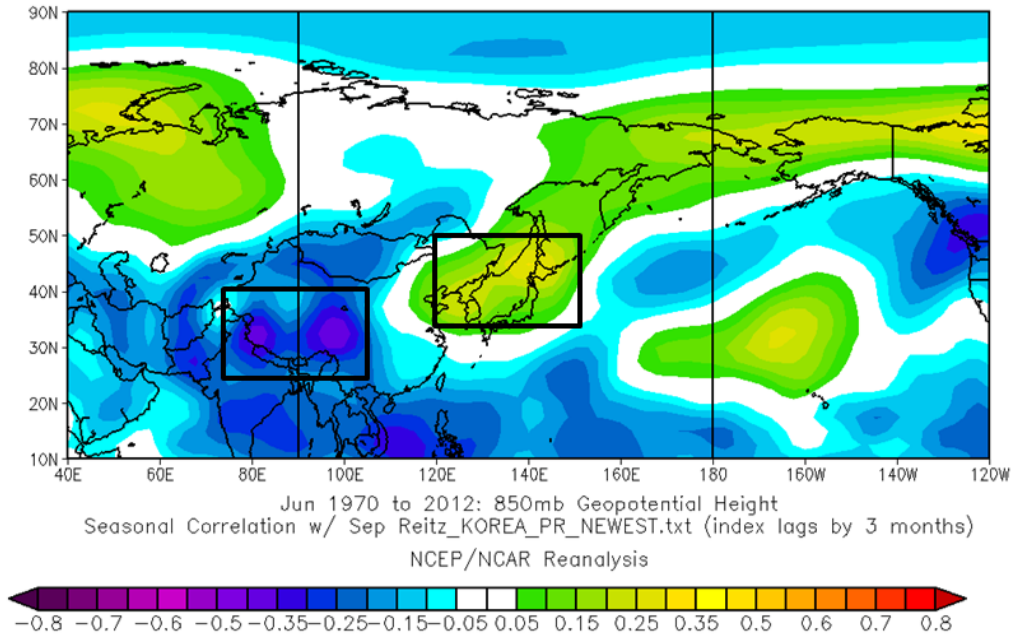


Figure 108. Inputs for KPI_SEP3, used as a predictor for Sep PR.

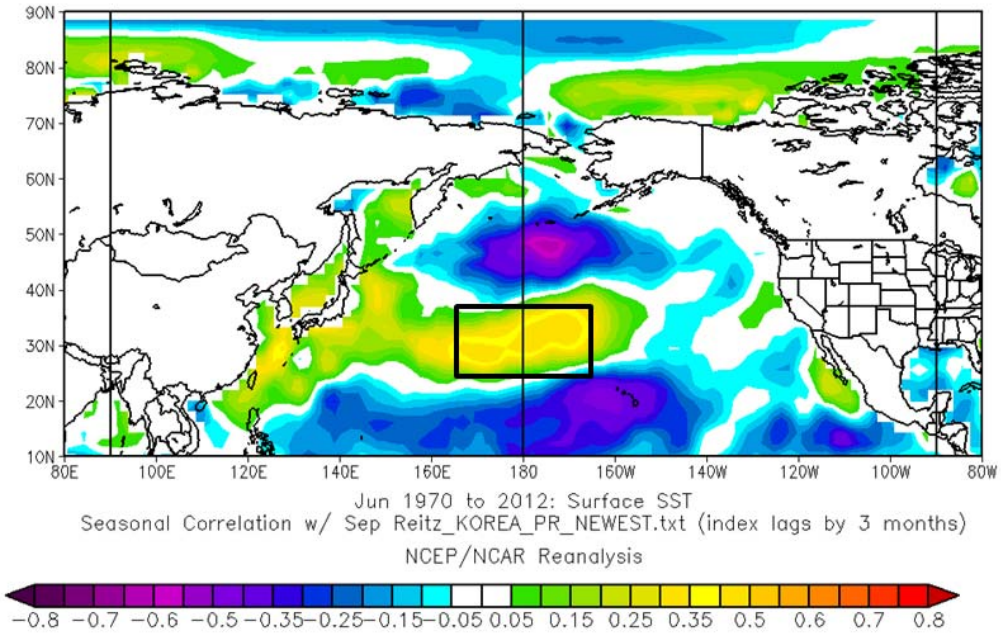


Figure 109. SST_PSEP3, used as a predictor for Sep PR.

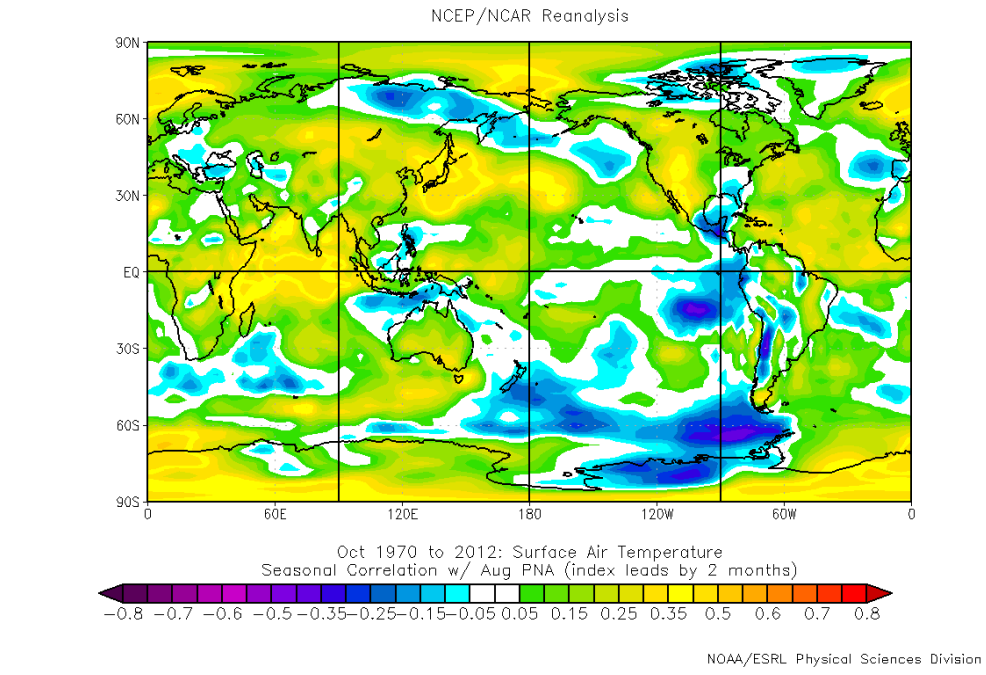


Figure 110. Aug PNA, used as a predictor for Oct surface air temperatures.

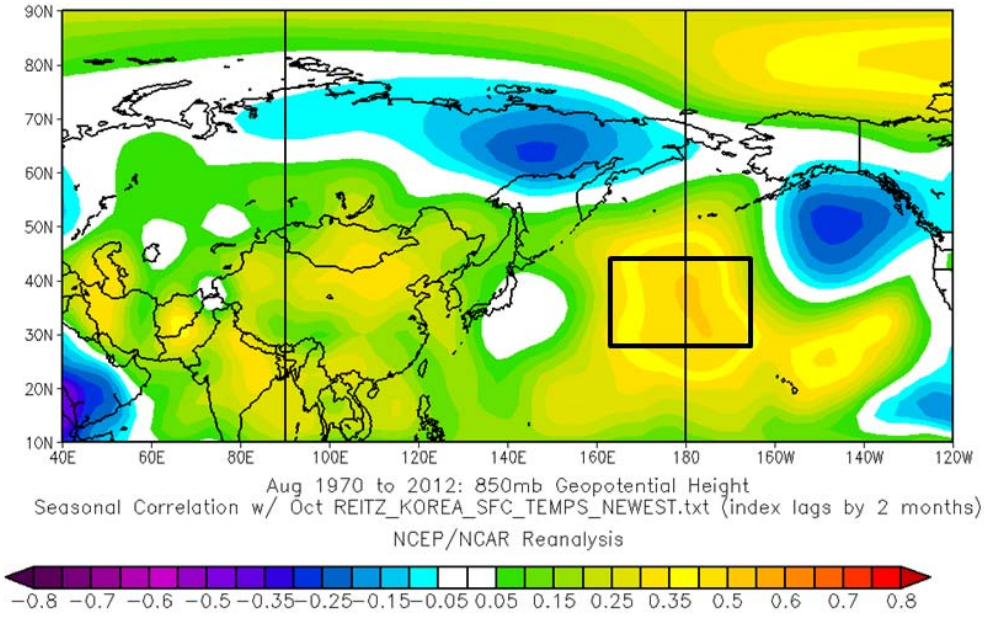


Figure 111. Inputs for KTI_OCT2, used as a predictor for Oct surface air temperatures.

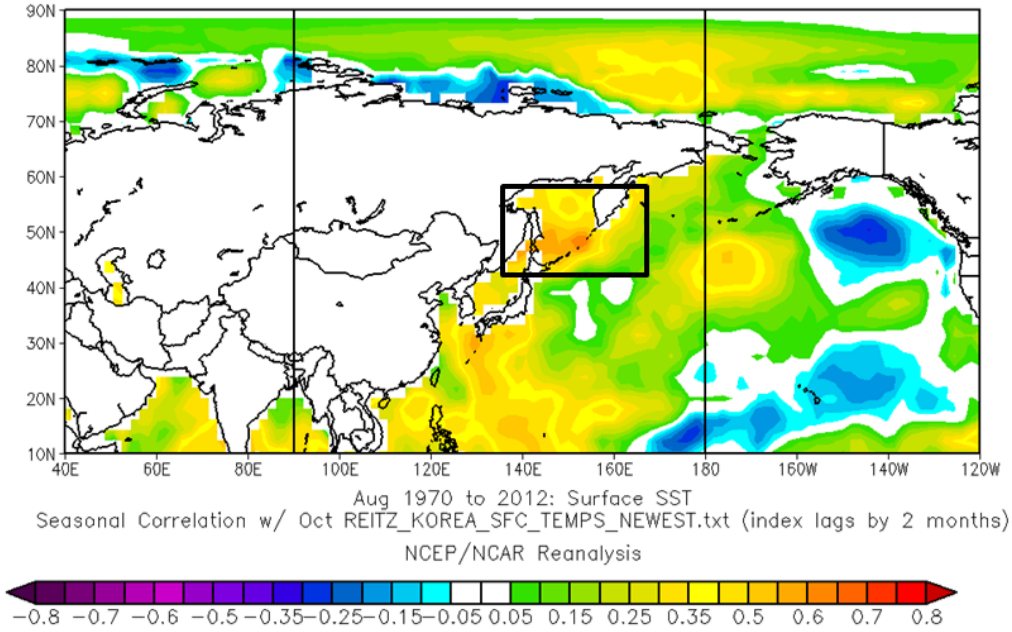


Figure 112. SST_TOCT2, used as a predictor for Oct surface air temperatures.

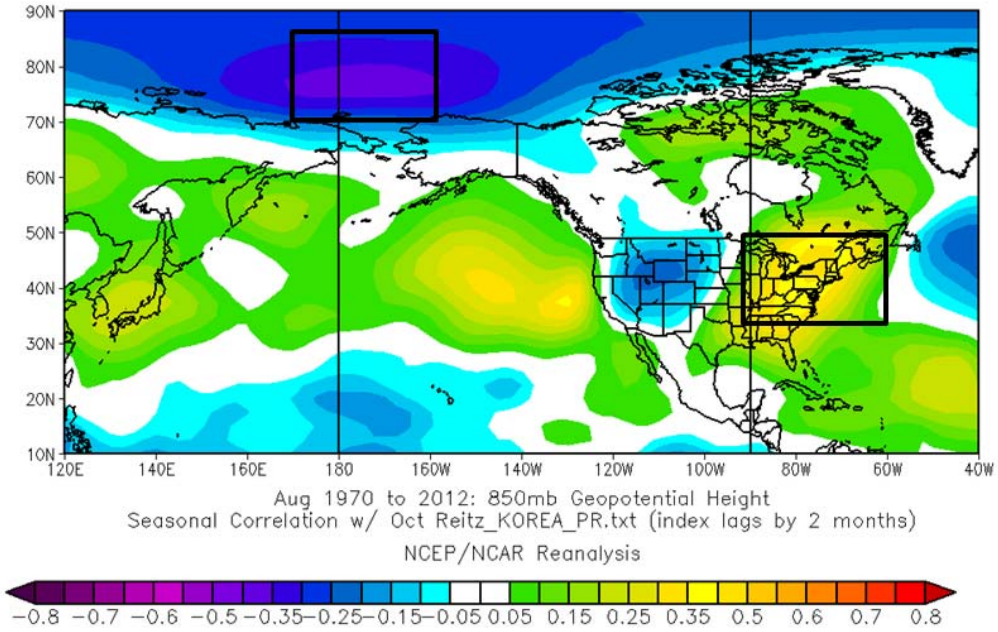


Figure 113. Inputs for KPI_OCT2, used as a predictor for Oct PR.

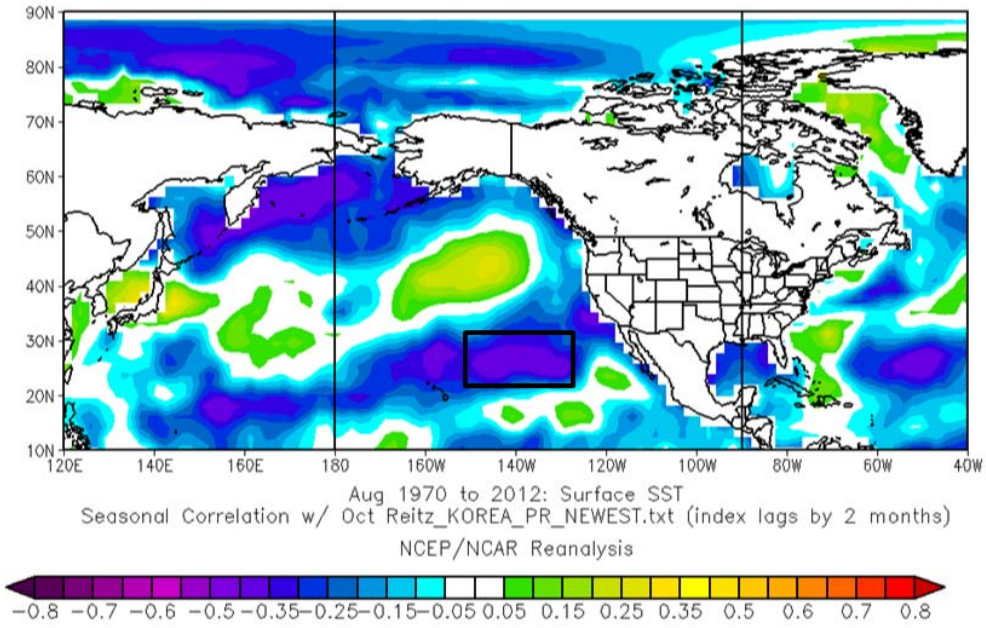


Figure 114. SST_POCT2, used as a predictor for Oct PR.

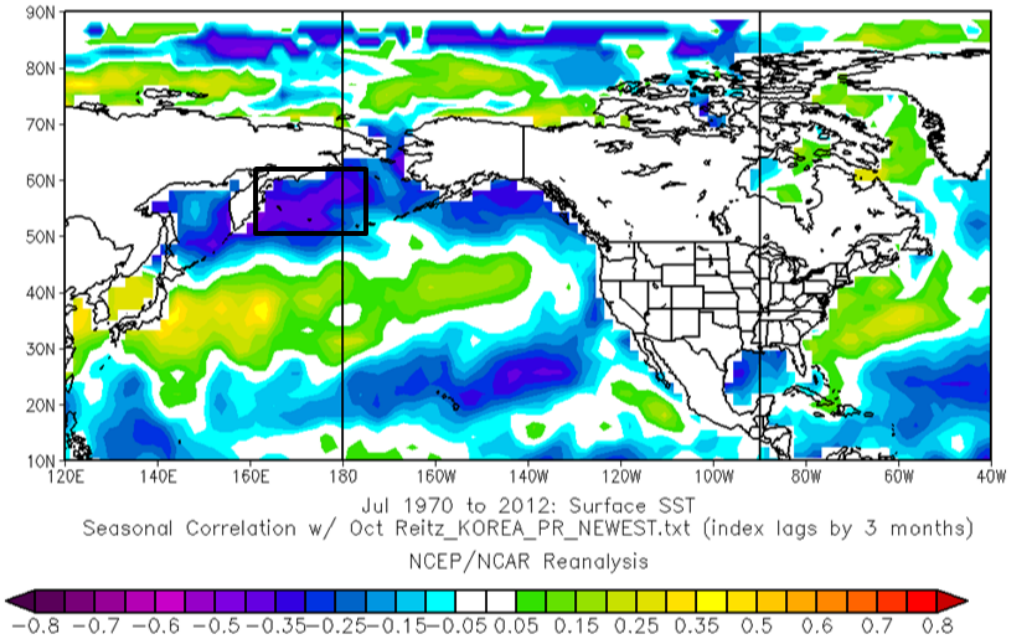


Figure 115. SST_POCT3, used as a predictor for Oct PR.

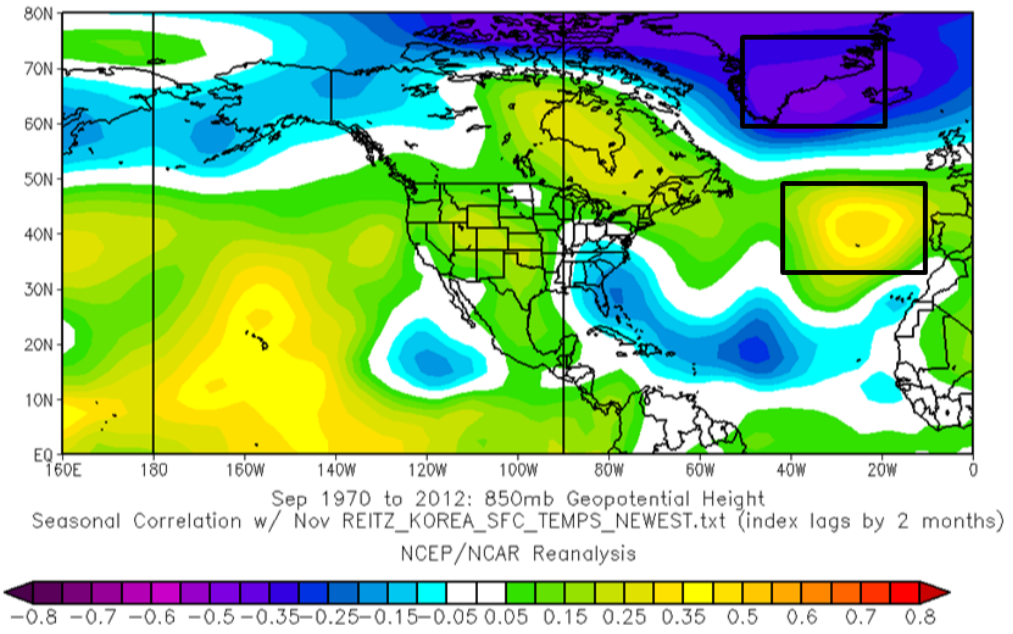


Figure 116. Inputs for KTI_NOV2, used as a predictor for Nov surface air temperatures.

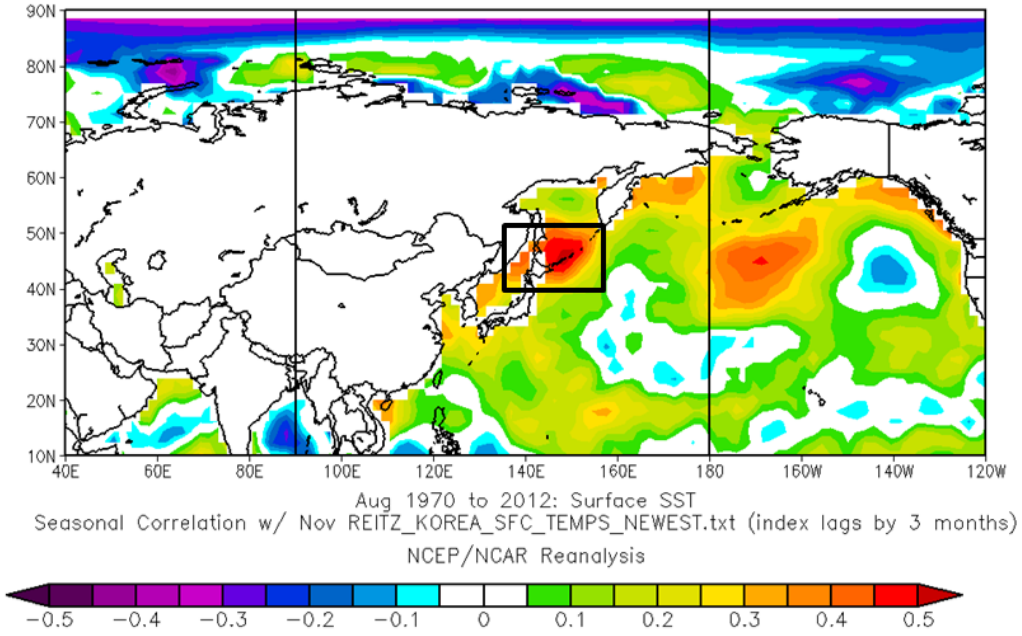


Figure 117. SST_TNOV3, used as a predictor for Nov surface air temperatures.

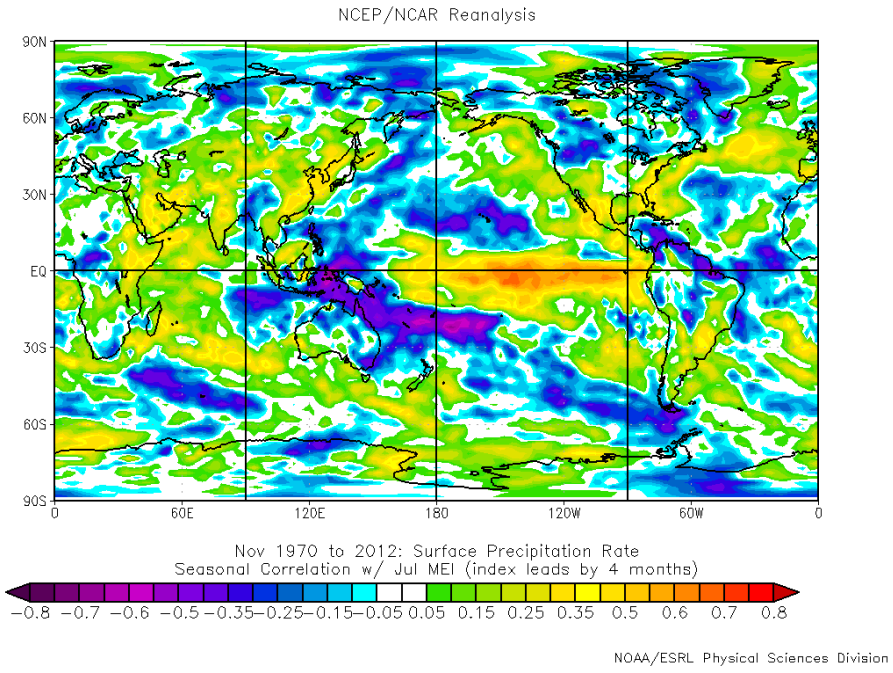


Figure 118. Jul MEI, used as a predictor for Nov PR.

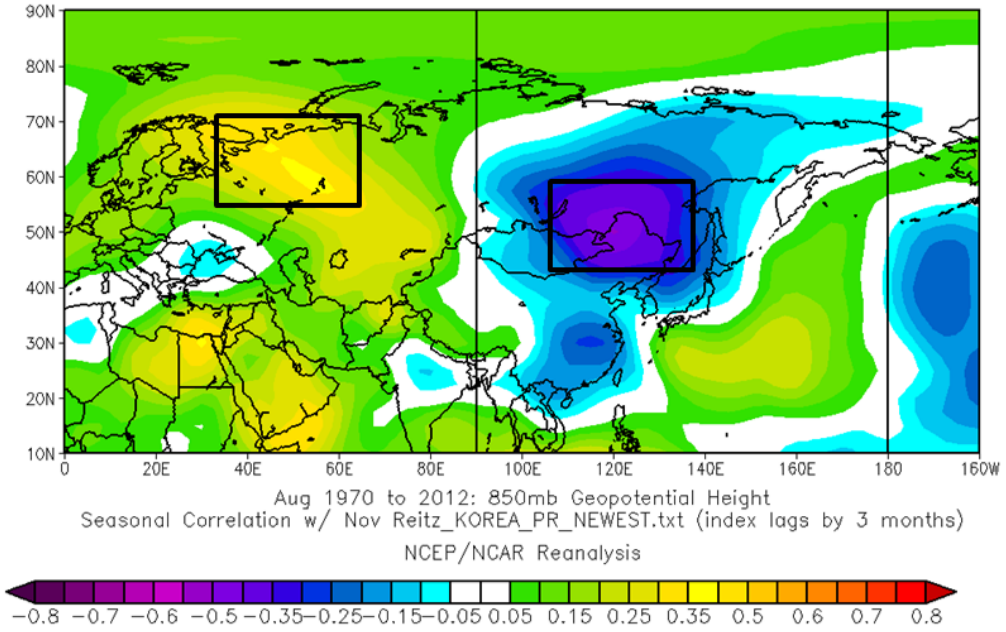


Figure 119. Inputs for KPI_NOV3, used as a predictor for Nov PR.

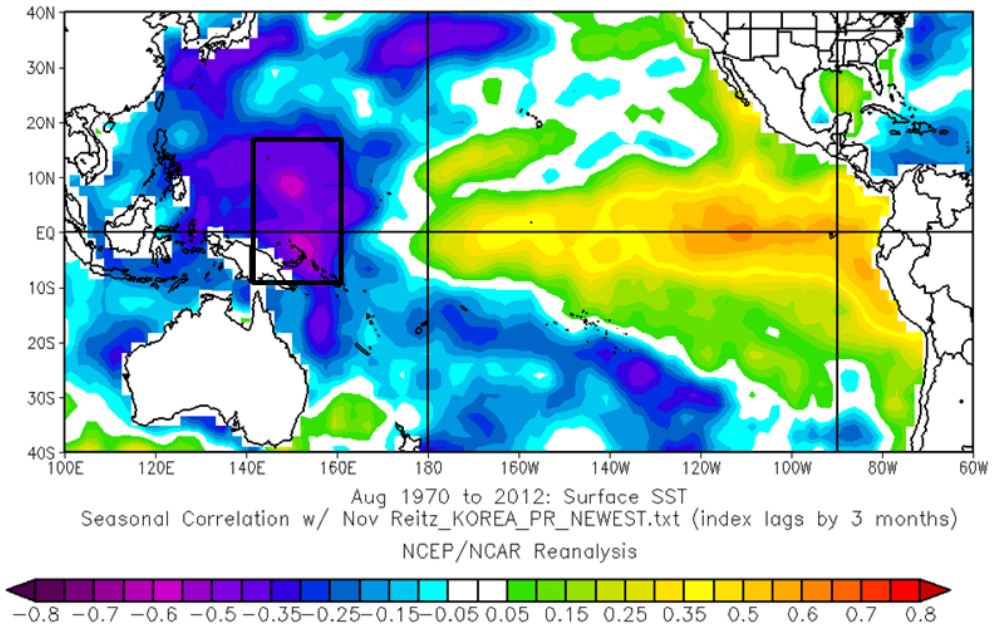


Figure 120. SST_PNOV3, used as a predictor for Nov PR.

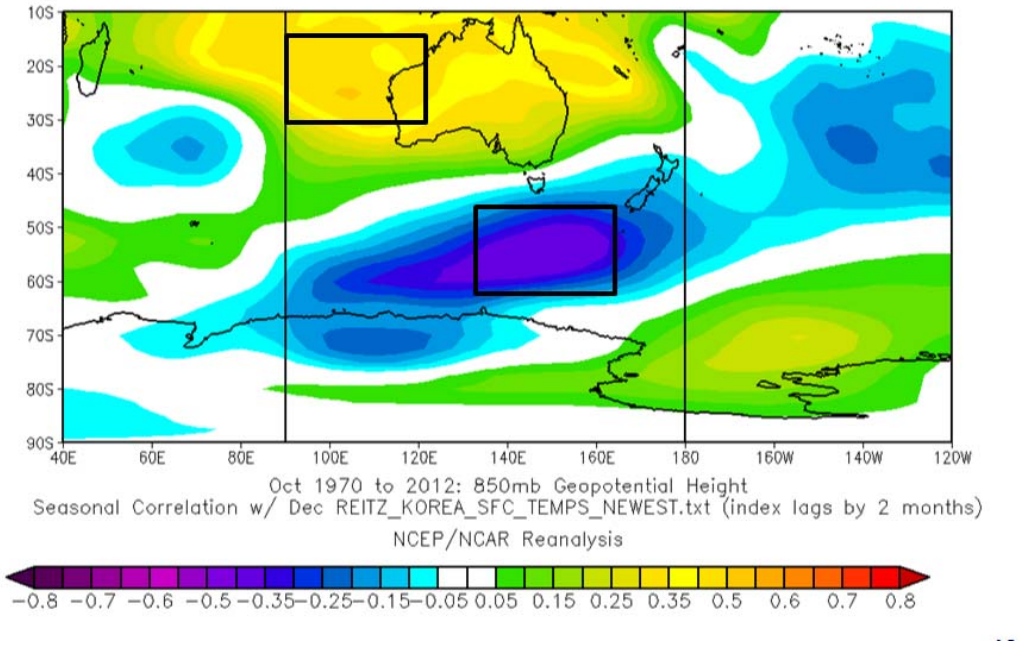


Figure 121. Inputs for KTI_DEC2, used as a predictor for Dec surface air temperatures.

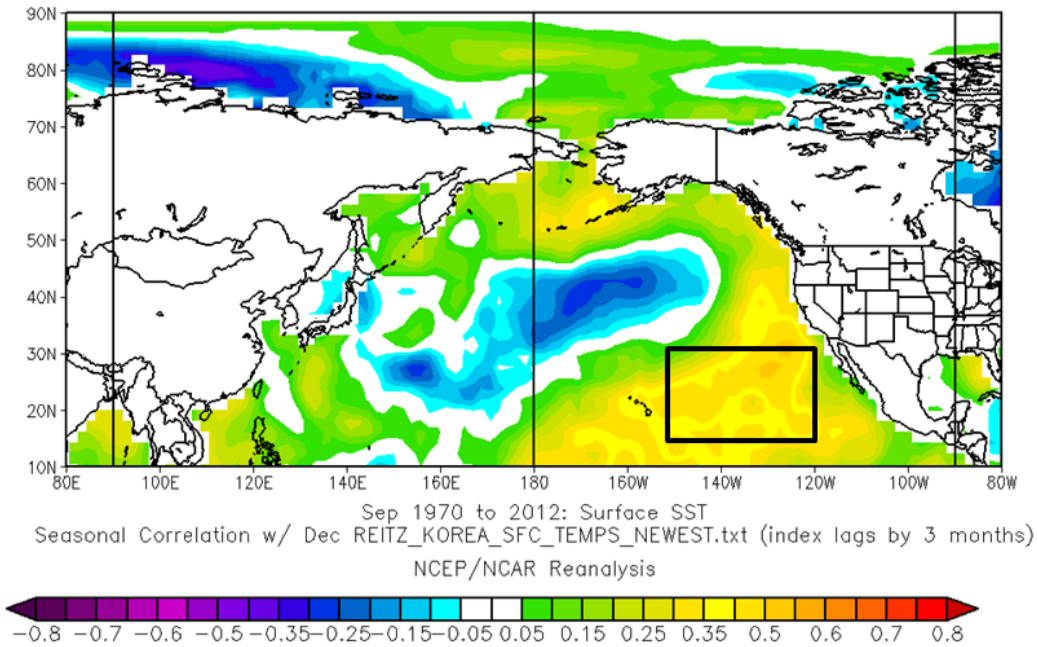


Figure 122. SST_TDEC3, used as a predictor for Dec surface air temperatures.

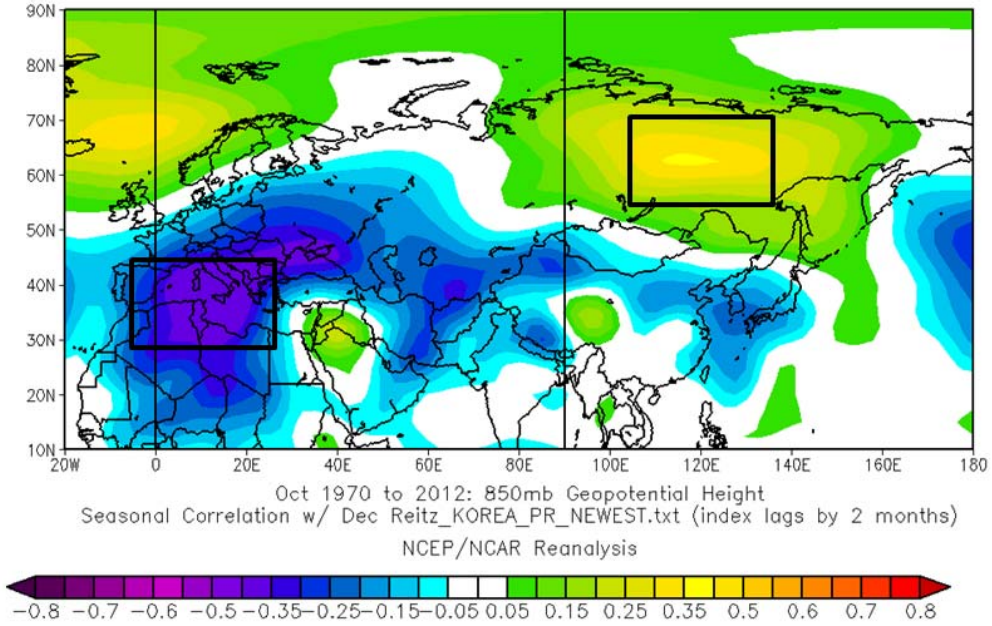


Figure 123. Inputs for KPI_DEC2, used as a predictor for Dec PR.

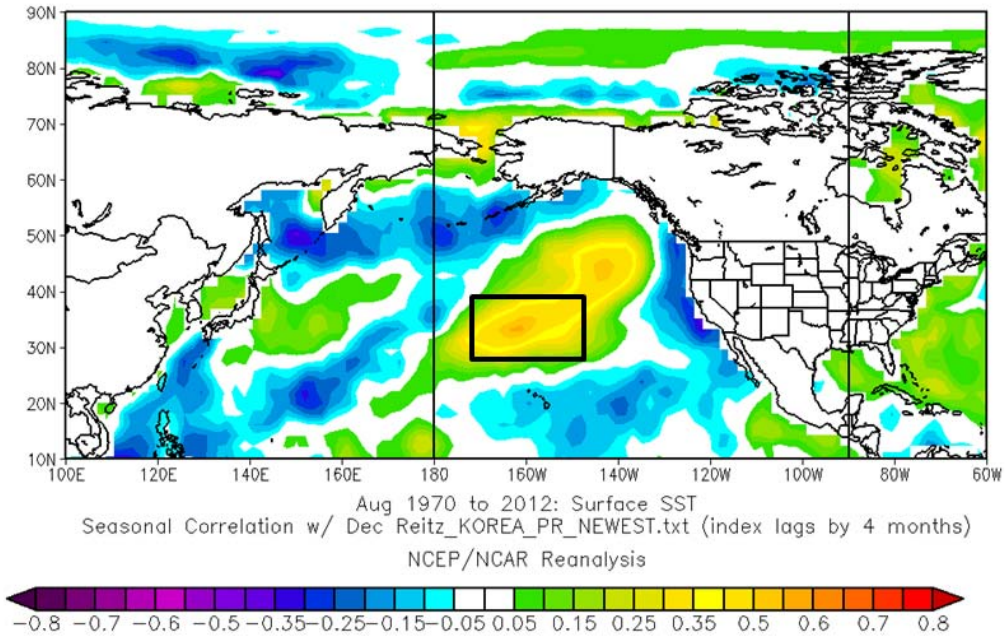


Figure 124. SST_PDEC4, used as a predictor for Dec PR.

THIS PAGE LEFT INTENTIONALLY BLANK

# APPENDIX B. HINDCASTING RESULTS

This appendix contains the hindcast results for all months for both surface temperatures and PR. The captions will be abbreviated in this appendix and the following description will be used.

Each figure shows the comparison of Korean surface air temperature (or PR) anomaly hindcasts and the corresponding observed anomalies (blue) for 1970–2012 for the indicated month. See Figures 44 and 45 for examples of detailed captions.

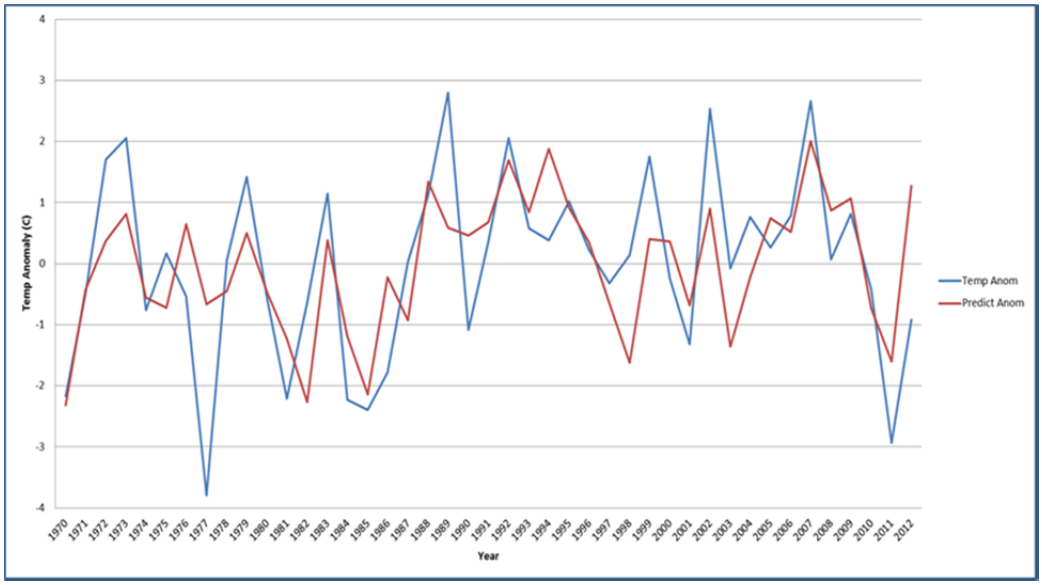


Figure 125. Jan Surface air temperature hindcasting results, 1970–2012.

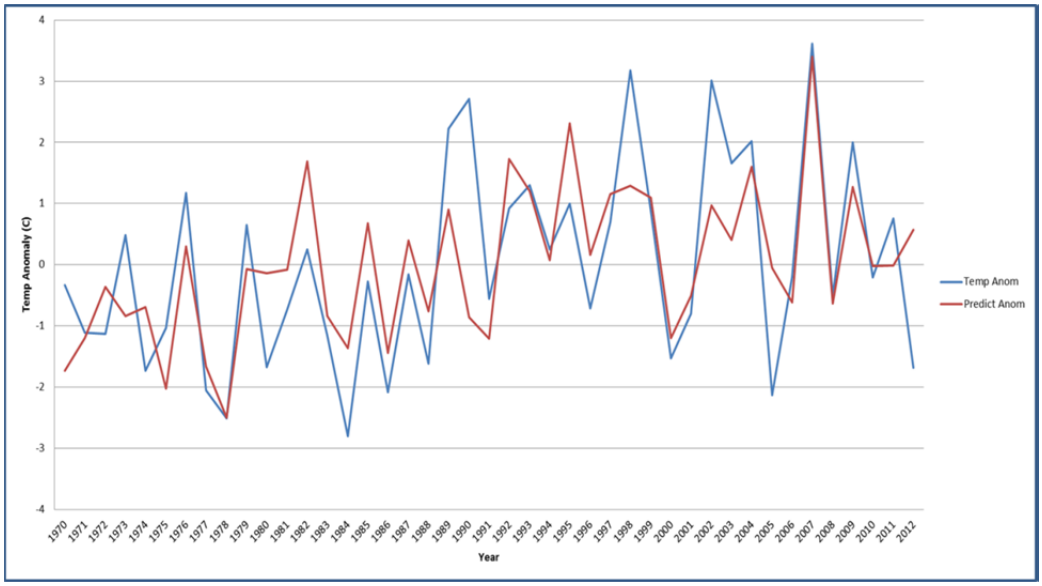


Figure 126. Feb surface air temperature hindcasting results, 1970–2012.

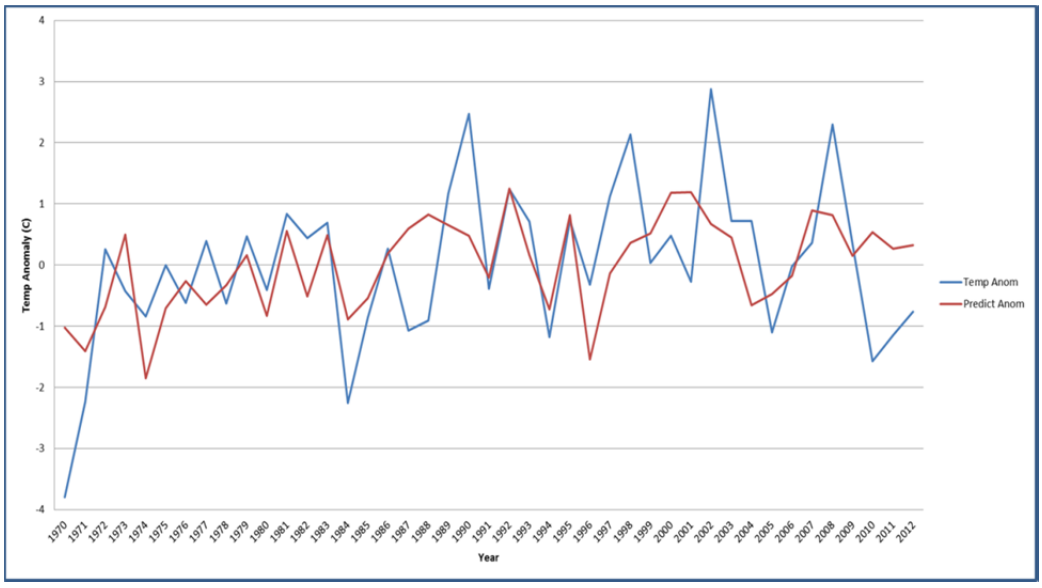


Figure 127. Mar surface air temperature hindcasting results, 1970–2012.

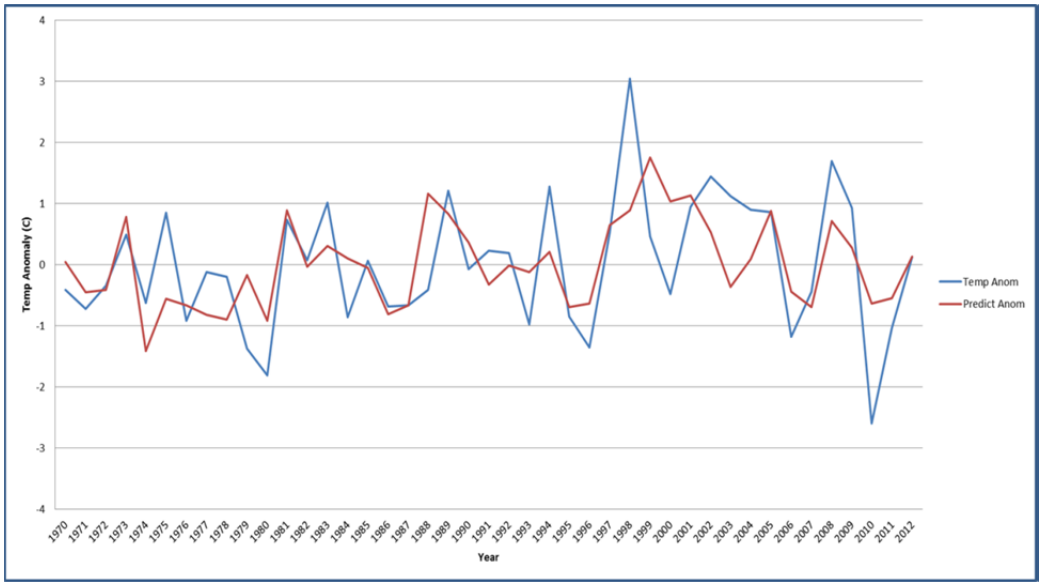


Figure 128. Apr surface air temperature hindcasting results, 1970–2012.

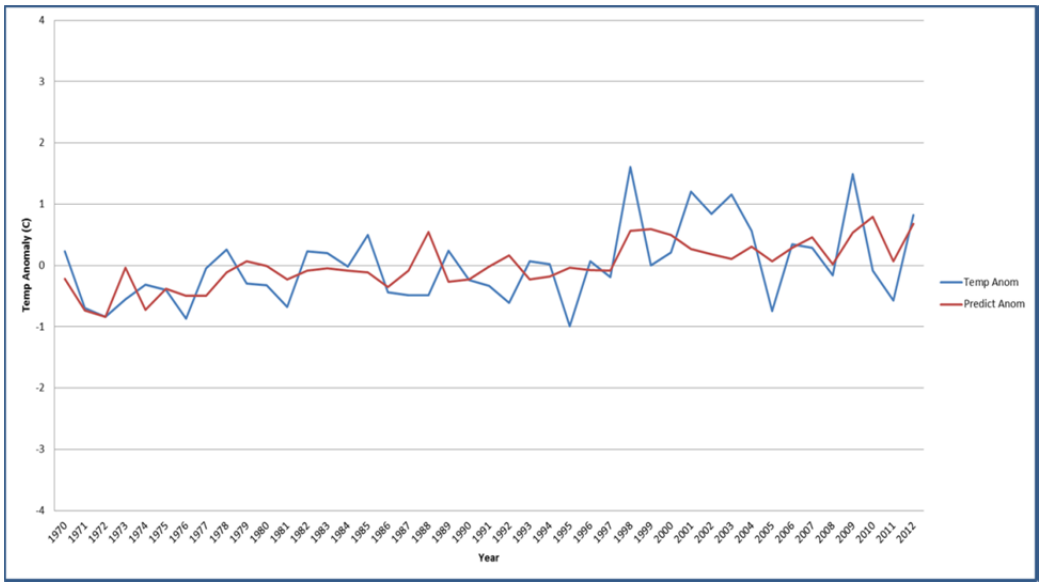


Figure 129. May surface air temperature hindcasting results, 1970–2012.

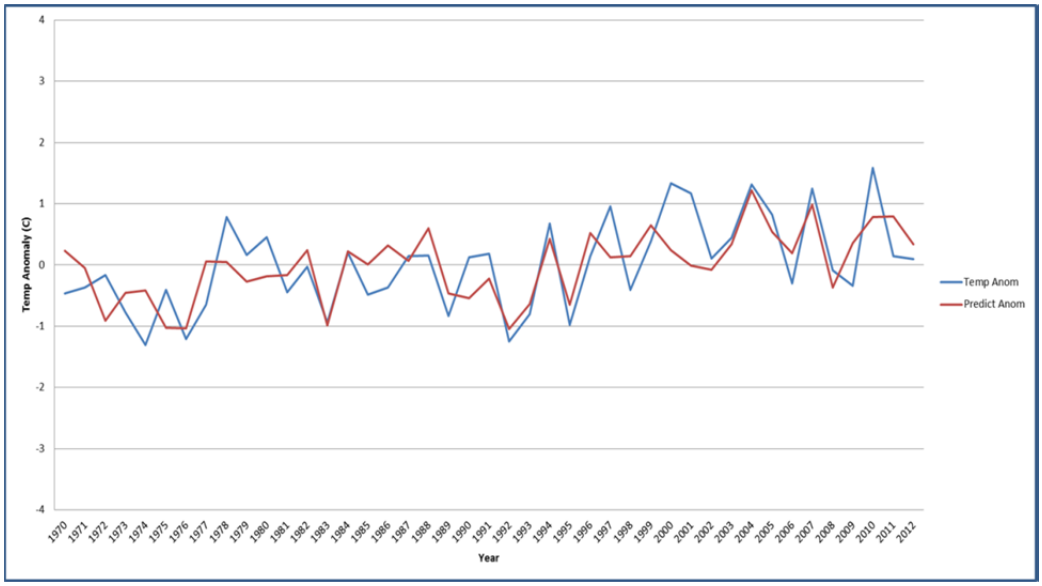


Figure 130. June surface air temperature hindcasting results, 1970–2012.

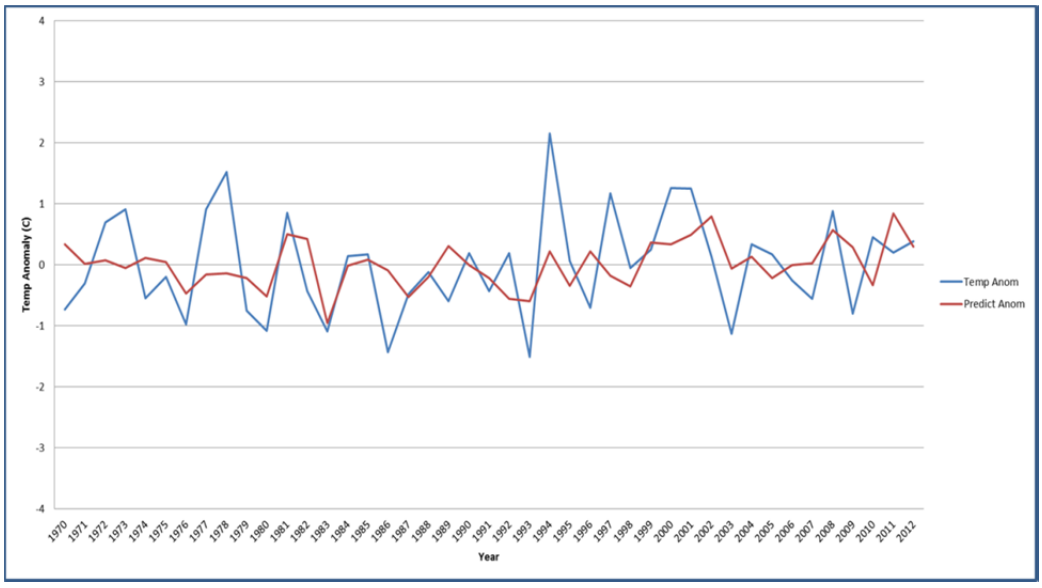


Figure 131. July surface air temperature hindcasting results, 1970–2012.

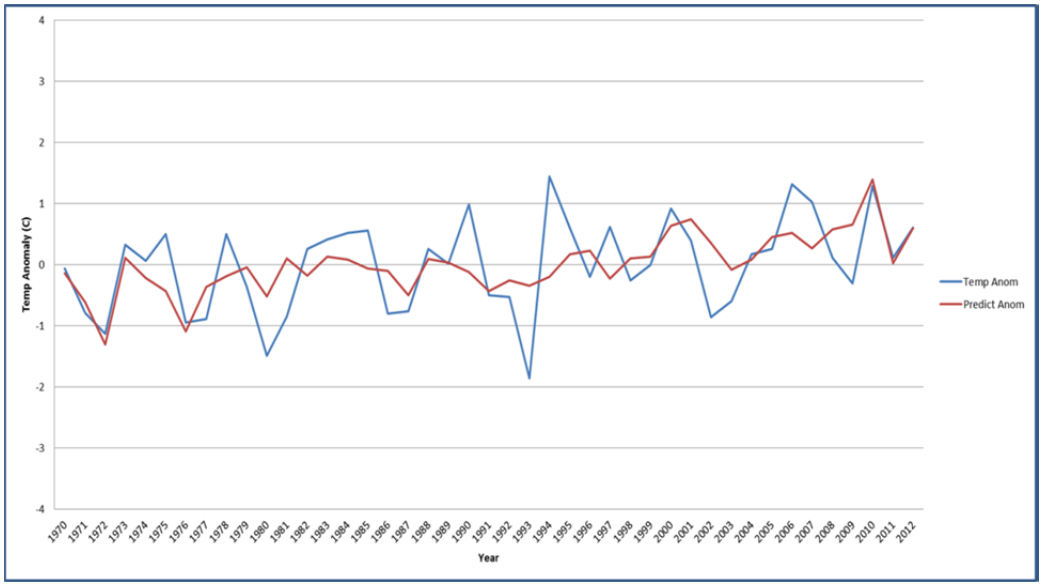


Figure 132. Aug surface air temperature hindcasting results, 1970–2012.

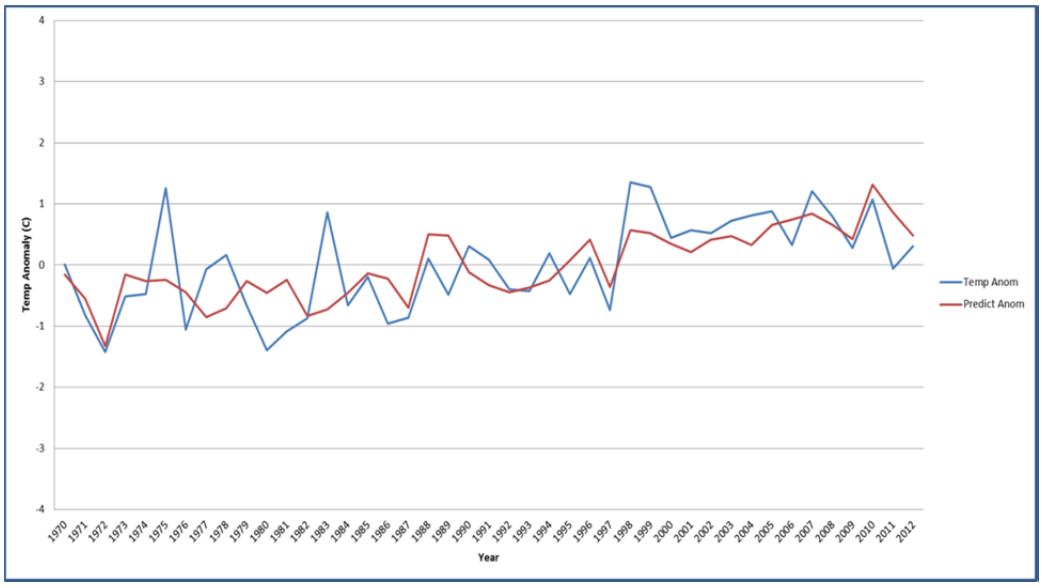


Figure 133. Sep surface air temperature hindcasting results, 1970–2012.

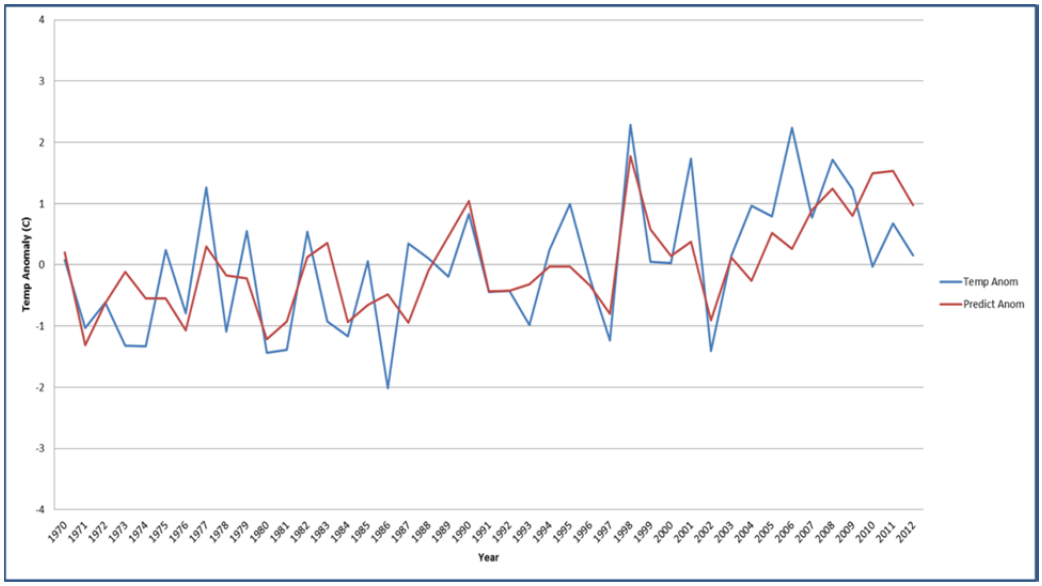


Figure 134. Oct surface air temperature hindcasting results, 1970–2012.

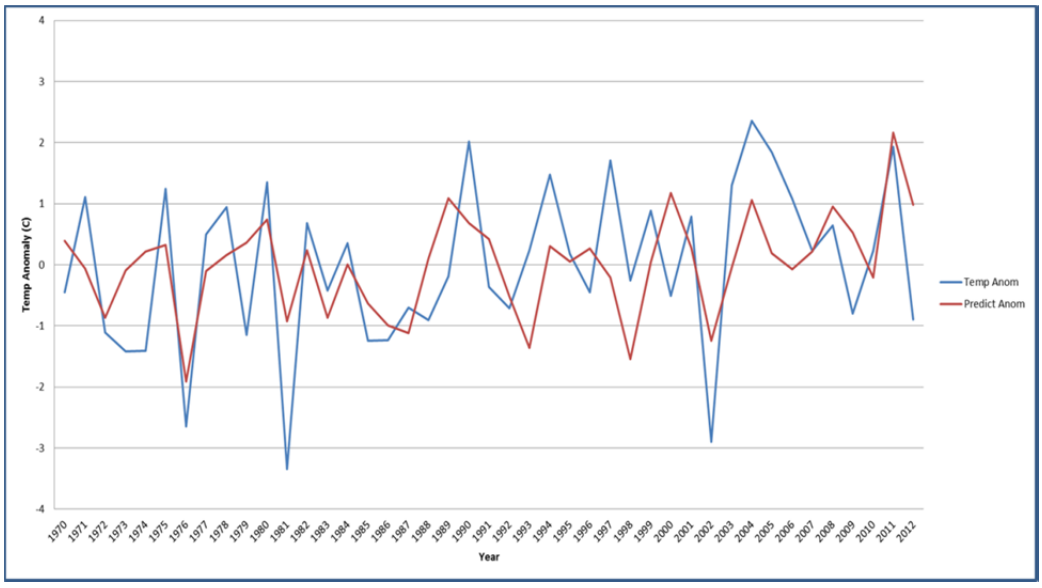


Figure 135. Nov surface air temperature hindcasting results, 1970–2012.

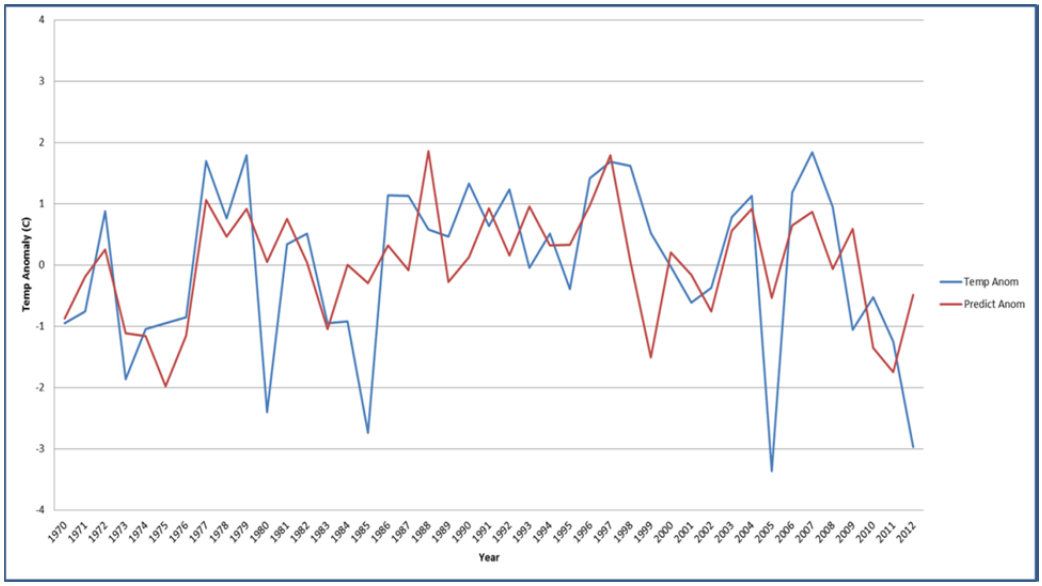


Figure 136. Dec surface air temperature hindcasting results, 1970–2012.

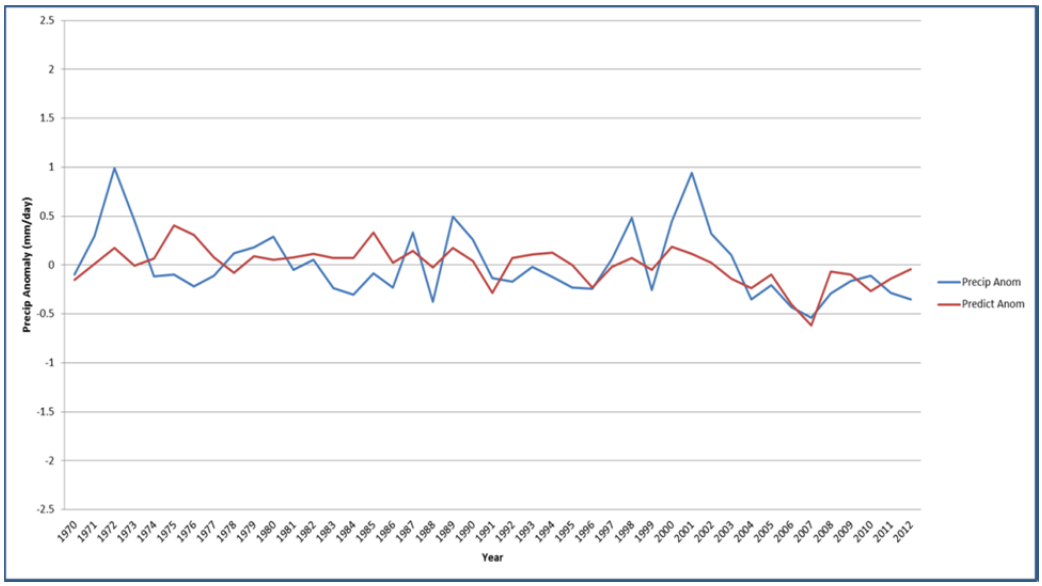


Figure 137. Jan PR hindcasting results, 1970–2012.

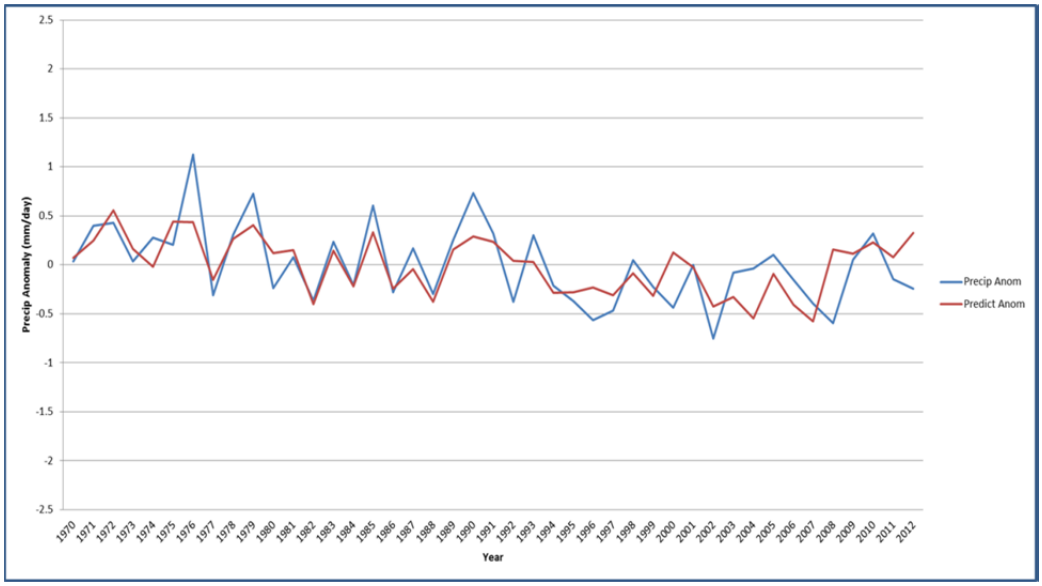


Figure 138. Feb PR hindcasting results, 1970–2012.

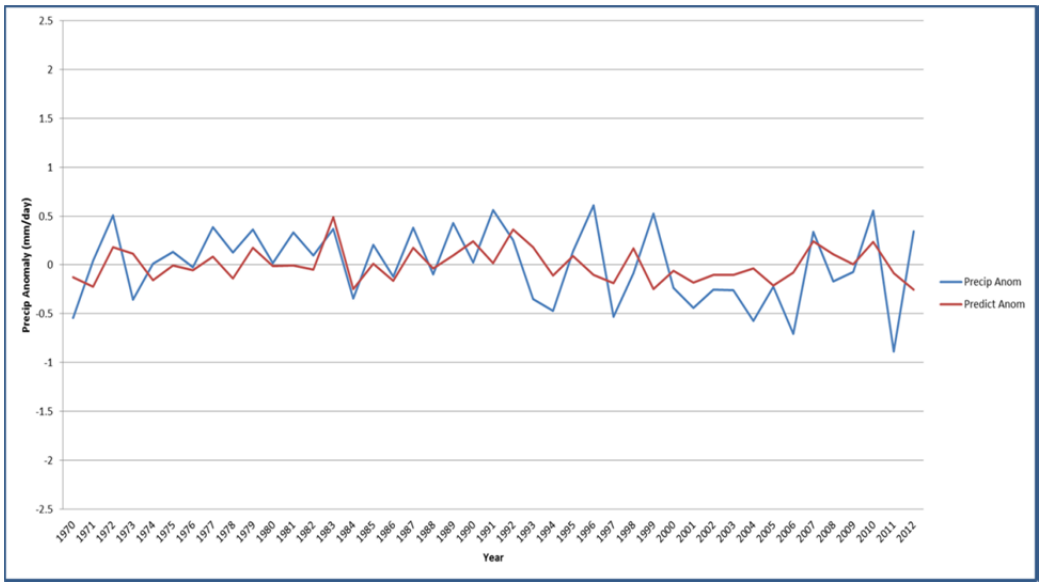


Figure 139. Mar PR hindcasting results, 1970–2012.

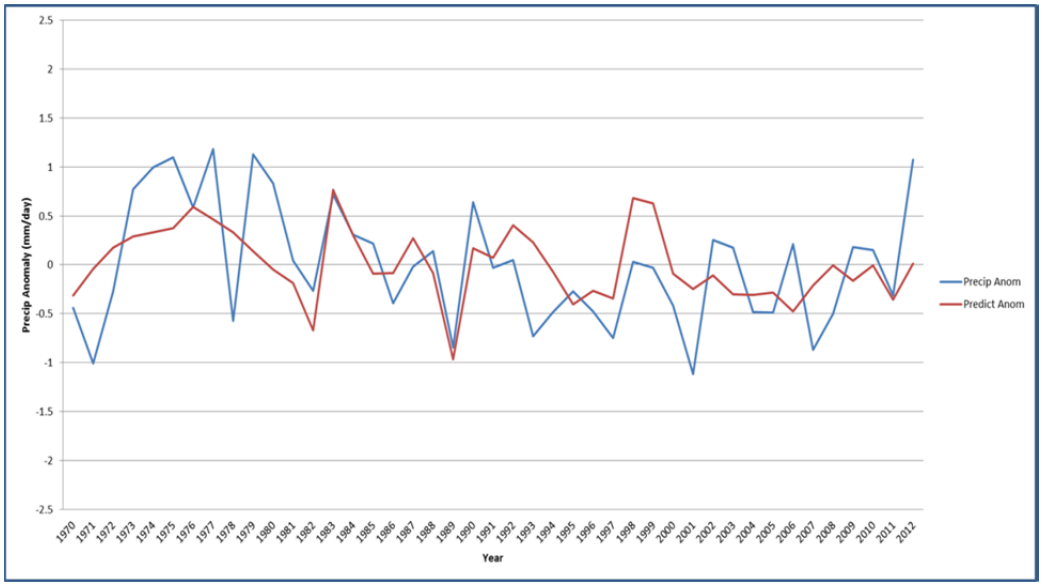


Figure 140. Apr PR hindcasting results, 1970–2012.

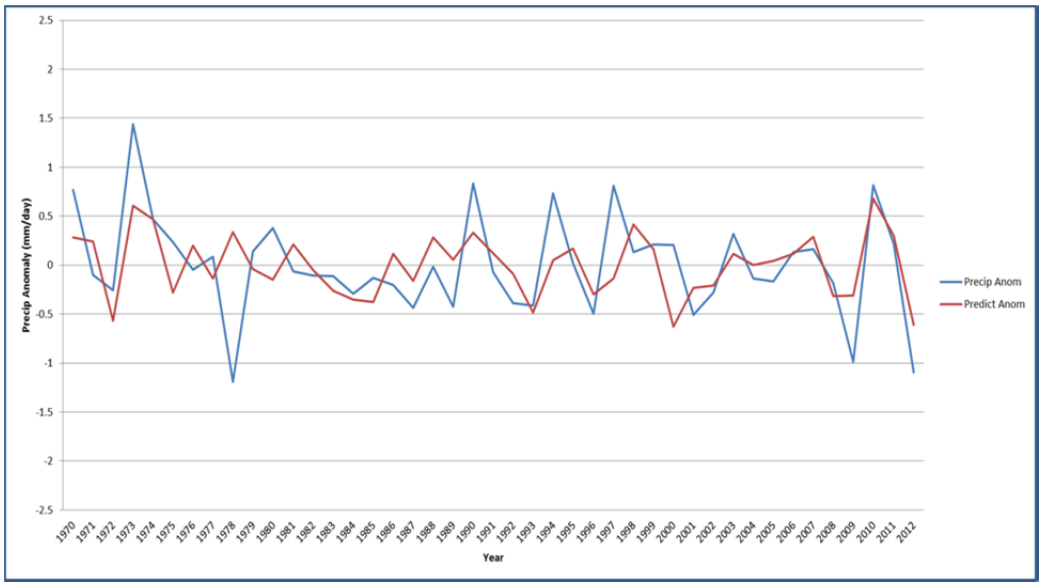


Figure 141. May PR hindcasting results, 1970–2012.

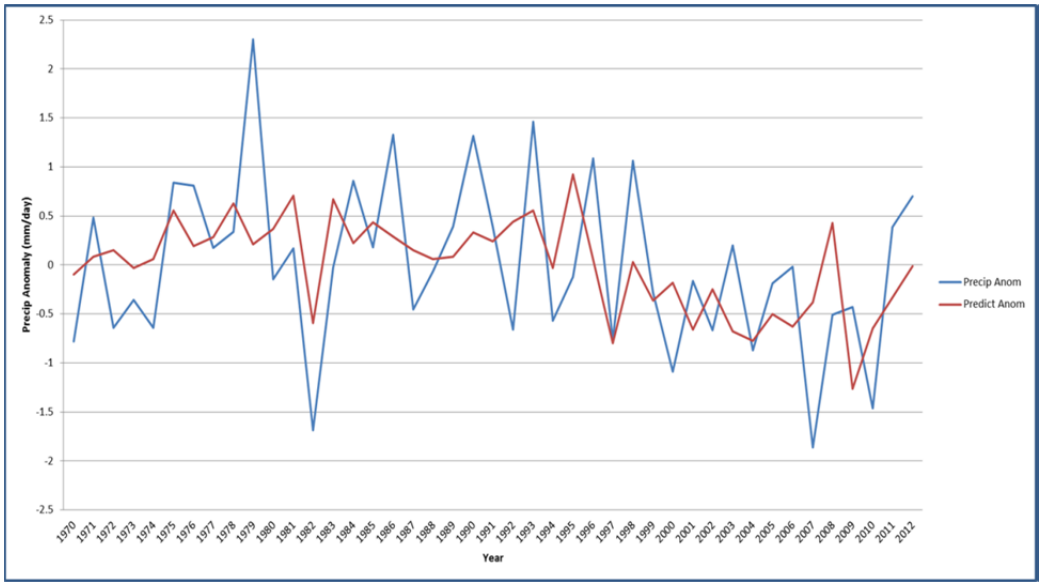


Figure 142. June PR hindcasting results, 1970–2012.

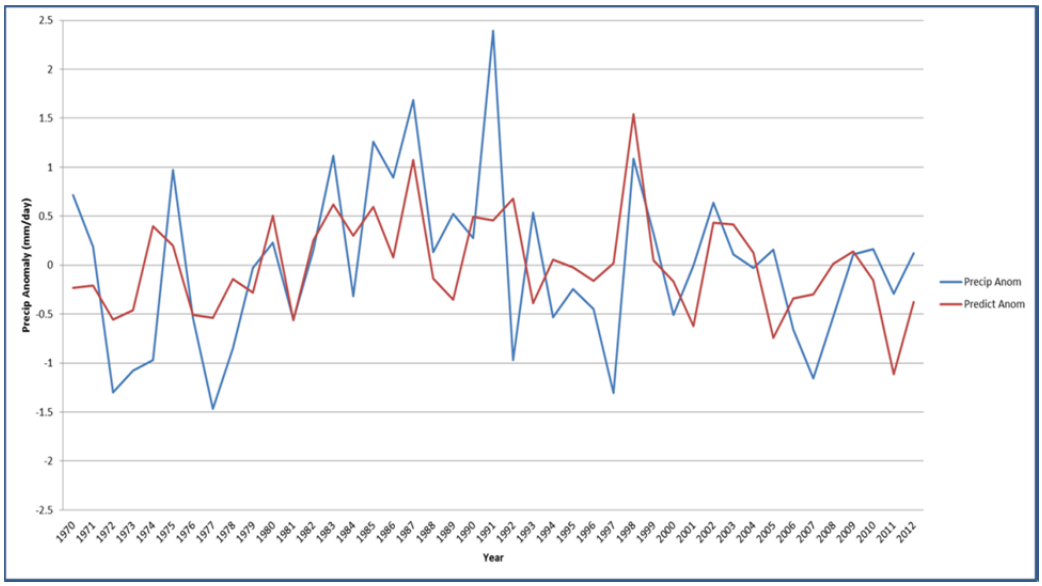


Figure 143. July PR hindcasting results, 1970–2012.

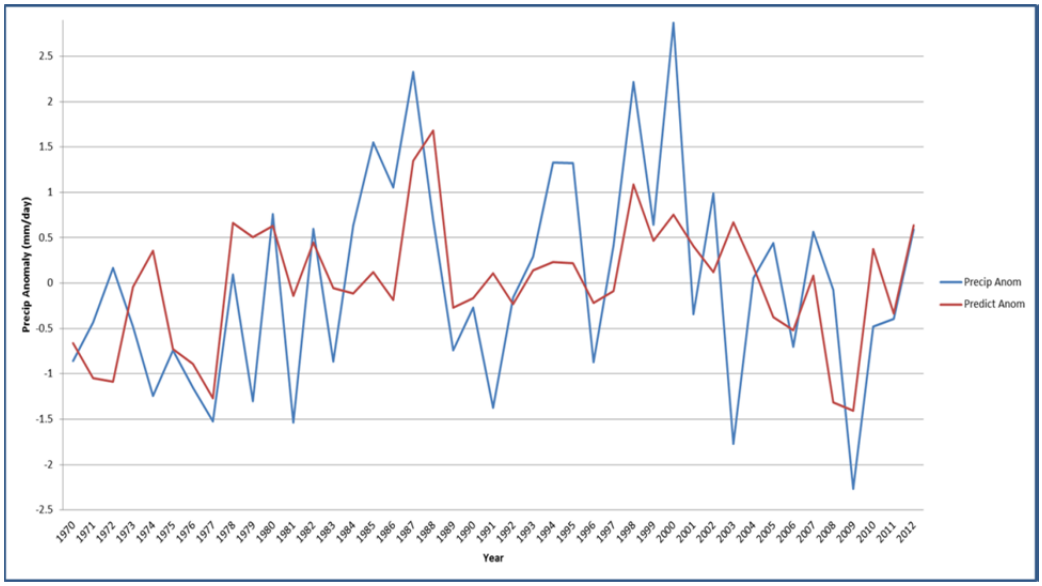


Figure 144. Aug PR hindcasting results, 1970–2012.

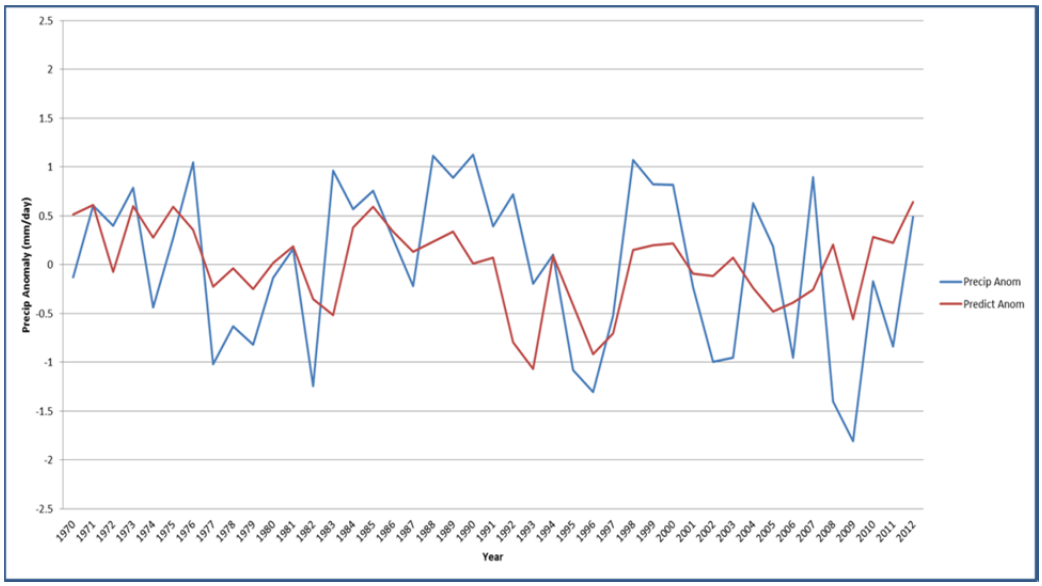


Figure 145. Sep PR hindcasting results, 1970–2012.

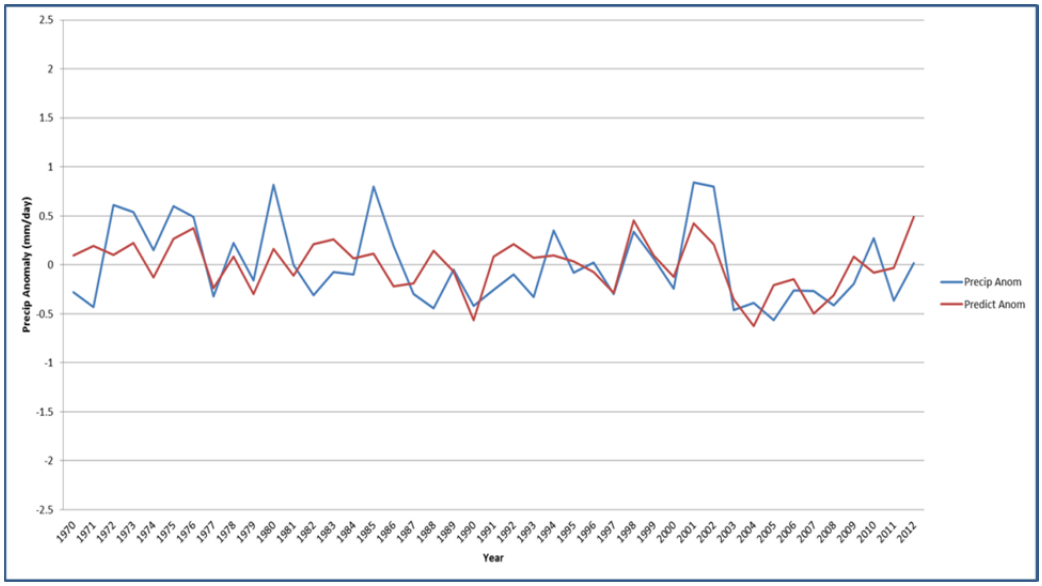


Figure 146. Oct PR hindcasting results, 1970–2012.

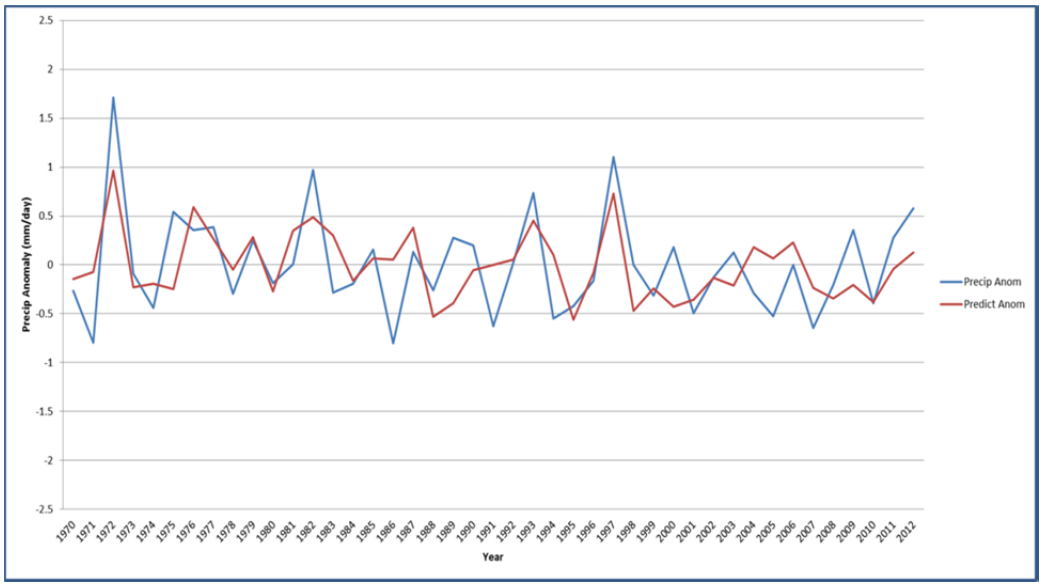


Figure 147. Nov PR hindcasting results, 1970–2012.

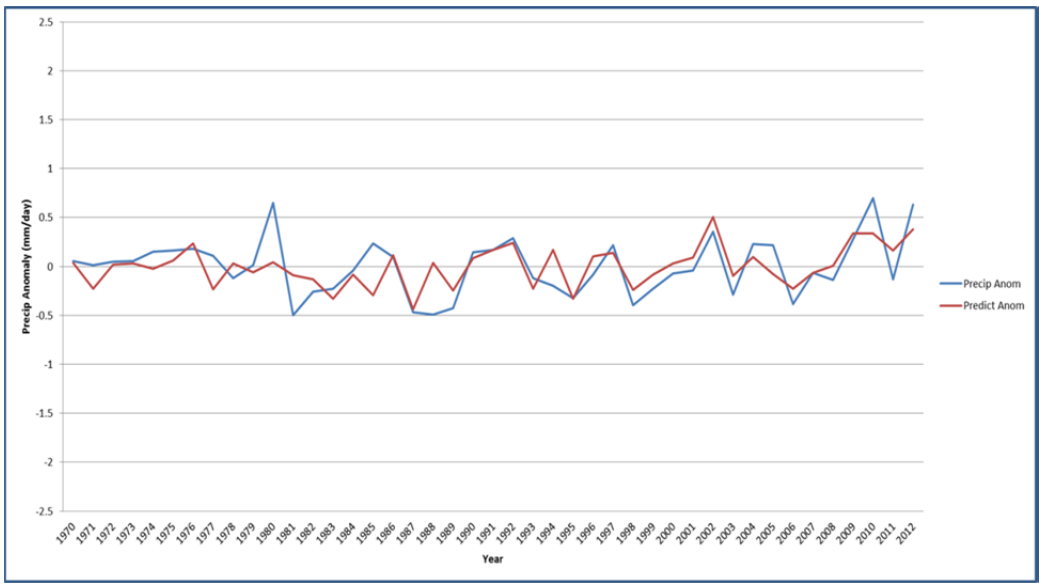


Figure 148. Dec PR hindcasting results, 1970–2012.

THIS PAGE LEFT INTENTIONALLY BLANK

# LIST OF REFERENCES


14th Weather Squadron (14 WS), cited 2012: [Available online at https://notus2.afccc.af.mil.]

America.gov, cited 2013: Briefing by Defense Secretary Gates and ROK Minister Lee. [Available online at http://www.america.gov/st/texttrans-english/2008/Oct/20081020121847eaifas0.7119104.html.]

Barnston, A. G., S. J. Mason, L. Goddard, D. G. DeWitt, and S. E. Zebiak, 2003: Multimodel ensembling in seasonal climate forecasting at IRI. *Bull. Amer. Meteor. Soc*., **84**, no. 12, 1783–1796, doi:10.1175/BAMS-84–12–1783.

Beijing Climate Center (BCC), cited 2013. [Available online at http://bcc.cma.gov.cn/Website/index.php?ChannelID=22.]

Bridgman, H., and J. Oliver, 2006: *The Global Climate System*, Cambridge University Press, 331 pp.

Climate Prediction Center (CPC), cited 2013: [Available online at http://www.cpc.ncep.noaa.gov/.]

DeHart, J., 2011: Long-range forecasting in support of operations in Pakistan. M.S. thesis, Dept. of Meteorology, Naval Postgraduate School, 83 pp.

Earth Systems Research Laboratory (ESRL), Physical Sciences Division, cited 2013: [Available online at http://www.esrl.noaa.gov/psd/.]

FindLaw, cited 2013: Korean Armistice Agreement, 1953. [Available online at http://news.findlaw.com/cnn/docs/korea/kwarmagr072753.html.]

Ford, B. W., 2000: El Niño and La Niña Effects on Tropical Cyclones: The mechanisms. M. S. thesis, Dept of Meteorology, Naval Postgraduate School, 190 pp.

Giese, P., 2004: *Korea: A full year study*, AFCCC, 80 pp.

Gillies, S., 2012: A statistical multimodel ensemble approach to improving long-range forecasting in Pakistan. M.S. thesis, Dept. of Meteorology, Naval Postgraduate School, 123 pp.

American Meteorological Society (AMS), cited 2013: [Available online at http://glossary.ametsoc.org/wiki/Teleconnection.]

Gong, D. Y., and C. H. Ho, 2003: Arctic Oscillation signals in the East Asian summer monsoon. *J. Geophys*. Res., **108**, 4066, doi:10.1029/2002JD002193.

Ha, K. J., and S. S. Lee, 2007: On the interannual variability of the Bonin high associated with the East Asian summer monsoon rain. *Climate Dynamics*, **28**, 67–83.

Hoffman, R. N., and E. Kalnay, 1983: Lagged average forecasting, an alternative to Monte Carlo forecasting. *Tellus*, **35A**, 100–118.

International Research Institute for Climate and Society (IRI), cited 2013: [Available online at: http://portal.iri.columbia.edu/portal/server.pt.]

Japan Meteorological Agency (JMA), cited 2013. [Available online at http://www.jma.go.jp/jma/en/Activities/forecast.html.]

Kalnay, E., and Co-Authors, 1996: The NCEP/NCAR 40-year reanalysis project, *Bull Amer. Meteor. Soc.*, **77**, no. 3, 437–471.

Kistler, R., and Co-Authors, 2001: The NCEP–NCAR 50-year reanalysis: monthly means CD-ROM and documentation. *Bull. Amer. Meteor. Soc*., **82**, no. 2, 247–267.

Korean Meteorological Administration (KMA), cited 2013. [Available online at http://web.kma.go.kr/eng/irwp/info_kma_lrf_sys.pdf.]

Latif, M., and T. P. Barnett, 1994: Causes of decadel climate variability over the North Pacific and North America. *Science,* **266**, 634–637

Leathers, D. J., B. Yarnal, M. A. Palecki, 1991: The Pacific/North American teleconnection pattern the United States climate. Part I: Regional temperature and precipitation Associations. *J. Climate*, **4**, 517–528.

Lemke, B., 2010: Long-range forecasting in support of operations in the Horn of Africa. M.S. thesis, Dept. of Meteorology, Naval Postgraduate School, 125 pp.

Li, Y., and N.C. Lau, 2011: Impact of ENSO on the atmospheric variability over the North Atlantic in late winter—role of transient eddies. *J. Climate,* **25**, 320-342.

Murphree, T., 2012a: MR3610 Course Module 6: *Introduction to Advanced Climate Support for National Security*. Dept. of Meteorology, Naval Postgraduate School, Monterey, California, 76 pp.

Murphree, T., 2012b: MR3610 Course Module 16: *El Niño, La Niña, and the Southern Oscillation- Part 1*. Dept. of Meteorology, Naval Postgraduate School, Monterey, California, 25 pp.

Murphree, T., 2012c: MR3610 Course Module 23: *North Atlantic Oscillation and Arctic Oscillation*. Dept. of Meteorology, Naval Postgraduate School, Monterey, California, 66 pp.

National Snow & Ice Data Center (NSIDC), cited 2013: All about Arctic climatology and meteorology. [Available online at http://nsidc.org/arcticmet/patterns/arctic_oscillation.html.]

Nitta, T., 1987: Convective activities in the tropical western Pacific and their impact on the Northern Hemisphere summer circulation, *J. Meteor. Soc. Japan*, **65**, 373-390.

Park, T., C. Ho, and S. Yang, 2010: Relationship between the Arctic Oscillation and Cold Surges over East Asia. *J. Climate,* **24**, 68–83.

Saha, S., and Co-Authors, 2010: The NCEP Climate Forecast System Reanalysis. *Bull. Amer. Meteor. Soc*., **91**, no. 8, 1015–1057, doi:10.1175/2010BAMS3001.1.

Thompson, D. W. J., and J. M. Wallace, 1998: The Arctic Oscillation signature in the wintertime geopotential height and temperature fields. Geophys. Res. Lett., **25**, no. 9, 1297–1300.

Tournay, R., 2008: Long-range forecasting of Korean summer precipitation. M.S. thesis, Dept. of Meteorology, Naval Postgraduate School, 121 pp.

University Corporation for Atmospheric Research (UCAR), cited 2013: [Available online at http://rda.ucar.edu/pub/cfsr.html.]

USA Today, cited 2013: N. Korea: Joint exercise pushes countries to 'brink of war'. [Available online at http://usatoday30.usatoday.com/news/world/2010–11–26-korea_N.htm.]

van den Dool, H., 2007: *Empirical Methods in Short-Term Climate Prediction*. Oxford University Press, 215 pp.

van den Dool, H., and Z. Toth, 1991: Why do forecasts for "near normal" often fail? *Wea. Forecasting*, **6**, 76–85.

Vorhees, D., 2006: The impacts of global scale climate variations on Southwest Asia. M.S. thesis, Dept. of Meteorology, Naval Postgraduate School, 161 pp.

Walker, G., 1932: World Weather V. *Memoirs of the Royal Meteorological Society*, **4**, no. 36, 53–84.

Watanabe, M., 2004: Asian jet waveguide and a downstream extension of the North Atlantic Oscillation. *J. Climate,* **17**, 4674–4691.

Wikimedia Commons, cited 2013: [Available online at http://commons.wikimedia.org/wiki/File:East_Asia_topographic_map.png.]

Wilks, D., 2006: *Statistical Methods in the Atmospheric Sciences*, Academic Press, 627 pp.

Willmott, C.J., S.M. Robeson and J.J. Feddema, 1994: Estimating continental and terrestrial precipitation averages from rain-gauge networks. *International Journal of Climatology*, **14**, 403–414.

Yang, S., K.M. Lau, S.H. Yoo, J.L. Kinter, K. Miyakoda, and C.H. Ho, 2004: Upstream subtropical signals preceding the Asian summer monsoon circulation. *J. Climate*, **17**, 4213–4229.

# INITIAL DISTRIBUTION LIST

1. Defense Technical Information Center
   Ft. Belvoir, Virginia

2. Dudley Knox Library
   Naval Postgraduate School
   Monterey, California

3. Capt. Nicholas Reitz
   Naval Postgraduate School
   Monterey, California

4. Prof. Tom Murphree
   Naval Postgraduate School
   Monterey, California

5. Mr. David Meyer
   Naval Postgraduate School
   Monterey, California

6. Air Force Weather Technical Library
   Asheville, North Carolina

7. Capt. Shane Gillies
   14th Weather Squadron
   Asheville, North Carolina